

“SHEAR STRESS TRANSFER ACROSS CONCRETE TO CONCRETE AND STEEL TO CONCRETE INTERFACES”

Otgonchimeg Davaadorj

A thesis submitted

in partial fulfillment of the requirements

for the degree of

MASTER OF SCIENCE in Civil Engineering

University of Washington

2018

Committee:

Paolo M. Calvi

John F. Stanton

Marc O. Eberhard

Jeffrey W. Berman

Program Authorized to Offer Degree:

Civil and Environmental Engineering

©Copyright 2018
Otgonchimeg Davaadorj

University of Washington

Abstract

“SHEAR STRESS TRANSFER ACROSS CONCRETE TO CONCRETE AND STEEL TO CONCRETE INTERFACES”

Otgonchimeg Davaadorj

Chairs of the Supervisory Committee:

Paolo M. Calvi

John F. Stanton

Civil and Environmental Engineering

This research project investigates shear transfer across concrete-to-concrete and steel-to-concrete interfaces where “sliding shear” failure is critical. Experimental data available in the literature were collected and statistically analyzed. Based on the experimental data available for concrete-to-concrete interfaces, a strength prediction model was calibrated and proposed. The performance of this new model, built on the framework of the model proposed by Mattock (2001), was compared against current design code provisions and some of the available models proposed by others over the years.

The database assembled for steel-to concrete interfaces was also used to examine the performance of some of the existing design equations and strength models. In addition, the analysis of the database led to the identification of a number of important gaps in the literature.

Amongst those, the lack of tests on embed plates subjected to combined shear and bending actions was of particular concern. Thus, an experimental program involving a total of five specimens was planned and conducted. The main variables considered were the load eccentricity and the stud distribution across the embed plate. The results of the experiments shed some light on the complex mechanisms that contribute to the interface strength, providing some preliminary insight and qualitative information on the aspects that should be incorporated in a rational design model.

In the sub-discipline of concrete engineering, shear transfer across both concrete-to-concrete and steel-to-concrete interfaces is treated as a frictional phenomenon, whereas, in the steel sub-discipline, shear transfer across steel-to-concrete interfaces is treated as a dowel action phenomenon. Both approaches can predict similar strengths if they are suitably calibrated, but some of the subtleties of the behavior of steel-to-concrete interfaces appear to be better modeled using the dowel action approach.

Acknowledgements

I would like to thank Dr. Paolo M. Calvi and Dr. John F. Stanton for their excellent support and guidance throughout the completion of this research.

I would also like to thank my fellow graduate student friends here at the University of Washington for sharing their insights and the time we spent together. You made this past two years a better journey!

Thanks to the undergraduate research assistants who helped me build the test specimens.

I am thankful for the funds received from Daniel P. Jenny PCI Fellowship and ACI Stewart C. Watson memorial scholarship programs.

I am also, forever thankful for the Government of Mongolia for making it possible for me to pursue CEE degree in the USA in the first place. State Training Fund for Young Mongolian Scholars in Science and Technology Fields was the biggest help for me to pursue the best education possible.

Dedication

This thesis is dedicated to my family who love and support me unconditionally. My parents, Davaadorj and Bolormaa, encouraged me in every way possible to pursue my dreams and continue my education. Thank you for believing in me. The same applies to both of my older siblings, Uuganbayar and Uranchimeg, and their families. The strongest support came from the other side of the world!

Энэхүү магистрын дипломын ажилыг намайг үнэн сэтгэлээсээ хайрлаж, тусалж дэмждэг гэр бүлийнхэндээ зориуллаа. Миний аав Даваадорж, ээж Болормаа нар намайг хүсэл мөрөөдлөө дагаж боловсролоо үргэлжлүүлэн ахиулахыг боломжит бүхий л аргаар урам зоригжуулан дэмжиж байсан. Надад итгэсэнд баярлалаа. Миний ах Ууганбаяр, эгч Уранчимэг, болон тэдний гэр бүлүүд ч мөн адил тэр бүхнийг хийсэн. Хамгийн хүчтэй туслалцаа дэлхийн нөгөө талаас ирсэн шүү!

Nomenclature

A_s or A_{vf} = Area of shear reinforcement crossing the shear interface

A_{cr} = Area of crack/shear interface

ρ_v or ρ = ratio of area of shear reinforcement to area of shear interface

V_n = Nominal interface shear strength

v_n = Nominal interface shear strength per unit interface area

v_u = Measured ultimate interface shear strength per unit interface area

Q_n = shear strength of one stud

q_n = shear strength per unit area of shear reinforcement

f_y = yielding strength of steel reinforcement

E_s = Young's modulus

ρf_y = clamping stress

ρf_u = ultimate clamping stress

f_{cm} = mean compressive strength of concrete

f'_c = concrete compressive strength

$f'_{c,cr}$ = critical compressive strength as defined in section 4.1.2.4.

f_u = ultimate tensile strength of steel reinforcement

$s_{long.}$ = spacing of studs in the longitudinal direction of applied shear load

$s_{trans.}$ = spacing of studs in the transverse direction of applied shear load

h_s = height of stud

μ = shear friction coefficient

μ_e = effective shear friction coefficient

λ = concrete weight modification factor

Φ = safety factor

COV=coefficient of variation

Std. DEV=standard deviation

R ratio=ratio of calculated over test shear strength of any design model.

PCI = Precast/Prestressed Concrete Institute

ACI = American Concrete Institute

AASHTO = American Association of State Highway and Transportation Officials

CSA = Canadian Standards Association

EN = EuroCode 2

ASTM = American Society for Testing and Materials

MO = Monolithically cast

CJ = Cold Joint (cast at different times)

U = Uncracked

P = Pre-cracked

R = Roughened

S = Smooth

NW = Normal weight concrete

SLW = Sanded lightweight concrete

ALW = All lightweight concrete

Table of Contents

Abstract.....	iii
Acknowledgements.....	iv
Dedication	v
Nomenclature	vi
Table of Contents.....	viii
List of Figures	xi
List of Tables	xviii
1. Introduction	1
1.1 Background	1
1.1.1 Shear Friction Theory	3
1.1.2 Dowel Action Approach	6
1.2 Research Motivation.....	6
1.3 Scope of Research	7
1.4 Thesis Content	8
2. Literature Review.....	9
2.1 Previous Studies:.....	9
2.1.1 Concrete to concrete interfaces:	9
2.1.2 Steel to concrete interfaces:.....	24
2.2 Miscellaneous models.....	32
2.3 Code Provisions.....	37
3. Database	48
3.1 Introduction	48
3.2 Concrete to Concrete Interface Data.....	48
3.2.1 Schematics of the database	49
3.2.2 Timeline of test programs.....	51
3.2.3 Detailed interpretation of the database by parameters	54
3.3 Steel to Concrete Interface Data	60
3.3.1 Schematics of the database	62

3.3.2	Timeline of Test Programs	64
3.3.3	Detailed interpretation of the database by parameters	66
4.	Analysis of Concrete to Concrete Interface Data.....	77
4.1	Introduction	77
4.2	Influence of Parameters.....	80
4.2.1	Overview	80
4.2.2	Effects of clamping stress and concrete strength.....	84
4.2.3	Effect of Yielding Strength of Shear Reinforcement	88
4.2.4	Effect of Concrete Type.....	90
4.2.5	Effects of Other Parameters	97
4.3	Proposed Model.....	99
4.3.1	Development of the Model.....	99
4.3.2	Calibration process and performance of the model	104
4.3.3	Performance ranking of all available models.....	110
4.3.4	Comparison of the proposed model and Code Provisions	114
5.	Analysis of Steel to Concrete Interface Data	123
5.1	Introduction	123
5.2	Influence of Parameters.....	124
5.2.1	Combined Effects of Concrete Compressive Strength and Clamping Stress	125
5.2.2	Effect of Tensile Strength of Shear Studs and Interface Preparations	127
5.2.3	Effect of Concrete Type.....	129
5.2.4	Effect of Stud Spacing	132
5.2.5	Effects of Other Parameters	133
5.3	Model comparisons	134
5.3.1	Performance Rankings of Available Models	134
5.3.2	Detailed Performance of Code Provisions	137
6.	Experimental Program	140
6.1	Introduction	140
6.2	Specimen Design and Test setup	141
6.2.1	Reinforced Concrete Blocks	143
6.2.2	Formwork.....	146

6.2.3 Placement of embed plates	147
6.2.4 Lifting system	148
6.2.5 Reinforcement and pipes.....	149
6.2.6 Concrete casting, surface preparation.....	151
6.3 Materials	153
6.3.1 Concrete mixture	153
6.3.2 Embed plates.....	156
6.4 Test Setup and Instrumentation	160
6.4.1 Test Setup	160
6.4.2 Specimen Instrumentation	165
6.5 Test Results	170
6.5.1 Specimen “2-0-0.92”	171
6.5.2 Specimen “4-0-0.92”	177
6.5.3 Specimen “2-2-0.92”	183
6.5.4 Specimen “2-2-0.25”	188
6.5.5 Specimen “2-2-0.50”	193
6.5.6 Summary of Test Results.....	198
6.6. Discussion of Results.....	201
6.6.1 Specimen 2-0-0.92	205
6.6.2 Specimen 4-0-0.92	206
6.6.3 Specimen 2-2-0.92	208
6.6.4 Specimen 2-2-0.25	210
6.6.5 Specimen 2-2-0.50	212
7. Summary, Conclusions and Recommendations.....	214
7.1 Summary	214
7.2 Conclusions	215
7.3 Recommendations for Design Equations.....	217
7.4 Recommendations for Future Work	217
References	219
Appendix A: Concrete-to-concrete interface database	225
Appendix B: Steel-to-concrete interface database.....	236

List of Figures

Figure 1.1.1: Diagonal web shear failure in a prestressed concrete beam (UW Big Beam Competition team media, 2016).....	1
Figure 1.1.2: Examples of interfaces that are critical in sliding shear	2
Figure 1.1.1.1: Shear friction mechanism scheme (Sneed and Shaw, 2013).....	3
Figure 1.1.2.2: Simplified shear force transfer scheme (Sneed and Shaw, 2013)	4
Figure 1.1.1.3: Common sliding shear friction test set-ups	5
Figure 2.1.1.1: Typical push-off specimens (Hanson, 1960)	9
Figure 2.1.1.2: Typical Push-off specimens (Anderson, 1960).....	10
Figure 2.1.1.3: Comparison between test data and the Birkeland &Birkeland model (1966)	12
Figure 2.1.1.4: Zia’s relationship between shear strength and clamping stress	13
Figure 2.1.1.5: Details of Hofbeck et al. (1969) test specimens	14
Figure 2.1.1.6: Test set ups included in Mattock and Hawkins, 1972	16
Figure 2.1.1.7: Effect of f_c' (Mattock and Hawkins, 1972)	16
Figure 2.1.1.8.a: Corbel type specimen (Mattock et al. 1975).....	18
Figure 2.1.1.8.b: Push-off specimen (Mattock et al. 1975)	18
Figure 2.1.2.1: typical solid-slab push-out test set up (Viest, 1956).....	25
Figure 2.1.2.2: Effect of stud diameter (Viest, 1956).....	25
2.1.2.3: Stud strength vs. flange thickness (Roddenberry, 2002).....	30
Figure 2.1.2.4: Evaluation of concrete formulas of AISC (2005), EC4, and proposed models (Pallares and Hajjar, 2010).....	32
Figure 2.3.1: Roughness definition (EN 1992-1-1)	44
Figure 3.2.2.1: Cumulative test numbers with time	52
Figure 3.2.2.2: Timeline of major milestones	53
Figure 3.2.3.1: NW data sorted by yielding strength of reinforcement	55
Figure 3.2.3.2: LW data sorted by yielding strength of reinforcement	55
Figure 3.2.3.3: NW data sorted by clamping stress	56
Figure 3.2.3.4: LW data sorted by clamping stress.....	57
Figure 3.2.3.5: NW data sorted by compressive strength of concrete.....	58
Figure 3.2.3.6: LW data sorted by compressive strength of concrete.....	58

Figure 3.2.3.7: NW data sorted by size of shear reinforcement.....	59
Figure 3.2.3.8: LW data sorted by size of shear reinforcement.....	60
Figure 3.3.1.1: Common types of steel to concrete interface test configurations.....	61
Figure 3.3.2.1: Cumulative test numbers with time	65
Figure 3.3.2.2: Timeline of studies on strength of shear studs.....	66
Figure 3.3.3.1: NW data sorted by ultimate strength of reinforcement	67
Figure 3.3.3.2: LW data sorted by ultimate strength of reinforcement	68
Figure 3.3.3.3: NW data sorted by ultimate clamping stress.....	69
Figure 3.3.3.4: LW data sorted by ultimate clamping stress	69
Figure 3.3.3.5: NW data sorted by compressive strength of concrete.....	70
Figure 3.3.3.6: LW data sorted by compressive strength of concrete.....	71
Figure 3.3.3.7: NW data sorted by diameter of studs.....	72
Figure 3.3.3.8: LW data sorted by diameter of studs	72
Figure 3.3.3.9: NW data sorted by height to diameter ratios of studs.....	73
Figure 3.3.3.10: LW data sorted by height to diameter ratios of studs.....	73
Figure 3.3.3.11: NW data sorted by longitudinal spacing to diameter ratios of studs.....	74
Figure 3.3.3.12: LW data sorted by longitudinal spacing to diameter ratios of studs.....	75
Figure 3.3.3.13: NW data sorted by transverse spacing to diameter ratios of studs	76
Figure 3.3.3.14: LW data sorted by transverse spacing to diameter ratios of studs.....	76
Figure 4.2.1.1: 3D shear strength plot for MO-U NW tests	80
Figure 4.2.1.2: Shear strength contour plot for MO-U NW tests.....	81
Figure 4.2.1.3: 3D shear strength plot for MO-P NW tests.....	82
Figure 4.2.1.4: Shear strength contour plot for MO-P NW tests	82
Figure 4.2.1.5: 3D shear strength plot for CJ-R NW tests	83
Figure 4.2.1.6: Shear strength contour plot for CJ-R NW tests.....	84
Figure 4.2.2.1: MO-U NW tests, grouped by f_c'	85
Figure 4.2.2.2: MO-U NW tests, cohesion vs f_c'	86
Figure 4.2.2.3: MO-U NW tests, friction coefficient vs f_c'	86
Figure 4.2.2.4: MO-P NW tests, grouped by f_c'	87
Figure 4.2.2.5: CJ-R NW tests, grouped by f_c'	87
Figure 4.2.2.6: CJ-S NW tests, grouped by f_c'	88

Figure 4.2.3.1: MO-P NW tests with $2.5\text{ksi} < f_c' < 4.5\text{ ksi}$, grouped by f_y	89
Figure 4.2.3.2: CJ-R NW tests with $2.5\text{ksi} < f_c' < 4.5\text{ ksi}$, grouped by f_y	89
Figure 4.2.4.1: MO-U NW tests in the specified f_c' range	91
Figure 4.2.4.2: MO-U LW tests in the specified f_c' range	91
Figure 4.2.4.3: MO-P NW tests in the specified f_c' range.....	92
Figure 4.2.4.4: MO-P LW tests in the specified f_c' range	93
Figure 4.2.4.5: CJ-R NW tests in the specified f_c' range	94
Figure 4.2.4.6: CJ-R LW tests in the specified f_c' range	94
Figure 4.2.4.7: CJ-S NW tests in the specified f_c' range.....	95
Figure 4.2.4.8: CJ-S LW tests in the specified f_c' range	96
Figure 4.2.4.9: Comparisons of λ vs ρf_y among interfaces.....	97
Figure 4.3.1.1: Example 3D surface of the trial model 3.....	102
Figure 4.3.1.2: Example 3D surface of the final model.....	103
Figure 4.3.1.3: Example comparison between Mattock 2001 and DCS model (MO-U interface)	104
Figure 4.3.2.1: Contour plots of RMSD values for MO-U, MO-P, CJ-R, and CJ-S interfaces.....	105
Figure 4.3.2.2: Upper limit activations at smallest f_c' available and at $f_{c, crit}'$ (MO-U NW).....	107
Figure 4.3.2.3: Proposed model surfaces for NW monolithic interfaces.....	108
Figure 4.3.2.4: Proposed model surfaces for SLW monolithic interfaces.....	108
Figure 4.3.2.5: Proposed model surfaces for ALW monolithic interfaces	109
Figure 4.3.2.6: Proposed model surfaces for NW cold-joint interfaces.....	109
Figure 4.3.2.7: Proposed model surfaces for SLW cold-joint interfaces.....	110
Figure 4.3.2.8: Proposed model surfaces for ALW cold-joint interfaces	110
Figure 4.3.4.1: Ln(R) ratios vs. f_c' (MO-U interface)	115
Figure 4.3.4.2: R ratios vs. ρf_y (MO-U interface).....	116
Figure 4.3.4.3: Bin counts of R ratios (MO-U interface)	117
Figure 4.3.4.4: Ln(R) ratios vs. f_c' (MO-P interface).....	117
Figure 4.3.4.5: R ratios vs. ρf_y (MO-P interface)	118
Figure 4.3.4.6: Bin counts of R ratios (MO-P interface).....	118
Figure 4.3.4.7: Ln(R) ratios vs. f_c' (CJ-R interface)	119
Figure 4.3.4.8: R ratios vs. ρf_y (CJ-R interface).....	120
Figure 4.3.4.9: Bin counts of R ratios (CJ-R interface).....	120

Figure 4.3.4.10: Ln(R) ratios vs. f_c' (CJ-S interface)	121
Figure 4.3.4.11: R ratios vs. ρf_y (CJ-S interface)	121
Figure 4.3.4.12: Bin counts of R ratios (CJ-S interface).....	122
Figure 5.2.1.1: 3D shear strength plot for NW tests (Steel interface).....	125
Figure 5.2.1.3: 3D shear strength plot for LW tests (Steel interface).....	127
Figure 5.2.2.1: NW tests with $f_c' < 5.5$ ksi grouped by f_u (Steel interface).....	128
Figure 5.2.2.2: NW tests with $4 \text{ ksi} < f_c' < 6 \text{ ksi}$ grouped by f_u (Steel interface).....	129
Figure 5.2.3.1: NW, concrete failure tests in the specified f_c' range.....	130
Figure 5.2.3.2: LW, concrete failure tests in the specified f_c' range	130
Figure 5.2.3.3: NW, stud failure tests in the specified f_c' range.....	131
Figure 5.2.3.4: LW, stud failure tests in the specified f_c' range.....	132
Figure 5.2.4.1: NW tests vs. ratios of longitudinal spacing over diameter of studs	133
Figure 5.2.4.2: NW tests vs. ratios of transverse spacing over diameter of studs	133
Figure 5.3.2.1: Ln(R) ratios vs. f_c' (steel to concrete interfaces) —North American Code Provisions	138
Figure 5.3.2.2: R ratios vs. ρf_u (steel to concrete interfaces).....	139
Figure 5.3.2.3: Bin counts of R ratios (steel to concrete interfaces)	140
Figure 6.1.1: Example steel-to concrete joints (Design of Steel-to-Concrete Joints Design Manual II) ...	141
Figure 6.2.1: Specimen naming convention.....	142
Figure 6.2.2: A typical specimen	143
Figure 6.2.1.1.a: Reinforcement types.....	144
Figure 6.2.1.1.b: Reinforcement types cont.	144
Figure 6.2.1.2: Spacing details of reinforcement cage.....	145
Figure 6.2.1.3: Spacing details shear reinforcement	145
Figure 6.2.1.4: Reinforcement cage side by side views	146
Figure 6.2.1.5: Reinforcement cage and steel pipes in place	146
Figure 6.2.2.1: Assembled formwork.....	147
Figure 6.2.3.1: Embed plate securement.....	147
Figure 6.2.3.2: Embed plate placement.....	148
Figure 6.2.4.1: Lifting rods and their coil inserts	148
Figure 6.2.5.1: Strain gauge wires going out of the formwork.....	149
Figure 6.2.5.2: Frame with plugs for the steel pipes	150

Figure 6.2.5.3: Rebar cage and steel pipes secured in place	150
Figure 6.2.5.4: Strain gauge wires secured to the nearest rebar	151
Figure 6.2.5.5: Strain gauge wires protected for casting process.....	151
Figure 6.2.6.1: Casting day.....	152
Figure 6.2.6.2: Moisture curing set up for test specimens	153
Figure 6.3.1.1: Slump test result	154
Figure 6.3.1.2: Compressive strength test set up	154
Figure 6.3.1.3: Compressive strength trend with time	155
Figure 6.3.2.1: Dimensions of shear studs (taken from a catalog of “Tru-Weld”).....	156
Figure 6.3.2.2: Sample stud shanks.....	157
Figure 6.3.2.3: Machined stud shanks for tensile tests	158
Figure 6.3.2.4.a: Test set up for tensile strength of studs	159
Figure 6.3.2.4.a: Test set up for tensile strength of studs (close-ups).....	159
Figure 6.3.2.5: Stud shank test (necking and fracture photos).....	159
Figure 6.3.2.6: Stress-strain relationship of shear stud shanks in tension.	160
Figure 6.4.1.1: Load transfer system.....	161
Figure 6.4.1.2.a: 6”x6 HSS tubes for 4-stud specimens	162
Figure 6.4.1.2.b: 5”x5” HSS tube for 2-stud specimen	162
Figure 6.4.1.3.a: Back side swivel being checked for component fitting (bolts were tightened in place later).....	163
Figure 6.4.1.3.b: The guide held-down for welding preparation (the horizontal hold-downs were removed after welding)	163
Figure 6.4.1.4.a: Actuator sitting on timber pieces	163
Figure 6.4.1.4.b: Back of the actuator.....	163
Figure 6.4.1.5: Assembled gizmo	164
Figure 6.4.1.6.a: Concrete block in place	165
Figure 6.4.1.6.b: Pre-stressing set up.....	165
Figure 6.4.2.1: Installed Strain gauges (before and after M-Coat application)	166
Figure 6.4.2.2: Typical completely protected strain gauges	167
Figure 6.4.2.3: Close up of displacement sensors and the tip of actuator gizmo.....	168
Figure 6.4.2.4: Locations of Optotrak sensors	169
Figure 6.4.2.5: Complete test set up.....	170

Figure 6.5.1: Monotonic loading direction	171
Figure 6.5.1.1: Specimen 2-0-0.92 at P=25 kips.....	172
Figure 6.5.1.2.a: Specimen 2-0-0.92 at P=35kips.....	172
Figure 6.5.1.2.a: Close-up of Specimen 2-0-0.92 at P=35kips.....	172
Figure 6.5.1.3: Crack patterns near embed plates after failure (Specimen 2-0-0.92)	173
Figure 6.5.1.4: Specimen 2-0-0.92's slip and separation after unloading	173
Figure 6.5.1.5: Specimen 2-0-0.92's sheared studs and local concrete crack profile.....	174
Figure 6.5.1.7: Shear force vs. slip (Specimen 2-0-0.92).....	176
Figure 6.5.1.8: Shear force vs. uplift (Specimen 2-0-0.92).....	176
Figure 6.5.1.9: Shear force vs. base rotation (Specimen 2-0-0.92).....	177
Figure 6.5.2.2.a: Specimen 4-0-0.92 at P=60kips.....	178
Figure 6.5.2.2.b: Close up of Specimen 4-0-0.92 at P=60kips.....	178
Figure 6.5.2.3: Crack patterns near embed plates after failure (Specimen 4-0-0.92)	179
Figure 6.5.2.5: Concrete profile around the studs after failure (Specimen 4-0-0.92)	180
Figure 6.5.2.6: Shear force vs strains in the studs (Specimen 4-0-0.92).....	181
Figure 6.5.2.7: Shear force vs. slip (Specimen 4-0-0.92)	181
Figure 6.5.2.8: Shear force vs. uplift (Specimen 4-0-0.92).....	182
Figure 6.5.2.9: Shear force vs. base rotation (Specimen 4-0-0.92).....	182
Figure 6.5.3.1: Specimen 2-2-0.92 before testing (West side)	183
Figure 6.5.3.2.a: Specimen 2-2-0.92 at P=25 kips (East side)	183
Figure 6.5.3.2.b: Specimen 2-2-0.92 at P=35 kips (East side)	183
Figure 6.5.3.3: Specimen 2-2-0.92 at P=38 kips.....	184
Figure 6.5.3.4: Specimen 2-2-0.92 after failure	185
Figure 6.5.3.5: Concrete profile around the studs after failure (Specimen 2-2-0.92)	185
Figure 6.5.3.6: Shear force vs strains in the studs (Specimen 2-2-0.92).....	186
Figure 6.5.3.7: Shear force vs. slip (Specimen 2-2-0.92).....	187
Figure 6.5.3.8: Shear force vs. uplift (Specimen 2-2-0.92).....	187
Figure 6.5.3.9: Shear force vs. base rotation (Specimen 2-2-0.92).....	188
Figure 6.5.4.1: Comparison between P=60 and 70 kips holds (Specimen 2-2-0.25)	189
Figure 6.5.4.2: Specimen 2-2-0.25 at P=80 kips.....	189
Figure 6.5.4.3: Specimen 2-2-0.25 after failure	190

Figure 6.5.4.4: Photographs of slip and crack width after failure (Specimen 2-2-0.25)	190
Figure 6.5.4.5: Shear force vs strains in the studs (Specimen 2-2-0.25)	191
Figure 6.5.4.6: Shear force vs. slip (Specimen 2-2-0.25)	192
Figure 6.5.4.7: Shear force vs. uplift (Specimen 2-2-0.25)	192
Figure 6.5.4.6: Shear force vs. base rotation (Specimen 2-2-0.25)	193
Figure 6.5.5.1: Specimen 2-2-0.50 at P=55 kips	194
Figure 6.5.5.2.a: Concrete crack pattern at P=60 kips (Specimen 2-2-0.50)	194
Figure 6.5.5.2.b: Concrete crack pattern at P=65 kips (Specimen 2-2-0.50)	194
Figure 6.5.5.3: Specimen 2-2-0.50 after failure	195
Figure 6.5.5.4: Concrete profile around the studs after failure (Specimen 2-2-0.50)	195
Figure 6.5.5.5: Shear force vs strains in the studs (Specimen 2-2-0.50)	196
Figure 6.5.5.6: Shear force vs. slip (Specimen 2-2-0.50)	197
Figure 6.5.5.7: Shear force vs. crack width—uplift (Specimen 2-2-0.50)	197
Figure 6.5.5.8: Shear force vs. base rotation (Specimen 2-2-0.50)	198
Figure 6.5.6.1: Load vs. slip relationship of all specimens	199
Figure 6.5.6.2: Schematics of failure mode analysis with respect to load eccentricity	201
Figure 6.6.1: Free body diagram of Method 1	202
Figure 6.6.2: Exaggerated crack width profile along the base plate	203
Figure 6.6.3: Stud deformation scheme	204
Figure 6.6.1.1: Normal force vs. slip (Specimen 2-0-0.92)	205
Figure 6.6.1.2: Resisting forces vs. slip (Specimen 2-0-0.92)	206
Figure 6.6.2.1: Normal force vs. slip (Specimen 4-0-0.92)	207
Figure 6.6.2.2: Resisting forces vs. slip (Specimen 4-0-0.92)	208
Figure 6.6.3.1: Normal force vs. slip (Specimen 2-2-0.92)	209
Figure 6.6.3.2: Resisting forces vs. slip (Specimen 2-2-0.92)	210
Figure 6.6.4.1: Normal force vs. slip (Specimen 2-2-0.25)	211
Figure 6.6.4.2: Resisting forces vs. slip (Specimen 2-2-0.25)	212
Figure 6.6.5.1: Normal force vs. slip (Specimen 2-2-0.50)	213
Figure 6.6.5.2: Resisting forces vs. slip (Specimen 2-2-0.50)	214

List of Tables

Table 2.1.1.1: Shear friction coefficients and maximum shear stress values (Shaikh, 1978).....	20
Table 2.1.1.2: Proposed modifications to the 6 th edition of PCI Design Handbook (Tanner, 2008).....	23
Table 2.2.1: Table of coefficients (Hamadi and Regan, 1980)	35
Table 2.3.1: Table of coefficients (ACI 318-14—Shear friction provisions)	38
Table 2.3.2: Table of coefficients (ACI 318-14—Interface shear provisions).....	38
Table 2.3.3: Table of coefficients (PCI Design Handbook 7 th ed.)	39
Table 2.3.4: Table of coefficients (PCI Design Handbook 6 th ed.)	40
Table 2.3.5: Table of coefficients (AASHTO LRFD Bridge Design Specifications. 7 th ed.).....	41
Table 2.3.6: Table of coefficients (CSA, 2014)	42
Table 2.3.7: Conversion between compressive strengths (EN 1992-1-1).....	43
Table 2.3.8: Table of coefficients (EN 1992-1-1).....	43
Table 3.2.1.1: Test configurations (concrete-to-concrete interfaces).....	49
Table 3.2.1.2: Summary of database (concrete-to-concrete interfaces).....	50
Table 3.2.2.1: Tabulated descriptions of the major milestones	53
Table 3.3.1.1: Summary of database (steel-to-concrete interface) (continues on the next page)	62
Table 4.1.1: List of works that are partially or completely excluded from calibration data (concrete to concrete interface).....	79
Table 4.2.2.1: Summarized coefficients of cohesion and shear friction (MO-U NW data).....	85
Table 4.2.4.1: MO-U, comparison between LW and NW concrete test results	92
Table 4.2.4.2: MO-P, comparison between LW and NW concrete test results	93
Table 4.2.4.3:CJ-R, comparison between LW and NW concrete test results.....	95
Table 4.2.4.4:CJ-S, comparison between LW and NW concrete test results	96
Table 4.2.5.1: Suggested reference works for effects of other parameters which may increase shear strength.....	97
Table 4.2.5.2: Suggested reference works for effects of other parameters which may decrease shear strength.....	98
Table 4.3.1.1: Summary of coefficients of the final model.....	103
Table 4.3.2.1: The coefficients resulting in mathematical min sum (RMSD).....	106
Table 4.3.3.1: Performances of available models – Monolithic interfaces (Ranked from top to bottom)	112
Table 4.3.3.2: Performances of available models – Cold-joint interfaces (Ranked from top to bottom)	114

Table 5.2.3.1: Concrete failure tests— comparison between LW and NW concrete test results	131
Table 5.2.3.2: Stud failure tests— comparison between LW and NW concrete test results	132
Table 5.3.1.1: Performances of available models – both NW and LW concretes (Ranked from top to bottom)	135
Table 5.3.1.2: Performances of available models – NW concrete (Ranked from top to bottom).....	136
Table 5.3.1.3: Performances of available models – LW concrete (Ranked from top to bottom).....	136
Table 6.2.1: Test matrix	142
Table 6.3.1.1: Compressive strengths of concrete at different ages.....	155
Table 6.3.2.1: Properties of embed plates.....	156
Table 6.3.2.2: Properties of shear studs (provided by the manufacturer)	157
Table 6.3.2.3: Diameters of the sample stud shanks at different lengths.....	158
Table 6.3.2.4: Gauge length information for stud tests.....	158
Table 6.4.2.1: Stud instrumentation scheme.....	165
Table 6.5.1: Brief test descriptions and dates	171
Table 6.5.6.1: Summary of test results	198

1. Introduction

1.1 Background

The response of concrete structures to shear loading is complicated for several reasons, including the effects of cracking, disturbances to the stress field due to geometric irregularities, and the presence and amount of reinforcement. The complexity of the behavior is reflected in the complexity and diversity of the shear design provisions in specifications such as ACI 318-14.

In a plain concrete member with uniform geometry, applied pure shear stress can be resolved into pure tension and compression at 45° to the applied shear stress, as shown in Figure 1.1.1. Concrete is generally weaker in pure tension than in pure shear, so the first major event is generally tension cracking at an inclined angle. Most instances of “shear” cracking are, in fact, diagonal tension cracking. After cracking, the response depends strongly on the reinforcement.

Simply supported pre-stressed beam set up (before loading):



Web shear failure at mid-point of the beam:



Figure 1.1.1: Diagonal web shear failure in a prestressed concrete beam (UW Big Beam Competition team media, 2016)

However, sometimes the capacity/demand ratio is higher in tension than in shear, and sliding failure along the shear plane becomes the first major event and the potential mode of failure. Examples include:

- A cold joint between bodies of concrete cast at different times (Figure 1.1.2.a).
- The interface between concrete cast against another material, such as steel (Figure 1.1.2.b).
- A concrete element whose geometry causes a crack to form at an angle nearly parallel to the direction of the shear stress, such as in a bracket or corbel.

a. Interfaces between precast/prestressed concrete bridge girders and cast-in-place concrete deck:



(Source: <http://www.biggsardosa.com/home/index.php/36-construction/bridge-inspections-cm>)

b. Interfaces between dissimilar materials:



(Source: <http://www.jp-uk.com/blog/category/cast-in-channel-fixings/page/2/#>)

Figure 1.1.2: Examples of interfaces that are critical in sliding shear

In such cases, the shear strength corresponding to failure by sliding must be evaluated. Any reinforcement crossing the potential crack plane helps to resist the shear loading, but the mechanics of the behavior of the cracked, reinforced concrete have not yet been established beyond question. In one view, the bodies of the concrete on the two sides of the crack ride over each other and move apart because of the crack roughness. That movement induces tension strain and stress in the reinforcement crossing the crack, which in turn creates compression, and hence friction, between the two concrete faces. The friction resists the applied shear force. This view is referred to as “Shear Friction” and is discussed in more detail in Section 1.1.1. In a second view, the load is resisted primarily by shear stress in the steel itself, and tension in the reinforcement (and hence friction) plays no part. This view is referred to as “Dowel Action” and will be discussed in Section 1.1.2.

The two approaches cannot be separated on the basis of simple mechanics. In the shear friction approach, the friction force is proportional to the tension force in the steel, and hence to its cross-sectional area. In the dowel action approach, the shear resistance of the steel is also proportional to its cross-sectional area. Researchers and regulatory agencies have tended to treat the phenomenon as one of shear friction in concrete-concrete interfaces and one of dowel action in steel-concrete interfaces.

It is likely that both behaviors contribute to shear resistance even in the simplest case of pure shear. If the loading includes bending or axial force as well and the steel crossing the interface is subjected to

direct tension, the internal mechanics become more complicated and the magnitude of the contributions of the two behaviors becomes more difficult to establish.

The two resistance mechanisms have been calibrated against test results and material constants chosen to make the predicted strengths match reasonably well to the measured ones. Consequently, codes such as ACI 318-14 contain different coefficients of friction for different types of interface. Such an empirical approach may be practical for design in situations where the prototype resembles the test configuration, but rational extensions to different situations are not possible. For example, no unified approach exists to guide the designer in cases of both combined loading (such as shear and bending) and pure shear. Furthermore, different agencies (e.g. ACI, AASHTO, PCI) provide different coefficients of friction, allow the use of a cohesion factor in addition to friction, or use an “effective” coefficient of friction that depends on the load. Application of rules from a different code leads to a different predicted strength for the same physical structure. This is not rational.

1.1.1 Shear Friction Theory

In the 1960’s, Mast (1968), Birkeland and Birkeland (1966), Hofbeck, et al. (1969) first introduced the idea of shear friction. These early shear friction models are based on test results from tests where monolithically cast normal strength concrete specimens were loaded in shear to failure. The most common test setups were: monotonically loaded vertical or horizontal push-off, pull-off, modified push-offs with load applied at an angle or eccentrically (Fig. 1.1.1.3).

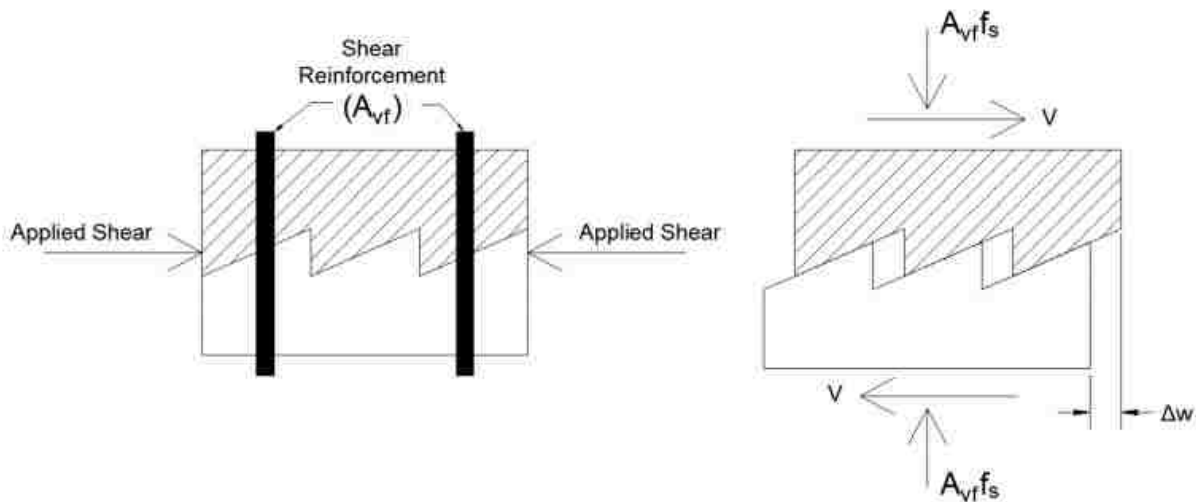


Figure 1.1.1.1: Shear friction mechanism scheme (Sneed and Shaw, 2013)

At nominal strength, the separation and slip are assumed sufficient to stress the reinforcement to yield (Figure 1.1.1.1). Tension force in the reinforcement is assumed to be:

$$N = A_s f_y$$

This tension force provides clamping forces across the shear interface as shown in Figure 1.1.1.2. As a result, the nominal shear strength is given by the

$$V_n = \mu N = \mu A_s f_y$$

Where μ is the coefficient of friction

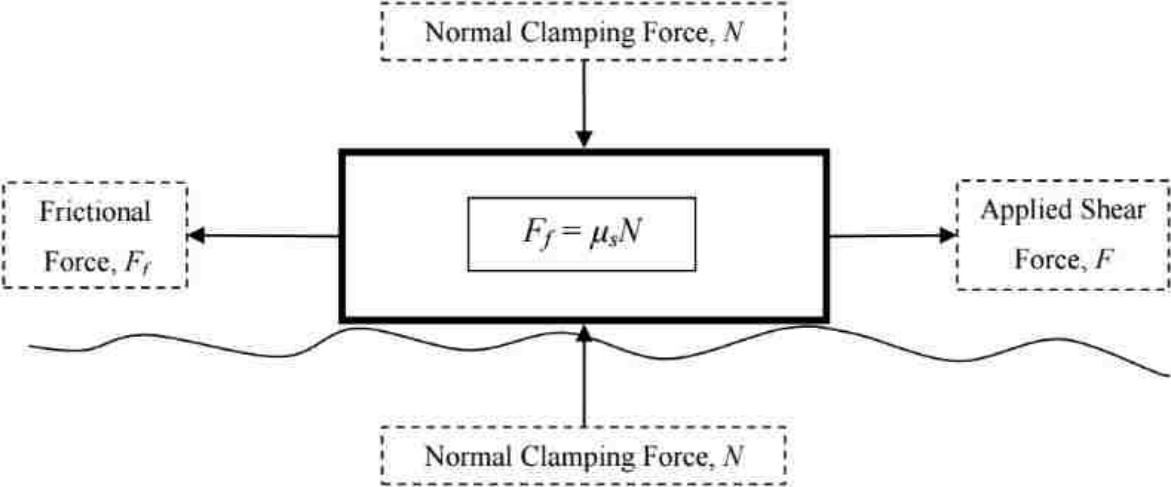


Figure 1.1.2.2: Simplified shear force transfer scheme (Sneed and Shaw, 2013)

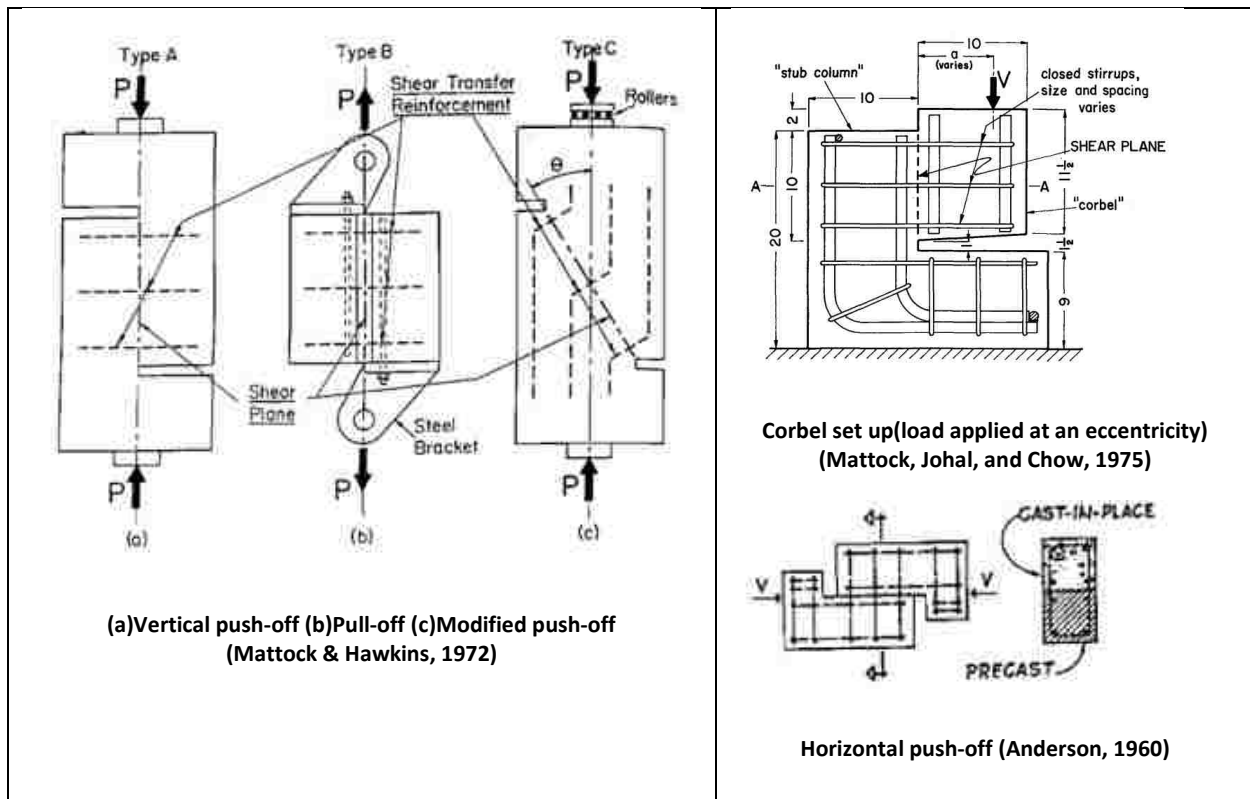


Figure 1.1.1.3: Common sliding shear friction test set-ups

Prior to cracking at the critical interface, cohesion is likely to contribute to shear, in addition to friction. The earlier shear friction models neglected the effects of cohesion, but a significant amount of research has been conducted subsequently, and has addressed various parameters including cohesion. Such parameters include, the interface preparation type, the density and compressive strength of the concrete, the amount and yield strength of the transverse reinforcement, and the presence of external tensile or compressive force. Those studies led to modifications to the basic friction model and resulted in the following main types of modeling:

1. Parabolic shear strength relations developed by Raths (1977), Loov (1978), and Birkeland (1968).
2. Effective shear friction method first introduced by Shaikh (1978) later adopted by PCI.
3. Models based on statistical analysis, such as Walraven (1987).
4. Slip-dependent relation models by Walraven and Reinhardt (1981), Gambarova and Karakoç (1983), Li et al. (1989), and Vecchio and Collins (1986).

These models and others are discussed in more detail in Section 2.1 and Section 2.2.

1.1.2 Dowel Action Approach

Most steel-framed buildings use composite beams, consisting of a rolled steel beam attached to the concrete floor by welded studs. The studs must transfer shear between the top flange of the beam and the slab. Research associated with the steel industry has addressed the modeling and design of these connections, and has treated the problem as one of dowel action. The strength is taken as the smaller of the stud failure strength, related to the stud area and steel strength, and the concrete failure strength, related to f'_c and E_c . Early work by (Newmark et al. 1952) was based on steel channel connectors, rather than studs, and used a “beam on flexible foundation” model. Channel connectors must be hand-welded, and so are more labor-intensive and expensive than studs, which can be shot into place quickly and economically. Studs now dominate the market and the models used are based on their expected plastic behavior.

The behavior of the system is quite complex, because the studs bend, the concrete crushes locally where the stud bears on it and splits transversely due to the prying action of the studs. The bent stud is no longer oriented at right angles to the interface, so tension and shear in the stud both contribute to the resistance parallel to the interface. The length to diameter ratio of the stud and the anchorage value of the head then affect the tension strength that can be mobilized and the relative importance of the contributions of the shear and tension in the stud. The behavior is further complicated by the fact that most slabs are not solid, but rather cast on cold-formed metal deck. Empirical modification factors are provided in the AISC Specifications to account for these effects.

In steel-concrete composite beams, most of the studs carry almost pure shear, so push-off tests provide a suitable basis for developing a model. (Near the end of the beam, the eccentricity of the load plays a bigger role, and the behavior is no longer pure shear). However, if a steel plate is embedded with studs into a concrete wall for the purpose of subsequently welding a beam to it, the stud group will be subjected to moment as well as shear. Some studs will then experience tension that will likely reduce their shear resistance. Present versions of the dowel action model offer no guidance for this situation.

1.2 Research Motivation

Concrete-to-concrete interfaces and steel-to-concrete interfaces have been modeled using different approaches, and consequently different design equations have been developed and embodied in the related codes. Current concrete design codes, including ACI 318, the AASHTO LRFD specifications, and

the PCI Design Handbook, use shear friction theory for prediction of interface shear transfer. However, their details differ. Examples are:

1. ACI: shear friction (friction only)
2. ACI: interface shear transfer (cohesion only)
3. AASHTO: cohesion and shear friction, acting together.
4. PCI: effective shear friction (friction coefficient depends on the load or clamping force across the interface)

These codes do not explicitly consider the contribution of the dowel action of reinforcing bars to the shear strength.

Unlike the above-mentioned code approaches, the design equations in the AISC Specifications are based on models that treat the shear transfer across steel to concrete surfaces as being transferred by dowel action of the transverse reinforcement that crosses the interface.

Even with Individual codes, the provisions contain some internal discrepancies, because the models have been calibrated by researchers using only limited data.

Desirable objectives are to minimize the discrepancies between codes, such as ACI 318 and AASHTO LRFD, and to shed light on the detailed mechanics and overall applicability of the dowel action and shear friction models. Ideally, many more experiments would be conducted, each designed to isolate the effect being investigated, and carefully instrumented to measure that effect. In the absence of the resources needed for such a test program, the best alternative is to assemble a comprehensive database, evaluate the existing models against it, and modify the best one or develop a new one based on the results.

1.3 Scope of Research

The primary objective of this research project is to investigate interface shear transfer problems and to develop a simple shear transfer design approach applicable to various interface types including monolithically cast (uncracked and precracked) concrete interfaces, and cold-joint (cast at different times) intentionally roughened or smooth concrete interfaces. Another goal of this study is to examine shear transfer behaviors of steel to concrete interfaces. To achieve this goal, the following tasks were undertaken:

1. Assemble a comprehensive database including all the available experimental data (for all interface types).
2. Critically analyze the available data and identify the importance of various parameters with respect to interface behavior.
3. Evaluate the reliability of the main shear friction models available in the literature, as well as the reliability of current and previous versions of applicable shear design code and identify gaps in the literature.
4. In the event that the available models provide unsatisfactory performance, calibrate a new model of interface behavior that better reflects the actual stress transfer mechanisms.
5. Design and conduct an experimental program to investigate aspects of the response of interfaces that have received limited attention over the course of past studies.
6. Provide preliminary recommendations for design procedures and future work.

1.4 Thesis Content

This thesis involves the following chapters:

Chapter 2: Literature Review Chapter 2 presents some background information pertaining to the main research works that are currently available in the literature. Applicable shear design code provisions from different countries are summarized, along with some of the available interface models that have been proposed by different authors over the years.

Chapter 3: Database Chapter 3 provides an overview of the comprehensive database that has been assembled pertaining to both steel to concrete and concrete to concrete interfaces. This chapter describes how the data was screened and selected, and how it was used to calibrate the new behavior model proposed as part of this research program.

Chapter 4 and 5: Analysis and Discussion Chapter 4 (concrete to concrete interfaces) and Chapter 5 (steel to concrete interfaces) provide a detailed overview of the main parameters that appear to affect the response of all types of interfaces subjected to shear stresses. These chapters also provide the basis for formulating the new behavior model that is proposed. Comparisons between existing models and available experimental results are included in these chapters.

Chapter 6: Experimental Program Chapter 6 summarizes the experimental program that was conducted on steel-to-concrete interfaces as part of this research. The specimen details, testing methodologies, experimental setup, test results etc. are discussed in detail.

Chapter 7: Summary and Recommendations Chapter 7 summarizes the key aspects of the research work, outlining the main findings and most notable conclusions. Recommendations for future investigations are also provided.

Appendices: The comprehensive database as well as other miscellaneous plots are included.

2. Literature Review

This chapter provides a brief overview of shear friction related research that is currently available in the literature. It includes results from previous experimental programs, a brief description of the main interface models developed over the years and an overview of current code provisions from different countries.

2.1 Previous Studies:

2.1.1 Concrete to concrete interfaces:

Hanson, 1960:

This work was the first extensive work to study composite action between precast girders and cast in place deck slab. To study the effects of various parameters' on the horizontal shear transfer across interfaces, 62 push-off tests as well as 10 T-shaped girders were tested (See Figure 2.1.1.1 for push-off specimen design). The compressive strength of concrete varied from 3,000 psi to 5,000 psi. However, the effects of the concrete strength on shear capacity was not studied exclusively. The test variables were adhesive bond between the cold-joint surfaces, roughness, presence of shear keys, and stirrup reinforcement ratio. Shearing stress and slip were recorded.

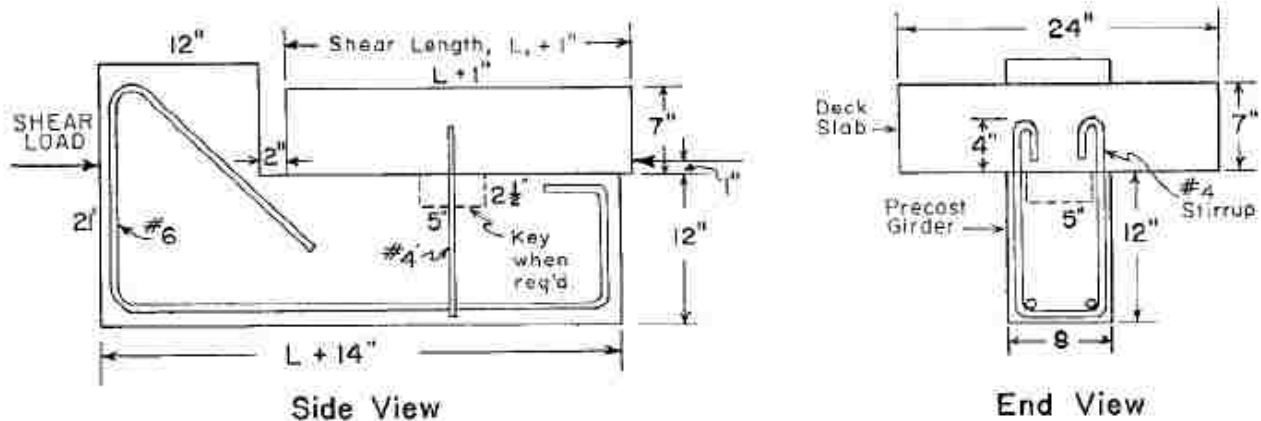


Fig. 1— Pushoff Specimen in Casting Position.

Figure 2.1.1.1: Typical push-off specimens (Hanson, 1960)

The results of the push-off tests showed the following:

1. The ultimate shear strength was proportional to the amount of reinforcement in the connection.
2. Although this test program did not intend to study the effects of the concrete strength, the peak shear stress was observed to be approximately proportional to the concrete strength.
3. Shearing strengths of the shear keys should not be added to the contribution of bond and roughness as large slips are required to engage the keys. The author advised to rely on a combination of bond, roughness, and stirrups instead. If shear keys are not avoidable, it may be necessary to assume the entire shear force is transferred by the keys only.

Anderson, 1960:

Anderson's research aimed to study the effects of higher compressive strength of concrete in composite construction. One side of the push-off specimens were roughened to amplitude of $\frac{1}{4}$ " and were characterized by concrete strength of 7,500 psi. The other side of the push-off specimens had strengths of 3,000 psi and 7,500 psi. The reinforcing ratio varied from 0.2% (2 #2 hoops) to 2.48% (4 #5 hoops) (See Figure 2.1.1.2).

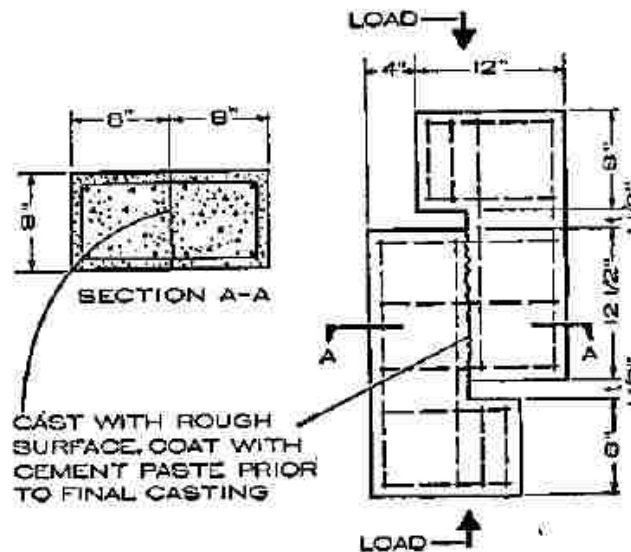


Figure 2.1.1.2: Typical Push-off specimens (Anderson, 1960)

Unlike Hanson (1960)'s setup, this test setup allowed for pure shear load testing. The results of this work suggested the following:

1. Cold-joint specimens behave monolithically until the applied loads reach 75% to 85% of the ultimate capacity, when loaded in pure shear.
2. The ultimate shear capacity is linearly proportional to the amount of reinforcement.
3. Doubling the concrete strength increased the shear capacity by more than 20% on average.

Birkeland and Birkeland, 1966:

After the Alaskan earthquake (1964), the precast industry recognized the importance of connection details. As a result, better design guidelines were necessary for shear connections. To meet that need, the original linear shear friction hypothesis was first introduced by the authors. The definition of shear friction is still what current design provisions are based on.

The authors stated that the ultimate shear force demand (V_u) should be achieved when the reinforcement reaches yielding point ($T_u = A_s f_y$). The tension force in the reinforcement is equal to the external clamping force P . Then, the friction force is equal to μP . They defined friction coefficients with $\tan \phi$ terms because of the surface profiles' analogy they adopted that is they idealized the interface as

a series of saw tooth ramps, having a slope of $\tan \Phi$. This hypothesis was evaluated using cold-joint test data from Hanson (1960), Anderson (1960) and an unpublished work of Mast (1962).

The authors concluded that the interface shear capacity can be defined as shown below:

$$V = \frac{V_u}{FS} = \frac{A_s f_y \tan \Phi}{FS}$$

Where:

$\tan \Phi = 1.7$ for monolithic concrete

$\tan \Phi = 1.4$ for roughened cold-joint

$\tan \Phi = 0.8$ to 1.0 for ordinary construction joints and for steel-to-concrete interfaces

The following tentative limitations were recommended:

yielding strength ($f_y \leq 60$ ksi)

ultimate shear stress on gross area ($v_u \leq 800$ psi)

reinforcing ratio ($\rho = \frac{A_s}{A_c} \leq 1.5\%$)

concrete strength $f'_c \geq 4,000$ psi

maximum reinforcing size=#6 rebar, or $\phi \frac{1}{2}$ " headed studs.

All but one of Hanson's rough bonded specimen were stronger than predicted. However, the data supported the hypothesis, but it needed to be further validated against more experimental data (See Figure 2.1.1.3). The 800 psi limit on ultimate shear stress was based on one unpublished test that was conducted when the specimen was only 1.5 days old (i.e. 1.5 days after casting) hence, was not suggested as permanent limit.

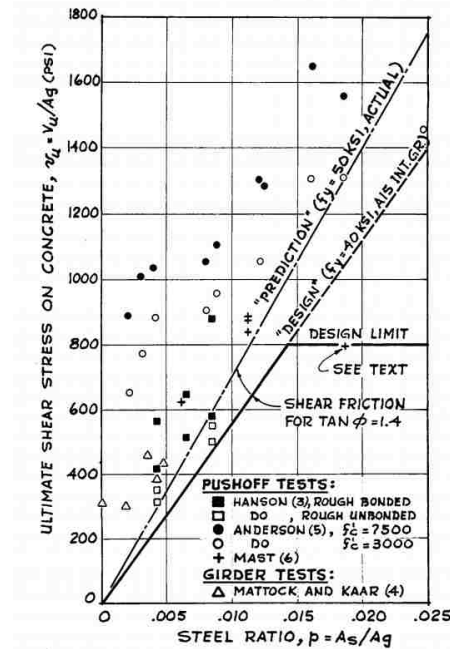


Figure 2.1.1.3: Comparison between test data and the Birkeland & Birkeland model (1966)

Mast, 1968:

Mast analyzed the previously available data from other researchers and recommended similar shear friction approach as Birkeland and Birkeland (1966). In the paper, Mast included design examples of connection details. He stated that accidental cracks prior to loading should be taken into account as it is common in practice. Also, he noted that the consideration of existing pre-cracks should be essential for a conservative design. Since cracks would exist, rational models such as shear friction models can be applied.

He recommended the same model as Birkeland and Birkeland (1966) with the following $\tan \Phi$ values:

- $\tan \Phi = 1.4$ for concrete to concrete—rough interface
- $\tan \Phi = 1.0$ for concrete to steel—composite beams
- $\tan \Phi = 0.7$ for concrete to steel—field welded inserts
- $\tan \Phi = 0.7$ for concrete to concrete—smooth interface

The limitations of the design method suggested by Mast include:

1. The shear friction hypothesis is not suitable for situations where slip or fatigue is critical.
2. To develop full yielding capacity of the reinforcement, the reinforcement must be properly anchored.
3. All available data at the time were based on normal weight concrete specimens, the design proposal may not be suitable for lightweight concrete members.
4. The proposed model is to reflect cracked specimens at low clamping stress.

- As the effects of high strength concrete and high clamping stress were neglected in the model, the clamping stress, ρf_y , should be limited to 15% of the concrete compressive strength. Further research was recommended.

Hofbeck, Ibrahim, and Mattock, 1969:

This study was conducted to study the shear transfer strength of reinforced (normal weight) concrete with or without a pre-crack along the shear plane. Shear transfer strengths of uncracked interfaces were determined using the Zia envelope to Mohr's circle (See Figure 2.1.1.4).

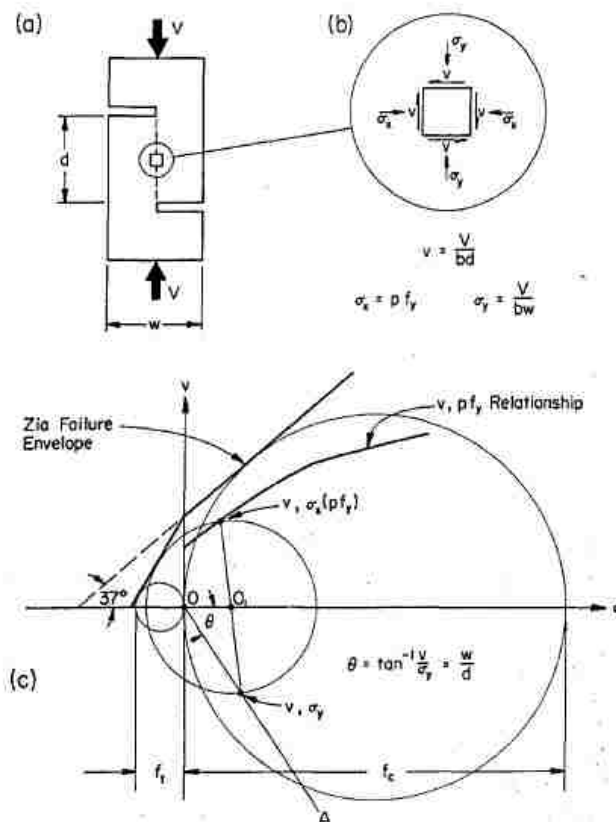


Figure 2.1.1.4: Zia's relationship between shear strength and clamping stress

A total of 36 push-off tests were conducted to study the following:

- Impact of an existing crack along the shear plane
- Influence of strength and different arrangements of reinforcement
- Influence of concrete compressive strength
- Dowel action of reinforcing bars crossing the shear plane
- Applicability of shear friction theory proposed by Birkeland and Birkeland (1966) and Mast (1968) when the shear plane is pre-cracked.

All specimens were horizontally cast on their side and then pre-cracks were formed using a linear force along the shear plane (See Figure 2.1.1.5). The pre-cracks were to simulate cracks unrelated to shear which may occur due to shrinkage, temperature change, accidental dropping, etc. This setup became the classic push-off test setup for the researchers in the same research field later on.

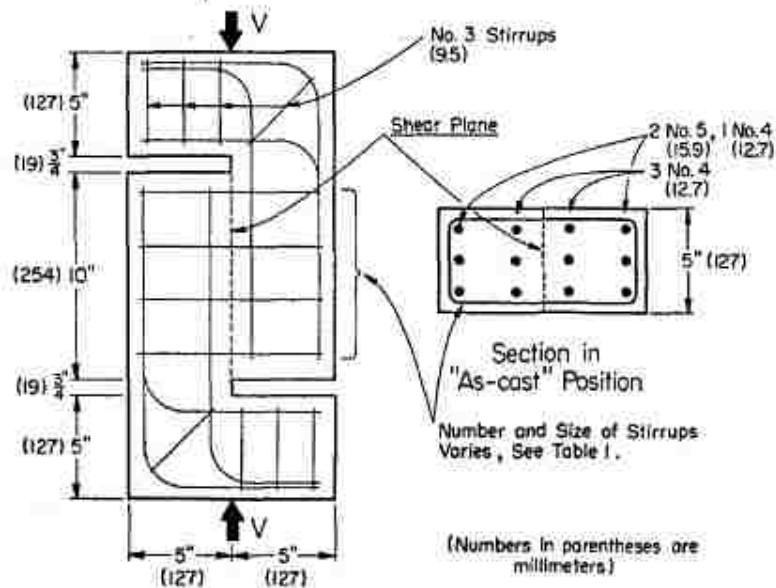


Figure 2.1.1.5: Details of Hofbeck et al. (1969) test specimens

The specimens had concrete compressive strength varying between 2500 psi and 4500 psi. The yield strength of the reinforcing bars varied between 50 and 66 ksi. The clamping stress varied between 0 and 1,500 psi. Reinforcing bars were bonded to the concrete except for 4 specimens that had partially unbonded bars (achieved using 2" long rubber sleeves). The rubber sleeves were used to eliminate the contribution of dowel action provided by the steel reinforcement, thus isolating the shear friction strength contribution. The specimens were placed vertically and loaded until failure as shown in Figure 2.1.1.5.

The authors concluded the following based on their research program:

1. Pre-existing cracks result in smaller ultimate shear strength compared to uncracked interfaces. The strength difference was observed to be about 250 psi for normal weight specimens, with concrete compressive strength of 4,000 psi, when the clamping stress, ρf_y , is between 200 and 1000 psi. Also, pre-cracked interfaces experience larger slip than their uncracked companions at all load levels.
2. When ASTM A432 steel (reinforcement with $f_y \leq 66.1$ ksi were used in the experiment) is used, the changes in yield strength, and the size and spacing between the reinforcement does not affect shear strength as long as ρf_y kept the same.

3. In pre-cracked specimens, a variation in f'_c does not affect the shear strength for shear reinforcement up to 600 psi. At higher ρf_y , the shear strength of higher compressive strength concrete increases. The concrete compressive strength sets an upper limit for clamping stress ($\rho f_y \leq 0.15 f'_c$). Beyond this upper limit, the shear strength increases as a function of ρf_y at a much slower rate.
4. The crack slips at different load levels was not affected by the presence of the rubber slip in uncracked specimens. The strength of the uncracked specimens was also not affected by the rubber sleeves (the difference was smaller than 10%). The dowel action contribution in pre-cracked specimens is significantly higher than it is in uncracked specimens. The slips in pre-cracked specimens with sleeves were about 6 times greater than in specimens without sleeves. The sleeves reduced the shear strength of pre-cracked specimens by 23 and 34%.
5. The shear friction theory gives conservative strength estimates for normal weight pre-cracked interfaces when intermediate or A432 steel is used if:

$$\tan \Phi = 1.4$$

$$\rho f_y \leq \text{smaller of } 0.15 f'_c \text{ or } 600 \text{ psi.}$$
6. For uncracked or roughened cold joint interfaces, the Zia failure envelope is reasonably suitable to determine a relationship between ultimate shear stress, v_u , and ρf_y .

Mattock and Hawkins, 1972:

This test program was the initial part of on-going research at the University of Washington at the time. The factors affecting shear transfer strength that were investigated are the characteristics of the shear plane, reinforcement, the concrete strength, and direct stress acting parallel and perpendicular to the shear interface. The factors except for direct stresses acting on the interface had been studied in Hofbeck et al. (1969), hence the results were included in this paper. Unlike the push-off tests conducted by Hofbeck et al. (1969), pull-off (Type B as shown in Figure 2.1.1.6) and modified pull-off (type C) tests were conducted to examine the direct stress effects. Hawkins and Mattock made conclusions concerning the design approach and the fundamental behavior of shear transfer.

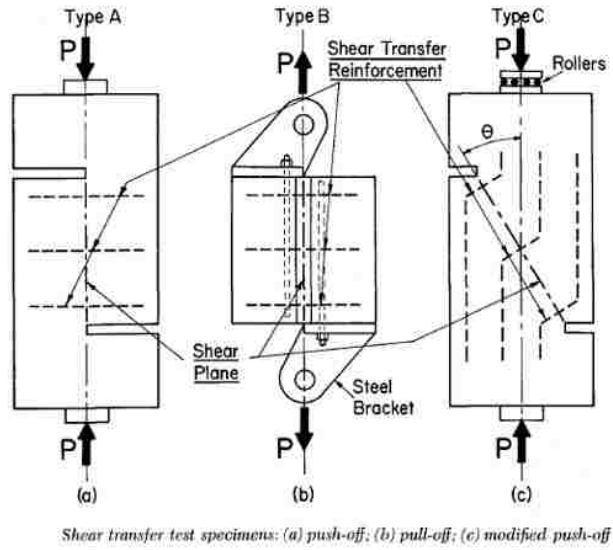


Figure 2.1.1.6: Test set ups included in Mattock and Hawkins, 1972

As discussed in Hofbeck et al. (1969), the authors stated that a pre-existing crack will result in a decrease of ultimate shear transfer strength and an increase in slip at all load levels. Different combinations of strength, size, and spacing of reinforcement can only affect shear transfer strength as part of clamping stress, ρf_y , for $f_y \leq 66$ ksi.

Also, the authors pointed out that the concrete compressive strength starts to play a role with respect to the strength of pre-cracked concrete interfaces when ρf_y is higher than a certain value. This ρf_y value (for this particular experimental program comparing specimens with concrete strength between 2,500 psi and 4,000 psi) is about 500 psi (See Figure 2..11.7).

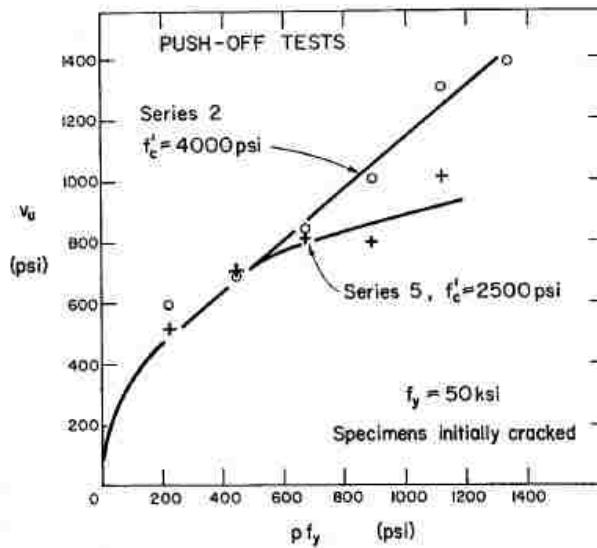


Figure 2.1.1.7: Effect of f'_c (Mattock and Hawkins, 1972)

Mattock and Hawkins observed that direct tension force perpendicular to the shear plane reduces the shear strength of initially uncracked interfaces but not that of pre-cracked interfaces. This was concluded by comparing pull-off and push-off test results. They also concluded that a compressive externally applied force that is perpendicular to the shear plane produces additional clamping stress; hence, it should be added to ρf_y to determine the total shear transfer strength.

The authors stated that the shear strength of uncracked interfaces is developed by a truss action that forms after diagonal tension cracking happens. Failure in initially uncracked specimens happens when the struts finally fail under a combination of axial and shear force. For moderately reinforced pre-cracked interfaces, the shear strength is mostly based on shear friction and dowel action against the sliding occurring at the shear plane. However, when large amount of reinforcement is provided, the precracked interface locks up and acts as an initially uncracked interface.

Another conclusion was that the shear friction design provisions of ACI 318-71 was conservative within its specified applicable ranges of parameters regardless of existence of pre-cracks. They also noted that a strength higher than the 800 psi upper limit of ACI 318-71 can be achieved with sufficient reinforcement and suggested the following equations for precracked interfaces:

$$v_u = 200psi + 0.8(\rho f_y + \sigma_n) \leq 0.3 f'_c$$

Where:

σ_n =externally applied normal stress (compression positive)

$$\rho f_y + \sigma_n \geq 200 psi$$

Mattock, Johal, and Chow, 1975:

A comprehensive study of shear transfer strength of reinforced concrete subjected to both monotonic and cyclic loading conditions took place at the University of Washington. Only the results pertaining to the monotonic tests are summarized in this section. The study was intended to study the effects of tensile normal force and moment acting on the shear plane. Other parameters studied were location, spacing and the amount of reinforcement. The report is based on corbel type push-off specimens and regular push-off test specimens with tension acting normal to the shear plane (See Figure 2.1.1.8.a and Figure 2.1.1.8.b). All specimens were normal weight, monolithically cast, pre-cracked or uncracked specimens with f'_c close to 4,000 psi.

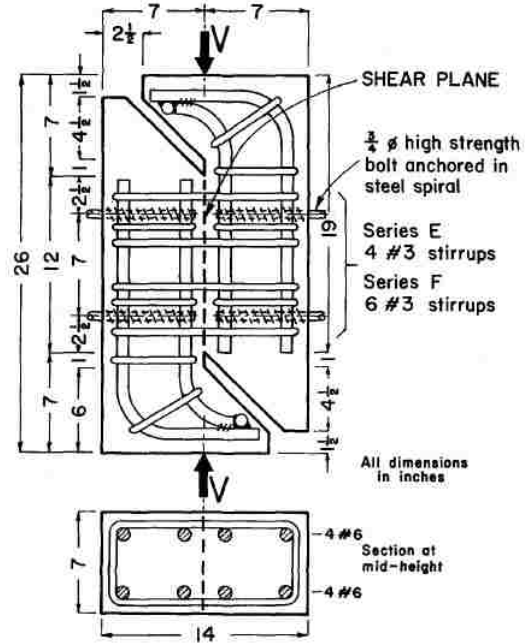
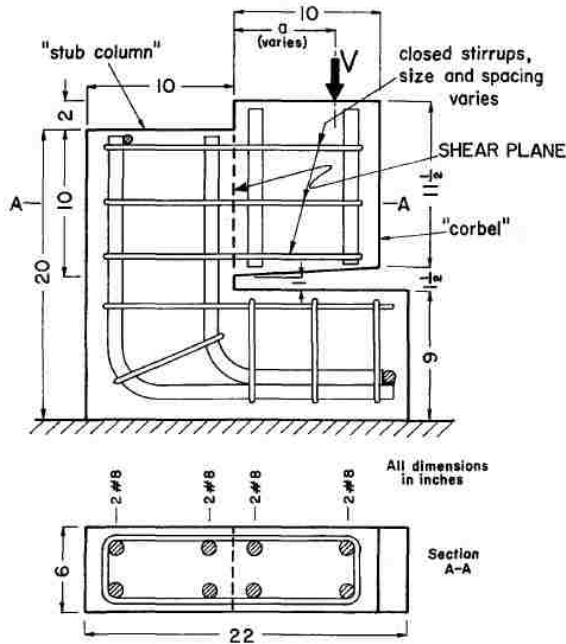


Figure 2.1.1.8.a: Corbel type specimen (Mattock et al. 1975) Figure 2.1.1.8.b: Push-off specimen (Mattock et al. 1975)

The corbel type specimens were used to study the effects of moment, by varying the load eccentricity. The push-off specimens were used to study the impact of externally applied tensile force acting on the shear plane. The externally applied normal tensile force was achieved through pulling $\phi 3/4$ " high strength anchor bolts (Figure 2.1.1.8.b).

The main conclusions that were drawn are:

1. The presence of moments at the shear plane that are less than or equal to the flexural strength of the shear interface do not reduce the interface shear capacity.
2. When the interface is subject to both moment and shear, the shear reinforcements need to be placed in the flexural tension zone to be fully effective.
3. Tension across the shear plane decreases the shear strength as if the clamping stress, ρf_y , was reduced proportionally to the tensile stress.
4. The PCI Design Handbook equation to be used when $\rho f_y > 600$ psi is conservative and the $\sigma_n + \rho f_y$ term should replace the ρf_y term.
5. Birkeland (1968) and Mattock (1974) equations (see equations below) are equally applicable to general shear transfer cases. Instead of shear friction equations, using these two equations multiplied by a capacity reduction factor would lead to economic designs.

Birkeland (1968):

$$v_n = 33.5 \sqrt{\rho f_y} \text{ psi}$$

Mattock (1974):

$$v_n = 0.8\rho f_y + 400\text{psi} \leq 0.3f'_c$$

Mattock, Li, and Wang, 1976:

Classic vertical push-off tests were conducted on uncracked and cracked specimens made of normal weight, sanded lightweight, and two types of all lightweight (rounded and angular aggregate) concrete. The specimens were reinforced with up to six #3 closed loop stirrups (total reinforcement area ranging from 0 to 1.32 in^2) in the shear plane. The specimens were grouped into ten series, 8 of which had $f'_c=4,000$ psi and two had $f'_c=2,500$ psi and 6,000 psi. The specimens were loaded monotonically until failure. They concluded the following:

1. Lightweight concrete has less shear transfer strength than normal weight concrete with identical compressive strength.
2. The shear transfer strength of all-lightweight concrete is not significantly affected by the aggregate type (rounded vs. angular).
3. The shear friction provisions of ACI 318-71 may be used if the shear friction coefficient, μ , is multiplied by a lightweight modification factors. For sanded lightweight concrete with ($Y \geq 105$ pcf), the modification factor should be 0.85. For all lightweight concrete ($Y \geq 92$ pcf), the modification factor should be 0.75.
4. The provisions of Section 6.1.9 of the PCI Design handbook do not conservatively predict the shear transfer strength of lightweight concrete.
5. New shear friction design equations were proposed by the authors for light weight concrete:

$$v_n = 0.8\rho f_y + 250\text{psi} \leq 0.2f'_c \text{ or } 1000\text{psi} \text{ (sand lightweight concrete, } Y \geq 105 \text{ pcf)}$$

$$v_n = 0.8\rho f_y + 200\text{psi} \leq 0.2f'_c \text{ or } 800\text{psi} \text{ (all lightweight concrete, } Y \geq 92 \text{ pcf)}$$

$$\rho f_y \geq 200\text{psi} \text{ (minimum reinforcement)}$$

Shaikh, 1978:

Shaikh analyzed and compared the models proposed by Mattock (1974), Birkeland and Birkeland (1969), and Raths (1977) using test data from Hofbeck et al. (1969), Mattock and Hawkins (1972), Mattock et al. (1975) and Mattock et al. (1976). Shaikh proposed revisions of the shear friction provisions of the PCI Design Handbook. Raths (1977) had previously observed a parabolic relationship between clamping stress and shear transfer strength and had proposed the following equation:

$$v_n = 37.42 \sqrt{\rho f_y} \text{ psi}$$

However, the equation Shaikh proposed resembled that of Birkeland and Birkeland (1969), but introduced an effective shear friction coefficient. The effective shear friction coefficient was intended to take into account the parabolic relationship between the shear strength and the parameter ρf_y

observed by Raths, and the concrete type modification proposed by Mattock (1976). Shaikh suggested that the required shear reinforcement should be as follows:

$$A_v = \frac{V_u}{\Phi f_y \mu_e}$$

$$\mu_e = \frac{1000 C_s^2 \mu}{v_u}$$

Where (See Table 2.1.1 for numerical values):

C_s^2 = concrete modification factor (1.0 for NW concrete, 0.85 for sanded lightweight concrete, and 0.75 for all lightweight concrete).

μ = shear friction coefficient based on interface type.

Φ = capacity reduction factor (0.85 for shear)

Table 2.1.1.1: Shear friction coefficients and maximum shear stress values (Shaikh, 1978)

Interface condition	μ	Maximum v_u (psi)
Monolithic	1.4	$0.3 f_c' C_s^2 \leq 1,200 C_s^2$
Cold-joint (roughened)	1.0	$0.25 f_c' C_s^2 \leq 1,000 C_s^2$
Cold-joint (smooth)	0.4	$0.15 f_c' C_s^2 \leq 600 C_s^2$
Concrete to steel	0.6	$0.20 f_c' C_s^2 \leq 800 C_s^2$

Hoff (1993):

Hoff studied the shear transfer behavior of high strength lightweight concrete for Arctic applications. The concrete compressive strength varied between 8,290 psi to 11,020 psi and had two types of lightweight aggregates (pelletized or crushed). The reinforcement of the specimens were made with Grade 60 steel with actual strength varying from 53.6 to 72.1 ksi. The main parameters investigated were the compressive strength of concrete and the reinforcement ratio. All the specimens were precracked with a line load. The results of the study showed that both higher reinforcement ratio and higher compressive strength result in higher shear friction strength. Also, he observed that pelletized aggregate concrete and crushed aggregates have similar strengths but the pelletized smooth aggregate concrete results in more abrupt slips. He concluded that the shear friction provisions of ACI 318-99 were applicable but more conservative lightweight concrete modification factors should be utilized.

Walraven and Stroband (1994):

The authors investigated the shear friction strength of high strength concrete. The specimens were pre-cracked and had concrete compressive strength of 14,360 psi. The yielding strength of the shear reinforcement was 86.3 ksi. The clamping stress varied between 483 and 2,166 psi. They checked the model proposed by Hsu and Mau (1988):

$$v_n = k \sqrt{\rho f_y f'_c} \text{ psi}$$

$k = 0.66$ for monolithic concrete

They concluded that the expected shear transfer capacity of high strength concrete reduces by 25% to 45% compared to what is predicted by the Hsu (1988) model. They suggested that this kind of reduction was due to the fact that the aggregates in high strength concrete fracture and create a smooth shear interface, while the cracks tend to form around the aggregates in normal weight concrete.

Mattock (2001):

Mattock examined the shear friction capacity of high strength concrete using test data from 8 previous studies. He concluded that the shear friction provisions of ACI 318-99 were overly conservative for modeling high strength concrete due to their strict strength upper limits (such as limiting the shear strength to the smaller of $0.2f'_c$ and 800 psi). He proposed a simple set of equations which would allow for more economical design by taking the concrete strength into account:

- For monolithic or cold-joint (roughened) interfaces:

- a. When $\rho f_y + \sigma_{nx} \geq K_1/1.45$:

$$v_n = K_1 + 0.8(\rho f_y + \sigma_{nx}) \leq K_2 f'_c \text{ and } K_3 \text{ (psi)}$$

Where:

Monolithic NW concrete: $K_1=0.1f'_c$ but no more than 800 psi, $K_2=0.3$ and $K_3=2,400$ psi.

CJ-R NW concrete: $K_1=400$ psi, $K_2=0.3$ (where f'_c taken as smaller f'_c of the two concretes), and $K_3=2,400$ psi.

SLW concrete: $K_1=250$ psi, $K_2=0.2$ and $K_3=1,200$ psi.

ALW concrete: $K_1=200$ psi, $K_2=0.2$ and $K_3=1,200$ psi.

- b. When $\rho f_y + \sigma_{nx} \leq K_1/1.45$:

$$v_n = 2.25(\rho f_y + \sigma_{nx}) \text{ (psi)}$$

- For cold-joint (smooth) interfaces:

$$v_n = 0.6\lambda\rho f_y \leq 0.2f'_c \text{ and } 800 \text{ (psi)}$$

- For concrete to steel interfaces:

$$v_n = 0.7\lambda\rho f_y \leq 0.2f'_c \text{ and } 800 \text{ (psi)}$$

Kahn and Mitchell (2002):

The authors conducted 50 push-off tests with uncracked, pre-cracked, and cold-joint interfaces with varying reinforcement ratio and concrete compressive strengths. Concrete strengths varied between 6,800 psi and 17,900 psi. The transverse reinforcement ratio ranged between 0.37% and 1.47% (clamping stress of 278 psi and 1245 psi). They used the same specimen design used in previous research programs in order to obtain comparable test results. The specimens with cold-joint interfaces were not intentionally roughened but all the interfaces except for two interfaces had 0.25" amplitude roughness.

Kahn and Mitchell concluded that the design approach from ACI 318-99 code provisions were applicable to high strength concretes (up to $f'_c = 18,000$ psi). However, they proposed a revised design equations for cold-joints and uncracked interfaces that take advantage of high strength concrete:

$$v_u = 0.05f'_c + 1.4 \rho f_y \leq 0.2f'_c \text{ (psi)}$$

They recommended to keep the yield strength of transverse reinforcement limited to 60 ksi. This would limit the slip along smooth cracks in high strength concrete and would keep uniform friction coefficients for high and normal strength concretes. They suggested to remove the 800 psi limit from the ACI code provisions but to keep the $0.2f'_c$ limit. The authors suggested that the shear friction coefficient should be 1.4 regardless of the interface type (monolithic and CJ-R) for all concrete strengths. This was because the model proposed resulted in conservative estimate when used with $\mu=1.4$ and f_y limited to 60 ksi. Also, they pointed out that the strength of two specimens with CJ-S interfaces was conservatively predicted by their model.

Tanner (2008):

Tanner examined the effective shear friction formulas used in the PCI Design Handbook (4th, 5th and 6th ed.) and the original formulas developed by Shaikh (1978) and Raths (1977). Test data were compared with these equations and mathematical clarifications and modifications were proposed regarding the use of effective shear friction. He pointed out several issues that may result in inconsistent design:

1. Interchanging use of V_u (demand) and V_n (capacity). As the strength reduction factor Φ for shear is reduced from 0.85 to 0.75 in different editions of the PCI Design Handbook, the calculated μ_e values corresponding to different V_n values differ between different versions of the code provisions.
2. μ_e should be equal to μ when $V_n = V_{n,max}$.
3. It is unclear whether μ_e should be a function of the concrete strength reduction factor, λ , or of λ^2 .

To eliminate the issues identified, he proposed to use the following modifications to the PCI Design Handbook (6th ed.) design provisions:

$$\mu_e = \frac{\mu V_{n,max}}{V_n} = \frac{\mu \Phi V_{n,max}}{V_u}$$

Table 2.1.1.2: Proposed modifications to the 6th edition of PCI Design Handbook (Tanner, 2008)

Interface	μ	Maximum μ_e	$V_{n,max}$
Monolithic	1.4λ	3.4λ	$0.30\lambda f'_c A_{cr} \leq 1,000\lambda A_{cr}$
Cold-joint (roughened)	1.0λ	2.9λ	$0.25\lambda f'_c A_{cr} \leq 1,000\lambda A_{cr}$
Cold-joint (roughened)	0.6λ	2.2λ	$0.20\lambda f'_c A_{cr} \leq 800\lambda A_{cr}$
Concrete to steel	0.7λ	2.4λ	$0.20\lambda f'_c A_{cr} \leq 800\lambda A_{cr}$

Where:

A_{cr} =area of shear-crack interface, $V_{n,max}$ =maximum nominal shear capacity.

λ =concrete strength reduction factor (NW: 1.0, SLW: 0.85, ALW: 0.75).

The $V_{n,max}$ values shown in Table 2.1.1.2 were adopted in the 7th edition of the PCI Design Handbook. The upper limits on μ_e for Monolithic and CJ-R interfaces were adopted without the λ factors. However, the effective shear friction approach was no longer allowed for CJ-S and concrete to steel interfaces in the 7th edition of the PCI manual.

Harries, Zeno, and Shahrooz (2012):

Cold-joint specimens with varying amount of transverse reinforcement were tested. Companion specimens with ASTM A615/A615M ($f_y=60$ ksi) and ASTM1035/1035M ($f_y=100$ ksi) grade reinforcements were built and tested to examine the effects of high strength steel in shear transfer strength. The reinforcing bar sizes were #3 and #4 and the compressive strength of the concretes were 5,800 psi and 7,120 psi on the test day. They noted that assuming that the shear reinforcements will yield at ultimate condition may be misleading as their measured stress in the reinforcement was only 17 ksi. Thus, they concluded that the reinforcement ratio affects the shear transfer capacity, while the steel grade does not. They developed and proposed a model:

$$V_n = \alpha A_{cv} f'_c + 0.002 A_{vf} E_s \leq 0.20 A_{cv} f'_c$$

$$\alpha=0.075, 0.040, \text{ and } 0 \text{ for (MO-U, CJ, MO-P respectively)}$$

They used the same upper limit ($0.2f'_c$) as the ACI 318-08 code provisions as this was consistent with their test results. The authors stated that the peak steel and concrete capacity components do not occur simultaneously. Hence, the second term in their model comes into play after the shear interface undergoes some opening.

Shaw and Sneed (2014):

To examine the applicability of the shear friction concept to lightweight concretes, 36 specimens made of normal weight, sanded lightweight, and all lightweight concrete were tested. All tests were cold-joint

specimens with either intentionally roughened to at least 0.25" amplitude roughness or not intentionally roughened (smooth). They concluded the following based on their test results:

1. Specimens with the same amount of reinforcement, compressive strength and interface preparation have similar shear transfer strengths regardless of their concrete unit weight.
2. The shear strength increases with the compressive strength of the concrete.
3. The shear friction provisions of ACI 318-11 and PCI Design Handbook were conservative for all lightweight and sanded lightweight concrete. This held true even when the concrete modification factor, λ , was taken as 1.0. They concluded that there is no shear transfer strength reduction for cold-joint interfaces associated with lower concrete unit weight as long as the other parameters stay the same.

Barbosa, Trejo, and Nielson (2017):

To examine the effects of high strength steel and size of reinforcing bars, a total of 20 push-off tests with Grade 420 (60 ksi) and Grade 550 (80 ksi), #4 and #5 bars were conducted. All specimens were designed to have similar shear strengths when used AASHTO (2015) code provisions. They concluded the following based on their test results:

1. Increasing f_y resulted in higher shear strength when #5 bars were used but the increase appeared negligible when #4 bars were used.
2. AASHTO code provisions can be revised to allow for use of f_y up to 80 ksi despite the inconsistency observed for the different rebar sizes. However, additional research is recommended.
3. The post peak sustained shear loads were consistently higher for Grade 550 (80 ksi) than they were for tests with Grade 420 (60 ksi) steel.

2.1.2 Steel to concrete interfaces:

Viest (1956):

12 solid-slab pushout tests on specimens with 1/2", 5/8", 1" and 1-1/4" diameter studs were conducted (See Figure 2.1.2.1). All specimens were loaded monotonically until failure. The concrete slabs were made of Type I cement, sand and gravel. The maximum size of gravel was 1". The average concrete compressive strength varied between 3,260 and 4,390 psi among specimens. The ultimate strength of the shear studs was between 63.3 and 73.6 ksi.

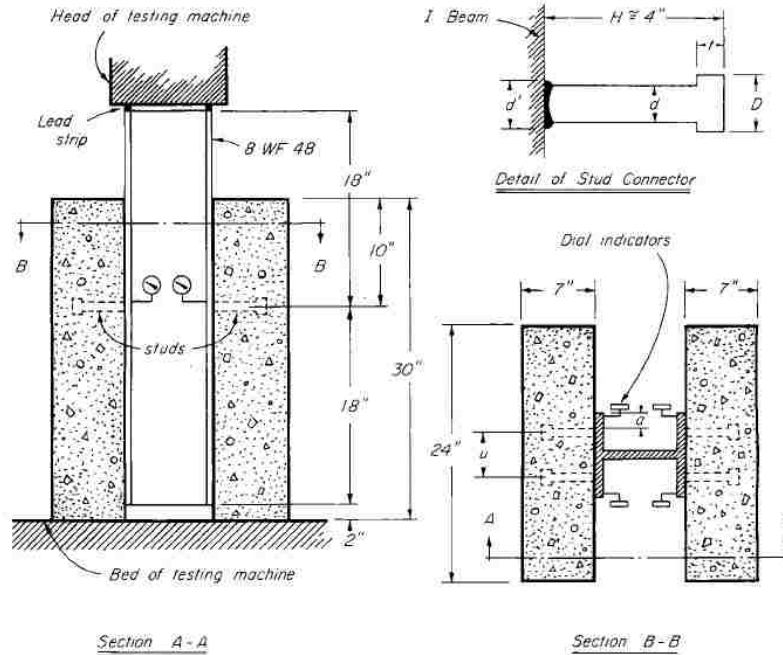


Figure 2.1.2.1: typical solid-slab push-out test set up (Viest, 1956)

The main conclusions of this study were:

1. Load capacities at constant slips differ between specimens with different concrete compressive strengths. Higher concrete compressive strength increases the shear capacity somewhat proportionally to $\sqrt{f'_c}$.
2. Transverse spacing between shear studs has no significant effect on the shear strength.
3. Viest defined the loads where shear slips transition from "small slips" to "big slips" (slip at yielding or 0.003") as "critical loads". The critical shear capacity of the studs increases with the stud diameter (See Figure 2.1.2.2). The critical load is proportional to d^2 for $d < 1$ " and proportional to d when $d \geq 1$ ". It was also noted that the critical loads for small diameter studs are governed by yielding while bigger studs are limited by arbitrary chosen slip limit of 0.003".

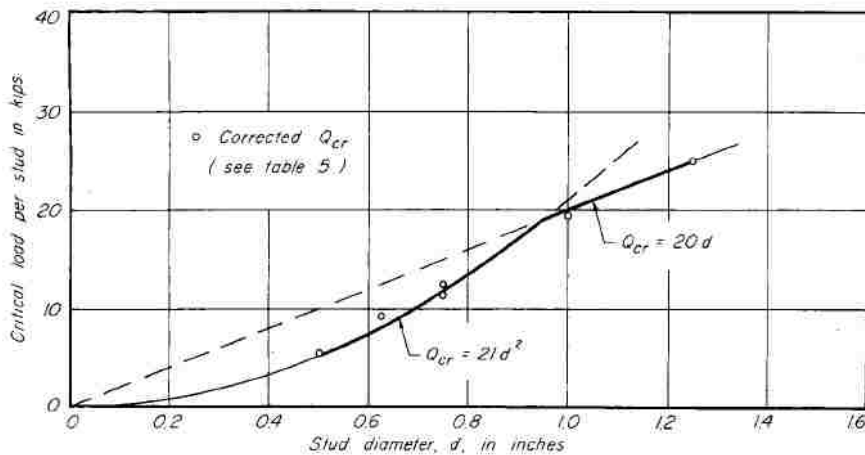


Figure 2.1.2.2: Effect of stud diameter (Viest, 1956)

Viest proposed equations for critical loads:

$$\text{For } d < 1": \quad Q_{cr} = 5.25d^2 f'_c \sqrt{\frac{4000}{f'_c}}$$

$$\text{For } d \geq 1": \quad Q_{cr} = 5df'_c \sqrt{\frac{4000}{f'_c}}$$

Where:

Q_{cr} = critical load (lbs.)

d = stud diameter (in.)

f'_c = concrete strength (psi)

Chinn (1965):

10 push-out tests similar to Viest (1956) tests were conducted. Chinn used 1/2", 5/8", 3/4", and 7/8" diameter studs and normal and lightweight concrete. The length of the studs was chosen to be approximately 4 times their diameters. The flanges of the I-beams were greased to minimize shear friction effects. Chinn introduced the "useful capacity" and notated this term as Q_{uc} . This capacity can be found at the intersection of lower and upper linear portions of load vs. slip curves of the tests. Chinn formulated the useful capacity as follows:

$$Q_{uc} = 6.5d^2 f'_c \sqrt{\frac{4,000}{f'_c}}$$

All specimens failed through stud shearing except for a test with 7/8" diameter studs which failed because of slab cracking. He formulated the ultimate strength as follows:

$$Q_u = 39.22d^{1.766} \text{ (kips)}$$

He found that the ultimate shear strengths were up to 43% higher than the direct shear strengths of the studs. This means that some of the forces were carried by friction and possibly the weld roots. He conducted 2 beam tests to confirm his push-out test results.

Davies (1967):

A total of 20 half-scale solid slab push-out tests were completed. The specimens had different number, spacing and geometrical pattern of shear studs. All studs were 2" long, 3/8" diameter studs. The steel beam flanges to which the studs were welded were greased to minimize shear friction. The author found that the specimens with two studs had about 25% more strength when the studs were placed in a row perpendicular to the load rather than parallel to the load. The author concluded that the ultimate strength varies linearly with longitudinal spacing. Also, when there were three studs in a row, the ultimate strength was more sensitive to spacing compared to the specimens with 2 studs.

Goble (1968):

The purpose of this study was to investigate the failure mode shift from thin flange pull-out failure to failure in the studs.

A total of 41 specimens was constructed with 1/2", 5/8", and 3/4" diameter studs welded to the steel flanges with thicknesses varying between 0.128" and 0.442". The concrete strength also varied from specimen to specimen. The author observed that the flange pull-out failure occurred when the ratio between the stud diameter and the flange thickness was greater than 2.7. He noted that the strength of the stud does not reduce at the failure mode shift. He proposed stud strength equations:

- For stud shear mode failure:

$$q_u = C d_s^2 \sqrt{f'_c}$$

$$C = 882$$

d_s = diameter of shear connector (in.)

f'_c = compressive concrete strength (psi.)

q_u = ultimate strength of stud shear connector (kips)

This equation is similar to the equation proposed by Slutter and Driscoll (1965) (where $C = 930$). However, the model by Slutter and Driscoll (1965) was for $f'_c \leq 4,000$ psi while Goble's specimens were stronger than 4,000 psi.

- Flange pull-out failure mode:

$$q_u = 4.70 t_f d_s^2 f_u$$

f_u = flange ultimate strength (ksi)

Ollgaard, Slutter, and Fisher (1971):

A total of 48 solid slab push-out tests with 5/8" and 3/4" diameter studs were conducted. The number and diameter of studs, concrete compressive and split tensile strengths, modulus of elasticity, aggregate type and unit weight of concrete were the variables considered in this study. Two types of NW concrete (crushed limestone and natural river gravel) and three types of lightweight concrete (rounded expanded shale, cubical to irregular expanded shale, and expanded slate) were used. Stud shearing, concrete failure, and mixed failures were observed.

The authors observed the following:

1. For concrete failures, cracks in lightweight concrete were larger than in normal weight concrete.
2. Lightweight concrete crushes below the studs causing the studs to stay straight under loading.
3. Specimens with one row of studs always failed in stud shearing.
4. Specimens with one and two rows of studs have the same strengths per stud.

5. The strength of lightweight specimens was typically 15-25% lower than that of normal weight specimens.
6. The studs rotated significantly near the welds in both types of concrete specimens.
7. Inelastic deformations in both types of concrete were considerable.
8. Shear strength per stud was nearly proportional to the cross section area of the studs.
9. Between 3.5 ksi and 5 ksi concrete compressive strengths, there was no apparent correlation between compressive strength and shear strength. However, when the compressive strength decreases noticeably, the shear strengths of the studs decrease noticeably as well.
10. Concrete compressive strength and modulus of elasticity affect the shear capacity more than the split tensile strengths and the density of concrete.
11. Ultimate conditions usually are controlled by the concrete capacity rather than by the studs. However, for smaller studs, the shear strength would be more dependent on the tensile strength of the studs.

The authors discussed that the model by Slutter and Driscoll (1965) is not applicable to lightweight concrete and showed that the model is not conservative using their test data. The authors produced a model that better fits the data:

- Shear strength of studs embedded in normal and lightweight concrete solid slab. [kips]

$$Q_u = 1.106A_s f_c'^{0.3} E_c^{0.44}$$

- Simplified equation for design purposes:

$$Q_u = 0.5A_{sa} \sqrt{f_c' E_c}$$

(The effect of concrete weight is included in E_c term).

- Load-slip relationship for continuous loading:

$$Q = Q_u (1 - e^{-18s})^{2/5}$$

$Q = \text{load (kips)}, s = \text{slip in inches}.$

An upper limit is set when $\sqrt{f_c' E_c}$ reaches 130 which corresponds to $Q_u/A_s = 65\text{ksi}$. The authors believe that this upper limit is related to the tensile strength of the connectors.

Hawkins (1973):

A total of 47 push-out tests were conducted to study the effects of mechanical properties of the studs, concrete compressive strength, inclusions of reinforcement in the slabs, use of lightweight concrete, diameter of the studs, and height to stud diameter ratio. The failure types were cracking of the slabs, shearing of the studs, punch-out, and pull-out.

Based on his test results, the author's main observations were:

1. The stud steel material has no effect until significant inelastic deformation occurs, at shear stress beyond 17 ksi.
2. The ultimate slip increases as the concrete compressive strength or the height of the stud increases. However, the ultimate slip decreases as the stud diameter or the yielding strength of the stud increases.
3. Reinforcement in slabs increases the range of shear stress-slip curve. With proper reinforcement, it is possible to produce either shearing, pull-out or punch-out failure of the studs.
4. The shear transfer strength is inversely proportional to the stud diameter.
5. The ultimate strength increases with ultimate slip. For pull-out failures, the ultimate slips are small. To avoid pull-out failures, the height to diameter ratios of the studs should be greater than 4.0.
6. The parameter with the biggest impact on the shear strength is the concrete compressive strength; the shear strength is proportional to $\sqrt{f'_c}$.
7. At smaller slips, the stud material does not noticeably impact the shear capacity but at higher slips, the shear capacity is proportional to the tensile strength of the studs. The yielding strength has no significant impact as the strength is controlled by the ultimate tensile strength of the studs.

The author proposed the following model for prediction of load-slip relationship:

$$v_s = 2.86Kf_u \left[\frac{f'_c}{d_s} \right]^{1/2} \ln(240s + 1) * 10^{-3}$$

$v_s = \text{shear stress in psi, } s = \text{slip in inches.}$

$K = 1.0 \text{ or } 0.85$ (for normal weight and lightweight concrete respectively)

It was also noted that the assumption of the stud behaving like a dowel on an elastic foundation works for lower loads. For higher loads, the above equation should be used.

Jayas and Hosain (1988):

The authors performed 18 full-size push-out and 4 pull-out tests. Five of the tests were performed on solid slabs. For the solid slab tests, the failure modes were shearing of studs, crushing of concrete near the studs and longitudinal shearing of the concrete slab. Depending on stud spacing, the failure mode shifted. When the studs in the solid slabs were spaced more than 6 times the stud diameter, the studs sheared off. However, when the studs were spaced closer, the failure occurred in the concrete. The shear strengths of the specimens with the studs spaced closer were about 7% lower than that of specimens with farther spaced studs. Due to this observation, the authors recommended to reduce the expected stud strength when longitudinal spacing is less than 6 times the stud diameter.

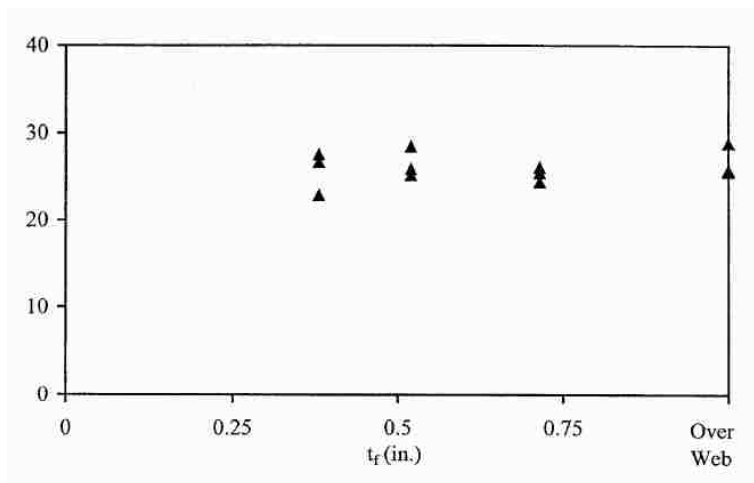
Lyons (1994):

In this work, Lyons conducted push-out tests on 48 solid slabs and 87 ribbed slabs with steel decks. All solid slab tests except for two failed in stud shearing. The other two specimens failed in concrete pull-out mode. Lyons concluded the following for solid slabs:

1. The cold-working process of increasing the tensile strength of the studs decreases their ductility which adversely affects their performance. The author believes that this is due to the high strength stud's inability to redistribute stress under loading. High strength studs ($F_u=84$ ksi) fail at lower slips than standard studs ($F_u=67$ ksi).
2. Lower unit weight and low strength concretes allow for greater deformation in the studs. This causes tensile force in the studs which reduces the shear capacity of the studs.
3. A significant portion of the shear strength comes from shear friction. Shear friction capacity allows for the steel to concrete interface to have higher shear capacity than the ultimate shear capacity of the studs.
4. The upper limit ($A_s F_u$) in ASIC (Load 1993) is unconservative. A more appropriate upper limit would be $0.8A_s F_u$. This upper limit does not represent the failure shift between concrete and stud failures.

Roddenberry (2002):

Roddenberry conducted 24 solid-slab tests and 93 composite slab tests, and bare stud tests. Her objective was to study the effects of friction, normal load, and stud distribution within ribs of the composite slabs, concrete strength, and stud properties on shear strength. Stud diameters ranged between 3/8" and 7/8". 12 of the solid slab tests were conducted to investigate flange thickness to which the studs were welded. The thickness of the flange varied from 0.38" to 0.715". The stud diameter over flange thickness ratio was kept smaller than 2.7 as it was the suggested maximum value in Goble (1968) work. She found out that the flange thickness does not cause significant difference in the shear strength as long as the ratio was kept smaller than 2.7 (See Figure 2.1.2.3).



2.1.2.3: Stud strength vs. flange thickness (Roddenberry, 2002)

Also, she noted that the strengths measured were underestimated by the equations proposed by Ollgaard (1971).

6 tests had modified interface. A flat metal sheet was placed in between the steel beam and concrete slabs. Roddenberry noticed that having a sheet metal between the concrete slab and the steel beam significantly reduces the strength of shear studs as the sheet metal reduces the interface shear friction. The stud strength was about 85% of the strength of the studs in specimens without sheet metal.

The remaining 6 tests had varying applied normal load. The author observed that having compressive normal load increases shear friction hence the shear strength. The AISC equations give adequate predictions of the strengths of studs in solid slabs when normal load is applied. When there is no normal load applied, the stud strengths are less than 90% of the AISC predictions.

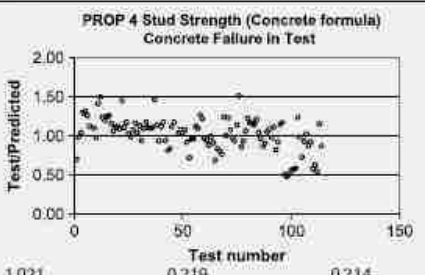
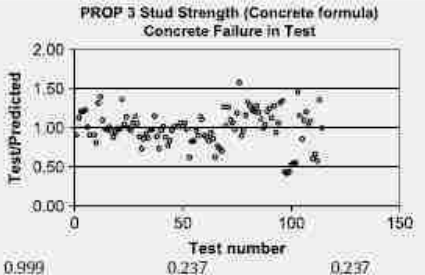
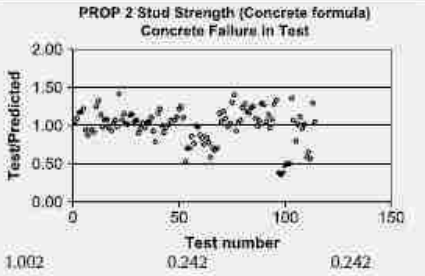
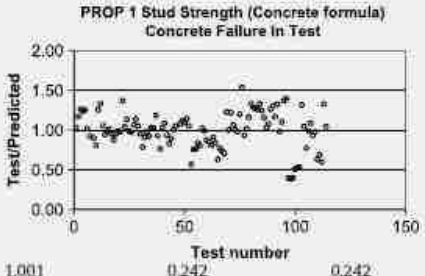
Pallares and Hajjar (2010):

The authors reviewed a total of 391 monotonic and cyclic solid slab tests using experiments of headed stud anchors. The authors proposed equations for limit states of concrete and steel failures and also discussed premature pryout failure. The authors recommend shear strength values for the seismic behavior of stud connectors. This paper reviews and compares available shear models and applicable code provisions including AISC (2005), ACI 318-05, PCI Design Handbook (6th ed.), and Eurocode 4.

The authors grouped the test results by their failure types and evaluated the accuracy of strength upper limits of code provisions for steel and concrete failures. The main conclusions drawn were:

1. The most common concrete failure in composite construction is pryout failure rather than break-out failure. This is due to limited front-to-edge and side-to-edge distances in composite constructions.
2. AISC formula's limit state for steel failure ($A_s F_u$) is accurate for steel failures if a resistance factor of 0.65 is applied. This 0.65 factor results in reliability index of 4.
3. EC-4 (2004) provides conservative results in most cases of both steel and concrete failures with its resistance factors applied.
4. PCI 6th ed. and ACI 318-05 are more accurate than AISC (2005) when the failure mode is concrete failure.
5. Alternative choices of concrete failure formula are proposed to AISC (2005) (See Figure 2.1.2.4).
6. Based on the available data, $h_{ef}/d > 6.5$ (here: h_{ef} is the shank length) or $h/d > 7$ (here: h is the total height of the stud) ensure steel failure. This ratio should be checked in future research.
7. A reduction factor of 0.75 is suitable for seismically loaded stud strengths if the monotonic strength is determined by including the resistance factor proposed in this work.

	Formula for $Q_{cr,c}^a$	μ	σ	C.O.V.	ϕ	
					$\beta = 3$	$\beta = 4$
AISC 2005	$0.5A_s\sqrt{f_c'}E_c$	0.827	0.250	0.302	0.49	0.41
EC-4	$C_s 0.5\sqrt{f_c'E_{cm}}$	0.965	0.249	0.258	0.61	0.52
Proposal 1	$17.00DA_s (f_c')^{0.452} (E_c)^{0.041}$					
		1.001	0.242	0.242	0.65	0.56
	$17A_s (f_c')^{0.45} (E_c)^{0.04}$	1.013	0.245	0.242	0.66	0.57
Proposal 2	$6.214A_s (f_c')^{0.209}$					
		1.002	0.242	0.242	0.65	0.56
	$6.2A_s (f_c'E_c)^{0.2}$	1.098	0.265	0.242	0.71	0.62
Proposal 3	$18.197A_s (f_c')^{0.479} (h)^{0.215}$					
		0.999	0.237	0.237	0.65	0.57
	$18A_s (f_c')^{0.5} (h)^{0.2}$	0.997	0.237	0.237	0.65	0.57
Proposal 4	$8.915\lambda (f_c')^{0.476} (d)^{1.373} (h)^{0.564}$					
		1.021	0.219	0.214	0.69	0.61
	$9\lambda (f_c')^{0.5} (d)^{1.4} (h)^{0.6}$	0.955	0.206	0.216	0.64	0.56



^a Optimized formula/Simplified formula. Units: kips, inches.

Figure 2.1.2.4: Evaluation of concrete formulas of AISC (2005), EC4, and proposed models (Pallares and Hajjar, 2010)

2.2 Miscellaneous models

Common notations:

v_{cr} is shear stress across the crack interface.

v_n is the ultimate shear strength.

σ_{cr} is the normal stress across the crack plane (not necessarily the normal stress at ultimate condition).
 s-slip
 w-crack width
 c-cohesion
 f_{cu} -concrete cube strength

Strength-only models for concrete-to-concrete behavior:

- **Loov (1978):**

Loov was the first author to include the compressive strength of concrete in the shear strength of concrete interface equation. The empirical equation proposed was:

$$v_n = k \sqrt{\rho f_y f'_c} \text{ psi}$$

$k = 0.5$ for initially uncracked monolithic concrete

- **Walraven (1987)**

An empirical model proposed by Walraven based on his statistical analysis of data:

$$v_n = C_3 (0.007 \rho f_y)^{C_4} \text{ psi}$$

$$C_3 = 16.8 f'_c{}^{0.406} \text{ and } C_4 = 0.0371 f'_c{}^{0.303}$$

- **Kono & Tanaka (2000):**

(Metric units)

$$v_n = k * (0.67 * \rho f_y + 2.84)$$

Where $k = 0.02 * f'_c + 0.2$ (for $f'_c \leq 40 \text{ Mpa}$)

otherwise $k = 1.0$

Not applicable to: plain surface and $\rho f_y \geq 7.6 \text{ MPa}$

- **Mansur & Vinayagam (2008):**

(Metric units)

(Applicable to only MO-P interfaces.) This is a 3-linear-branch method.

-1st branch (If $\rho f_y / f'_c \leq 0.075$:)

$$v_n = 2.5 * \rho f_y$$

-2nd branch (If $0.075 \leq \frac{\rho f_y}{f'_c} \leq \frac{0.3 \frac{0.56}{f'_c{}^{0.385}}}{0.55} = 0.545 - \frac{1.018}{f'_c{}^{0.385}}$:)

$$v_n = 0.56 * f_c'^{0.615} + 0.55 * \rho f_y$$

-3rd branch (If $0.545 - \frac{1.018}{f_c'^{0.385}} \leq \frac{\rho f_y}{f_c'}$)

$$v_n = 0.3 * f_c'$$

- **Lin & Chen (1989):**

(Metric units)

$$v_n = \mu_e \rho f_y \leq \left\{ \begin{array}{l} 0.3 * f_c' \\ 12.46 \text{ MPa} \end{array} \right\}$$

$$\mu_e = \left(\frac{1.75 \sqrt{f_c'}}{\rho f_y + \sigma_{ext}} \right)^{0.5}$$

- **Tsoukantas and Tassions (1989):**

(Metric units)

-CJ-S:

$$v_n = 0.4 * \sigma_{cr}$$

-CJ-R:

$$v_n = 0.5 * \sqrt[3]{f_c'^2 * \sigma_{cr}}$$

Comprehensive shear strength vs. slip models for concrete-to-concrete behavior

- **Hamadi and Regan (1980):**

(Metric units)

$$v_{cr} = k \frac{S}{W} = kr$$

k=5.4N/mm² for gravel aggregate

k=2.7N/mm² for expanded clay aggregate

$$V_{cr} \leq V_n = C + \mu \sigma_{cr}$$

Table 2.2.1: Table of coefficients (Hamadi and Regan, 1980)

Surface	C [MPa]	μ
Natural gravel	4.0	0.7
Expanded clay	2.0	0.3

- **Walraven and Reinhardt (1981)**

Linear aggregate interlock relationship:

(Metric units)

$$\sigma_{cr} = -\frac{f_{cu}}{20} + [1.35w^{-0.63} + (0.191w^{-0.552} - 0.15)f_{cu}]s$$

$$v_{cr} = -\frac{f_{cu}}{30} + [1.8w^{-0.80} + (0.234w^{-0.707} - 0.20)f_{cu}]s$$

- **Gambarova and Karakoç (1983):**

(Metric units)

Rough crack model:

$$\sigma_{cr} = k_1 k_2 \sqrt{w} \frac{r}{(1+r^2)^{0.25}} v_{cr}$$

$$v_{cr} = v_0 \left[1 - \left(\frac{2w}{a} \right)^{1/2} \right] r \frac{k_3 + k_4 |r|^3}{1 + k_4 r^4}$$

Where:

$$r = s/w$$

a = maximum aggregate size

$$k_1 k_2 = 0.62, \quad k_3 = 2.45/v_0, \quad k_4 = 2.44(1 - (4/v_0))$$

$$v_0 = 0.25 f'_c$$

- **Li et al., (1989):**

Simplified method based on contact density theory:

(Metric units)

$$\sigma_{cr} = 3.83 f'_c{}^{1/3} \left[\frac{\pi}{2} - \cot^{-1} r - \frac{r}{1+r^2} \right]$$

$$v_{cr} = 3.83 f_c'^{1/3} \frac{r^2}{1 + r^2}$$

- **Vecchio and Collins (1986):**

(Metric units)

-The ultimate shear stress of the crack:

$$v_n = 0.18 * v_{ci \ max} + 1.64 * f_{ci} - 0.82 * \frac{f_{ci}^2}{v_{ci \ max}}$$

Where the maximum shear stress a crack can resist at restrained crack width, w:

$$v_{ci \ max} = \frac{\sqrt{f_c'}}{0.31 + \frac{24w}{a + 16}}$$

Where:

f_{ci} = positive compressive stress due to internal and external loads.

a=the maximum aggregate size

Models for steel-to-concrete interfaces:

- **Buttry (1965):**

$$Q = Q_u(1 - e^{-18s})^{2/5}$$

Where:

Q = load (kips)

s = slip in inches.

- **Newmark *et al.*, (1952):**

In their test program, they used steel channel anchors as shear reinforcement of their push-out specimens. The main assumption in their model was that the channel flange welded to the steel beam is infinitely rigid while the web of the channel is infinitely long and flexible. Also, they assumed that the concrete under the rigid portion of the channel has stiffness K and the concrete under the flexible portion has stiffness K/n.

Simplified equations:

Unit pressure exerted by the stiff portion of the connector to the adjacent concrete:

$$f_{co} = \frac{Q}{Yw}$$

Maximum steel stress in connector:

$$f_{max} = \frac{Q}{k_1 Yw}$$

Deflection of the stiff portion (slip):

$$y_0 = \frac{Q}{k_2 Y}$$

Where:

$$Y = \frac{t}{2} + h \quad k_1 = \frac{1.6}{\frac{f_{co}}{f_c} + 1.8} \quad k_2 = \frac{2.3 \cdot 10^6 \text{ psi } w}{\frac{f_{co}}{f_c} + 0.6} \frac{1}{h}$$

t = thickness of web,

h = thickness of flange,

w = width of channel,

Q = load applied in lb

- **Oehlers and Johnson (1987):**

The mean strength of stud connectors in push-out specimens:

$$P = 5A_s F_u \left(\frac{E_c}{E_s} \right)^{0.4} \left(\frac{f_{cu}}{F_u} \right)^{0.35}$$

f_{cu} = cube strength

2.3 Code Provisions

- **ACI 318-14—Shear Friction:**

f_y is limited to 60 ksi.

Permanent net compression across the shear plane shall be permitted to be added to $A_{vf} f_y$.

λ : normal weight:1, sand-light-weight:0.85, all-light-weight: 0.75

Generally, (reinforcement at 90°, no external normal force applied):

$$V_n = A_{vf} f_y \mu$$

If shear reinforcement is at an angle, α , other than 90°:

$$V_n = A_{vf} f_y (\mu \sin \alpha + \cos \alpha)$$

$$v_n = \rho f_y (\mu \sin \alpha + \cos \alpha)$$

Table 2.3.1: Table of coefficients (ACI 318-14—Shear friction provisions)

Case	Interface type	μ	$V_{n,max} = V_u / \Phi$
1	Concrete to concrete, cast monolithically	1.4 λ	For NW concrete (monolithic or roughened): Least of $\left\{ \begin{array}{l} 0.2f'_c A_c \\ (480 + 0.08f'_c) A_c \end{array} \right\}$ For all other cases: Lesser of $\left\{ \begin{array}{l} 0.2f'_c A_c \\ 800A_c \end{array} \right\}$
2	Concrete to hardened concrete with roughened interface	1.0 λ	
3	Concrete placed against hardened concrete not intentionally roughened	0.6 λ	
4	Concrete anchored to as-rolled structural steel by headed studs or by reinforcing bars	0.7 λ	

- **ACI 318-14—Interface shear transfer:**

When $V_u > \Phi(500b_v d)$: V_{nh} shall be taken as V_n in accordance with the shear-friction provision of ACI.

When $V_u \leq \Phi(500b_v d)$: See table below:

Table 2.3.2: Table of coefficients (ACI 318-14—Interface shear provisions)

Shear transfer reinforcement	Concrete surface preparation	V_{nh} , [lb]
$A_v \geq A_{v,min}$	Concrete placed against hardened concrete intentionally roughened to a full amplitude of approximately 1/4"	Lesser of: $\left\{ \begin{array}{l} \lambda \left(260 + 0.6 \frac{A_v f_y t}{b_v s} \right) b_v d \\ 500b_v d \end{array} \right\}$
	Concrete placed against hardened concrete not intentionally roughened	80 $b_v d$
Other cases	Concrete placed against hardened concrete intentionally roughened	80 $b_v d$

$$A_{v,min} \text{ shall be greater of } \left\{ \begin{array}{l} 0.75\sqrt{f'_c} \frac{b_w s}{f_y} \\ 50 \frac{b_w s}{f_y} \end{array} \right\}$$

- **PCI Design Handbook 7th Edition (2011):**

This provision allows the use of “effective shear friction” for monolithic and intentionally roughened interfaces. The use of the effective shear friction is not applicable to smooth cold-joints and steel to concrete interfaces.

f_y is limited to 60 ksi.

When, axial tension is present, additional reinforcement $A_n = \frac{N_u}{\Phi f_y} = \frac{N_n}{f_y}$

λ : normal weight:1, sand-light-weight:0.85, all-light-weight: 0.75

$\Phi=0.75$

Generally, (reinforcement at 90°, no external normal force applied):

Case 1 and 2:

$$\mu_e = \frac{\Phi 1000 \lambda A_{cr} \mu}{V_u} = \frac{1000 \lambda A_{cr} \mu}{V_n}$$

$$A_{vf} = \frac{V_u}{\Phi f_y \mu_e} = \frac{V_n}{f_y \mu_e}$$

$$v_n = \rho f_y \mu_e = \sqrt{1000 \rho f_y \lambda \mu}$$

Case 3 and 4:

$$A_{vf} = \frac{V_u}{\Phi f_y \mu} = \frac{V_n}{f_y \mu}$$

$$v_n = \rho f_y \mu$$

Table 2.3.3: Table of coefficients (PCI Design Handbook 7th ed.)

Interface	μ	Maximum μ_e	$V_{n,max}$
Monolithic	1.4 λ	3.4	$0.30 \lambda f'_c A_{cr} \leq 1,000 \lambda A_{cr}$
Cold-joint (roughened)	1.0 λ	2.9	$0.25 \lambda f'_c A_{cr} \leq 1,000 \lambda A_{cr}$

Cold-joint (smooth)	0.6λ	N/A	$0.20\lambda f'_c A_{cr} \leq 8000\lambda A_{cr}$
Concrete to steel	0.7λ	N/A	$0.20\lambda f'_c A_{cr} \leq 800\lambda A_{cr}$

- **PCI Design Handbook 6th Edition (2004):**

In this older version of the PCI Design Handbook, the “effective shear” friction approach was allowed for all interface types.

The amount reinforcement normal to the crack interface required by the 6th edition of the PCI Design Handbook:

$$A_{vf} = \frac{V_u}{\Phi f_y \mu}$$

$$\mu_e = \frac{1000\lambda A_{cr} \mu}{V_u}$$

The following table values were used:

Table 2.3.4: Table of coefficients (PCI Design Handbook 6th ed.)

Interface	μ	Maximum μ _e	V _{n,max}
Monolithic	1.4λ	3.4	$0.30\lambda^2 f'_c A_{cr} \leq 1,000\lambda^2 A_{cr}$
Cold-joint (roughened)	1.0λ	2.9	$0.25\lambda^2 f'_c A_{cr} \leq 1,000\lambda^2 A_{cr}$
Cold-joint (roughened)	0.6λ	2.2	$0.20\lambda^2 f'_c A_{cr} \leq 8000\lambda^2 A_{cr}$
Concrete to steel	0.7λ	2.4	$0.20\lambda^2 f'_c A_{cr} \leq 800\lambda^2 A_{cr}$

- **AASHTO LRFD Bridge Design Specifications 7th Edition (2014):**

This provision allows for use of cohesion terms unlike the provisions of ACI and PCI.

f_y is limited to 60 ksi.

$$\rho f_y \geq 0.05 \text{ ksi}$$

$$V_{ri} = \Phi V_{ni} \geq V_{ui}$$

Where resistance factor $\Phi=0.9$ and 0.7 for normal and light weight concrete respectively.

Generally, (when the shear reinforcement is perpendicular to the shear interface):

$$V_{ni} = cA_{cv} + \mu(A_{vf}f_y + P_c) \leq \text{smaller of } K_1f'_cA_{cv} \text{ or } K_2A_{cv}$$

$$v_{ni} = c + \mu(\rho f_y + \sigma_c) \leq \text{smaller of } K_1f'_c \text{ or } K_2$$

If shear reinforcement bars are inclined at angle, α , relative to the shear interface:

$$v_{ni} = c + \mu(\rho f_y \sin \alpha + \sigma_c) + \rho f_y \cos \alpha \leq \text{smaller of } K_1f'_c \text{ or } K_2$$

Table 2.3.5: Table of coefficients (AASHTO LRFD Bridge Design Specifications, 7th ed.)

Concrete type and interface type	c (ksi)	μ	K_1	K_2 (ksi)
Cast-in-place slab on girder(NW concrete, Roughened)	0.28	1.0	0.3	1.8
Cast-in-place slab on girder(LW concrete, Roughened)	0.28	1.0	0.3	1.3
Monolithic (NW concrete)	0.40	1.4	0.25	1.5
Monolithic (LW concrete), Cold-joint (LW, Roughened)	0.24	1.0	0.25	1.0
Cold-joint (NW concrete, Roughened)	0.24	1.0	0.25	1.5
Cold-joint (Smooth)	0.075	0.6	0.2	0.8
Concrete to steel	0.025	0.7	0.2	0.8

Note: All interfaces must be clean and free of laitance; an intentionally roughened cold-joint must be roughened to an amplitude of 0.25”.

- **CSA (2014):**

In this provision, a shear crack is assumed to occur across shear plane and cohesion and shear friction resist the relative displacement.

Factored shear stress resistance, v_r :

General equation:

$$v_r = \lambda \Phi_c (c + \mu \sigma_{tot}) + \Phi_s \rho f_y \cos \alpha$$

$$\lambda (c + \mu \sigma_{tot}) \leq 0.25 f'_c$$

resistance factor for concrete, $\Phi_c = 0.65$

resistance factor for steel, $\Phi_s = 0.85$

Table 2.3.6: Table of coefficients (CSA, 2014)

Case	Interface description	c	μ
a	For concrete placed against hardened concrete with the surface clean but not intentionally roughened	0.25 MPa (36.259 psi)	0.60
b	For concrete placed against hardened concrete with the surface clean and intentionally roughened to a full amplitude of at least 5 mm	0.50 MPa (72.519 psi)	1.00
c	For concrete placed monolithically	1.00 MPa (145.038 psi)	1.40
d	For concrete anchored to as-rolled structural steel by headed studs or by reinforcing bars	0.00 MPa	0.60

For monolithically cast or intentionally roughened (to a full amplitude of 5mm) interfaces the following equation can be used in lieu of the general equation:

$$v_r = \lambda \Phi_c k \sqrt{\sigma_{tot} f'_c} + \Phi_s \rho f_y \cos \alpha$$

$$k = 0.5 \text{ for roughened}$$

$$k = 0.6 \text{ for monolithic}$$

Note: Here $\sigma_{tot} = \rho f_y \sin \alpha + \sigma_c$ (in CSA code, σ_{tot} is notated as σ and σ_c is external normal stress applied).

- **EN 1992-1-1 (2004): Euro code 2: 6.2.5 Shear at the interface between concrete cast at different times.**

(Metric units)

Notations and their equations:

-Strength reduction factor for concrete cracked in shear:

$$v = 0.6 * \left(1 - \frac{f_{ck}}{250}\right)$$

-Characteristic compressive cylinder strength of concrete at 28days:

$$f_{ck} \text{ (in our notation system, } f'_c \text{)}$$

-Design compressive strength

$$f_{cd} = \alpha_{cc} f_{ck} / \gamma_c$$

α_{cc} = unfavorable effects factor on compressive strength (Recommended value=1.0)

γ_c = partial safety factor (Persistent and transient design situation=1.5, accidental design situation=1.2)

-Design value of concrete tensile strength:

$$f_{ctd} = \alpha_{ct} f_{ctk,0.05} / \gamma_c$$

α_{ct} = unfavorable effects factor on tensile strength (Recommended value=1.0)

$$f_{ck} = 50 \text{ for C50/60}$$

Table 2.3.7: Conversion between compressive strengths (EN 1992-1-1)

$f_{cm} = f_{ck} + 8 \text{ (MPa)}$
$f_{ctm} = 0.3 * f_{ck}^{(2/3)} \leq C50/60$
$f_{ctm} = 2.12 * \ln \left(1 + \left(\frac{f_{cm}}{10} \right) \right) > C50/60$
$f_{ctk;0.05} = 0.7 * f_{ctm}$ 5% fractile

Design shear resistance at the interface cast at different times:

$$v_{rdi} = c f_{ctd} + \mu \sigma_n + \rho f_{yd} (\mu \sin \alpha + \cos \alpha) \leq 0.5 v f_{cd}$$

external compressive stress, $\sigma_n \leq 0.6 f_{cd}$

if σ_n is tension, its magnitude is negative and $c f_{ctd}$ term goes to zero.

$$45^\circ \leq \alpha \leq 90^\circ$$

Table 2.3.8: Table of coefficients (EN 1992-1-1)

Case	Interface description	c	μ
------	-----------------------	---	-------

Very smooth	Cast against steel, plastic or specially prepared wooden molds.	0.025	0.5
smooth	A slip formed or extruded surface, or a free left without further treatment after vibration	0.20	0.6
rough	A surface with at least 3mm roughness at about 40mm spacing, achieved by raking, exposing of aggregate or other methods	0.40	0.7
indented	A surface indentations complying with the figure below	0.50	0.9

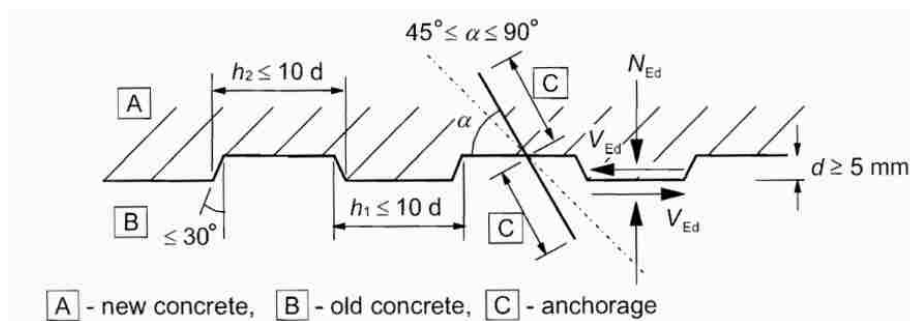


Figure 2.3.1: Roughness definition (EN 1992-1-1)

- **MC90 (CEB-FIP, 1990) equations for aggregate interlock:**

(Metric units)

For $s < 0.1\text{mm}$:

$$v_{cr} = 5v_n s$$

v_{cr} is shear stress across the crack interface.

v_n is the ultimate shear strength.

For $s \geq 0.1\text{mm}$:

$$\left[\frac{v_{cr}}{v_n} \right]^4 - 0.5 \left[\frac{v_{cr}}{v_n} \right]^3 = 0.3s - 0.03$$

For rough interface:

$$v_n = 0.4f_c'^{2/3}\sigma_{cr}^{1/3}$$

For smooth interface:

$$v_n = 0.4f_c'^{2/3}\sigma_{external}^{1/3}$$

σ_{cr} is the normal stress across the crack plane.

Crack dilatancy: $w=0.6s^{2/3}$

- **AISC 14th ed. (2011):**

The entire horizontal shear at the interface between steel beam and concrete slab shall be assumed to be transferred by steel-headed stud or steel channel anchors. Other code provisions for shear strength of stud connectors have the same assumptions and the general form of the model as AISC provisions.

Strength of steel headed stud anchors:

The nominal shear strength of one steel-headed stud anchor embedded in a solid concrete slab or a slab with decking shall be determined as:

$$Q_n = 0.5A_{sa}\sqrt{f_c'E_c} \leq R_gR_pA_{sa}F_u$$

where:

A_{sa} = cross sectional area of stud

E_c = modulus of elasticity of concrete

F_u = specified minimum tensile strength of steel stud

$R_g = 1.0, R_p=0.75$ when no decking is present (solid slab)

Strength of steel channel anchors:

The nominal shear strength of one hot rolled channel anchor embedded in solid concrete slab shall be determined as:

$$Q_n = 0.3(t_f + 0.5t_w)l_a\sqrt{f_c'E_c}$$

Where:

l_a = length of channel anchor

t_f = thickness of flange of channel anchor

t_w = thickness of channel anchor web

Detailing requirements:

Stud spacing in the direction parallel to the shear force to be distributed: min of $4 d_s$

Stud spacing in the direction transverse to the shear force to be distributed: min of $6 d_s$

Max center to center spacing: $8 t_{slab}$

Besides requirements on spacing limitations, AISC specifies the max diameter of the shear stud to be 2.5 times the thickness of the flange.

- **CSA Steel Design Handbook (2010):**

In solid slabs with shear connectors:

$$Q_n = 0.5\Phi_{sc}A_{sc}\sqrt{f'_c E_c} \leq \Phi_{sc}A_{sc}F_u$$

A_{sc} = cross sectional area of stud

$F_u = 450\text{MPa} = 65.27\text{ksi}$ for commonly available studs (CSA W59 Type B studs)

$\Phi_{sc} = 0.8$ resistance factor

Detailing requirements:

$$d_s \leq 2.5t_f$$

Studs shall be headed or hooked with $h_s/d_s \geq 4$

- **EN (Eurocode 4, 1994):**

(Metric units)

Shear resistance of headed stud is determined as:

$$P_{rd} = 0.29\alpha d_s^2 \sqrt{f_{ck} E_c} \frac{1}{\gamma_v} \leq 0.8F_u \left(\frac{\pi d_s^2}{4} \right) \frac{1}{\gamma_v}$$

With:

Partial safety factor: $\gamma_v = 1.25$

$$\alpha = 0.2 \left(\frac{h_s}{d_s} + 1 \right) \text{ for } 3 \leq h_s/d_s \leq 4$$

$$\alpha = 1 \text{ for } \frac{h_s}{d_s} > 4$$

Limitations:

$$F_u \leq 500\text{MPa}$$

$$16\text{mm} \leq d_s \leq 25\text{mm}$$

- **AASHTO LRFD (2014):**

Shear strength of one stud shear connector embedded in a concrete bridge:

$$Q_n = 0.5A_{sc}\sqrt{f'_c E_c} \leq A_{sc}F_u$$

- **JSCE Guidelines (2007):**
(Metric units)

Stud strength is smaller of:

$$V_{stud} = \frac{31A_{ss}\sqrt{(h_{ss}/d_{ss}) f'_{cd}} + 10000}{\gamma_b}$$

$$V_{stud} = A_{ss}f_{stud}/\gamma_b$$

$$f'_{cd} = f'_c/\gamma_c$$

With:

$$\text{Member factor, } \gamma_b = 1.3$$

$$\text{Material factor for concrete, } \gamma_c = 1.3$$

Limitations:

$$13\text{mm} \leq d_{ss} \leq 32\text{mm}$$

$$400 \leq f_{stud} \leq 550\text{MPa}$$

$$14 \leq f'_c \leq 63\text{Mpa}$$

- **Ministry of Construction of China 2003:**
(Metric units)

$$Q_n = 0.43A_{sc}\sqrt{f_{cu} E_c} \leq 0.7A_{sc}F_u$$

- **GB50017-2003:**
(Metric units)

Design stud shear capacity:

$$N_v = 0.43A_s\sqrt{f'_c E_c} \leq 0.7A_{sc}F_u \gamma$$

$$\gamma = F_u/f_y$$

3. Database

3.1 Introduction

Substantial amount of studies have been conducted in the past as discussed in Chapter 2. In most instances, those works have been conducted independently of each other resulting in significantly different results. Code Provisions and models proposed in the past rely on a limited number of data (often using data from different test programs). To clear up the inconsistencies among the models, comprehensive database have been built for statistical analysis that will be described in Chapter 4 and 5.

Test results from previous works referenced in the applicable ACI, PCI, AASHTO and AISC code provisions and their reference papers as well as other recent research works were collected in the database. Data for steel to concrete and concrete to concrete interfaces were collected separately in the database. To best study shear transfer strength, only the test results of specimens that failed in shear or mainly in “shear mode” were selectively collected. Tests failed due to excessive cracks, spalling-out, splitting of slabs and prying-out in the concrete components, and poor anchorage of the shear reinforcement were not collected.

3.2 Concrete to Concrete Interface Data

Past test programs for concrete to concrete interfaces had different test configurations. The major types of tests include push off tests with axial loads normal (or at an angle) to the shear interface, inclined shear reinforcement crossing the interface, load applied eccentrically or loaded cyclically (See Table 3.2.1.1). To effectively address the most fundamental shear transfer, data from monotonically loaded classic push-off tests with no external axial force or moment with perpendicular shear reinforcement were mainly collected. (Some data from tests with other configurations were also collected but were not the focus of this study).

A total of 522 monotonically loaded (vertical or horizontal) pull/push-off and beam tests data make up the concrete to concrete interface database (including both classic and modified tests) (Appendix A) The parameters previously studied and believed to have potential impacts on the shear transfer strength of concrete interfaces include (but are not limited to):

- Concrete types (NW: normal weight, SLW: Sand lightweight, ALW: All lightweight)
- Compressive strength of concrete (f'_c)
- Interface types (MO-U: monolithic uncracked, MO-P: monolithic pre-cracked, CJ-R: roughened cold joint, CJ-S: smooth cold joint)
- Reinforcement details: diameter, angle relative to the interface, reinforcement ratio (ρ), yield strength (f_y), and average clamping stress (ρf_y).
- Externally applied loads.

These were the parameters reported by the majority of the previous experimental research programs, hence were collected in the database. No upper or lower limit on any parameter was set as a criteria for selecting data to collect. Data from tests which met this research program’s data selection criteria (based on failure modes and general test set up) were all collected.

Besides the above mentioned parameters, some scholars reported the following information:

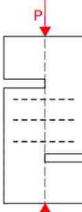
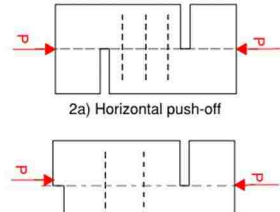
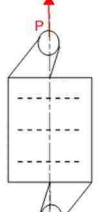
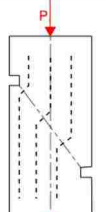
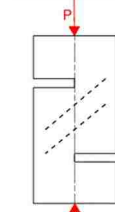
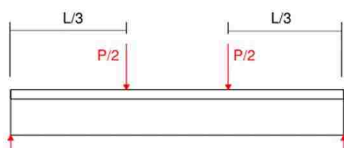
- Specimen properties (initial crack width, deformity of reinforcing bars, and maximum aggregate sizes)
- Test outputs (crack width and slip at ultimate load, strains in steel, load, slip and crack width at test termination if no loaded until ultimate load)

These values were collected in the database when reported or scalable plots for these parameters were provided.

3.2.1 Schematics of the database

The majority of the test programs for concrete-to-concrete interfaces had the configurations shown in Table 3.2.1.1.

Table 3.2.1.1: Test configurations (concrete-to-concrete interfaces)

Types of Configurations:					
Type 1	Type 2 a, b	Type 3	Type 4	Type 5	Type 6
 <p>1) Vertical push-off</p>	 <p>2a) Horizontal push-off 2b) Special horizontal push-off</p>	 <p>3) Pull-off</p>	 <p>4) Modified push-off</p>	 <p>5) Push-off with angled reinforcement</p>	 <p>6) Beam test</p>

The parameters were organized into three categories:

1. Parameters found in the study to be important
2. Other information provided by almost all researchers
3. Information provided by only a few researchers

The information pertaining to the first two categories is shown in Table 3.2.1.2. This research program concluded that the most critically influencing parameters were clamping stress, concrete compressive strength, and concrete and interface types (detailed discussion in Chapter 4.2). Reinforcement bar size and aggregate size were parameters of interest in other studies, but they have not received as much experimental attention as the previously mentioned parameters. Table 3.2.1.2 also indicates whether the work was referenced in any design code provisions.

Table 3.2.1.2: Summary of database (concrete-to-concrete interfaces)

Authors	Year	Codes based on the work?	Test set up and (# of tests, if multiple types)	extra comment (if applicable)	# Applicable tests in total	Interface	Concrete	Range of f_c' [ksi]	D_{agg} [in]	Range of f_y [ksi]	Range of p_{fy} [psi]	d_s [in]
Hanson	1960	yes	2b	small offset between load and interface	38	CJ-R, CJ-S	NW:38 LW:0	3.24-4.22	0.75	47-52	0-409.1	0.5
Hofbeck et al.	1969	yes	1		31	MO-U, MO-P	NW:31 LW:0	2.39-4.51	0.875	42.4-66.1	192-1454.2	0.375
Mattock and Hawkins	1972	yes	3 (6 tests) and 4 (12 tests)	modified push-offs: shear reinforcement is at 90° angle but load is applied at an angle to the interface	18	MO-U, MO-P	NW:18 LW:0	3.94-6.44	unreported	49.5-53.7	312-985	0.375
Mattock et al.	1975	yes	1		15	MO-U, MO-P	NW:15 LW:0	3.82-4.25	0.75	49.1-53.2	514-836	0.375
Mattock et al.	1976	yes	1		66	MO-U, MO-P	NW:13 LW:53	2.33-6	LW: 0.375, 0.5 NW: 0.75	47.7-53.6	0-1404	0.375
Kahn and Mitchell	2002	yes	1		45	MO-U, MO-P, CJ-R, CJ-S	NW:45 LW:0	6.81-17.96	0.75	69.5-83	278-1245	0.375
CTA	1974	no	6	shear strengths are smaller of V_uQ/lb and V_u/bd	2	CJ-S	NW:2 LW:0	4.06-5.5	unreported	N/A	0	N/A
CTA	1976	no	6	shear strengths are smaller of V_uQ/lb and V_u/bd	11	CJ-R, CJ-S	NW:11 LW:0	3.42-4.9	unreported	N/A	0	N/A
Walraven and Reinhardt	1981	no	1		23	MO-P	NW:23 LW:0	3.62-6.92	0.63, 1.26	62.9-73.6, 110 (1test)	154-2200	0.16-0.63
Frenay	1985	no	1		20	MO-P	NW:20 LW:0	6.72-9.88	0.63	66.7-79.8	747-1787	0.315
Hoff	1993	no	1		18	MO-P	NW:0 LW:18	8.29-11.02	0.75	53.6-72.1	280.8-657.2	0.375, 0.5
Walraven and Stroband	1994	no	1		6	MO-P	NW:6 LW:0	14.36	0.63	86.3	483-2166	0.315, 0.472
Jose	1998	no	2a and 2a with various interface preparations (CJ-R)	CJ-R specimen interfaces were prepared with various brooming angles	16	MO-U, CJ-R, CJ-S	NW:16 LW:0	5.31-7.54	0.75	N/A	0	N/A
Nagle and Kuchma	2007	no	5		16	MO-P	NW:16 LW:0	13.45-17.49	unreported	64.54-79.19	107-916.5	0.394-0.63

Mansur and Vinayagam	2008	no	1		19	MO-P	NW:19 LW:0	5.83-15.43	0.79	43.5, 76.9	194.4-2049.4	0.315, 0.394
Scott	2010	no	2a and 2a with different concrete blocks	8 tests had NW on one side LW on the other side. (noted as LW specimens in the database)	27	CJ-R	NW:9 LW:18	5.73-6.25	0.5, 1	60	0-287.5	0.5, 0.625
Crane	2010	no	1		20	CJ-R, CJ-S	NW:20 LW:0	12.2	0.75	73.5	0-551.3	0.375
Miller et al.	2011	no	1		8	CJ-R	NW:8 LW:0	5.8	1	61.5-67.3, 126-140	272.2-1033.8	0.375, 0.5
Sagaseta and Vollum	2011	no	1		6	MO-P	NW:6 LW:0	4.6, 7.7	0.394	79.8	335-678	0.315
Sneed and Shaw	2013	no	1		33	CJ-R, CJ-S	NW:12 LW:21	4.55-7.85	0.5	66.2	882.8	0.375
Rahal et al.	2015	no	1		15	MO-U	NW:15 LW:0	6.29-11.49	0.787	37.42, 59.18	135.4-1142.2	0.236, 0.315
Sneed et al.	2016	no	1		46	MO-U, MO-P, CJ-R, CJ-S	NW:4 LW:42	4.38-5.57	0.375, 0.75	72.2	649.8-1588.4	0.375
Barbosa et al.	2017	no	1	(collected fu values over fy values in the database)	20	CJ-R	NW:20 LW:0	4.15-4.58	0.375	67.6-93	302.5-560.6	0.5, 0.625

Note that Table 3.2.1.2 gives details of subset of the test programs that satisfy the data selection criteria of this research program which is to study direct shear failure as a main mode of failure. Hence, the actual total number of tests conducted in each program was equal or higher than what is reported in the table.

3.2.2 Timeline of test programs

The total number of shear friction tests conducted in the past is summarized in Figure 3.2.2.1. It shows that shear transfer strength studies on normal weight concrete interfaces were prevalent compared to lightweight concrete interfaces. The number of normal weight concrete tests surpass that of lightweight concrete tests significantly until the 2010's. Only in the 1970's and in the recent (since 2010), significant amount of lightweight concrete tests were conducted.

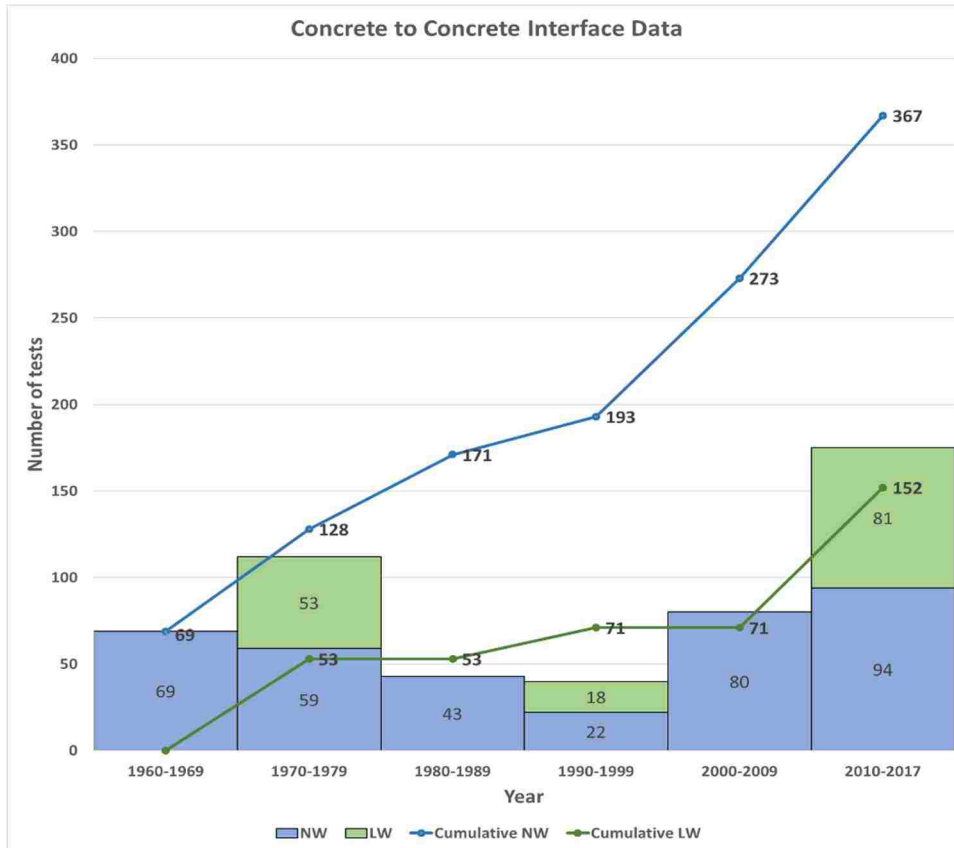


Figure 3.2.2.1: Cumulative test numbers with time

Figure 3.2.2.2 shows the major milestones of shear friction studies focusing on concrete-to-concrete interfaces as well as the applicable code provision changes throughout time. By looking at Figures 3.2.2.1 and 3.2.2.2, it is possible to see how much data was available at times when models and code provisions were proposed or changed. One example is that the very first ACI shear friction chapter was introduced when 69 documented direct-shear transfer tests (normal weight concrete only) were available. As more studies became available, codes changed accordingly.

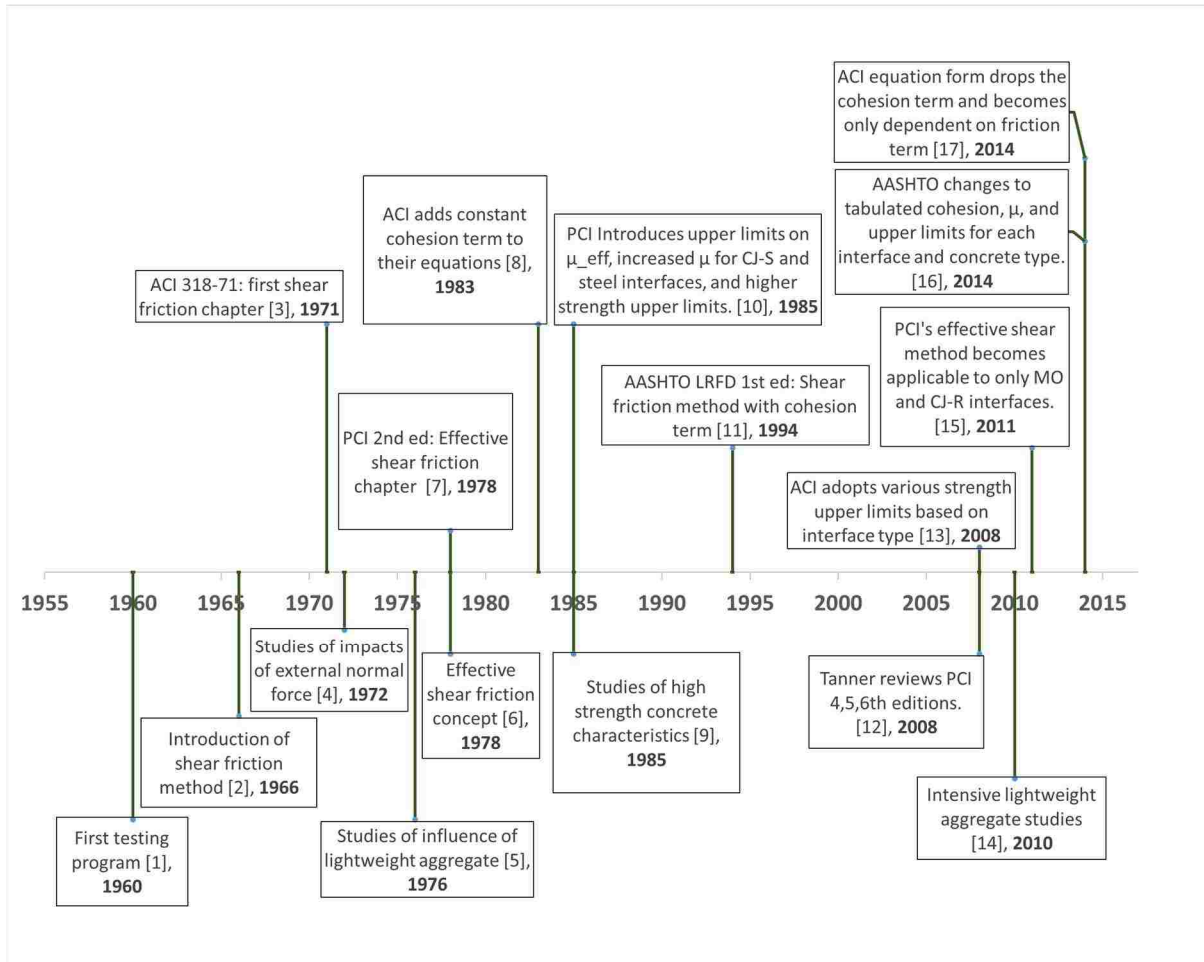


Figure 3.2.2.2: Timeline of major milestones

More thorough descriptions of the major milestones in Figure 3.2.2.2 are reported in Table 3.2.2.1 below:

Table 3.2.2.1: Tabulated descriptions of the major milestones

Timeline	Year	Description:
[1]	1960	Hanson (1960) test program takes place.
[2]	1966	First introduction of shear friction theory: Birkeland and Birkeland (1966) followed by Mast (1968) and Hofbeck (1969).
[3]	1971	ACI's first shear friction chapter (ACI 318-71).
[4]	1972	Mattock and Hawkins (1972) followed by Mattock (1975) study effects of external normal force.
[5]	1976	Mattock et al. (1976) first studies influence of lightweight aggregate.

[6]	1978	Shaikh's effective shear friction concept evaluation on Mattock (1974), Birkeland (1969), and Raths (1977) works.
[7]	1978	First appearance of effective shear friction in PCI (2 nd ed.). Shear friction coefficients of CJ-S and steel interfaces were 0.4 and 0.6 respectively. Corresponding upper limits were smaller than that of current PCI Handbook.
[8]	1983	ACI adopts constant cohesion terms (based on aggregate type) to friction term. Minimum clamping force was set to 200psi.
[9]	1985	Studies on impacts of high compressive strength concrete begin.
[10]	1985	PCI adopts higher upper limits. Shear friction coefficients for CJ-S, and steel interfaces were raised. Upper limits on effective shear friction coefficients were introduced.
[11]	1994	AASHTO LRFD (1 st ed.) Shear friction method that utilizes cohesion and external normal force. To take concrete/aggregate type into account, λ factor was in use.
[12]	2008	Tanner reviews PCI 4 th , 5 th , and 6 th editions and addressed mathematical flaws.
[13]	2008	ACI adopts various shear strength upper limits based on interface type.
[14]	2010	Lightweight concrete studies start to take place notably. Scott (2010), Sneed and Shaw (2013), and Sneed et al. (2016) etc.
[15]	2011	PCI's effective shear method becomes applicable to only MO and CJ-R interfaces. λ^2 term in equation of μ_{eff} becomes λ .
[16]	2014	AASHTO changes to tabulated cohesion, μ , and upper limits for each interface and concrete type.
[17]	2014	ACI equation form drops the cohesion term and becomes only dependent on friction term

3.2.3 Detailed interpretation of the database by parameters

Distribution of yielding strength of reinforcement (f_y):

In the database, data from tests with high strength (actual $f_y > 90$ ksi) steel reinforcement were noticeably rare. The majority of the database consisted of tests with regular strength steel ($f_y \leq 70$ ksi) and intermediate strength steel ($70 < f_y \leq 90$ ksi). This distribution trend of f_y (yield strength of shear reinforcement) is true for both populations of NW (normal weight) and LW (light weight) concrete tests (See Figures 3.2.3.1 and 3.2.3.2). Note that when the actual yielding strength was not reported the nominal yielding strength was collected.

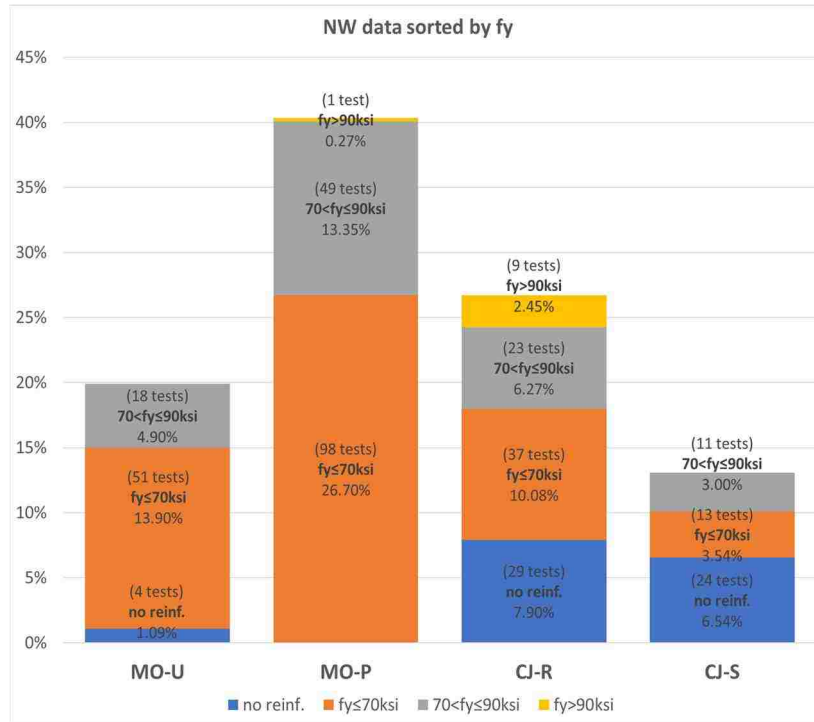


Figure 3.2.3.1: NW data sorted by yielding strength of reinforcement

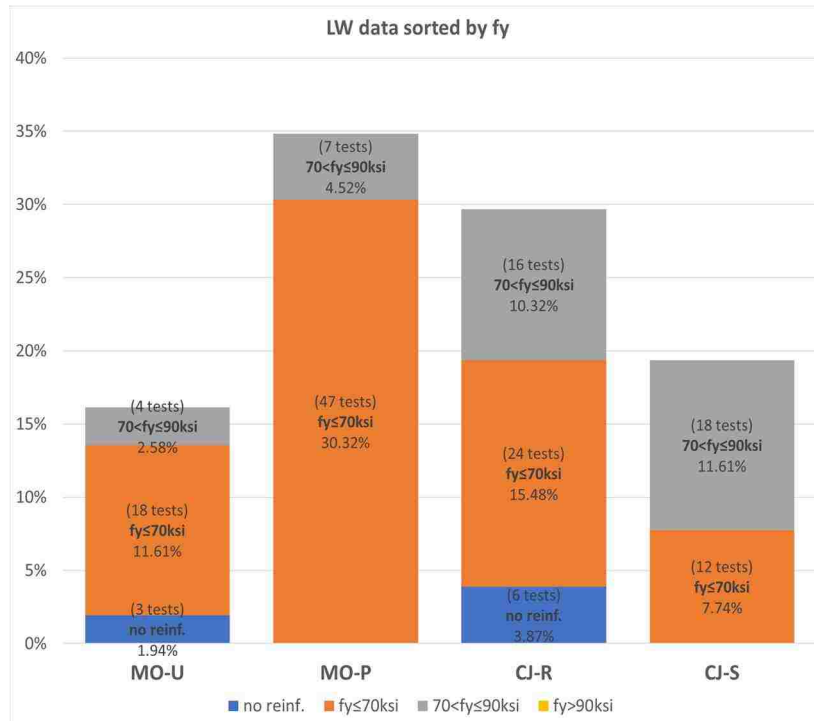


Figure 3.2.3.2: LW data sorted by yielding strength of reinforcement

Distribution of clamping stress (ρf_y):

Figures 3.2.3.3 and 3.2.3.4 show that a substantial number of tests have been conducted in all of the four major surface types, with the most conducted on MO-P specimens. For the great majority of tests, p_{fy} lay in the range 62.5 to 1400psi. There were more unreinforced normal weight concrete tests than unreinforced lightweight concrete tests.

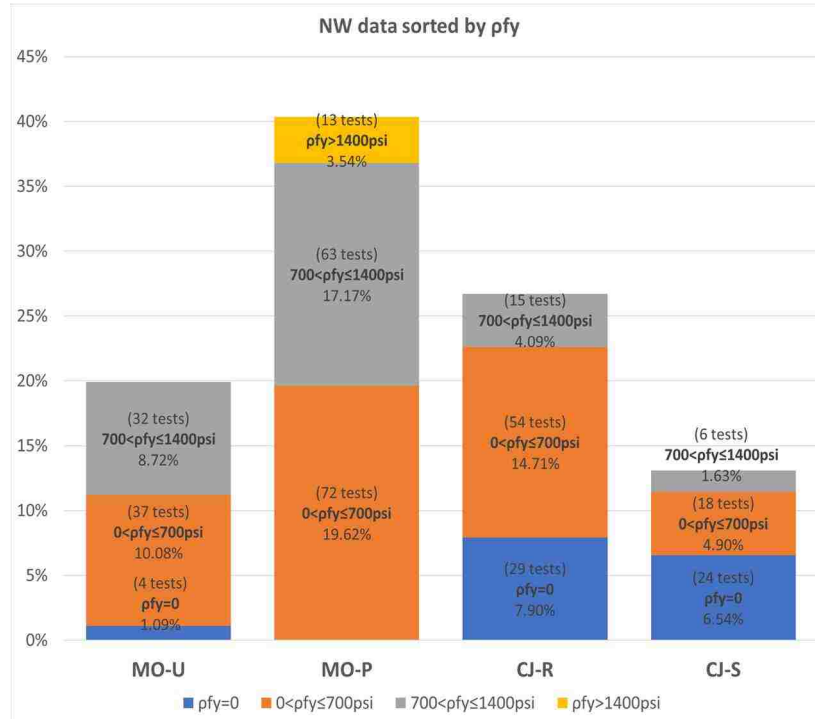


Figure 3.2.3.3: NW data sorted by clamping stress

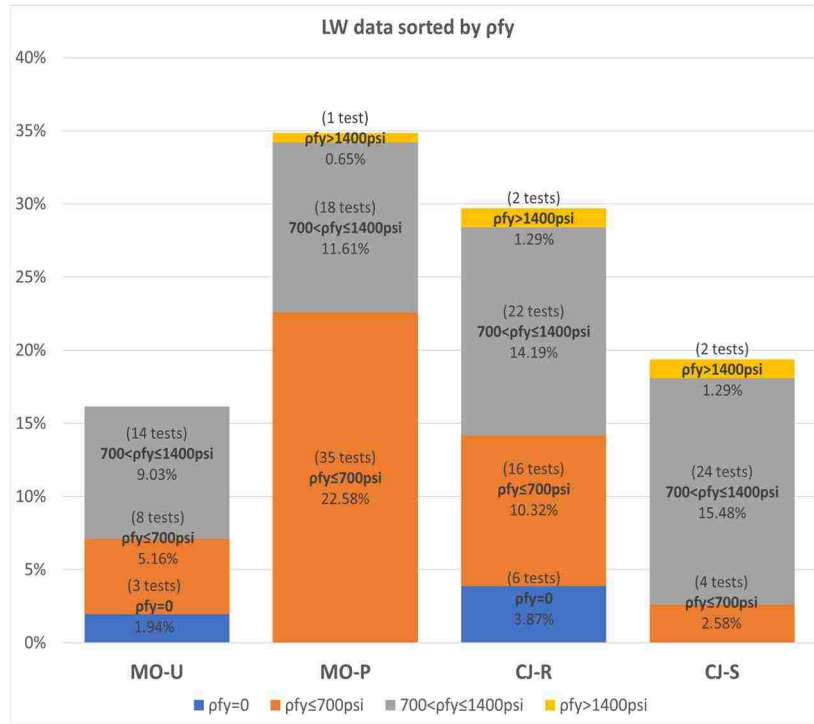


Figure 3.2.3.4: LW data sorted by clamping stress

Distribution of compressive strength of concrete (f'_c):

As shown in Figures 3.2.3.5 and 3.2.3.6, the concrete strength varied over a wide range, with about half of the NW concrete and the majority of the LW concrete tests carried out on specimens with $f'_c < 6$ ksi.

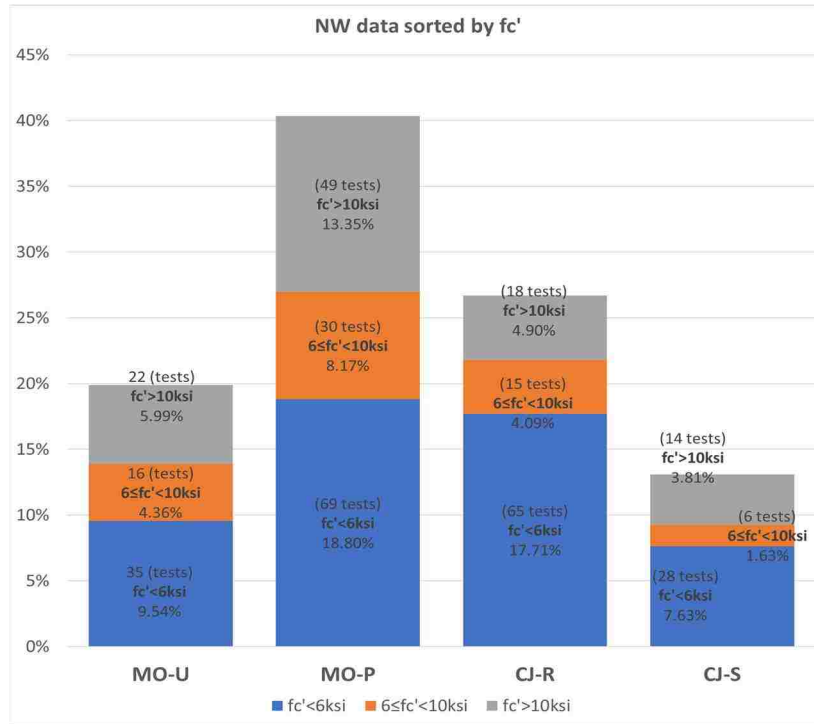


Figure 3.2.3.5: NW data sorted by compressive strength of concrete

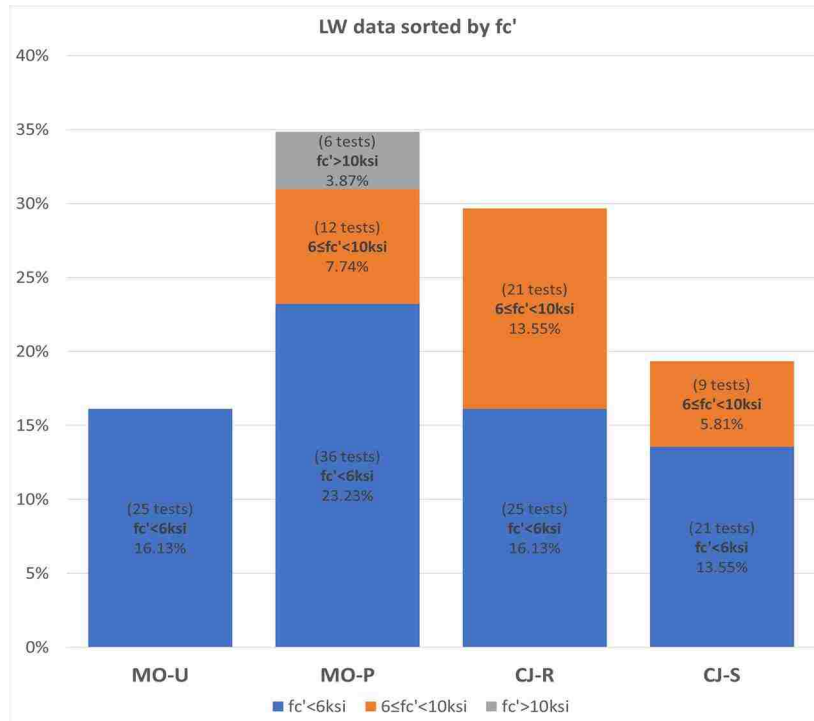


Figure 3.2.3.6: LW data sorted by compressive strength of concrete

Distribution of diameter of reinforcing bars (d_s):

The reinforcing bar diameters did not vary over a wide range. The range of bar sizes of test programs included in the database varies between 0.24" and 0.63". As can be seen in Figures 3.2.3.7 and 3.2.3.8, the majority of the tests were conducted on specimens with $d_s \leq 0.5"$.

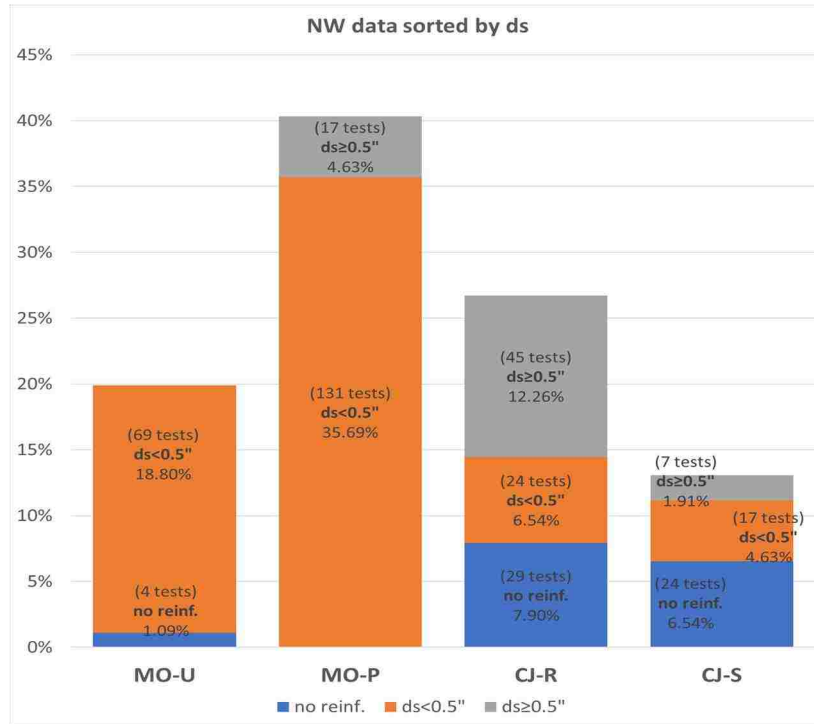


Figure 3.2.3.7: NW data sorted by size of shear reinforcement

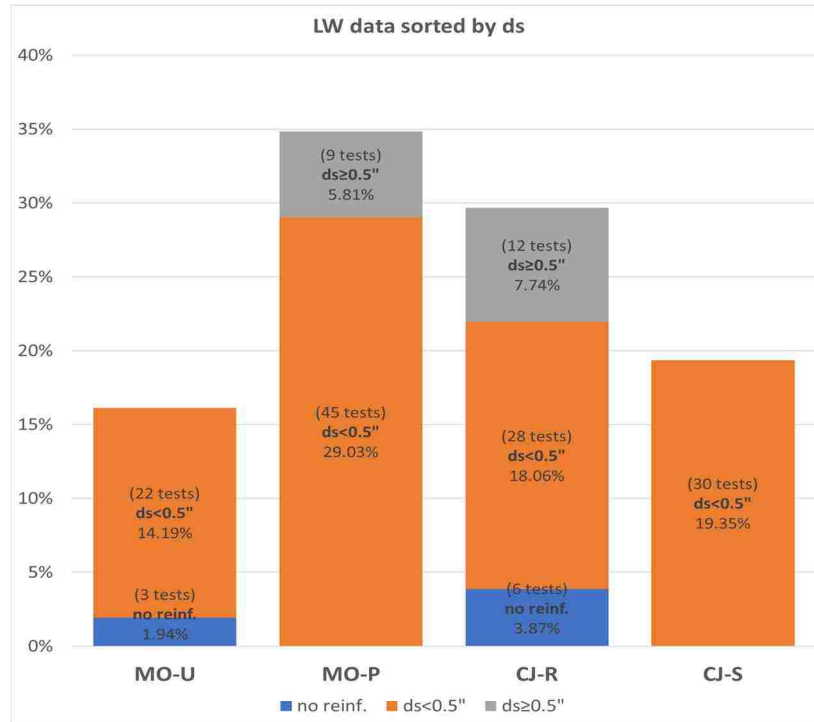


Figure 3.2.3.8: LW data sorted by size of shear reinforcement

3.3 Steel to Concrete Interface Data

A separate database was assembled for steel-to-concrete interfaces. The two types of interface were treated separately for several reasons. First, most of the tests described in the literature were conducted on specimens representing concrete slab/s connected by shear studs to a steel beam (Type C as shown in Figure 3.3.1.1). This configuration leads to moment as well as shear loading, so the total number and configuration of the studs become important. Secondly, the deflected shape of the shear studs differs from that of bar reinforcement in a concrete-to-concrete specimen. Third, research on concrete-to-steel interfaces has been conducted largely by groups related to the steel industry, and the behavior has been modeled in terms of stud shear strength rather than friction caused by stud tension.

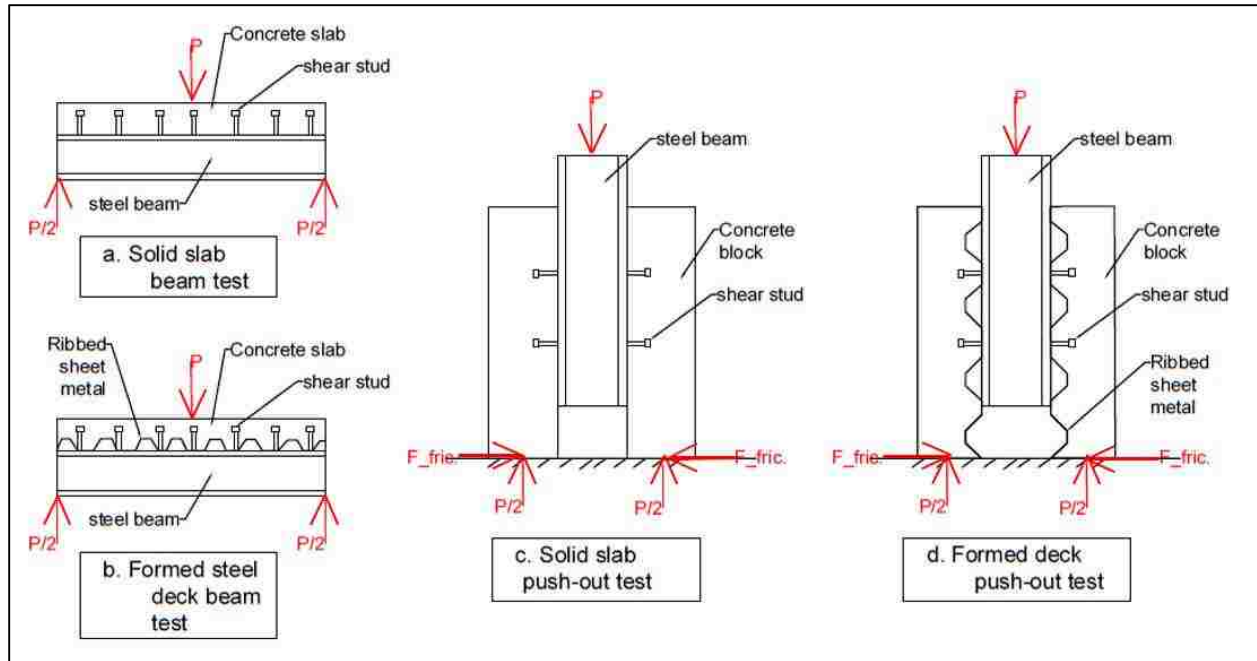


Figure 3.3.1.1: Common types of steel to concrete interface test configurations

The common test configurations for steel to concrete interfaces are shown in Figure 3.3.1.1. In these tests, the specimens were loaded monotonically or cyclically. This research program focused on collecting data from monotonically loaded from the beginning or partially cycled initially and then loaded to failure solid slab push-out tests.

The parameters collected in the database for steel to concrete interfaces include:

Data from 455 solid slab push-off tests have been collected in the steel to concrete interface database (Appendix B). The parameters reported (alongside with failure loads) were:

1. Concrete properties:
 - Concrete type (NW vs. LW concrete)
 - Thickness of concrete slabs
 - Concrete compressive strength
2. Interface properties:
 - Bond (greased or ungreased)
 - Externally applied normal load
 - Length and width of steel beam in contact with concrete
3. Stud properties
 - Diameter and height of studs
 - Number of studs
 - Configurations of studs and spacing
 - Yielding (if reported) and ultimate tensile strengths of studs

Section 3.3.1 through 3.3.3 provide more detailed discussion about the database both parameters wise and chronologically.

3.3.1 Schematics of the database

Table 3.3.1.1: Summary of database (steel-to-concrete interface) (continues on the next page)

	Authors	Viest	Shoup and Singleton	Chapman and Balakrishnan	Chinn	Buttry	Davies	Mainstone and Menzies	Steele	Goble
	Year	1956	1963	1964	1965	1965	1967	1967	1967	1968
	Codes based on the work?	yes	no	no	no	no	no	no	no	yes
	Interface bond	no	yes	no	no	unreported	no	no	unreported	yes
	external normal force (10%)	no	no	no	no	no	no	no	no	no
	# Applicable tests in total	12	9	9	10	22	20	11	18	21
	Concrete	NW:12 LW:0	NW:9 LW:0	NW:9 LW:0	NW:2 LW:8	NW:9 LW:13	NW:20 LW:0	NW:11 LW:0	NW:3 LW:15	NW:21 LW:0
Geometric variables:	# rows	1	2	1	1	1	1-4	1	1	1
	# studs per row	2, 4	2	2	2	2	1, 2	2	2	2
	# studs per plane	2, 4	4	2	2	2	2-4	2	2	2
	ds [in]	0.5-1.25	0.5-0.875	0.5, 0.75	0.5, 0.625, 0.875	0.5-0.75	0.375	0.75	0.749	0.5-0.75
	Hs [in]	3.84-4.08	3.9-8.44	2, 4	2-4	1.5-3.69	2	4	2.63	4
	tf [in]	0.683	unreported	0.717	0.38	unreported	0.38	0.55	unreported	0.192-0.442
	t slab [in]	7	unreported	6	6	6	2.5	6, 9	6	6
	Hs/ds	3.07-8	5.2-9.65	2.67-8	4-6.4	2-7.38	5.33	5.33	3.5	5.33-8
	ds/tf	0.73-1.83	uncalculable	0.7, 1.05	1.32-2.3	uncalculable	0.99	1.36	uncalculable	1.64-2.6
	sLong [in]	0	unreported	0	0	0	0-3.75	0	0	0
	sTrans [in]	1.86-4.12	unreported	2.5	4	4	0, 0.75, 1.5	3.75	4	2.5, 4
	sLong/ds	0	uncalculable	0	0	0	0-10	0	0	0
sTrans/ds	2.48-7.72	uncalculable	3.33, 5	4.57-8	5.33-8	0, 2, 4	5	5.34	4-5.33	
Material and reinforcement variables:	fy [ksi]	unreported	unreported	unreported	65	unreported	unreported	unreported	unreported	unreported
	fu [ksi]	63.3-73.6	63.23-75.67	66.4-78.4	70.15	59-78.3	85.3	unreported	76.2	unreported
	ρ [10^{-3}]	1.72-10.8	unreported	4.09, 9.2	4.03, 6.3, 12.35	unreported	9.2-18.41	11.04	unreported	3.60-5.15
	pfu [psi]	122.2-689	uncalculable	299.4-721.6	282.8, 441.91, 866.14	uncalculable	785.1-1570.2	uncalculable	uncalculable	uncalculable
	fc' [ksi]	3.26-4.39	3.44-4.9	2.92-4.88	4.4	3.03-5.64	4.7-6.9	3.78-5.26	2.88-4.42	4.36-7.36

	Authors	Dallam	Baldwin	Ollgaard et al.	Menzies	Hawkins	Oehlers	Mitchell and Hawkins	Jayas and Hossain	An and Cederwall	Lyons	Zhao
	Year	1968	1970	1971	1971	1973	1980	1984	1988	1994	1994	1994
	Codes based on the work?	no	no	yes	no	no	no	no	yes	no	no	no
	Interface bond	no	yes	yes	no	no	no	yes	yes	yes	yes	unreported
	external normal force (10%)	no	no	no	no	no	no	no	no	no	yes	no
	# Applicable tests in total	17	26	48	15	17	14	5	5	8	40	18
	Concrete	NW:2 LW:15	NW:2 LW:24	NW:21 LW:27	NW:6 LW:9	NW:17 LW:0	NW:14 LW:0	NW:5 LW:0	NW:5 LW:0	NW:8 LW:0	NW:23 LW:17	NW:18 LW:0
Geometric variables:	# rows	1	1	1, 2	1	1, 2	1	1, 2	2,3,4	2	2	1, 2
	# studs per row	2	2	2	2	2	1	1, 2	2	2	1, 2	1, 2
	# studs per plane	2	2	2, 4	2	2, 4	1	2	4-8	4	2, 4	1, 4
	ds [in]	0.5-0.875	0.5-0.875	0.625, 0.75	0.75	0.75, 0.875	0.51-0.87	0.75	0.63	0.748	0.56-0.75	0.866
	Hs [in]	3.5, 3.69	2.19-3.69	3	4	3, 4, 5	2.56, 3.94	3-5	2.99	2.95	4.19, 4.28	1.97-3.54
	tf [in]	0.688	0.688	0.56	0.55	0.45	unreported	0.375	0.56	0.748	0.52	unreported
	t slab [in]	6	6	6	9	unreported	4.53-6.89	4-6	4.02	5.91	5.75	unreported
	Hs/ds	4-7.38	3.5-7.38	4, 4.8	5.33	4-5.71	4.55-5.26	4-6.67	4.75	3.95	5.58-7.63	2.28-4.09
	ds/tf	0.73-1.27	0.73-1.27	1.17, 1.34	1.36	1.67, 1.94	uncalculable	2	1.12	1	1.08-1.44	uncalculable
	sLong [in]	0	0	0, 12	0	0, 12	0	0, 2.5, 12	4.02, 5.98, 12	9.84	18	0, 3.94
	sTrans [in]	4	4	4	3.75	2.5	0	0, 3	2.99	5.91	0, 3.28	0, 3.94
	sLong/ds	0	0	0, 16, 19.2	0	0, 16	0	0, 3.33, 16	6.38-19.05	13.16	24-32.14	0, 4.55
sTrans/ds	4.57-8	4.57-8	5.33, 6.4	5	2.86, 3.33	0	0, 4	4.75	7.89	0, 4.82	0, 4.55	
Material and reinforcement variables:	fy [ksi]	unreported	50.5-66.8	unreported	unreported	unreported	unreported	unreported	unreported	60.6	unreported	unreported
	fu [ksi]	59-78.3	59-78.3	70.2-70.9	unreported	61.8-85.8	83.54-101.96	62.5, 74.5	unreported	75.3	67, 84	61.9
	ρ [10 ⁻³]	2.84-8.71	2.84-8.71	4.21-8.42	11.05	8.03, 10.93, 12.62	unreported	5.67	5.74-11.49	6.57	2.17-6.41	unreported
	p _{fu} [psi]	222.6-513.7	222.6-513.7	298.6-597.1	uncalculable	496.4-985.8	uncalculable	354.2, 422.2	uncalculable	494.9	182.8-539.2	uncalculable
	fc' [ksi]	3.9-6.11	3-8.08	2.67-4.02	2.31-7.9	1.98-8.99	3.48-8.16	3.31-4.97	4.32, 4.38	4.46-13.23	2.76-6.75	3.13, 3.37

	Authors	Roddenberry	Okada et al.	Shim et al.	Anderson and Meinheit	Xu et al.	Xue et al.	Liu and Alkhatib	Spremic et al.	Su et al.
	Year	2002	2004	2004	2005	2011	2012	2013	2013	2014
	Codes based on the work?	yes	no	no	no	no	no	no	no	no
	Interface bond	yes	yes	no	yes	yes (5 tests) no (1test)	no	yes	no	no
	external normal force (10%)	yes (15 tests) no (3 tests)	no	no	no	no	no	no	no	no
	# Applicable tests in total	18	11	18	8	6	5	20	19	5
	Concrete	NW:18 LW:0	NW:0 LW:11	NW:18 LW:0	NW:8 LW:0	NW:6 LW:0	NW:5 LW:0	NW:20 LW:0	NW:19 LW:0	NW:5 LW:0
Geometric variables:	# rows	2	2, 3	2	2, 3	1, 3	1, 3	2	1, 2, 4	1-6
	# studs per row	1	2, 3	2	2	2, 3	2	1	1, 2	2, 6
	# studs per plane	2	4, 9	4	4, 6	2, 9	2, 6	2	4	2-36
	ds [in]	0.75	0.866	0.984-1.182	0.5	0.511	0.866	0.874	0.63	0.866
	Hs [in]	4	3.94, 5.91	6.1	1.81	3.15	7.87	3.94-7.87	3.94	7.87
	tf [in]	0.38, 0.52, 0.715	0.689, 1.28	0.551	0.5	0.787	1.181	0.394	0.689	0.787, 1.575
	t slab [in]	5.75	5, 91, 9.84	7.87, 8.66	15	3.94, 17.72, 21.65	15.75	9.06	5.5	15.75
	Hs/ds	5.33	4.55, 6.82	5.17-6.2	3.62	6.15	9.09	4.5, 6.76, 9	6.25	9.09
	ds/tf	1.04-1.97	0.68, 1.26	1.79-2.14	1	0.65	0.73	2.22	0.91	0.55, 1.1
	sLong [in]	18	4.33, 9.84, 13.78	9.84	3-6	0, 2.36	0-9.85	unreported	0-3.94	0, 3.94
	sTrans [in]	0	3.15, 3.94	3.94	3	1.97, 3.15	3.94	0	0-3.15	4.92, 5.91
sLong/ds	24	5, 11.36, 15.91	8.33-10	6, 9, 12	0, 4.62	0-11.36	unreported	0-6.25	0, 4.55	
sTrans/ds	0	3, 64, 4.55	3.33-4	6	3.85, 6.15	4.55	o	0-5	5.68, 6.82	
Material and reinforcement variables:	fy [ksi]	unreported	64.5	51.2	67.4	58	55.1	54.1	61.9	53.2
	fu [ksi]	64.9	76.9	66.1	75.5	69.6	68.9	70.2	76.5	69.6
	ρ [10 ⁻³]	3.44-3.78	6.07, 10, 13.65	14.95-21.53	14.5, 21.8	2.08, 9.37	3.96, 11.88	17.58	5.62	5.43, 17.55-30.08
	ρ fu [psi]	223.7-245.4	466.5, 768.5, 1049.6	988.9-1424	1098.1, 1647.2	145, 652.3	272.8, 818.4	1233.1	430.5	378.1, 1221.4-2093.9
	fc' [ksi]	3.44, 4.88	6.43-7.18	5.12-9.35	5.86-6.23	8.29, 10.77	8.08	6.57	4.19-4.96	8.43

As data collection criteria, monotonically loaded solid slab push out test type was selectively chosen over the other common test configurations shown in Figure 3.3.1.1. The solid slab push-out configuration consisted of greased or ungreased I/W-shaped steel beam in between solid slabs (plain slab). The number of rows and number of studs per row was a subject to vary from test program to another. Due to the selective data collection process, the total number of tests reported in the table above illustrate only a sub-set of each test programs that fit the data selection criteria.

3.3.2 Timeline of Test Programs

Figure 3.3.2.1 shows that the majority of the database came from 1965-1974. Since then, number of test programs focused on solid slab shear transfer slowed down. This can be explained by the fact that the methods of designing and constructing steel-to-concrete composite beams were developed in the 1960s and 1970s, and have changed little since then. Most of the testing have been done to support composite construction.

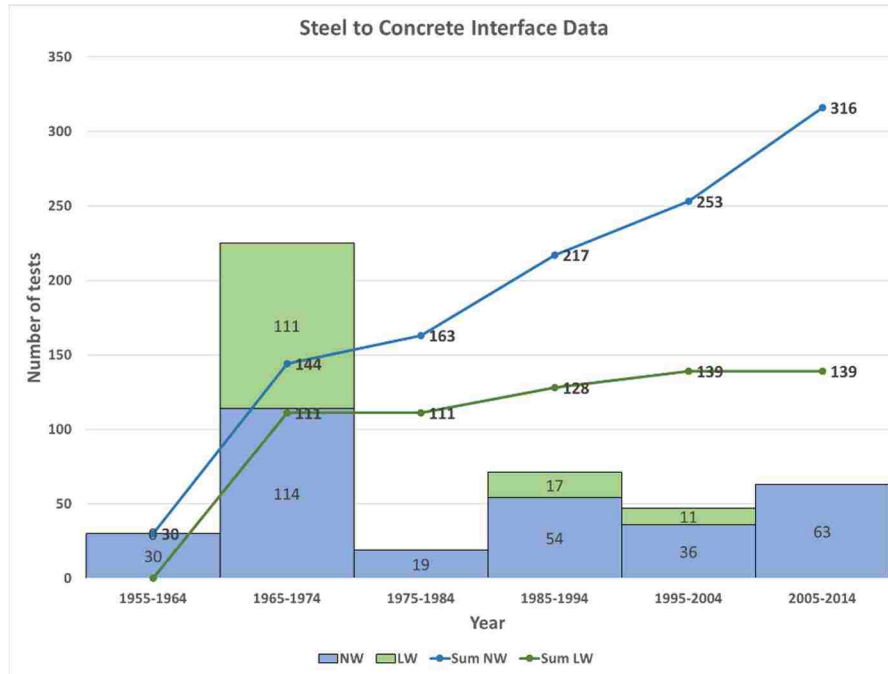


Figure 3.3.2.1: Cumulative test numbers with time

Figure 3.3.2.2 shows the major milestones of shear transfer studies focusing on steel-to-concrete interfaces throughout time.

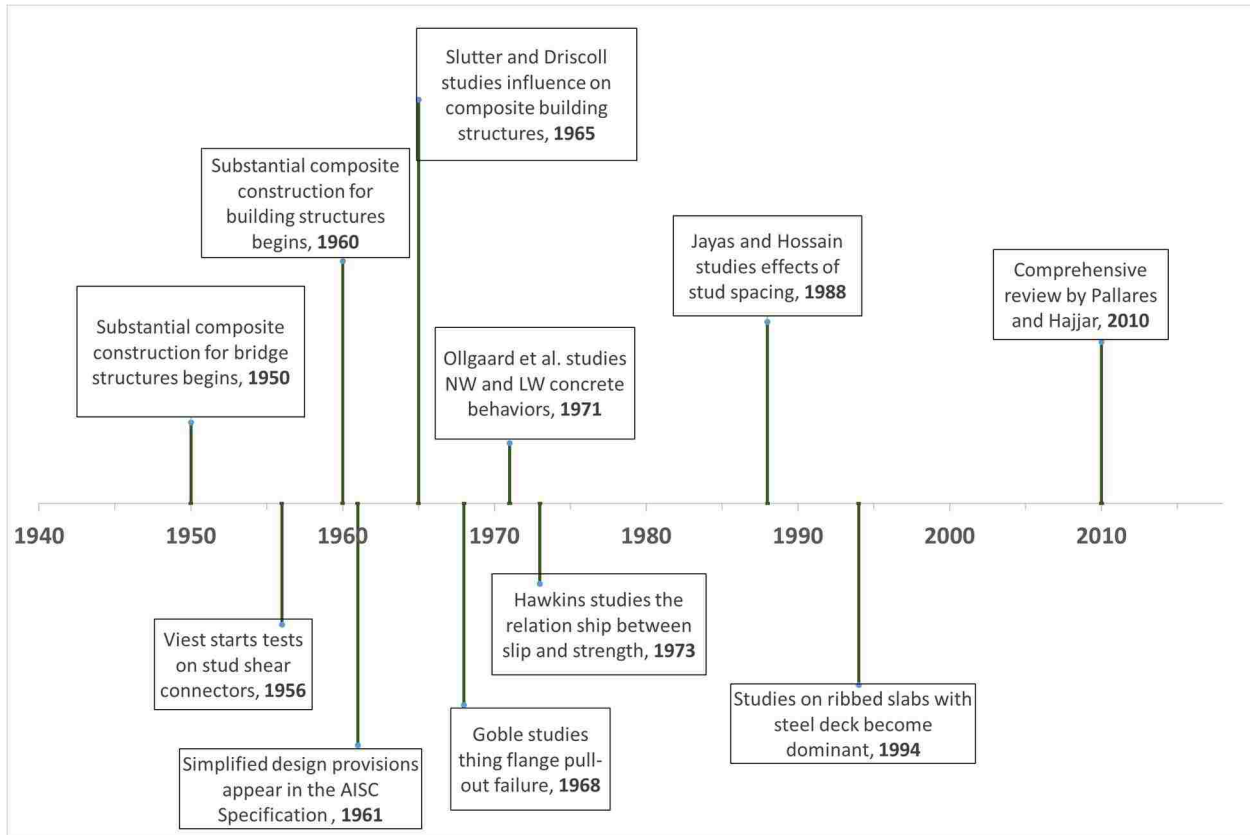


Figure 3.3.2.2: Timeline of studies on strength of shear studs

3.3.3 Detailed interpretation of the database by parameters

Some test programs did not report certain parameters and the shear interface bond (ungreased vs. greased). Thus, it was necessary to treat the unclear data separately for the detailed explanation of the database. In this section, when the parameter of interest was unreported or not calculable, the corresponding test program data counted in a group: “unreported” on each histogram. Also, when interface bond is not reported, they were grouped in a series: “unreported bond” as noted on the x axis of each histogram.

Distribution of ultimate strength of reinforcement (f_u):

Ultimate tensile strength of the stud was more commonly reported than yielding strengths in tests conducted on steel to concrete interfaces. On the other hand, the most tests conducted on concrete to concrete interfaces reported yielding strengths. This could be due to the fact that steel to concrete interface tests were conducted by groups of people whose main research interest lies in the steel industry while the concrete to concrete interface tests were completed by people whose interest lies in the concrete industry. Another possible reason is that welded shear studs may not have significantly distinct yielding strength than the ultimate strength especially in the heat affected zone.

However, several test programs (from well before the 1990's) did not report the ultimate tensile strength, f_u , of studs. Some of them reported that they used “common” shear studs at the time of the test. In those cases, approximate ultimate tensile strength were problematic to track down.

As shown in Figure 3.3.3.1 and Figure 6.3.3.2, the vast majority of the both total NW and LW concrete data is based on tests with $f_u \leq 80$ ksi.

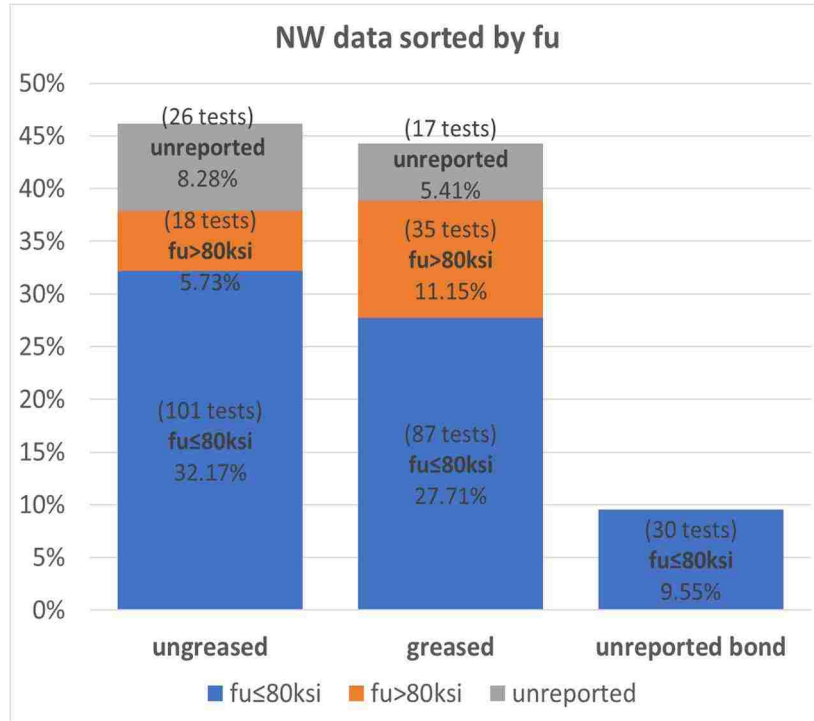


Figure 3.3.3.1: NW data sorted by ultimate strength of reinforcement

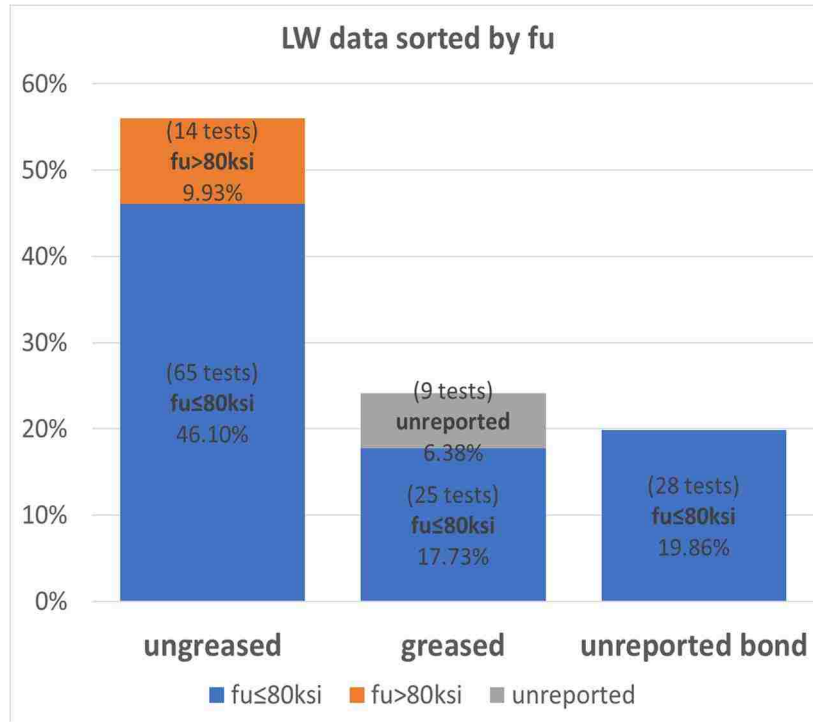


Figure 3.3.3.2: LW data sorted by ultimate strength of reinforcement

Distribution of ultimate clamping stress (ρf_u):

The majority of the test programs reported the tensile strength rather than the yielding strength of the shear studs. Therefore, unlike concrete-to-concrete interface database, steel-to-concrete interface database is able to give more information about the ultimate clamping stress, ρf_u , rather than “regular” clamping stress, ρf_y .

Figures 3.3.3.3 and 3.3.3.4 show that the majority of the tests have been conducted on specimens with $\rho f_u \leq 800$ psi. In about half of the specimens, the interface was greased, with the goal of eliminating friction so that its contribution could be determined by comparison with ungreased specimens.

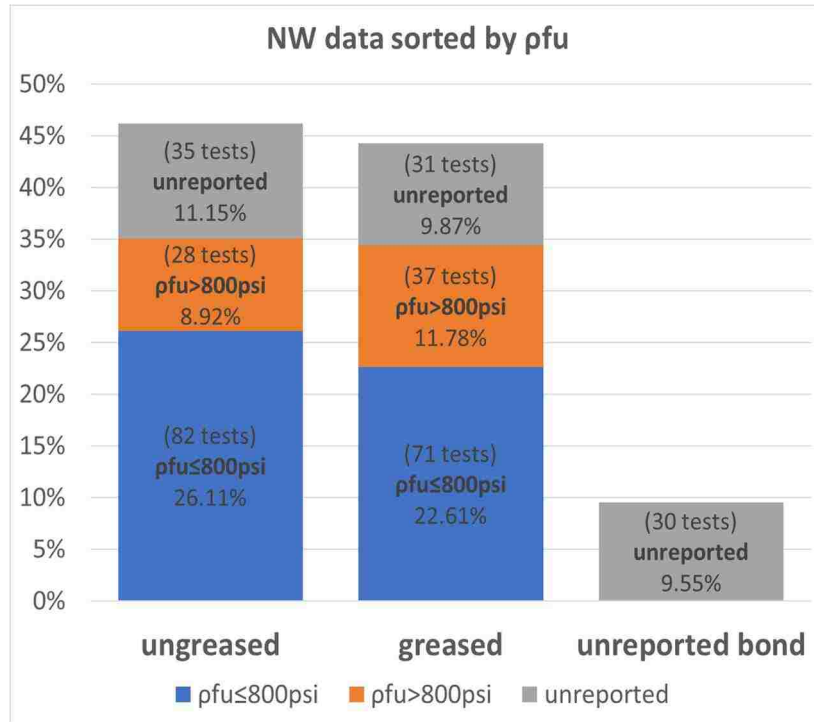


Figure 3.3.3.3: NW data sorted by ultimate clamping stress

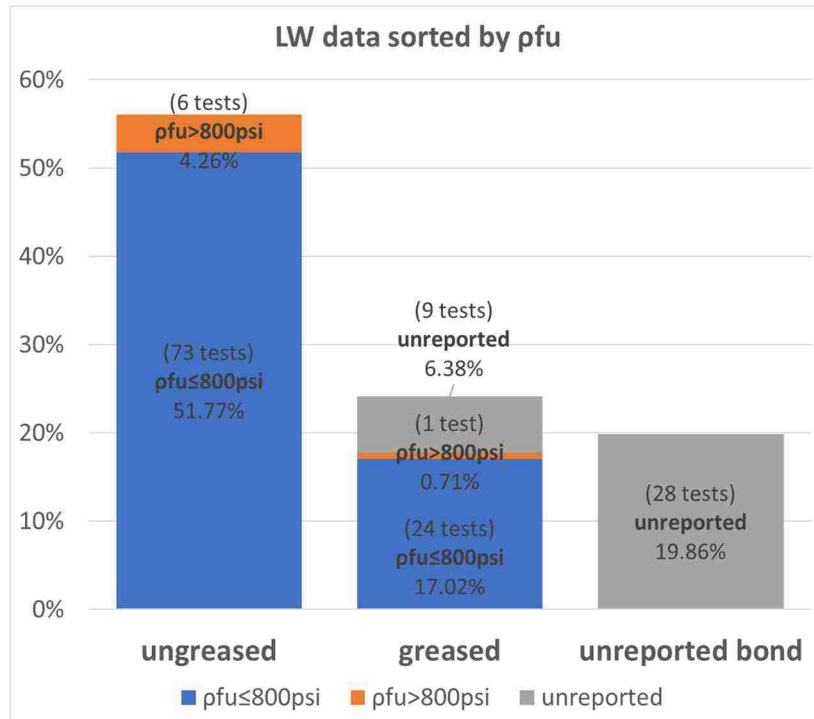


Figure 3.3.3.4: LW data sorted by ultimate clamping stress

Distribution of compressive strength of concrete (f'_c):

As shown in Figures 3.3.3.5 and 3.3.3.6, the majority of both NW and LW data are from tests with regular strength concrete slabs ($f'_c < 6$ ksi). As can be seen from the Figures 3.3.3.5 and 3.3.3.6, high strength concrete tests were rare in the steel-to-concrete interface database. This reflects the fact that slabs typically do not need high strength concrete, because their flexural strength is largely controlled by the reinforcement.

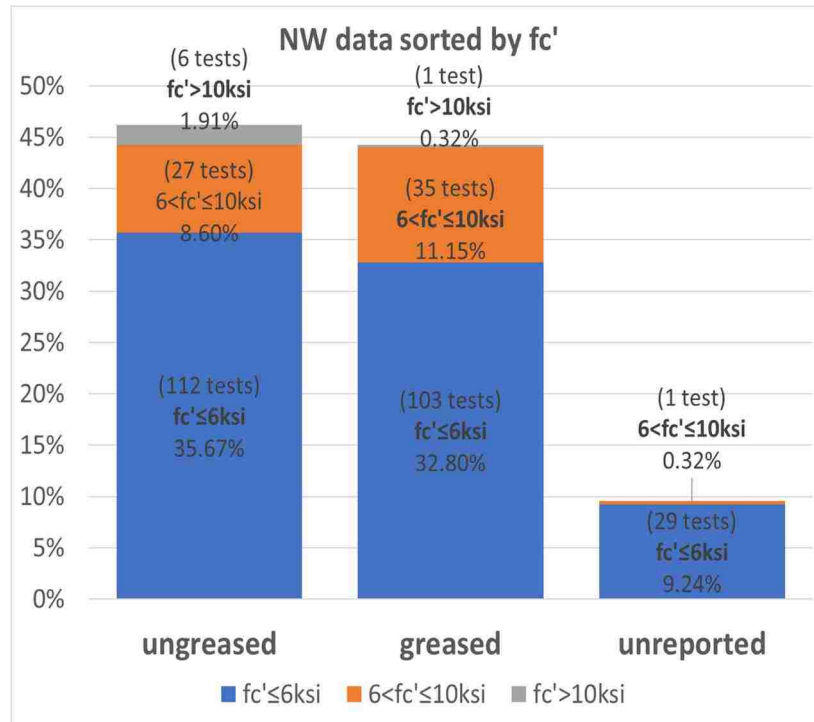


Figure 3.3.3.5: NW data sorted by compressive strength of concrete

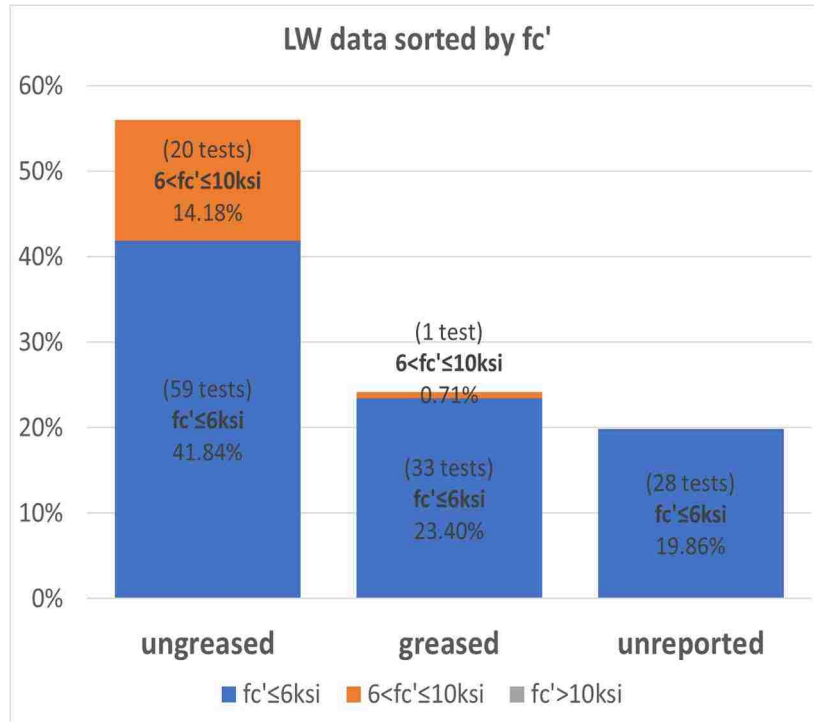


Figure 3.3.3.6: LW data sorted by compressive strength of concrete

Distribution of stud diameter (d_s):

The database consist of tests with studs with diameters varying from 0.375 to 1.25 inch. Figures 3.3.3.7 and 3.3.3.8 show the distribution of database with respect to diameter of shear studs. The distribution shows that the majority of the data has stud diameter smaller than 1".

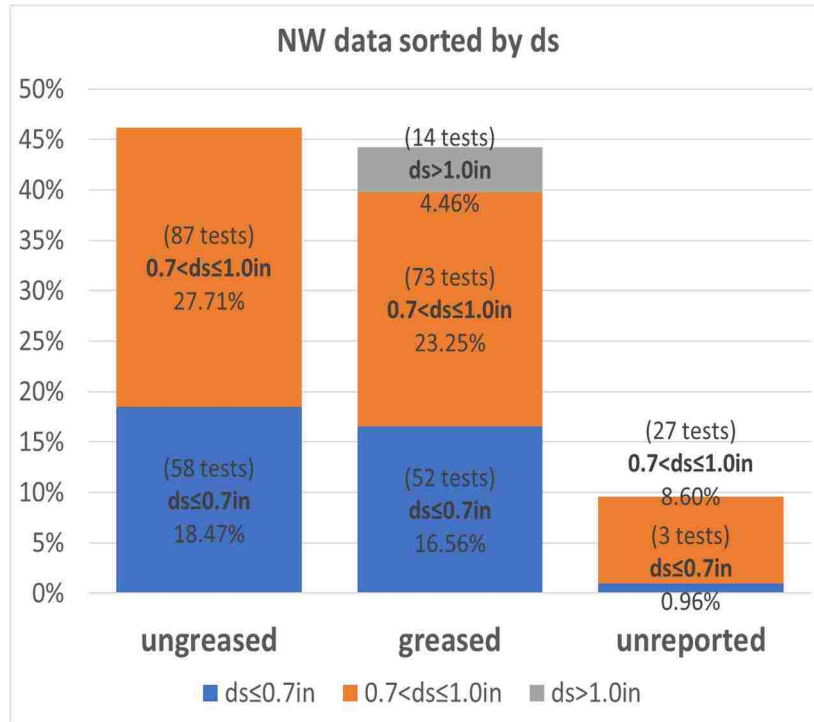


Figure 3.3.3.7: NW data sorted by diameter of studs

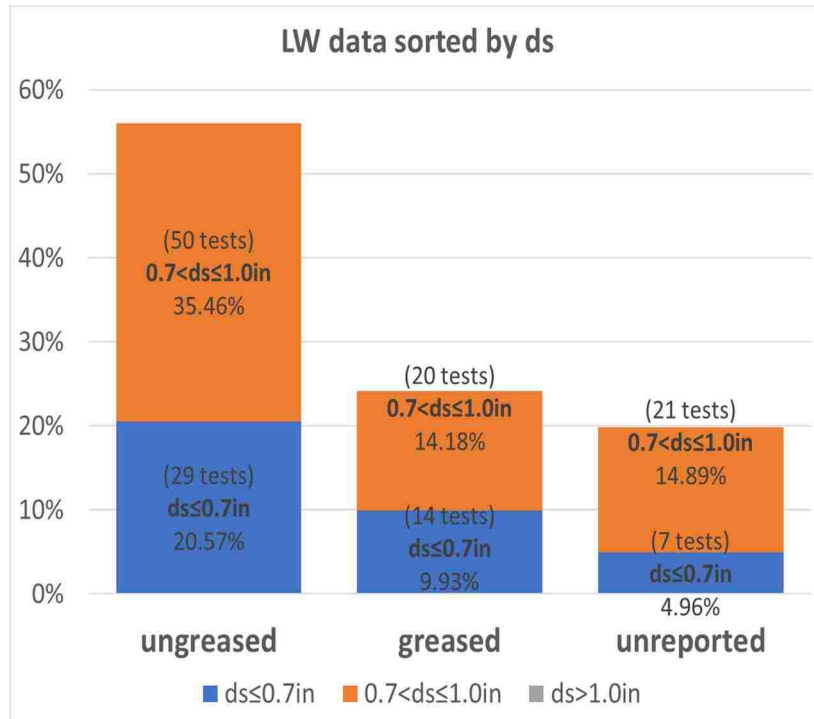


Figure 3.3.3.8: LW data sorted by diameter of studs

Stud height to diameter ratios (h_s/d_s):

The biggest h_s/d_s was 9.6. As shown in Figure 3.3.3.9, the majority of the NW tests and about half of the LW tests in the database had h_s/d_s bigger than 4.

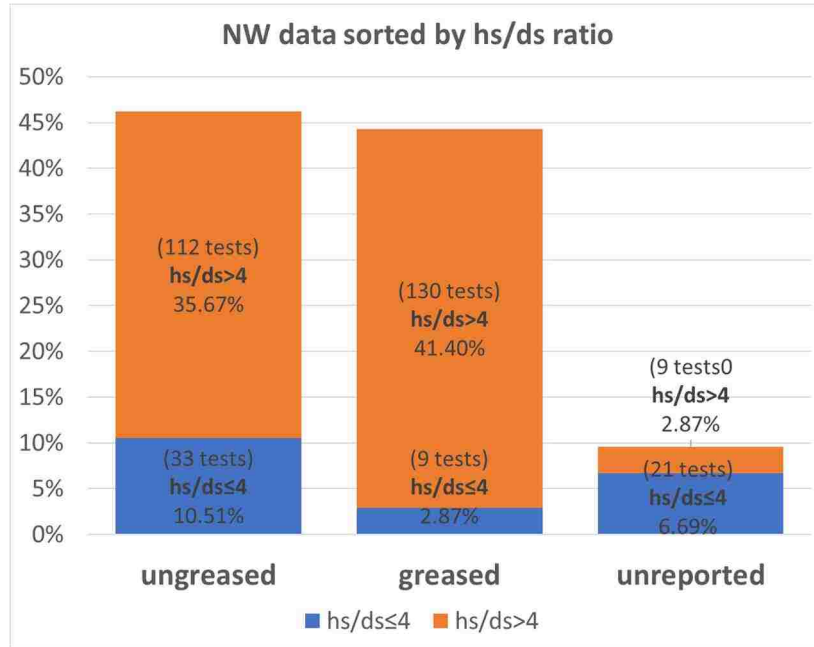


Figure 3.3.3.9: NW data sorted by height to diameter ratios of studs

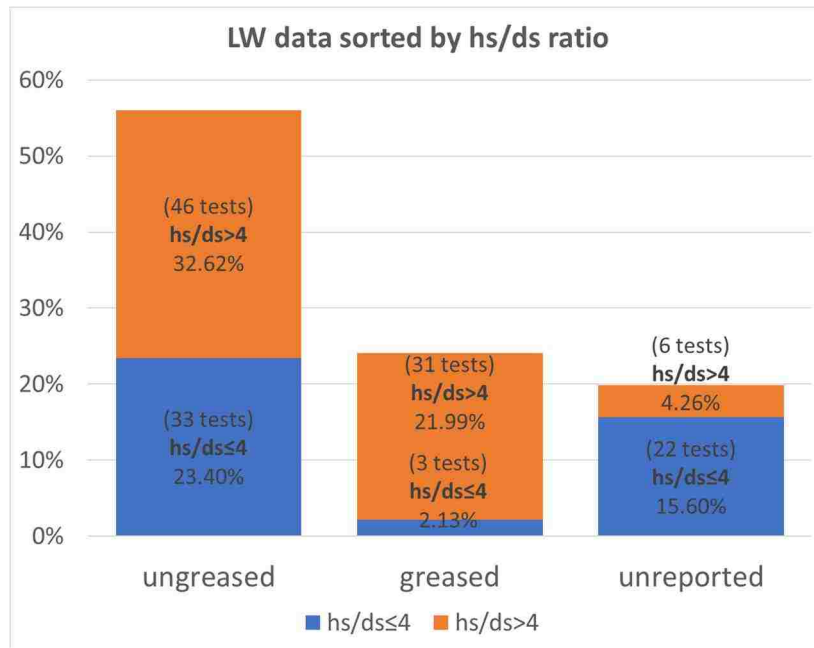


Figure 3.3.3.10: LW data sorted by height to diameter ratios of studs

Ratios of longitudinal spacing of studs to stud diameter (s_{long}/d_s):

The AISC code limit on minimum longitudinal spacing is 6. Figures 3.3.3.11 and 3.3.3.12 show that the majority of tests were spaced further than 6 times the stud diameter or had single rows in longitudinal directions.

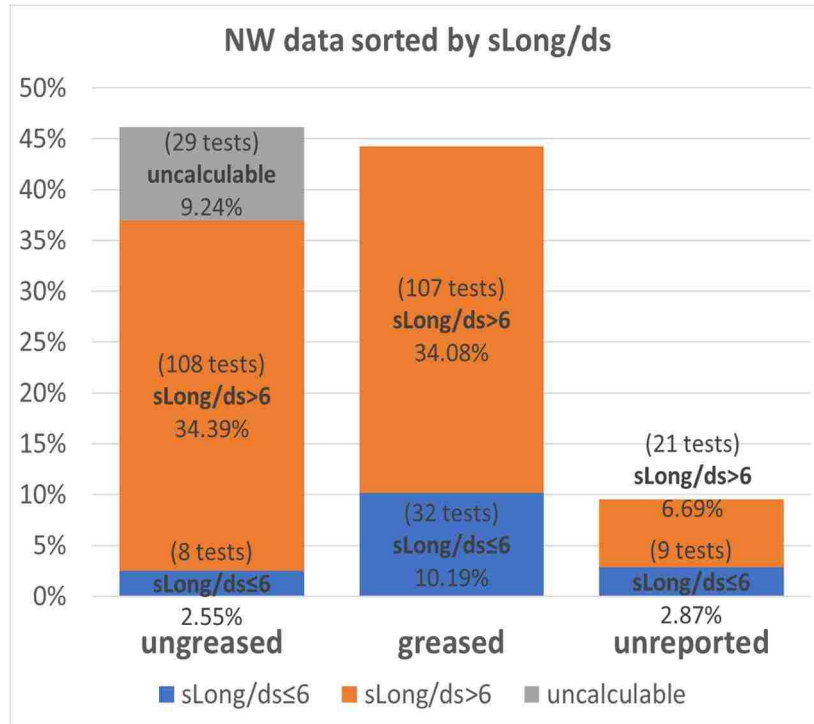


Figure 3.3.3.11: NW data sorted by longitudinal spacing to diameter ratios of studs

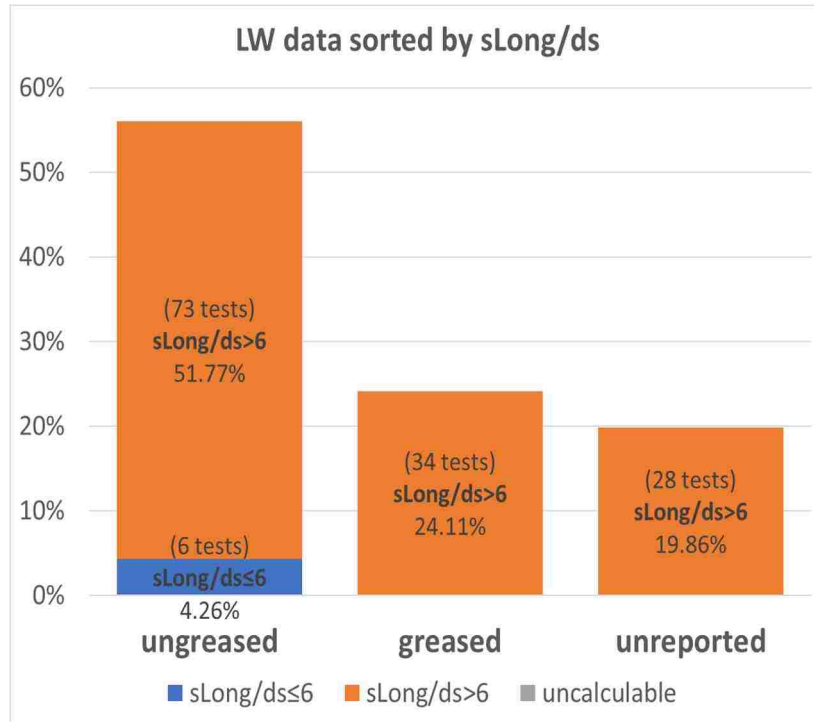


Figure 3.3.3.12: LW data sorted by longitudinal spacing to diameter ratios of studs

Ratios of transverse spacing of studs to stud diameter ($s_{trans.}/d_s$):

In Figure 3.3.3.13, it can be seen that about a quarter of NW data have transverse stud spacing smaller than or equal to 4. The rest of the NW data had longer transverse spacing than 4 times the stud diameter. As shown on Figure 3.3.3.14, there are only few LW tests in the database and the rest of LW data consist of test result that are well spaced or have single stud in transverse direction of applied load.

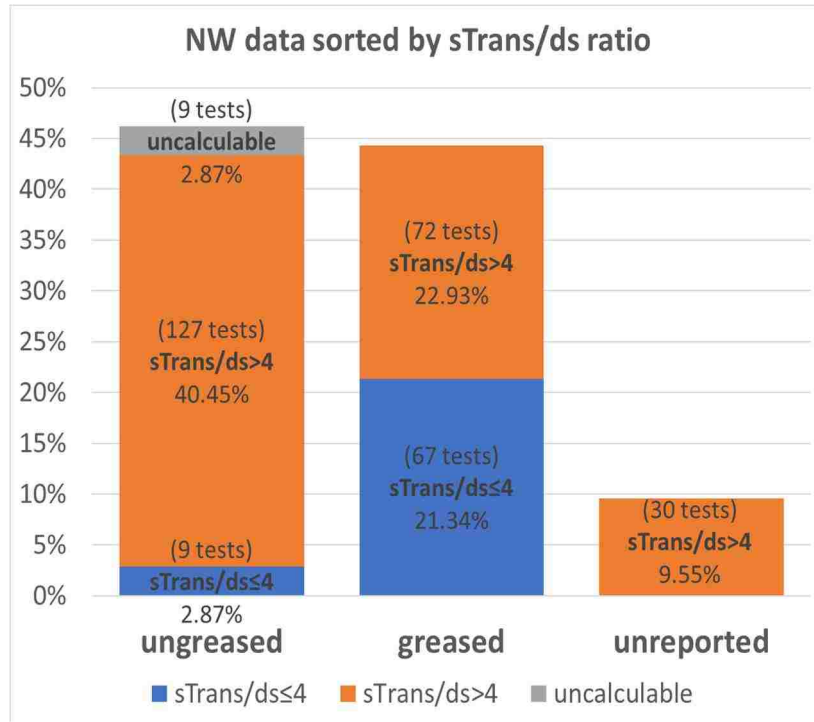


Figure 3.3.3.13: NW data sorted by transverse spacing to diameter ratios of studs

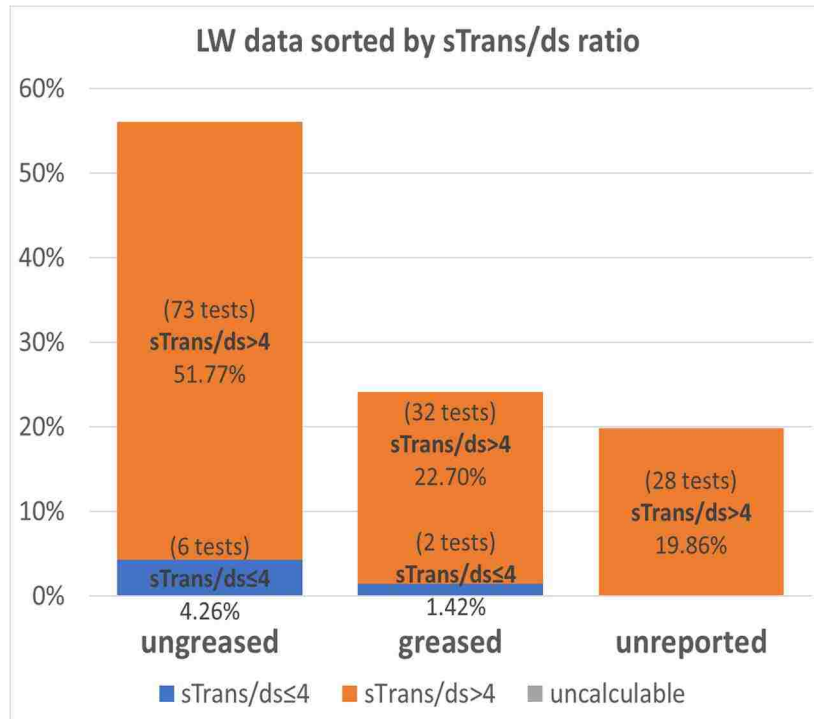


Figure 3.3.3.14: LW data sorted by transverse spacing to diameter ratios of studs

4. Analysis of Concrete to Concrete Interface Data

4.1 Introduction

The database consists of a total of 522 tests. In this chapter, the test results are analyzed to determine the parameters that have the most influence on the shear resistance. The parameters used in the tests can be assigned to two categories, one associated with materials and configuration, and the other with testing and loading procedures. The analysis largely follows the parameters.

Materials and configuration

Average contact pressure, ρf_y . This is included in all code requirements, and has been found by almost all researchers to be important. The shear resistance is generally taken to be linearly proportional to ρf_y , on the basis that friction is proportional to normal force.

Concrete compressive strength, f'_c . Stronger concrete has been found to lead to higher shear resistance, but again the nature of its influence is not clear. Many researchers have argued that the stronger concrete is better able to resist the breaking off of asperities, in which case the surface is ground smooth more slowly.

Surface type. Rougher surfaces have been found to lead to higher friction coefficients. However, difficulties exist in defining roughness, and the exact relationship between roughness and friction coefficient. Particularly for surfaces that are not intentionally roughened, the roughness is both low and indeterminate, and the value of the friction resistance shows considerable scatter. The four surface types used here are:

- MO-U. Monolithic uncracked.
- MO-P. Monolithic pre-cracked.
- CJ-R. Cold joint, roughened.
- CJ-S. Cold joint “smooth”, meaning not intentionally roughened.

Concrete density (normal or lightweight). Lightweight concrete has been found to offer lower shear resistance than normal weight concrete of the same compressive strength. The argument commonly given is that lightweight aggregate is weaker, and thus fractures off more easily, than “hard rock” aggregate. If that argument is correct, some measure of aggregate strength might be a better predictor of shear strength than concrete density. However, measures of aggregate strength are not standardized, so concrete density is the commonly accepted proxy parameter, and is used here.

The foregoing four parameters are the most commonly accepted as influencing shear strength. They are incorporated into most code-based design procedures. It should be noted that ρf_y , and f'_c are essentially continuous variables, and the surface type and concrete density are discrete. For concrete density, a continuous range of values is theoretically possible, but the available test data are limited to either lightweight or normal weight (LW or NW), so only those two values were used here.

Other parameters also affect shear strength, but in ways that have been less well investigated. Consequently the nature of their influence is less clear. They include:

Reinforcement yield stress, f_y . Higher yield stress will lead to higher tensile strain, and probably longer development length of the transverse reinforcement, both of which result in larger gap opening at the interface. This will lead to a larger slip at peak load, and possibly a different value of peak load.

Size and number of transverse bars. For a given ρf_y , fewer, larger diameter bars will have a different elastic shear stiffness, and may provide a different dowel action contribution to shear resistance. Dowel action is not counted explicitly in the shear friction strength, but it must provide some of the total resistance. Most tests have used bar diameters lying in a rather narrow range, so conclusive test data on the matter is not available.

Reinforcement orientation relative to the crack plane. A small number of investigators have studied the question, but it is a specialized question that was not included in the present research.

Concrete aggregate size. Larger aggregates may maintain more of the interlock strength at larger crack openings. Again, little test data is available, and most building applications today use aggregates of $\frac{3}{4}$ " or smaller. Some self-consolidating concrete contains no coarse aggregate, and might be expected to have lower shear-friction strength. Conclusive test data on SCC is not yet available.

Vibration techniques. One study was found that suggested that the level of vibration might affect the shear friction strength. Again the data is insufficient to be conclusive.

Test and loading procedures.

Presence of normal load. Tension or compression perpendicular to the interface have been found to affect the clamping force and friction. They did not form part of this study.

Combined loading in shear and moment. Behaviors of shear interfaces in response to a combination of shear and flexural load have not been thoroughly studied in general. Mattock et al. (1975) study address such combined loading, but it is corbel-specific. Combined loading on concrete-to-concrete interfaces was not included in this study.

Sustained load. Under sustained load, initial crack widths should develop further and the rate of displacement believed to be a function of time-dependent parameters of concrete. This was not a focus of this study.

Test stopped prematurely. A few test programs studied shear capacity of interfaces at certain pre-determined maximum allowable slips in consideration of serviceability. As a result, the ultimate shear strengths were not measured in those test programs. On the other hand, this study focused on the maximum shear capacity independently of crack opening and slip.

The foregoing parameters have been found to, or are believed to, influence shear resistance. The analysis that follows is used to investigate the nature and magnitude of the effects of the primary

parameters. In most cases their effects are investigated one at a time, although the effects of ρf_y and f'_c are investigated together, because they are linked.

Calibration Dataset

Because some of the tests focused on parameters that lay outside the main focus of this study, they were excluded from the analyses. The remaining dataset consisted of 380 tests, and is referred to here as the Calibration Dataset. The studies that were excluded, and the reasons for exclusion, are summarized in Table 4.1.1:

Table 4.1.1: List of works that are partially or completely excluded from calibration data (concrete to concrete interface)

Authors	Year	Reason for being completely or partially excluded from calibration
Mattock and Johal	1975	external normal (tension) load applied
Mattock and Hawkins	1972	external compression load caused by load applied at angle to the critical shear interface.
Nagle and Kuchma	2007	reinforcement at an angle other than 90° to the shear interface
Scott	2010	specimens consisted of NW and LW concrete, real f_y were not reported but only the nominal values
Miller	2011	very small number of high strength shear reinforcement tests ($f_y > 93\text{ksi}$)
Walraven and Reinhardt	1981	very small number of high strength shear reinforcement tests ($f_y > 93\text{ksi}$)
Frenay	1985	subjected to sustained loads before loaded to failure statically
Jose	1998	some specimens were broomed at an angle and some were specially vibrated so that the shear strength went up
When Applicable:		stopped loading before reaching ultimate load, or significant spalling occurred.
		Test results that seemed to have significant variation among the similar specimens from the same experimental program.

4.2 Influence of Parameters

4.2.1 Overview

Trial evaluations showed that the two continuous parameters, ρf_y and f'_c , had the largest influence on shear strength. Because there are only two such parameters, their influence can be shown on continuous 3-D surface plots. Such plots are presented in this section, for NW concrete alone, with the goal of illustrating the nature of their effect on shear strength. Best-fit numerical values for those effects are established in Section 4.2.2.

These 3D surface plots smooth the data and extrapolate where no data is available, and so should be taken to illustrate the trends, rather than as representing the precise values. For example, no data was available for certain f'_c values in between the minimum and maximum f'_c available, but the plots are extrapolated to those regions. The surfaces were extrapolated between the available minimum and maximum ρf_y and f'_c values in the corresponding calibration dataset. Furthermore, when multiple points exist in a region, the surface uses the average of those points.

In each case, the data is shown both as a surface plot and a contour plot. Note: v_u on the z axis is the ultimate shear strength capacity (the maximum shear stress carried in the test) rather than “factored” shear demand.

MO-U Interface:

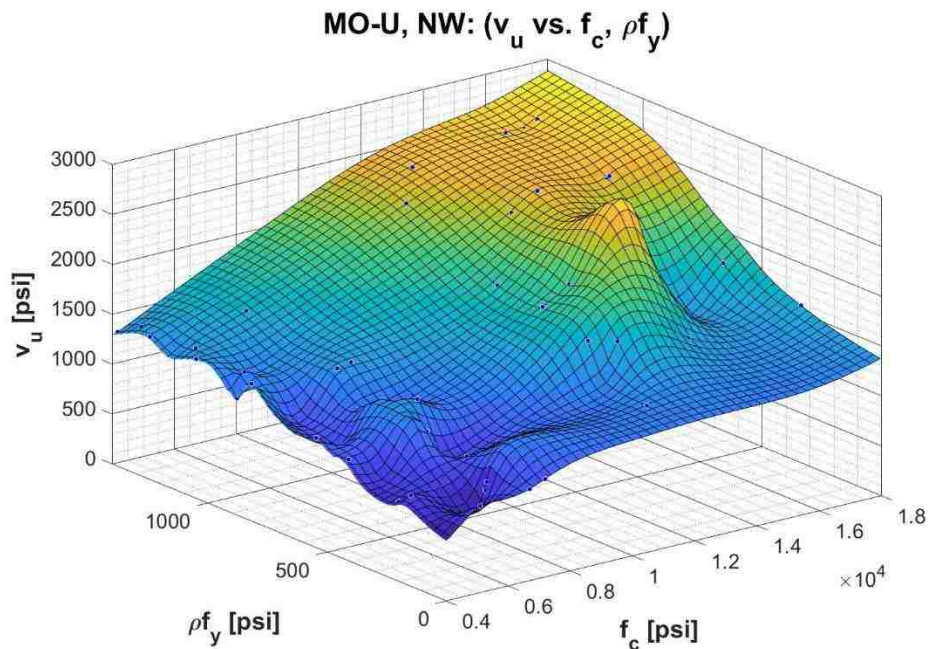


Figure 4.2.1.1: 3D shear strength plot for MO-U NW tests

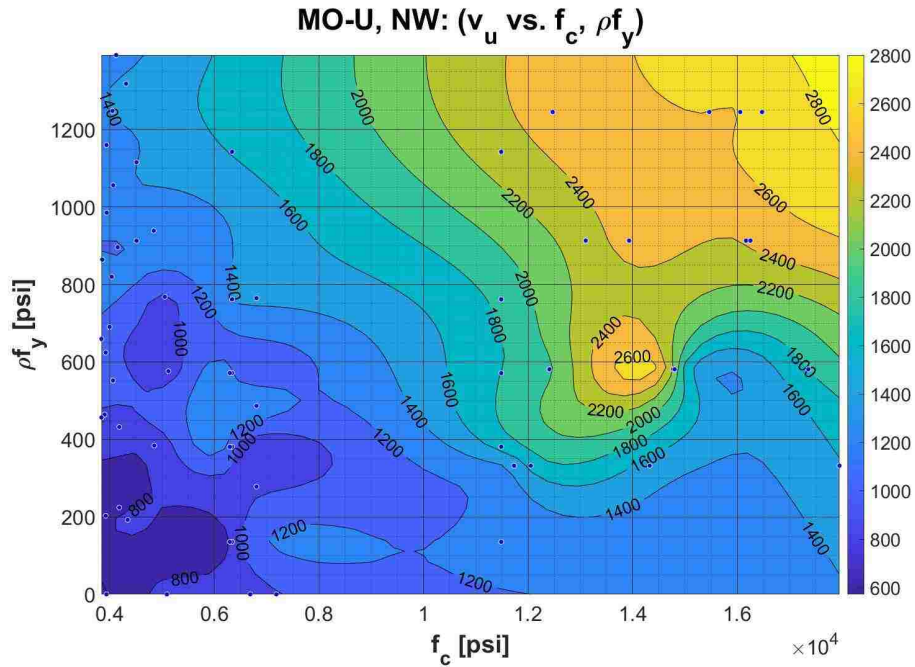


Figure 4.2.1.2: Shear strength contour plot for MO-U NW tests

The data for MO-U NW shows four major trends:

- The shear strength, v_u , generally increases with ρf_y .
- The shear strength is not zero when $\rho f_y = 0$, so some cohesive component of shear strength exists.
- The shear strength generally increases with f'_c .
- The shear strength increases much more slowly with ρf_y and f'_c at high values of those parameters. This phenomenon could be interpreted as an absolute upper bound on shear strength, or an upper bound on the usable value of f'_c , but the data is too sparse to be conclusive.

MO-P Interface:

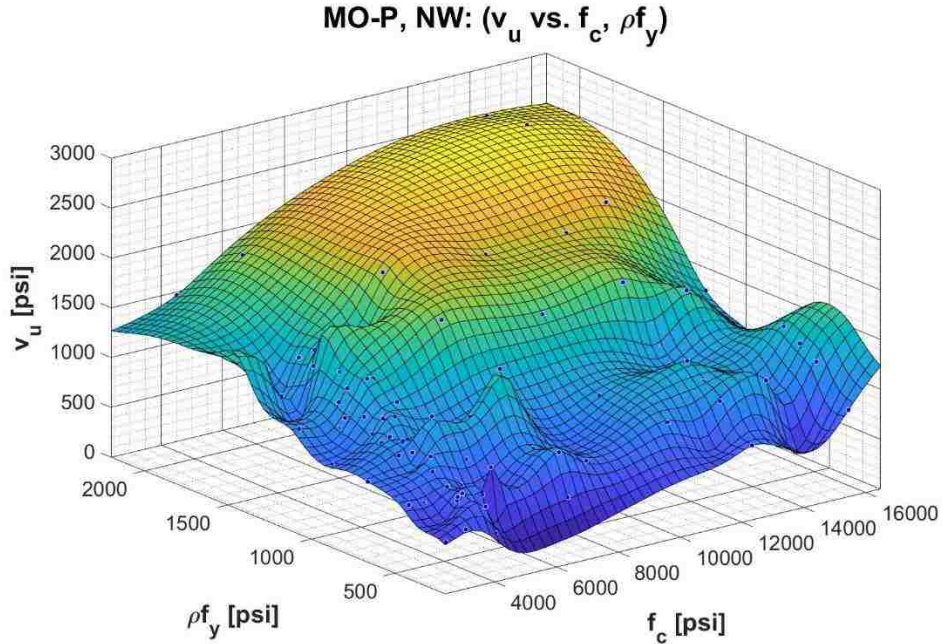


Figure 4.2.1.3: 3D shear strength plot for MO-P NW tests

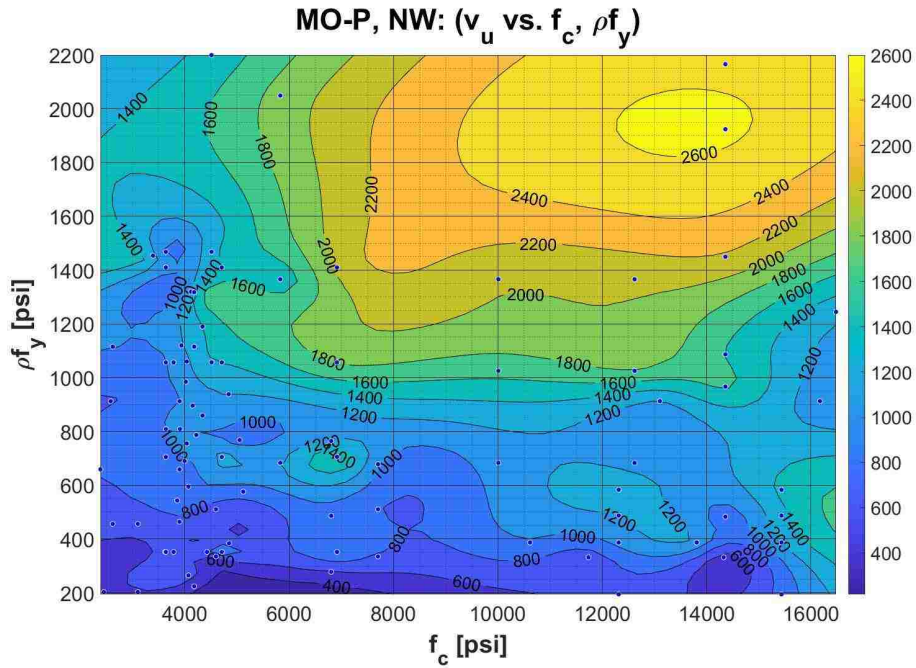


Figure 4.2.1.4: Shear strength contour plot for MO-P NW tests

The MO-P NW data showed the same trends as the MO-U-NW data, but the shear strengths were generally lower. At very high f_c , there are anomalous dips at $\rho f_y \approx 300$ psi and $\rho f_y \approx 1000$ psi. This is caused by sparsity of data and single anomalous data points in the center of the surface dips.

In both the MO-U NW and MO-P NW data, the irregularity of the surface, which indicates the scatter of the data, is greater at low ρf_y . This area of the 3D plots supports the existence of a cohesive component of shear strength, but is not totally conclusive. Cohesion depends on the tensile strength of the concrete, and so is expected to be more brittle, and hence, causes more scatter. At low ρf_y , the existence of cohesion seems to play a relatively important role and causes scatter in the data points. However, cracking will reduce cohesion, so the pre-cracked data should be expected to show less scatter at low ρf_y values, but this is not the case. Other explanations for the scatter at low ρf_y values are also plausible. For example, slight errors in the alignment of the test rig might have more influence on low-strength test specimens. Such information was not available through the test reports.

CJ-R Interface:

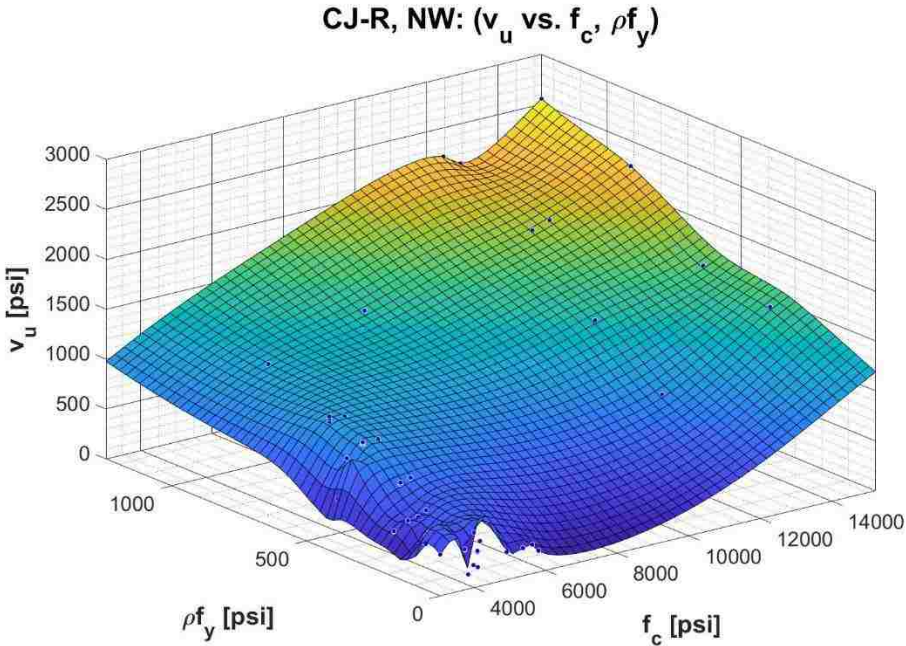


Figure 4.2.1.5: 3D shear strength plot for CJ-R NW tests

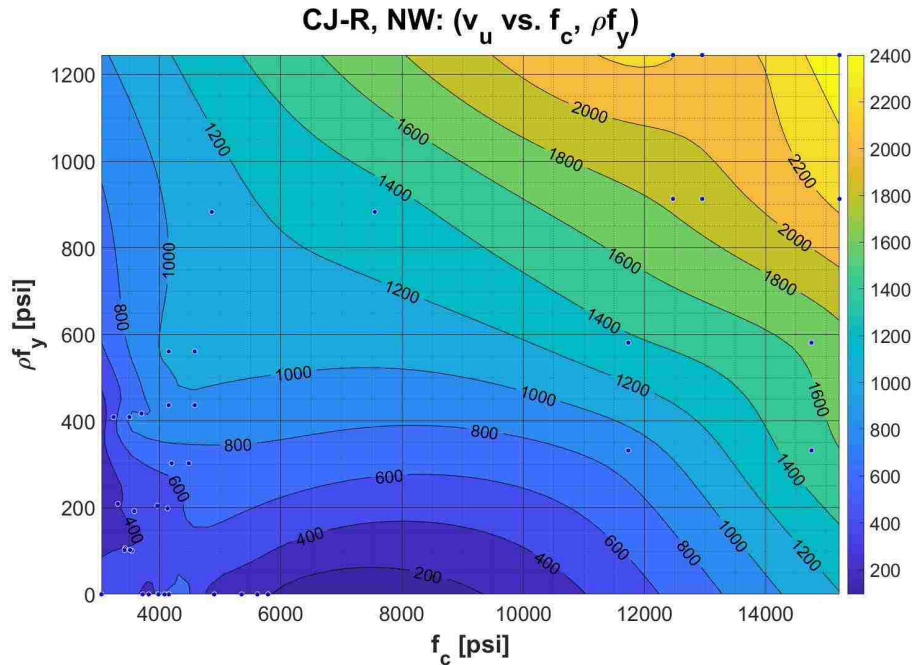


Figure 4.2.1.6: Shear strength contour plot for CJ-R NW tests

The CJ data is less voluminous than that for the MO data. The surface roughness is also not well-defined in test programs beyond the distinction of being “intentionally roughened” or not. Both features imply greater scatter and less reliability. This is particularly true for the CJ-S data, so only the CJ-R data is presented here. Note that the range of ρf_y and f_c for the CJ-R data are smaller than for the MO data, so the scales in the plots are different.

Despite these caveats, the overall trends are the same as for the MO specimens.

4.2.2 Effects of clamping stress and concrete strength

The plots presented in Section 4.2.1 show that these two variables are linked, so their influences are considered together in this section. The shear strength, v_u , increases with both parameters, so the analysis procedure was as follows:

- Treat the data for any one surface type and concrete density (LW or NW) as a separate subset.
- Within each subset, group the f_c values into three to five ranges, depending on the amount of data available.
- For each f_c range, plot v_u vs ρf_y .
- Fit a linear curve through the data, with a constant upper bound (in which case the curve becomes bilinear) if justified. Obtain the properties of the curve (zero v_u offset = cohesion, slope = μ , upper bound).
- Plot curve properties vs f_c . Fit a (bi)-linear curve to that data. Weight the data for each f_c by the number of points in the underlying v_u vs ρf_y curve.

An interesting outcome is that, for MO-U NW data, the shear strength can be characterized as:

$$v_u = c + \mu(\rho f_y) \leq v_{u,max}$$

Where:

$$c = c_0 + c_1 f'_c \leq c_{ub}$$

$$\mu = \mu_0 + \mu_1 f'_c \leq \mu_{ub}$$

$$v_{u,max} = v_{max0} + v_{max1} f'_c \leq v_{maxub}$$

This characterization is intended to help understand the data, and may be used to inform the evaluation and modification of existing models and development of a new one, if needed. The fitted curves chosen are linear, because the consistency and, in some regions, the volume, of data are judged to be insufficient to justify higher order polynomials.

For the MO-U NW data, the plots are shown in Figures 4.2.2.1 through 4.2.2.3. The values of the curve constants c_0 , c_1 , etc., are summarized in Table 4.2.2.1 for MO-U NW data.

Table 4.2.2.1: Summarized coefficients of cohesion and shear friction (MO-U NW data)

surface	density	c_0	c_1	c_{max}	μ_0	μ_1	μ_{max}
		(psi)	(psi/psi)	(psi)	(-)	(1e-5/psi)	(-)
MO-U	NW	273.4	0.0866	1212	0.2999	6.000	1.500

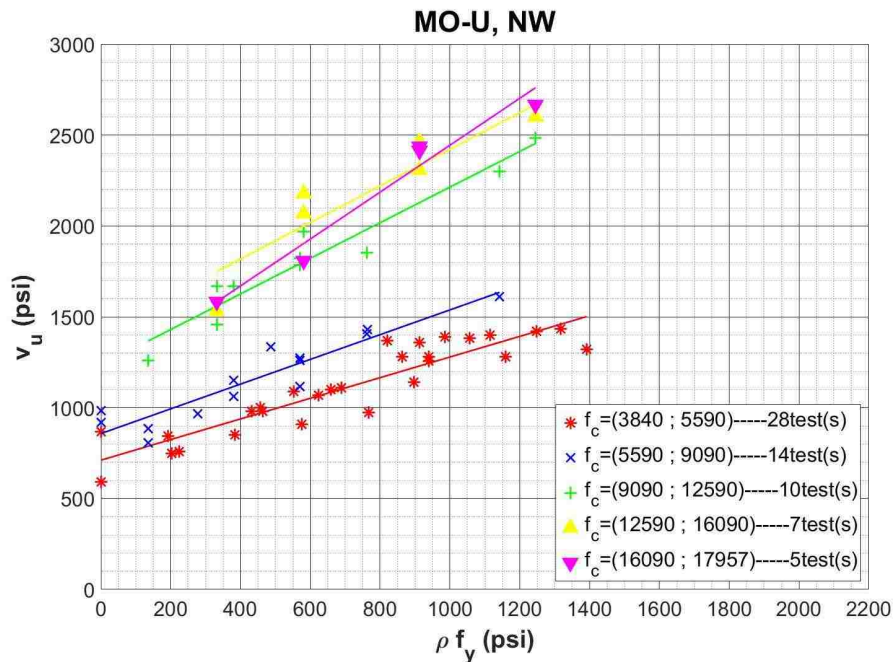


Figure 4.2.2.1: MO-U NW tests, grouped by f'_c

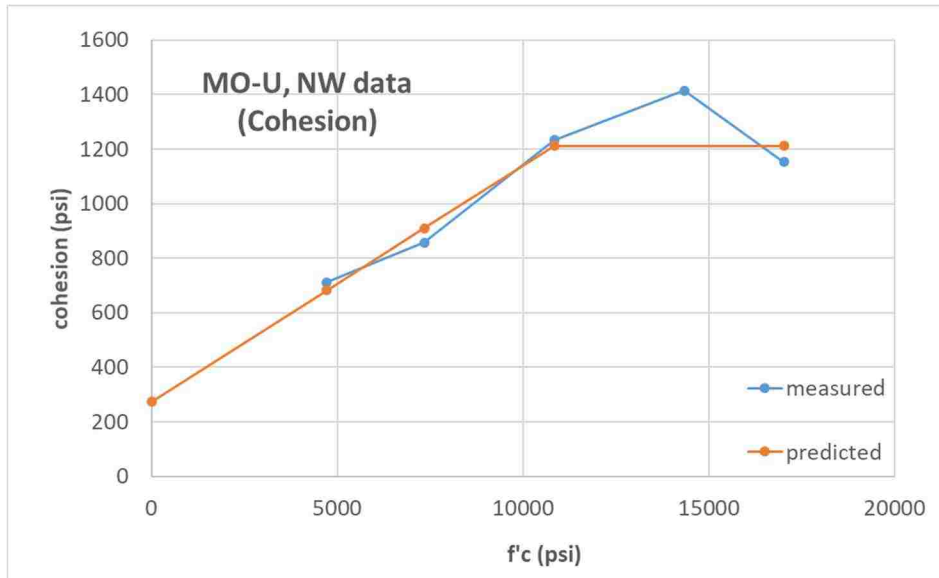


Figure 4.2.2.2: MO-U NW tests, cohesion vs f'_c

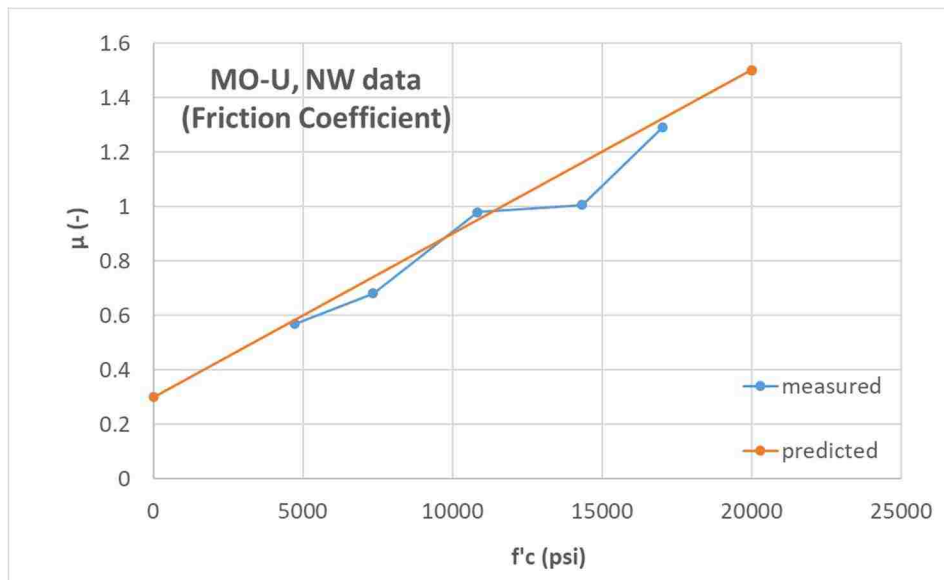


Figure 4.2.2.3: MO-U NW tests, friction coefficient vs f'_c

However, all the other datasets for different combinations of surface type and concrete density did not show a clear trend of increasing μ with increase of f'_c . The plots of ν_u vs $\rho f'_y$ for NW data for MO-P and CJ interfaces are shown in Figures 4.2.2.4 through 4.2.2.6 for comparison. They provide a visual evaluation of the amount of data available and the overall impact of f'_c in cohesion and shear friction. Overall, the shear strength seemed to increase with an increase of f'_c and eventually the shear strength stops growing at higher values of f'_c .

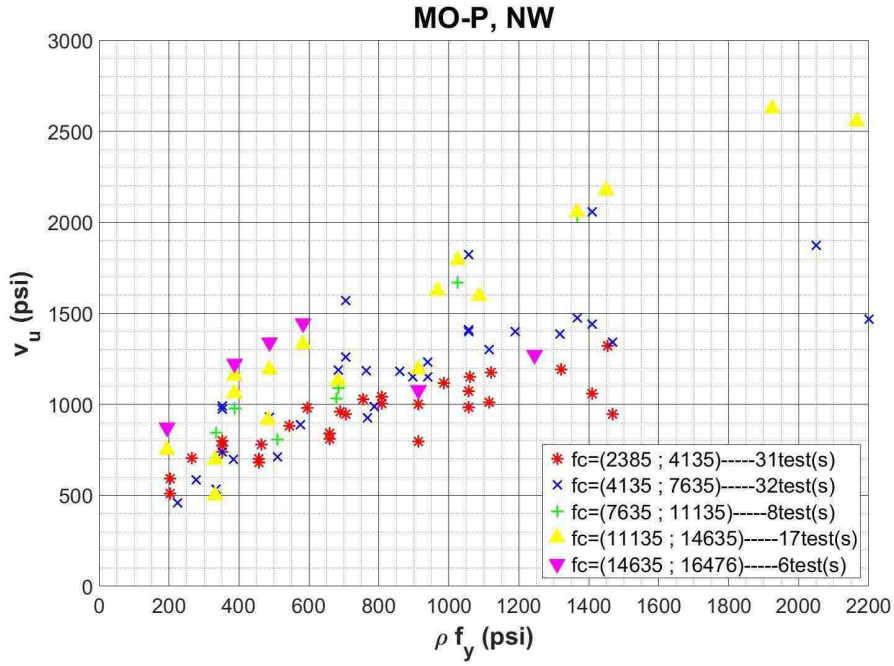


Figure 4.2.2.4: MO-P NW tests, grouped by f'_c

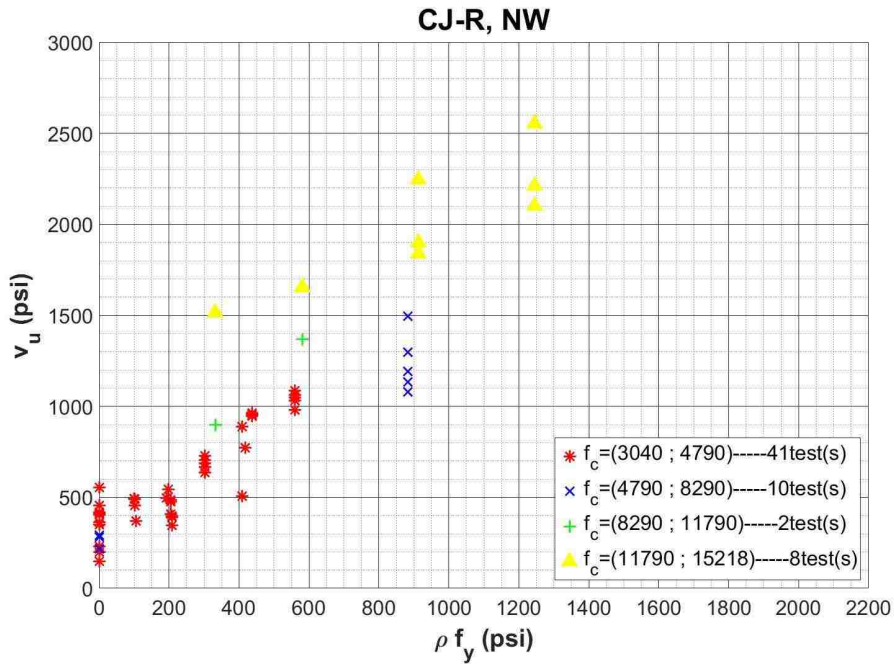


Figure 4.2.2.5: CJ-R NW tests, grouped by f'_c

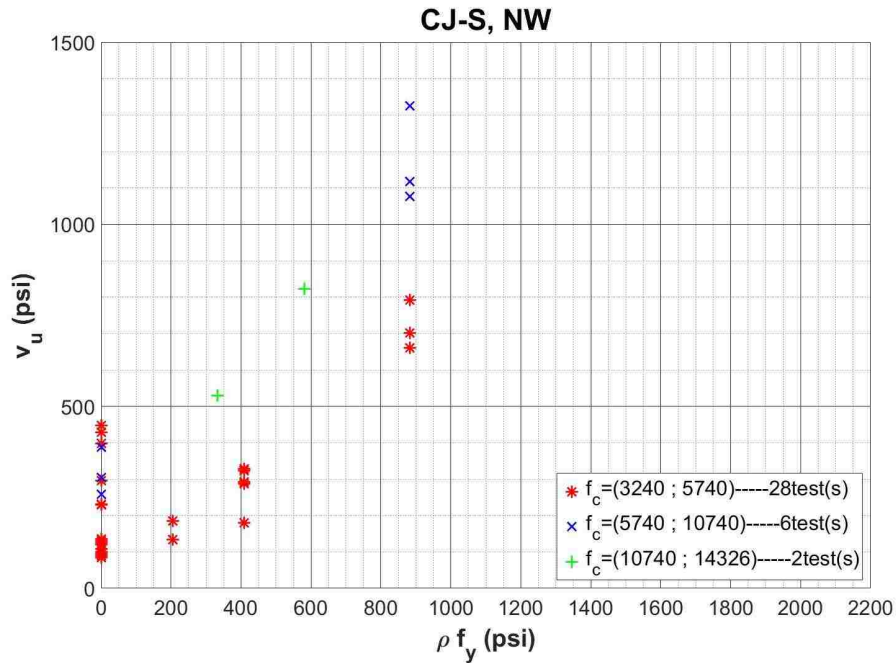


Figure 4.2.2.6: CJ-S NW tests, grouped by f'_c

4.2.3 Effect of Yielding Strength of Shear Reinforcement

To allow a smaller amount of reinforcement, high strength steel shear reinforcement is desired by designers. However, due to the upper limit on yielding strength in the applicable code provisions, reinforcements with $f_y > 60$ ksi are not permitted. There are only 5 test results with f_y between 110-140 ksi which is insufficient for drawing conclusions. The database has a reasonable amount of data with measured $f_y < 93$ ksi (up to Grade 80) which allows for analyzing data with $f_y < 93$ ksi only.

For the majority of the test programs, higher strength ($f_y > 80$ ksi) steel tend to be used only at high f'_c ; while lower strength ($f_y < 60$) or intermediate strength ($f_y = 60-80$ ksi) steel reinforcement were used with lower f'_c concrete. Due to such limited data distribution only few sets of data were able to show the effect of f_y . To eliminate the influence of the other parameters, shear strengths of NW concrete tests with $2.5 \text{ ksi} < f'_c < 4.5 \text{ ksi}$ for the following interfaces were shown:

- MO-P (See Figure 4.2.3.1)
- CJ-R reinforcement tests (See Figure 4.2.3.2).

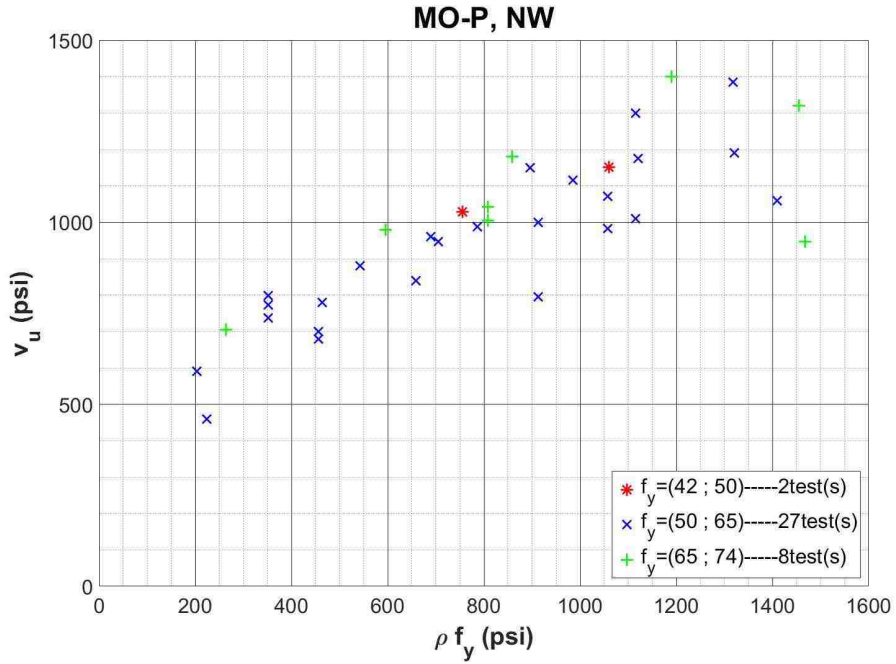


Figure 4.2.3.1: MO-P NW tests with $2.5\text{ksi} < f'_c < 4.5\text{ksi}$, grouped by f_y

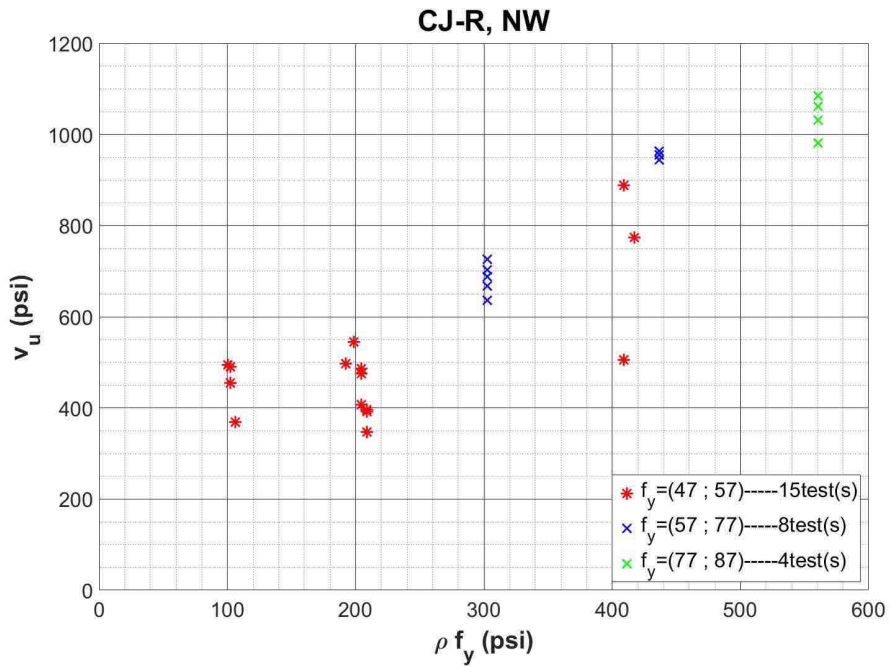


Figure 4.2.3.2: CJ-R NW tests with $2.5\text{ksi} < f'_c < 4.5\text{ksi}$, grouped by f_y

As shown in Figures 4.2.3.1 and 4.2.3.2, higher f_y steel reinforcement at least does not seem to decrease shear capacity at constant reinforcement ratio (when paired with NW concrete). The plots suggest that yielding strength of reinforcing steel up to Grade 80 should be allowed. This observation is

in agreement with Barbosa et al. (2017) where the authors observed that an increase in f_y (grade 60 vs. Grade 80) result in higher shear capacity when #5 bar used but negligible when #4 bar is used.

4.2.4 Effect of Concrete Type

In the current shear friction code provisions, lightweight concrete usage is permitted with the use of concrete modification factor, λ . Concrete modification factor is 0.85 for sand lightweight concrete and 0.75 for all lightweight concrete to account for reduced strength of lightweight concrete compared to normal weight concrete. To isolate the influence of concrete type (normal, sand lightweight and all lightweight) on shear strength, test results of NW concrete tests and LW concrete tests for each interface were compared in the same concrete compressive strength ranges.

In each plot, the concrete/aggregate type is indicated with additional marks on top of the main circle notations for applicable data chosen to plot. Each red solid line is the average shear strength value of the points that are in the range of ρf_y between the beginning and end of the line. The dashed lines are average values plus or minus the standard deviation of the points fall in the same range of ρf_y as the solid line. Counts of the points plotted are indicated below each line.

The maximum ρf_y in the data base is 2200psi for NW MO-P interface test data. Therefore, the x-axis of all plots in this section are set to a maximum of 2200 psi for ease of understanding and comparing the plots. Also, all the y-intercepts are not necessarily true cohesion terms at zero reinforcement. They are only there to help get better sense of the shear strength trend visually. For each interface, the ranges of f'_c for the applicable NW and LW concrete are listed. Only the data that falls in the range of common f'_c among the two ranges of f'_c are specified and plotted.

MO-U Interface:

The f'_c range of the database for MO-U interface:

NW: $3.8 < f'_c < 18$ ksi

LW: $f'_c < 5$ ksi

(Common among the above two ranges, hence plotted: $f'_c < 5$ ksi.)

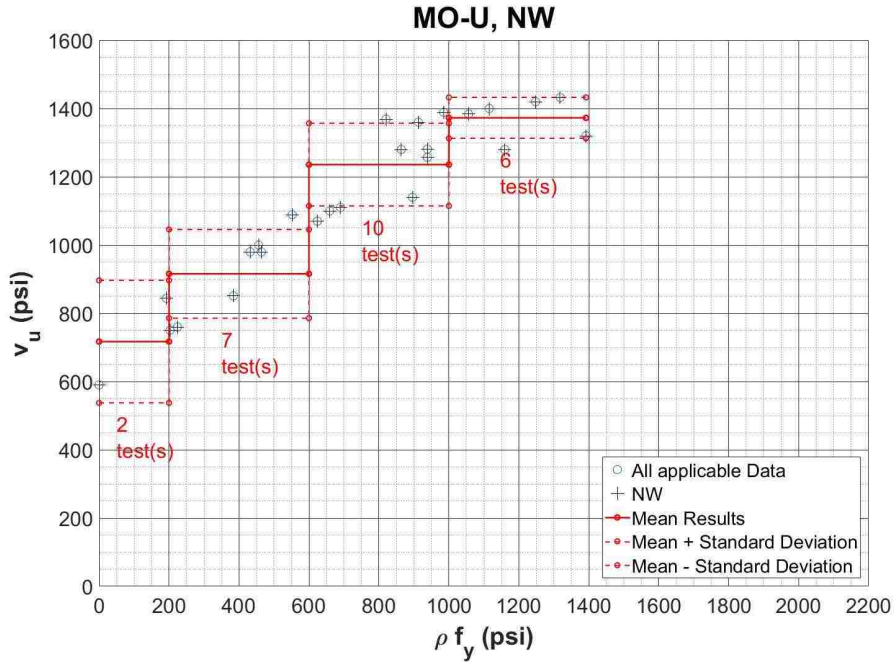


Figure 4.2.4.1: MO-U NW tests in the specified f'_c range

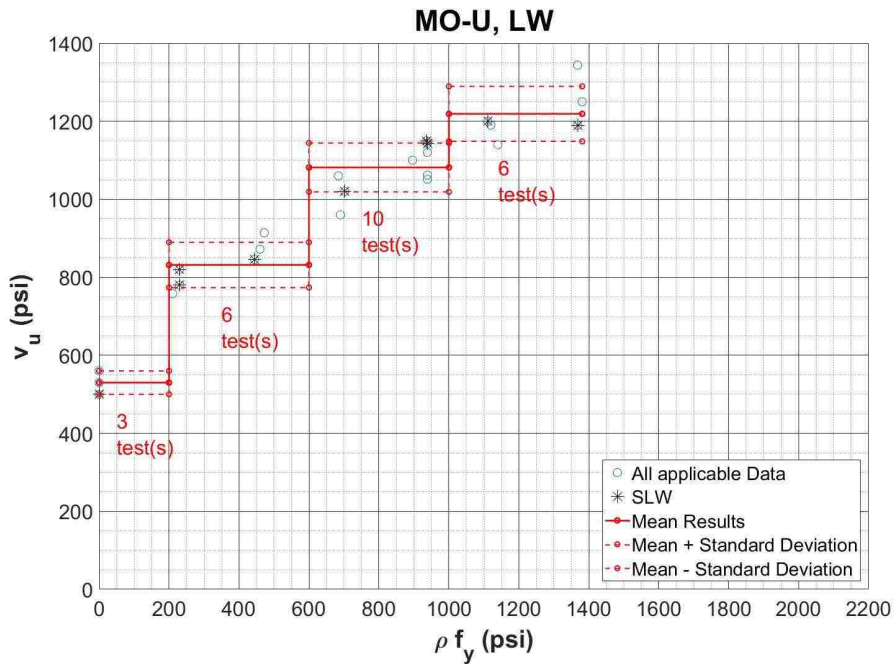


Figure 4.2.4.2: MO-U LW tests in the specified f'_c range

As shown in Figure 4.2.4.1 and 4.2.4.2, the ratio between the average shear strength, v_u , of LW data and NW data in each ρf_y range (separated with red circles) seem to be between 0.74-0.91 (See Table 4.2.4.1). This means that the use of a concrete modification factor of code provisions (between 0.75-

0.85) is generally close to real values for the MO-U interface. However, as can be seen in Figure 4.2.4.2, the strength difference between SLW and ALW concrete test results is inconsistent is insufficient to justify different ratios of 0.75 and 0.85.

Table 4.2.4.1: MO-U, comparison between LW and NW concrete test results

MO-U:	unit: [psi]				average
	100	400	800	1200	
ρf_y	100	400	800	1200	
$(\overline{v_{NW}})_{\pm}(\sigma_{NW})$	(717)+/-(180)	(916)+/-(130)	(1236)+/-(121)	(1373)+/-(60)	
$(\overline{v_{LW}})_{\pm}(\sigma_{LW})$	(530)+/-(30)	(832)+/-(58)	(1082)+/-(63)	(1219)+/-(71)	
$\lambda_{calc} = \frac{average\ v_{LW}}{average\ v_{NW}}$	0.74	0.91	0.88	0.89	0.85

MO-P Interface:

The f'_c range of the database for MO-P interface:

NW: $2.3 < f'_c < 16.5$ ksi

LW: $2.0 < f'_c < 11$ ksi

(Common among the above two ranges, hence plotted: $f'_c < 11$ ksi.)

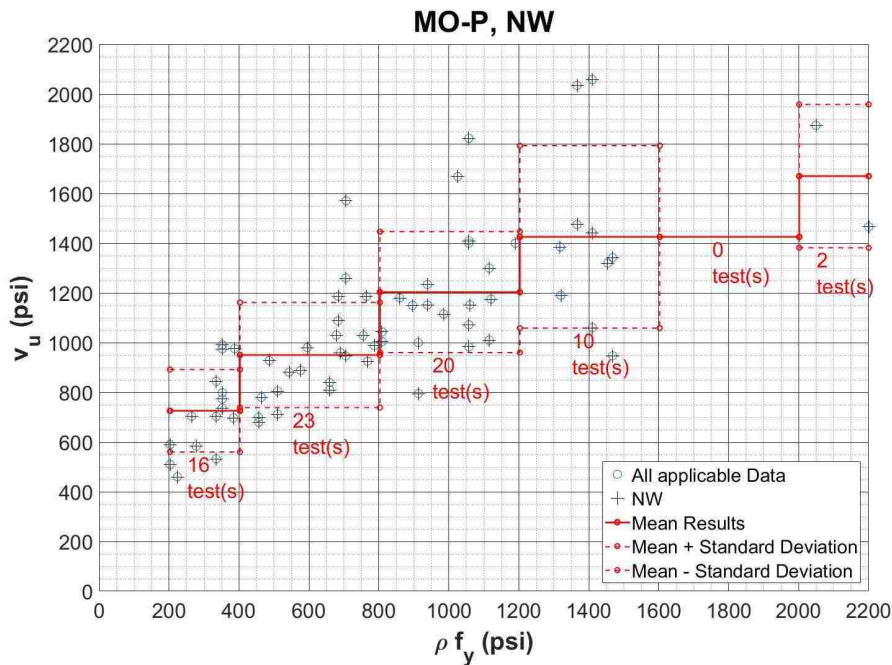


Figure 4.2.4.3: MO-P NW tests in the specified f'_c range

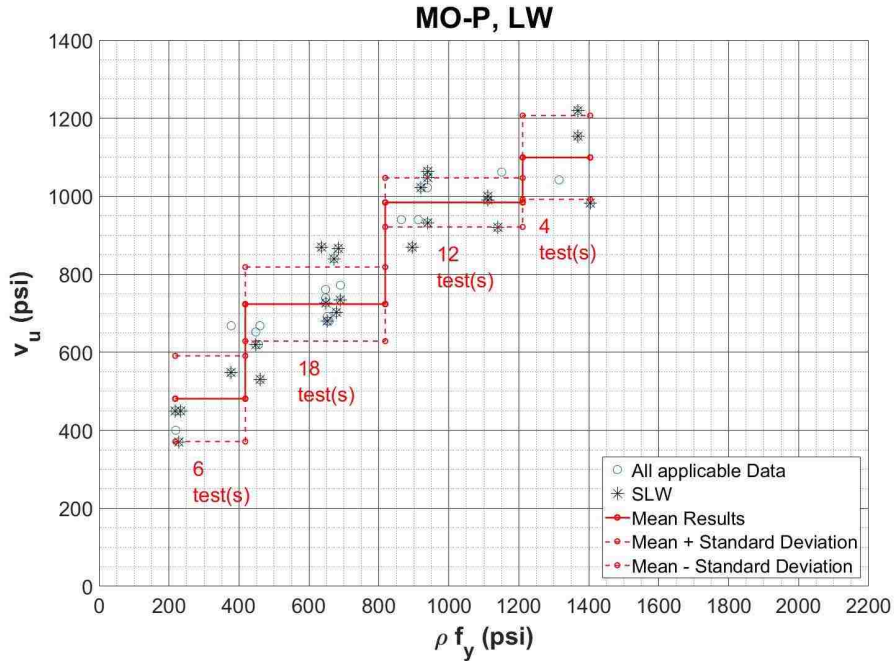


Figure 4.2.4-4: MO-P LW tests in the specified f'_c range

Unlike the MO-U interfaces, the strength ratios between NW and LW concrete data in each ρf_y ranges (separated with red circles) were between about 0.66-0.82 (See Table 4.2.4.2). This may bring the use of λ a bit on the unconservative side if the equation for NW concrete captured the shear strength absolutely accurate prior applying safety factors. Similar to the MO-U LW plot (Figure 4.2.4.2), the MO-P LW plot (Figure 4.2.4.4) shows the inconsistency of 0.85 to 0.75 ratios between SLW and ALW concrete tests.

Table 4.2.4.2: MO-P, comparison between LW and NW concrete test results

MO-P:	unit: [psi]				average
	ρf_y	300	600	1000	
$(\overline{v_{NW}})_{\pm}(\sigma_{NW})$		(726)+/-(166)	(950)+/-(211)	(1203)+/-(243)	(1425)+/-(367)
$(\overline{v_{LW}})_{\pm}(\sigma_{LW})$		(481)+/-(110)	(724)+/-(95)	(984)+/-(63)	(1100)+/-(107)
$\lambda_{calc} = \frac{average\ v_{LW}}{average\ v_{NW}}$		0.66	0.76	0.82	0.77

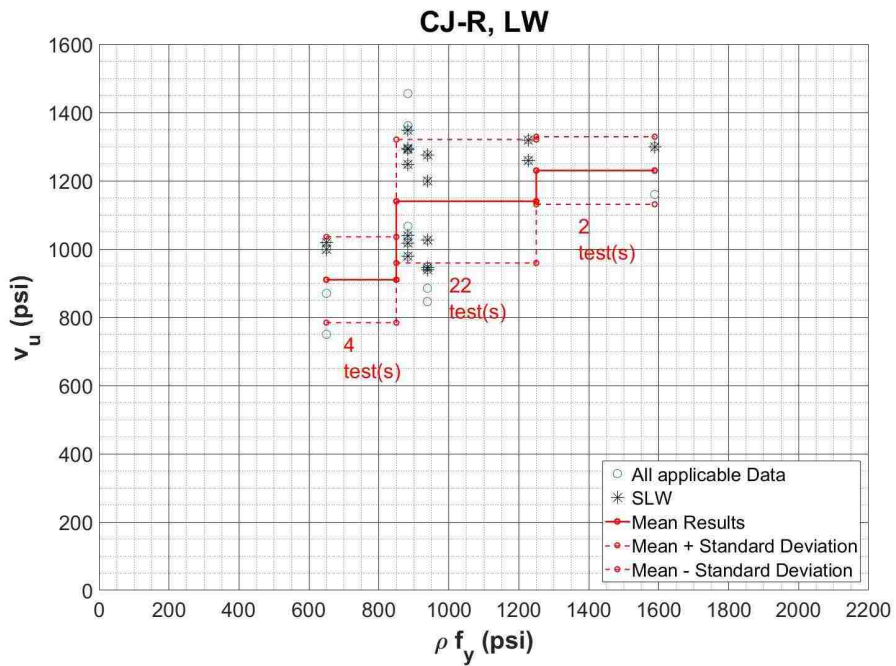
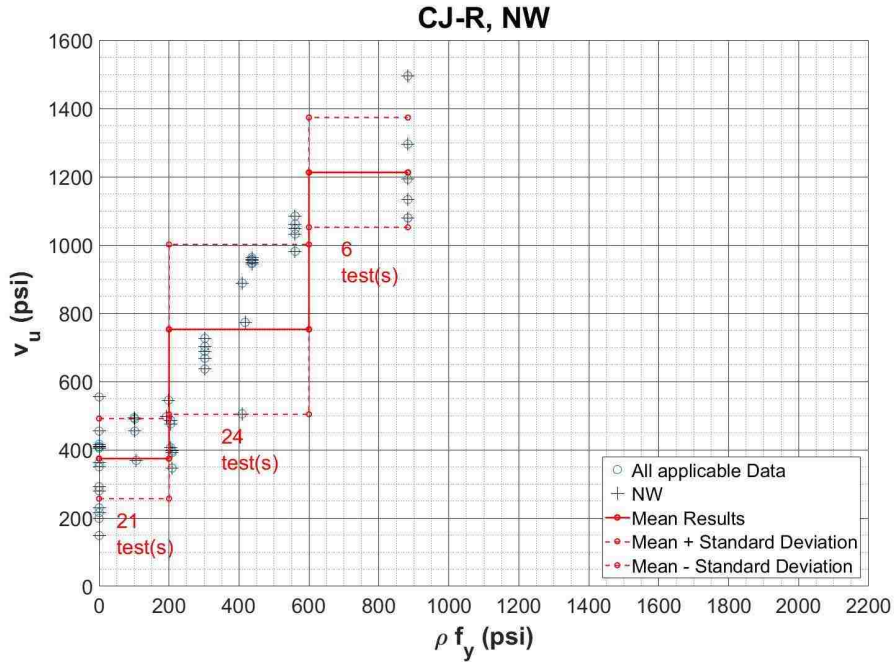
CJ-R Interface:

The f'_c range of the database for CJ-R interface:

NW: $3.8 < f'_c < 15.2$ ksi

LW: $4.4 < f'_c < 7.9$ ksi

(Common among the above two ranges, hence plotted: $f'_c < 7.9$ ksi.)



When NW and LW concrete tests at around $\rho f_y=700$ psi and $\rho f_y=900$ psi were compared, the strength ratios between them seem to be about 0.75 (See Table 4.2.4.3). This suggests that the current λ values in the codes are conservative for comparing LW concrete to NW concrete specimens.

Table 4.2.4.3: CJ-R, comparison between LW and NW concrete test results

CJ-R:	unit: [psi]
ρf_y	800
$(\overline{v_{NW}}) \pm (\sigma_{NW})$	(1213)+/-(161)
$(\overline{v_{LW}}) \pm (\sigma_{LW})$	(910)+/-(126)
$\lambda_{calc} = \frac{\text{average } v_{LW}}{\text{average } v_{NW}}$	0.75

CJ-S Interface:

The f'_c range of the database for CJ-S interface:

NW: $3.4 < f'_c < 14.4$ ksi

LW: $4.3 < f'_c < 7.9$ ksi

(Common among the above two ranges, hence plotted: $f'_c < 7.9$ ksi.)

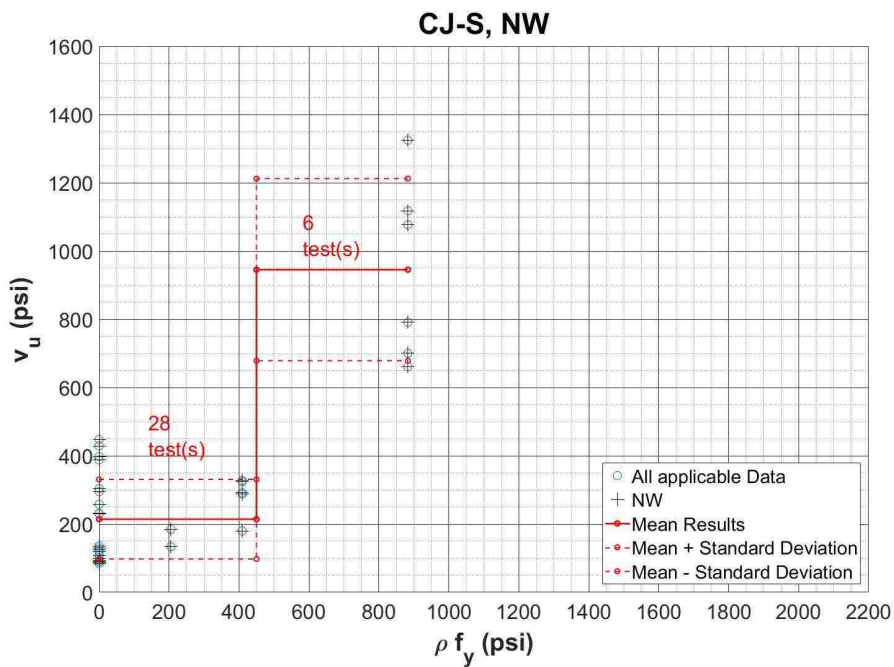


Figure 4.2.4.7: CJ-S NW tests in the specified f'_c range

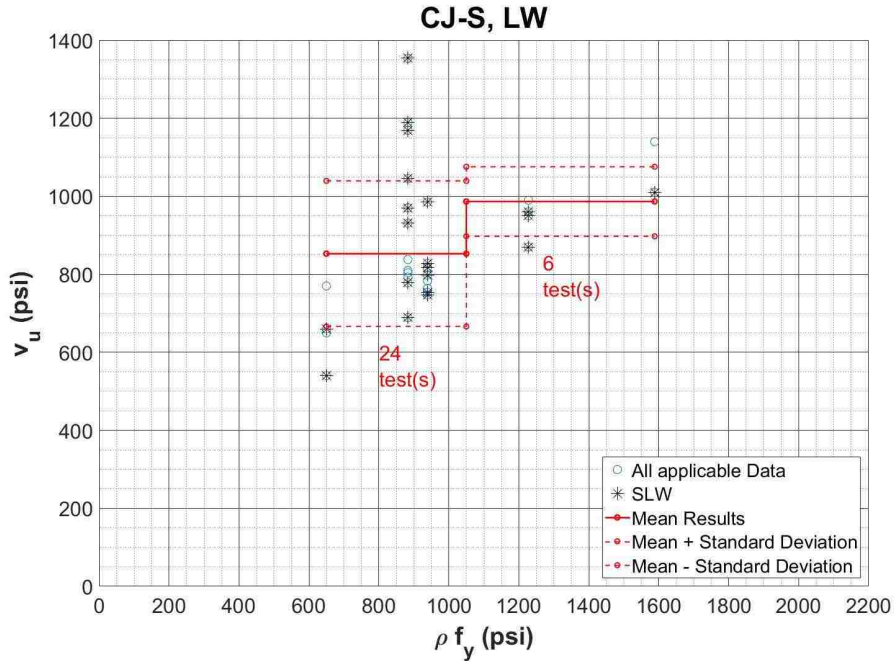


Figure 4.2.4.8: CJ-S LW tests in the specified f'_c range

Figure 4.2.4.7 and 4.2.4.8 show much variation in strength even at the same or at similar clamping stresses especially around $800 < \rho f_y < 900$ psi. All the LW CJ-S and NW CJ-S with non-zero reinforcement test data were collected from Sneed et al. (2013) and Sneed et al. (2016). The nature of CJ-S interface strength can be highly dependent on and sensitive to the method of surface preparation of the test. Depending on what type of form was used, the roughness of the interface can vary. (Perfectly smooth vs. somewhat rough but not intentionally roughened).

Despite all the variations in strength, the average strengths of NW and LW concrete were fairly close ($\lambda = 0.9$) at $\rho f_y = 800-900$ psi (See Table 4.2.4.4). It was also discussed in the work of Sneed et al. (2016) that shear strength of CJ-S interfaces were not dependent on unit weight of concrete.

Table 4.2.4.4: CJ-S, comparison between LW and NW concrete test results

CJ-S:	unit: [psi]
ρf_y	800
$(\overline{v_{NW}}) \pm (\sigma_{NW})$	(945) +/- (267)
$(\overline{v_{LW}}) \pm (\sigma_{LW})$	(853) +/- (187)
$\lambda_{calc} = \frac{average\ v_{LW}}{average\ v_{NW}}$	0.90

Summary of lightweight concrete factor:

Figure 4.2.4.9 summarizes all the lightweight concrete modification factors (λ) previously discussed in this section. This plot shows considerable variation of λ with ρf_y for interface types where variation of ρf_y is available. The average trends of MO interfaces suggest that the λ values used in the current versions of ACI and PCI code provisions should be kept the same. The only potential exception is that CJ-S interfaces seem to yield similar shear strengths for both NW and LW concrete data. However, further research is necessary to examine λ factors for CJ-S at different ρf_y ranges.

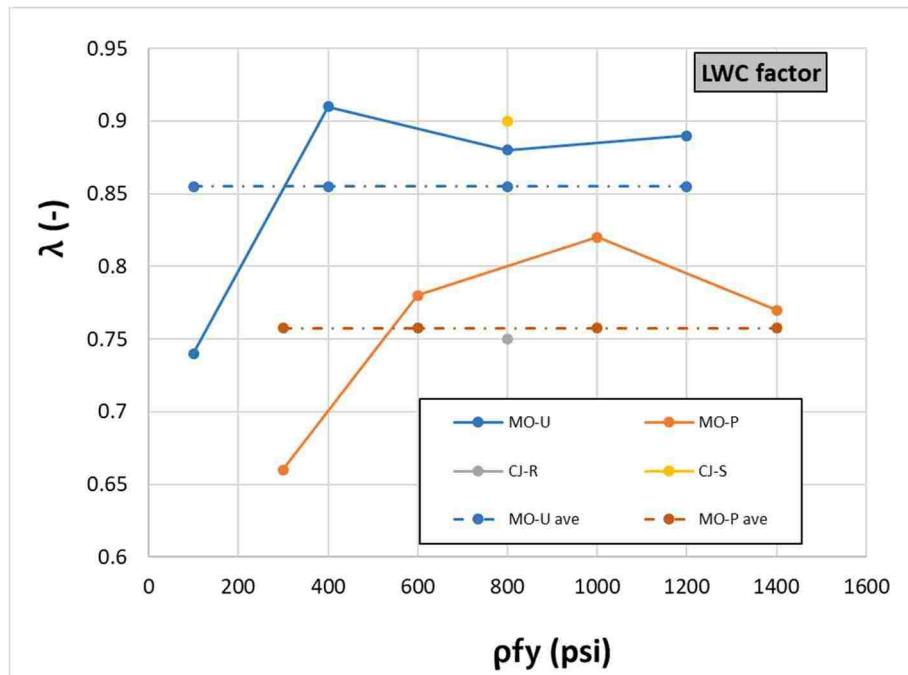


Figure 4.2.4.9: Comparisons of λ vs ρf_y among interfaces

4.2.5 Effects of Other Parameters

Due to limitations of the scope of the project and the extent of the database, the effects of other parameters could not be studied in depth. The following were notable based on preliminary observation and comments from the literature review (main references are indicated in parenthesis for each parameter):

Parameters which may increase shear strength:

Table 4.2.5.1: Suggested reference works for effects of other parameters which may increase shear strength

Parameters/variables	Suggested references:	Additional comments (if any):
Use of UHPC high strength concrete	Crane, 2010	

Subjecting specimens to sustained load prior to loading to failure	Frenay, 1985	
Extra vibration in the concrete preparation	Jose, 1985	
Bigger bars		the database only consist of test data where diameter of reinforcing steel was between 0.16"-0.63"
Light weight aggregate type (SLW vs ALW)	Sneed et al., 2013 Sneed et al. ,2016	Among the use of lightweight concrete, sand lightweight is believed to have higher shear strength than all-lightweight concrete
Externally loaded additional normal force	Mattock et al., 1975 Mattock and Hawkins, 1972	
Maximum aggregate size	Maekawa et al., 1989	The database range for max aggregate size is 0.5"-1.26" for NW concrete and 0.375"-0.75" for LW concrete. No significant impact was captured in any of the early stages of visual parameter examinations.)

Parameters which may decrease shear strength:

Table 4.2.5.2: Suggested reference works for effects of other parameters which may decrease shear strength

Parameters/variables	Suggested references:	Additional comments (if any):
angled reinforcement	Nagle and Kuchma, 2007 Mattock, 1973	When the shear reinforcement is crossing the interface at an angle other than 90° angle, clamping stress is usually taken as product of sine of the angle and nominal clamping stress. This research program did not focus on angled reinforcement.

nonstandard roughening methods (for CJ-R interface)	Jose, 1985	Unconventional roughening methods such as burlap roughening or brooming at an angle other than 90° angle
smooth small diameter bars	Mansur et al., 2008	

Further research is necessary to confirm the effects of the parameters mentioned above especially the ones which are not followed by any reference in parenthesis.

4.3 Proposed Model

4.3.1 Development of the Model

Motivation for model development

From literature review, models proposed by different scholars and shear friction design provisions in codes were collected (See Chapter 2 for available design equations). Most of the past models were based on, and checked against, either their own test data or data from a few chosen previous test programs. As addressed in Sections 3.2.1 and 3.2.2, the applicable design provisions also mostly relied on limited number of test data from the 1960s and the 1970s and have changed little since then. Using the database for concrete-to-concrete interfaces, the performances of the past models and shear friction design provisions were examined. The accuracies of the past models will be discussed in Section 4.3.4.

The main form of the design provisions including the ACI, PCI, and AASHTO is based on shear friction only or a constant cohesion term on top of it. This particular form does not provide a clear linkage to the physics of the shear transfer behavior. By looking at the common forms of past models and their performances, it was necessary to develop a new model. However, it should be noted that there were a few exceptional models that perform well for certain interfaces. One of the goals of this research program was to develop a statistically fitted unified model (using the database) that is simple and applicable to all concrete interface types.

Key observations from Section 4.2

Regarding the linked influence of f'_c and ρf_y :

- At small clamping stress, increase in f'_c does not effectively increase interface shear strength compared to cases where intermediate or high clamping stress is provided. This suggests that at small f'_c range, concrete controls shear strength of the interface. In the intermediate range of f'_c , the concrete components of the system is strong enough to enable the benefits of having higher ρf_y . This suggests that there should be a f'_c dependent upper limit to avoid overestimation of shear strength when weak concrete interface is highly reinforced.

- Also, as f'_c approaches certain high values (will be noted as $f'_{c,crit}$) the benefits from strong concrete maxes out and shear reinforcement start to control the shear strength of the interface. This value was close to 11 ksi when observable.
- It can be observed that the average shear strength at $\rho f_y = 0$ is not equal to zero for interfaces for which unreinforced test data were available. For such interfaces, approximate curves fitted to the corresponding data seemed to intercept y-axis (the shear strength axis) at non-zero y-values. Unreinforced test data were not available for MO-P interfaces and LW CJ-S. For conservativeness, it is better to set shear strength estimation of MO-P interface to zero when $\rho f_y = 0$.
- There appears to be a potential trend of μ increasing with f'_c for MO-U interface, but this trend will not be adopted in the new model both for simplicity and a small doubt about the trend.

Other observations:

- LW data generally have smaller shear strength than NW data. However, the same observation was not clearly true for CJ-S interface clearly. The average shear strengths of CJ-S NW data and LW data were close. However, it is necessary to mention that strength of CJ-S interface vary due to its nature of being sensitive to the variation of surface preparations. The number of CJ-S data points is also small. For conservativeness, the traditional λ values should be kept the same until further research.
- Up to Grade 80, all transverse reinforcement contributes equally to shear strengths of interfaces as long as the ρf_y is the same.

Based on the observations mentioned above several forms of models were tried:

Note that, in the models, the symbol v_n is used for the shear stress, because it refers to the nominal shear strength (i.e. capacity) to be used in design.

Model A: Initially to catch the effect of combination of higher f'_c and higher ρf_y resulting in higher shear strength, v_u , the following form was tried and calibrated against corresponding calibration data from the database:

$$v_n = (A_1 + A_2 f'_c)^{A_3} * (A_4 + A_5 \rho f_y)^{A_6} \text{ with } f'_c \text{ limited to certain } f'_{c,crit} \text{ values.}$$

(The exponents A_3 and A_6 were restricted to be in between 0 and 2 and the rest of the coefficients were set free.)

In the calibration process, either one of the following was minimized to solve for the coefficients:

$$\sum \left| \left(1 - \frac{v_{calc}}{v_{exp}} \right) \right| \text{ is minimized. (Better for small } v_u \text{)}$$

$$\sum |v_{exp} - v_{calc}| \text{ is minimized. (Better for big } v_u \text{).}$$

This form performed well resulting in overall good agreement with real test data mathematically. However, the main form of this model was judged to be too complicated for design purposes and was not suitable for explaining the mechanics of shear transfer.

Model B: The following simple form was then tried:

$$v_n = A_1 f_c'^{A_2} + A_3 \rho f_y^{A_4} \text{ with } f_c' \text{ limited to } f_{c,crit}'.$$

This form performed as well as model A and involves a smaller number of independent coefficients. Thus, upper limits were applied on top of this main form of the model.

Model C: The next form of the model was:

$$v_n = \lambda [A_1 f_c' + A_2 \rho f_y] \leq \min \left\{ \begin{matrix} K_1 f_c' \\ K_2 \end{matrix} \right\}$$

$$f_c' \leq f_{c,crit}'$$

$$f_{y,test} \leq 93 \text{ ksi (or GR 80)}$$

$\lambda = 1.0, 0.85,$ and 0.75 for normal, sand-lightweight, and all-lightweight concrete respectively.

All units are in psi.

Coefficients were solved mathematically. The upper bound coefficients K_1 and K_2 were chosen by manual trials based on real test data availability. It should be noted that, by definition, the amount of data available near the extreme shear stress values is limited. Therefore K_1 and K_2 values are tentative and likely to be revised as more high strength data becomes available. For each interface type (MO-U, MO-P, CJ-R, CJ-S), K_2 values were chosen to be rounded up or down values of the maximum v_u of the available data. K_1 values were chosen to make sure that in the combination ranges of small f_c' with high ρf_y , v_u would not be taking advantage of the high clamping stress when the concrete is not strong enough to support big loads.

Figure 4.3.1.1 is a 3D visualization of the model and explains each surface. Blue dots in the figure are some, but not all, of the calibration data. (Note that Figure 4.3.1.1 is not the representation of the final model and is only here as a visually aid for this earlier version of model.)

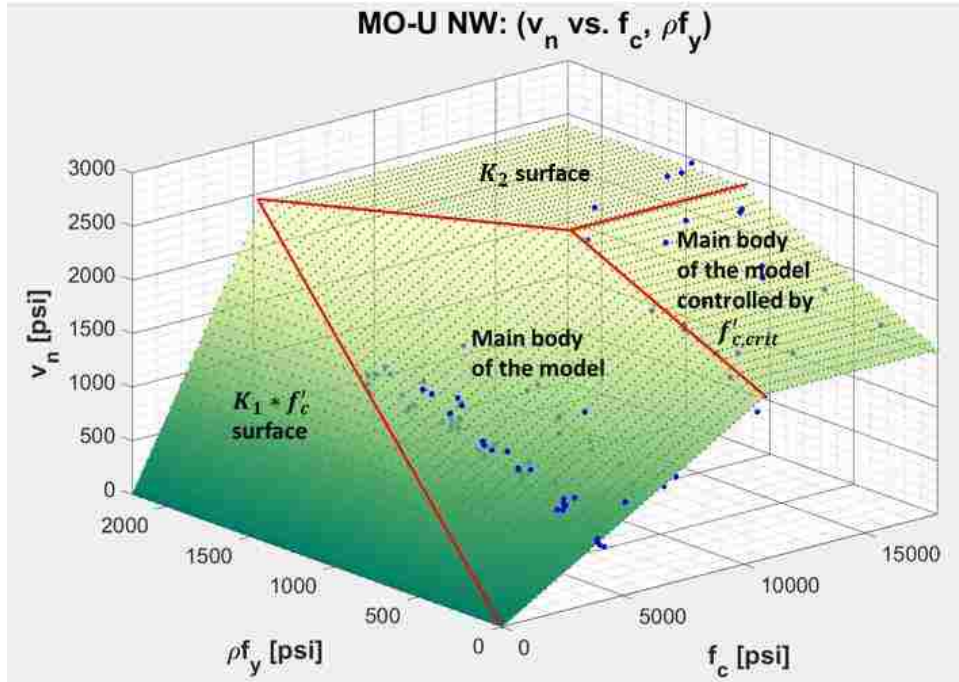


Figure 4.3.1.1: Example 3D surface of the trial model 3

However, the slopes that created the $K_1 f'_c$ upper limit were steep. This upper limit alone would imply that, at a combination of small f'_c and intermediate or high ρf_y , v_u would increase dramatically with a slight increase of f'_c . As a result, it became clear that adopting another upper limit (with a form: $K_i * f'_c + K_j$) was necessary. The method employed to manually choose this additional limit was connecting the $K_1 f'_c$ controlled (small f'_c and high ρf_y) region to the plateau surface (due to K_2) at smaller rate.

Although $f'_c = 0$ is not practical, the $K_1 f'_c$ limit surface needs to meet the ρf_y axis so that mathematically $v_u = 0$ when $f'_c = 0$.

Final Model: The final form of the model is:

$$v_n = \lambda(A_1 * f'_c + A_2 * \rho f_y) \leq \lambda \begin{pmatrix} K_1 * f'_c \\ K_2 * f'_c + K_3 \\ K_4 \end{pmatrix}$$

All units are in psi. Note that the subscripts of K values are different than in the previous models.

Notes:

$$f'_c \leq f'_{c,crit} = 11,000 \text{ psi}$$

$$f_{y,test} \leq 93 \text{ ksi (or GR 80)}$$

$$\lambda = \begin{cases} NW: 1.0 \\ SLW: 0.85 \\ ALW: 0.75 \end{cases}$$

λ may be dropped for CJ-S interface if additional experimental proof is provided.

Table 4.3.1.1: Summary of coefficients of the final model

	A_1	A_2	K_1	K_2	K_3 [psi]	K_4 for NW [psi]	K_4 for LW [psi]
MO-U	0.09	1.2	0.3	0.17	500	2400	1500
MO-P	0	1.2	0.3	0.17	500	2000	1400
CJ-R	0.04	1.2	0.25	0.17	330	2000	1400
CJ-S	0.02	0.75	0.13	-	-	1000	1000

In the final model, all the concerns mentioned in discussion of the trial model type 3 have been taken into account. The calibration of coefficients will be discussed in Section 4.3.2. As discussed in Chapter 3, the majority of the database is from NW concrete tests. All calibration NW data for each interface were fitted first and then concrete modification factor, λ , were applied to the model. All coefficients are tabulated in Table 4.3.1.1.

Figure 4.3.1.2 shows an example strength prediction surface created for MO-U NW interface and the controlling surfaces of all limits. Blue dots are real calibration points from the database. Some of the blue points are average shear strengths of multiple points at the same coordinates of ρf_y and f'_c when multiple tests with same parameters were available.

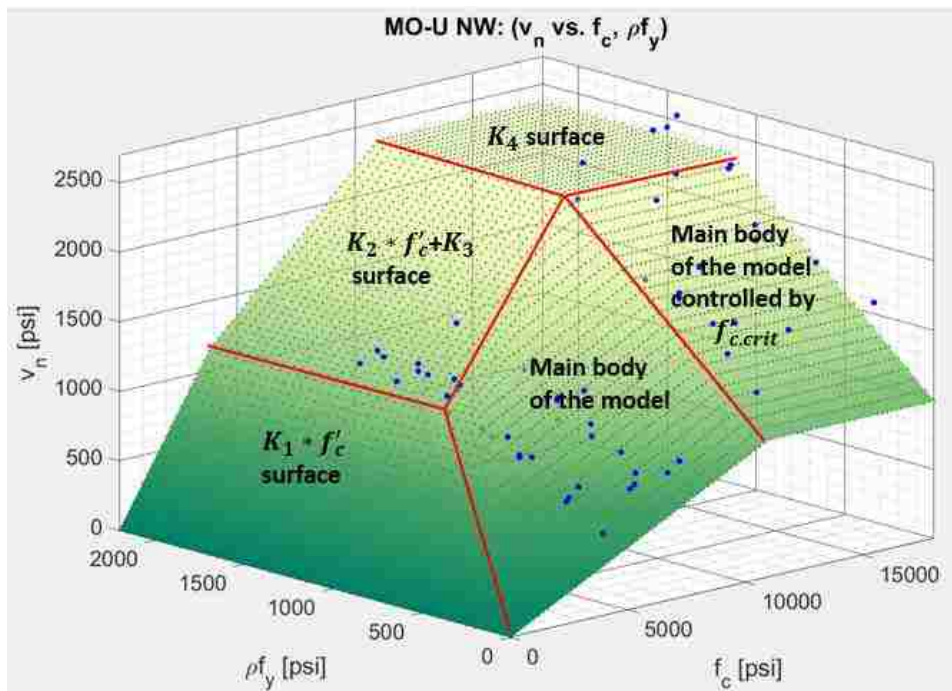


Figure 4.3.1.2: Example 3D surface of the final model

The K_4 upper bound limits were based on the highest shear stress values available in the database for each interface and concrete types. The K_4 values for LW datasets were chosen such that the

corresponding K_4 values multiplied by the concrete modification factors were close to the highest shear stresses available in the database.

In Section 4.2, for interfaces for which high f'_c data available, it was observed that the benefit of having high f'_c maxes out around 11 ksi. CJ-R and CJ-S interfaces did not have clear trend for $f'_{c,crit}$ due to lack of high f'_c data. Although high f'_c data for MO-P interface were available and $f'_{c,crit}$ seemed to be close to 7ksi. Even though $f'_{c,crit}$ seemed to be less than 11ksi for MO-P interface, surface for K_4 upper limit intersects the surface for $(K_2 * f'_c + K_3)$ upper limit before reaching f'_c well less than 11ksi. Thus, the $f'_{c,crit}$ characteristic gets activated at smaller f'_c than 11ksi making it possible to have a common $f'_{c,crit}$ for all interfaces. The common $f'_{c,crit}$ was chosen to be 11ksi for all interfaces.

It should be noted that the proposed model, DCS-Davaadorj-Calvi-Stanton, represents an updated version of the Mattock (2001) model. Figure 4.3.1.3 show an example comparison between the Mattock (2001) model and the proposed model using the MO-U NW dataset. The plot compares the models in two ways. First, the ratio of calculated/experimental strength value is plotted against ρf_y . The ratio is plotted using a log scale so that ratios of two and one half appear on the plot to have the same error. Second, a histogram of the number points is plotted against the ratio value. The average Ln(Ratio value) values for MO-U NW dataset are -0.132 and -0.253 for the DCS and Mattock(2001) models respectively.

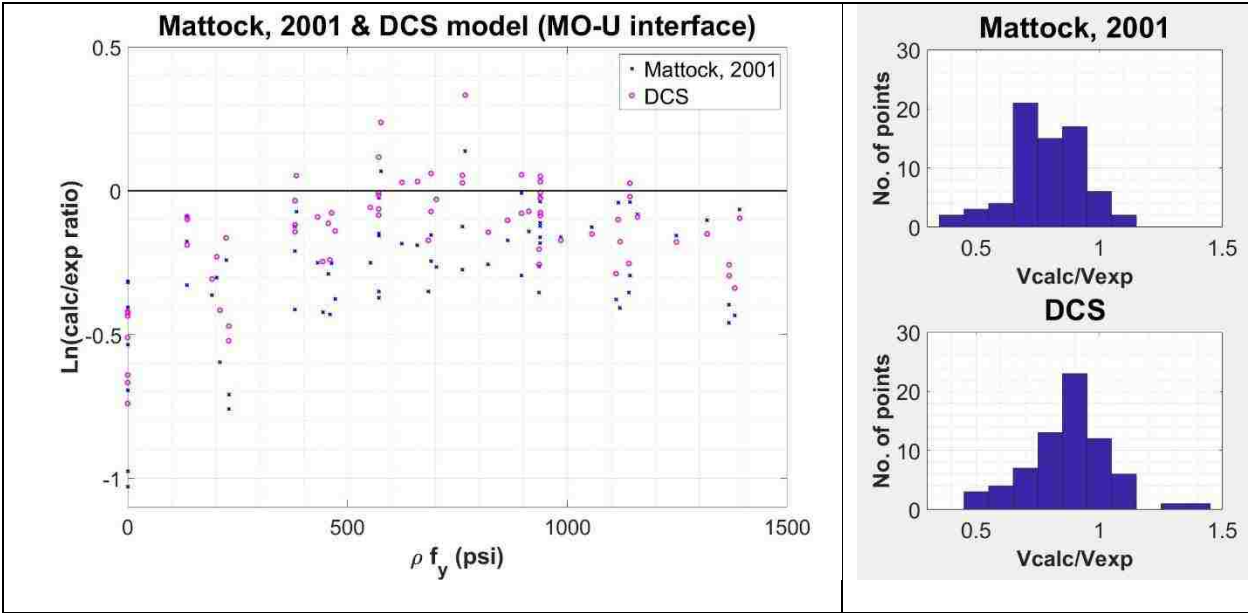


Figure 4.3.1.3: Example comparison between Mattock 2001 and DCS model (MO-U interface)

4.3.2 Calibration process and performance of the model

For purposes of calibration of the coefficients, the calibration data has been used to extrapolate more data. The extrapolation was done by fitting the calibration data to 3D surface (v_u vs. f'_c and ρf_y). The extrapolation was to make sure the model was inclusive of all ranges of f'_c and ρf_y including ranges with little or no corresponding real data.

A_1 and A_2 are solved mathematically (in MATLAB) such that the sum of root-mean-square-deviations (RMSD) of all v_u points on the extrapolated surface data and corresponding v_n values estimated by the model being proposed. Figure 4.3.2.1 shows the contoured sum of RMSD values for NW data of each interface type for all pairs of A_1 and A_2 considered. For these contour plots, $f'_{c,crit} = 11 \text{ksi}$ was used for all interfaces but none of the upper bound shear strength limits were applied.

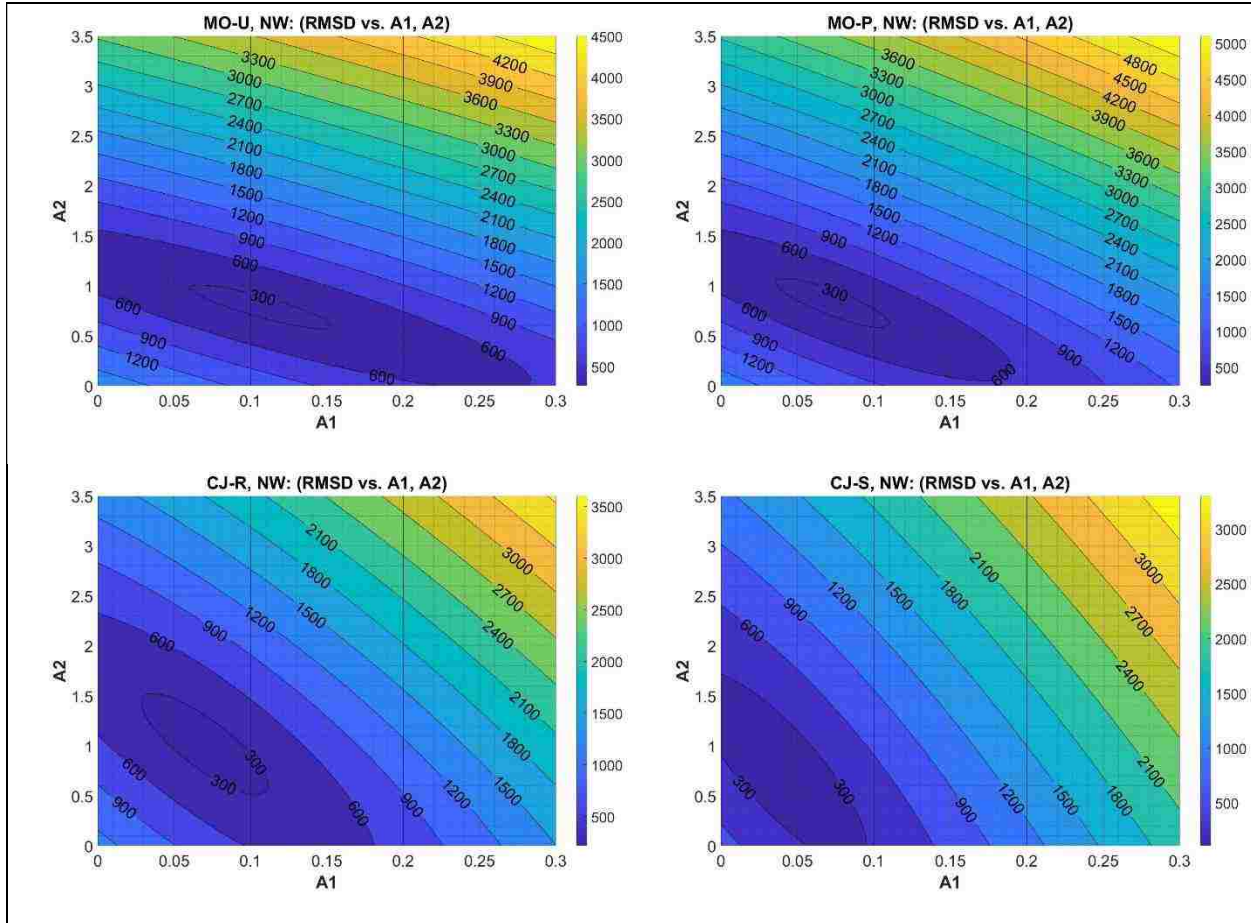


Figure 4.3.2.1: Contour plots of RMSD values for MO-U, MO-P, CJ-R, and CJ-S interfaces

In Figure 4.3.2.1, for all of the interface types, the contour surface is characterized by a long narrow valley that is much steeper in one direction than the other. This implies that, for each surface, there are many pairs of (A_1 , A_2) values that would give almost the same goodness of fit. In particular, those past and present models based solely on shear friction ($A_1=0$ and $A_2 \approx \mu$) would lie on the A_2 axis of these plots and could be made to give a nearly optimal fit in an overall sense simply by selecting the appropriate parameter values.

Most importantly, Figure 4.3.2.1 suggests that improving the shear transfer models is not about debating over shear friction coefficients (μ), rather is about considering the nature of each interface type while staying in the as small sum of RMSD contour levels as possible. This can be achieved by finding the balance between cohesion-like term ($A_1 * f'_c$) and the shear friction-like terms ($A_2 * \rho f_y$) in the model.

Table 4.3.2.1 lists the pairs of A_1 and A_2 that results in the absolute minimum sum of RMSD values for each interface. Picking the pairs of A_1 and A_2 which gives the absolute minimum sum of RMSD values results in the best models mathematically. However, the contour plots of RMSD values show other pairs of A_1 and A_2 of which corresponding sum of RMSD values are close the mathematical absolute minimum sum of RMSD values as well. These other options of pairs allow for being flexible with the coefficients such that the physics of the shear transfer mechanisms are better reflected.

Table 4.3.2.1: The coefficients resulting in mathematical min sum (RMSD)

	A_1	A_2	$RMSD_{min}$
MO-U	0.11	0.8	262.2
MO-P	0.07	0.85	240.2
CJ-R	0.07	1	212.4
CJ-S	0.04	0.75	102.8

After choosing A_1 and A_2 coefficients by formal optimization, the K coefficients were chosen manually by a trial and error method. The model forms and values were initially selected to be similar to those in current code provisions, and then the K values were manually changed to ensure the following:

- At the smallest f'_c value in the corresponding dataset available and at $f'_{c,crit}=11$ ksi, the estimated strengths controlled by the limits at those two f'_c would frame the majority of the real test data in a conservative manner. An example trial for K coefficients (boundaries resulting from the finalized A and K coefficients are shown) for MO-U NW dataset is shown in Figure 4.3.2.2. (The proposed model is shown here as “DCS—Davaadorj-Calvi-Stanton” model).

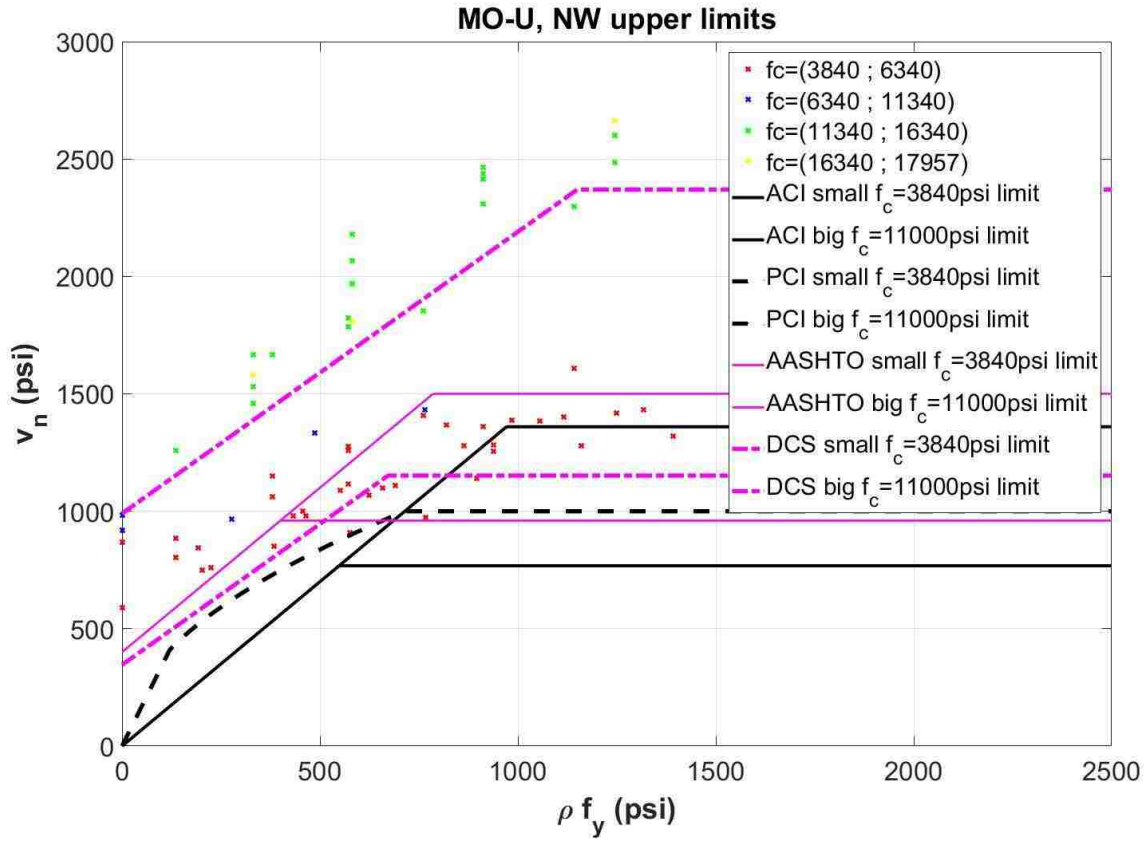


Figure 4.3.2.2: Upper limit activations at smallest f'_c available and at $f'_{c,crit}$ (MO-U NW)

In the finalized model, the term that serves as “cohesion” (A_1 coefficient) for the MO-P interface was chosen to be zero even though the mathematical minimum RMSD occurs at $A_1=0.07$. That was to ensure zero shear strength of precracked interface when no reinforcement is provided ($\rho f_y=0$). The A_1 coefficients for the other three interface types were also reduced below the values in Table 4.3.2.1. The coefficients were chosen to make sure that “cohesion” terms of the model result in conservative estimates on average when $\rho f_y=0$ for each interface.

Finally, to validate the manually chosen K values, the model was checked to ensure that the 3D MO-U model interface is at least as strong as the MO-P model interface. Similar checks were completed with the CJ-R and CJ-S interfaces.

Figures 4.3.2.3, through 4.3.2.5 show the 3D surfaces created by the proposed model for monolithic interfaces. In these figures, MO-U interfaces are bigger than or equal to MO-P interfaces in terms of predicted strength for all types of concrete (NW, SLW and ALW). Also they show the trend for the accuracy of the model compared to the real corresponding test data. More details on accuracy will be discussed in Section 4.3.4.

Similar plots for the cold-joint interfaces are shown in Figures 4.3.2.6 through 4.3.2.8. (The λ factor is not used for CJ-S interfaces in these plots). In these plots, it can be seen that the CJ-R interfaces are

predicted to have bigger strengths than CJ-S interfaces. Also, it is clear that not applying the lightweight concrete modification factor, λ , to the 3D model surface for CJ-S NW interface results in a conservative estimate. This holds true for the currently available data but should be checked again when more data becomes available.

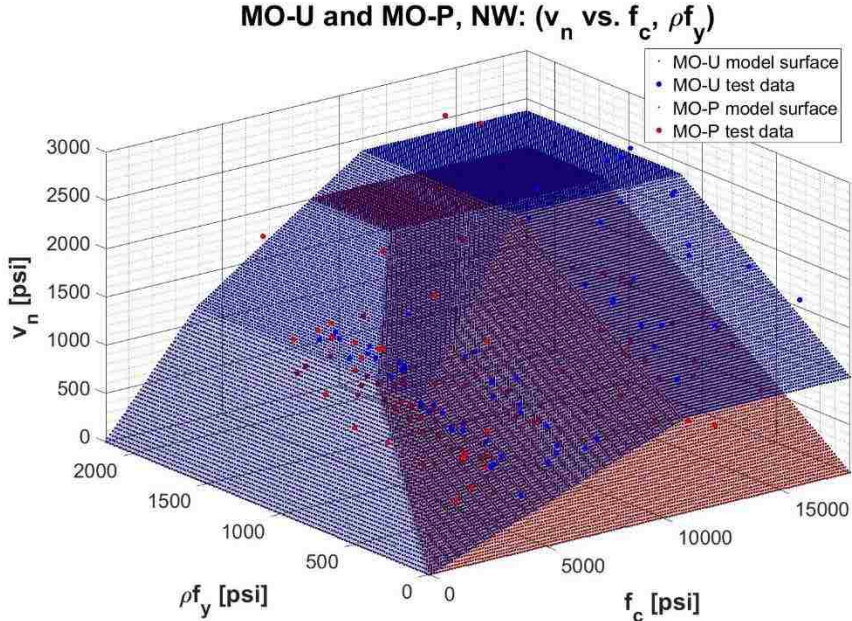


Figure 4.3.2.3: Proposed model surfaces for NW monolithic interfaces

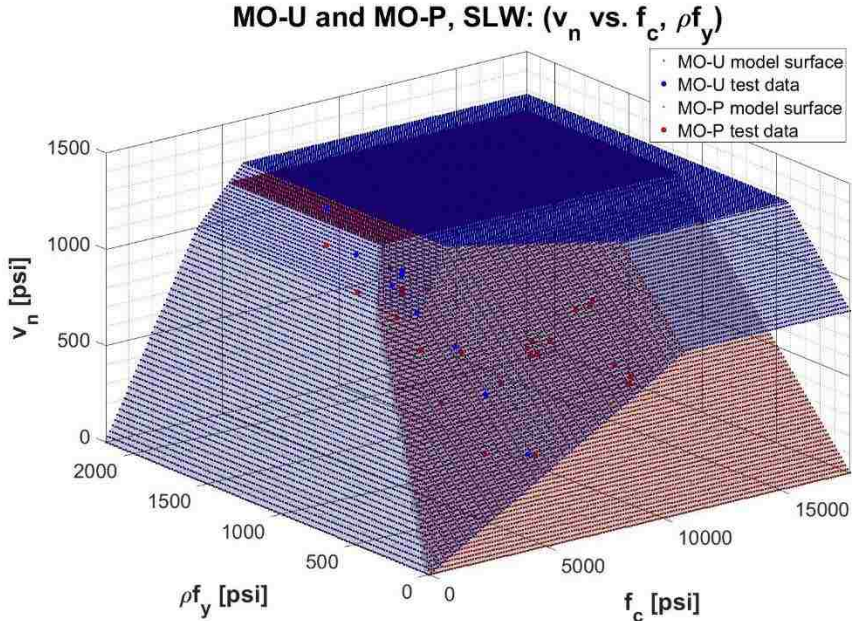


Figure 4.3.2.4: Proposed model surfaces for SLW monolithic interfaces

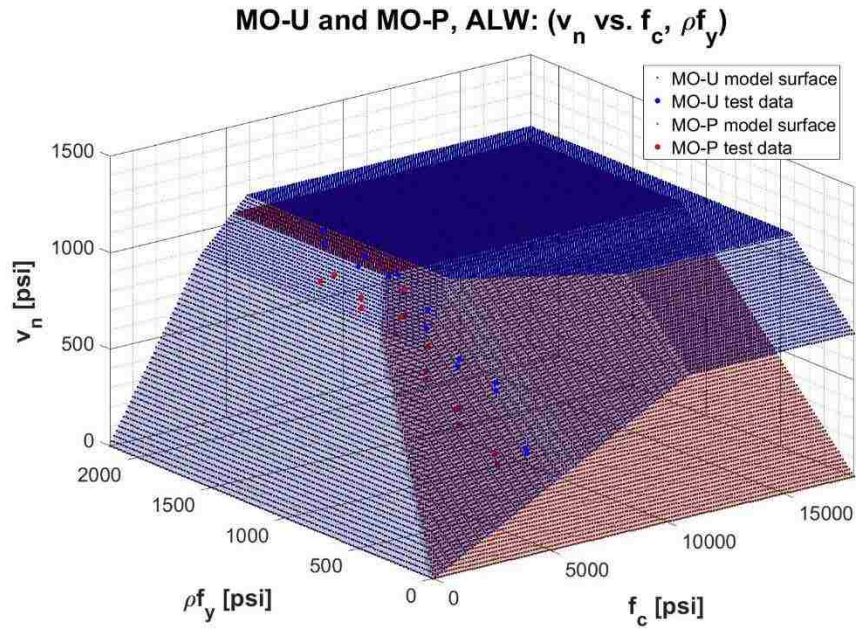


Figure 4.3.2.5: Proposed model surfaces for ALW monolithic interfaces

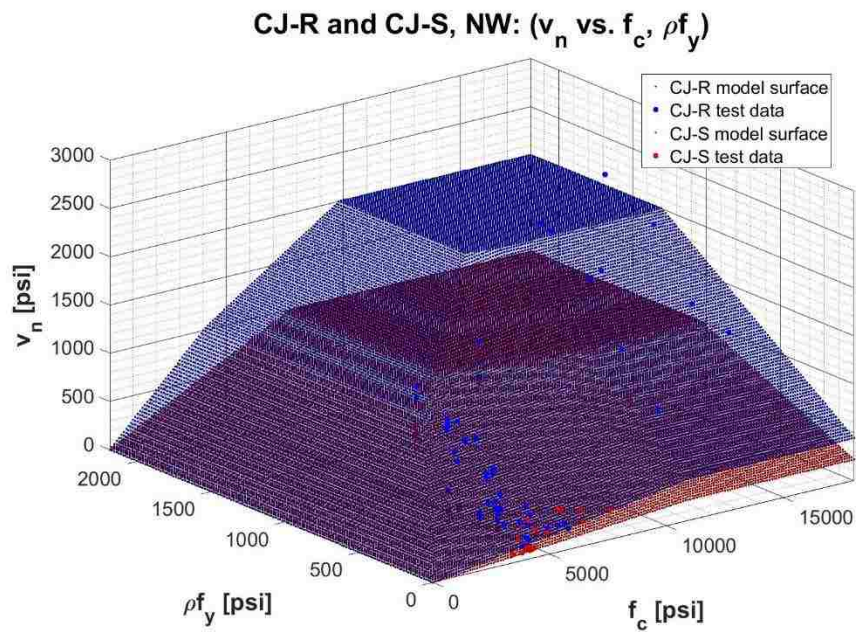


Figure 4.3.2.6: Proposed model surfaces for NW cold-joint interfaces

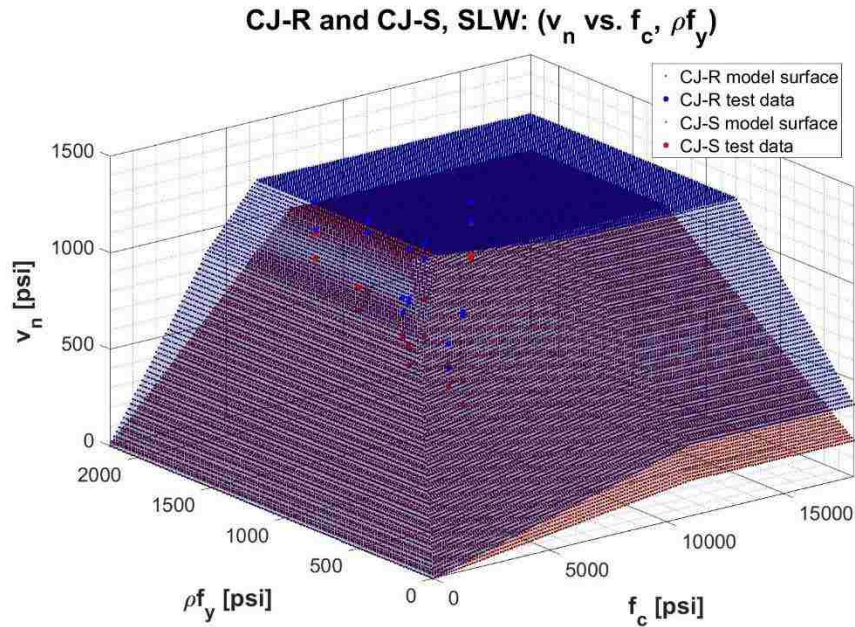


Figure 4.3.2.7: Proposed model surfaces for SLW cold-joint interfaces

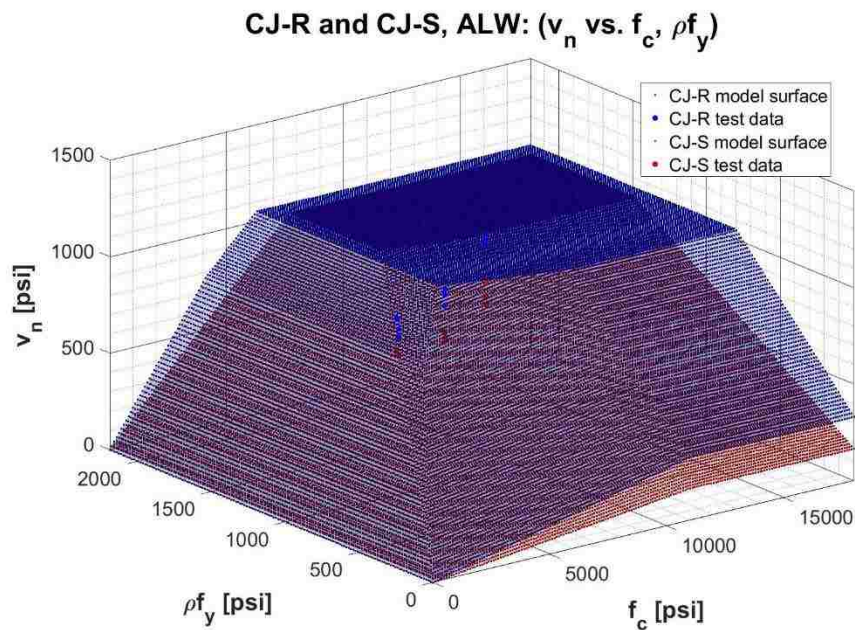


Figure 4.3.2.8: Proposed model surfaces for ALW cold-joint interfaces

4.3.3 Performance ranking of all available models

In determination of performances of available models, the ratio of calculated/test shear strength were statistically analyzed. The calculated values were those predicted by the various models, while the test values were from the database. In Tables 4.3.3.1 and 4.3.3.2, mean, standard deviation (std. DEV), coefficient of variation (COV) of the R ratios are summarized. Some of the available models were not

applicable to certain data points due to either concrete type, minimum reinforcement ratio, or lack of required geometrical details reported. Total number of calibration points used to solve the statistical parameters of R values for each model is also provided in Tables 4.3.3.1 and 4.3.3.2.

The rankings were determined based on the following sorting order:

- 1) The most numbers of applicable calibration points.
- 2) The smallest coefficient of variation.
- 3) Smallest absolute difference between mean R and 1.0.
- 4) Smallest standard deviation.

The above sorting order was chosen to ensure broader applicability of the design method (number of applicable points), consistency of the model accuracy (COV), and goodness of the accuracy (std. Dev and difference between mean R and 1.0). Fitting a model that applies to a wide range of data with good accuracy is more important than a model with better accuracy over a more limited range. Models with strict applicability restrictions can be checked against a smaller number of test results from the database. Also, models that resulted in a small COV but an R value further from 1.0 may perform well over all after a minor modification of the parameters. Hence, the smaller COV had higher priority in sorting than the difference between mean R and 1.0. Tables 4.3.3.1 and 4.3.3.2 clearly indicate that no single design provision or past model performs consistently to be one of the best models for all interface types while being applicable to the most number of data points.

Table 4.3.3.1: Performances of available models – Monolithic interfaces (Ranked from top to bottom)

Interface performance	MO-U				Interface performance	MO-P			
	Average	Std.DEV	COV %	applicable points		Average	Std.DEV	COV %	applicable points
Harries & Zeno (2012)	0.7405	0.1288	17.4008	70	Mattock (2001)	0.9888	0.143	14.46	117
DCS (2018)	0.8764	0.1638	18.6202	70	Mattock another update	1.0111	0.163	16.124	117
Mattock (2001)	0.7768	0.1495	19.2454	70	Hsu& Mau (1988)	1.2942	0.2174	16.796	117
Shaikh (1978)	0.7481	0.1636	21.8713	70	Lin & Chen (1989)	1.0281	0.1771	17.23	117
Kahn & Mitchell (2002)	0.9446	0.3006	31.8238	70	AASHTO 7th	0.98	0.1806	18.428	117
CSA (2014)	0.711	0.2515	35.3732	70	CSA (2014)	0.9292	0.1725	18.567	117
Walraven (1987)	0.8642	0.3232	37.393	70	Mansur & Vinagayam (2008)	1.1016	0.2101	19.071	117
Hsu& Mau (1988)	0.9225	0.3461	37.5245	70	Shaikh (1978)	0.9524	0.1843	19.349	117
Loov (1978)	0.6988	0.2622	37.5245	70	ACI 318 Shear Friction	0.7123	0.1474	20.699	117
PCI 7th ed.	0.6315	0.2446	38.732	70	Mattock (1974, 1976)	0.9388	0.1964	20.917	117
PCI 6th ed.	0.6315	0.2446	38.732	70	Walraven (1987)	1.2507	0.2721	21.755	117
MC 90 (CEB-FIP, 1990)	0.9221	0.3665	39.7434	70	PCI 7th ed.	0.8334	0.185	22.203	117
Raths (1977)	0.7589	0.3107	40.9412	70	PCI 6th ed.	0.8334	0.185	22.203	117
Birkeland (1968)	0.6692	0.274	40.9412	70	Raths (1977)	1.0185	0.2324	22.818	117
ACI 318 Shear Friction	0.5344	0.2336	43.7012	70	Birkeland (1968)	0.8982	0.205	22.818	117
Mast (1958)	0.7726	0.43	55.6544	70	DCS (2018)	0.7679	0.2003	26.081	117
Mattock another update	0.7774	0.1429	18.3796	67	Harries & Zeno (2012)	0.6347	0.1888	29.745	117
Mattock (1974, 1976)	0.7285	0.166	22.785	67	Mast (1958)	1.0464	0.3846	36.756	117
Lin & Chen (1989)	0.8469	0.1492	17.6186	63	MC 90 (CEB-FIP, 1990)	1.3573	0.5707	42.05	117
AASHTO 7th	0.847	0.1547	18.2653	63	Kono & Tanaka (2000)	0.757	0.1612	21.299	89
Kono & Tanaka (2000)	0.6173	0.1074	17.3957	50	Walraven & Reinhardt (1981)	-0.1843	5.2445	-2846.1	76
Vecchio & Collins (1986)	0.9136	0.2976	32.5712	30	Hamadi & Regan (1980)	0.7746	0.2519	32.52	76
Hamadi & Regan (1980)	0.4302	0.1789	41.5885	29	Vecchio & Collins (1986)	1.0559	0.4364	41.327	76
Gambarova & Karakoc (1983)	0.4997	0.265	53.0357	29	Li et al. (1989)	1.5751	0.7929	50.342	76
Li et al. (1989)	0.8407	0.4515	53.7009	29	Gambarova & Karakoc (1983)	1.1063	0.5675	51.294	76
Walraven & Reinhardt (1981)	0.6707	0.7727	115.213	29	Loov (1978)	N/A	N/A	N/A	0
EN 1992-1-1 (2004)	N/A	N/A	N/A	0	EN 1992-1-1 (2004)	N/A	N/A	N/A	0
Mansur & Vinagayam (2008)	N/A	N/A	N/A	0	Kahn & Mitchell (2002)	N/A	N/A	N/A	0
Tsoukantas & Tassions (1989)	N/A	N/A	N/A	0	Tsoukantas & Tassions (1989)	N/A	N/A	N/A	0

In Table 4.3.3.1, it can be seen that Walraven and Reinhardt (1981) model results in negative R ratios. This model was based on crack geometry (crack width and slip) which were not reported commonly. Majority of the strength calculation was done for this model by using scaled crack geometry from works when failure photographs or slip/width-load plots were provided. Therefore, it is possible that this model has been improperly analyzed.

The Harries and Zeno (2012) model performed the best of all models for the MO-U interfaces, about as well as the DCS model for MO-P interfaces, but (as shown below) worse for CJ interfaces. The main form of the Harries and Zeno model is similar to that of DCS model.

Harries & Zeno (2012):

(Imperial units)

$$v_n = \alpha f'_c + 0.002\rho E_s \leq 0.20f'_c$$

$\alpha=0.075, 0.0,$ and 0.040 for (MO-U, MO-P and CJ-R respectively)

The main difference between the Harries and Zeno model and the proposed model is that instead of f_y , the Harries and Zeno model utilizes $0.002 * E_s$ in place of f_y . If Young's modulus of the reinforcement steel is 29,000ksi, then $0.002 * E_s$ term is 58ksi. They compared performances of Grade 60 and 100 steel reinforcements and believed that the high strength steel do not yield at peak load. Also, peak contributions from steel and concrete do not happen simultaneously; the second term $0.002 \rho E_s$ comes into play after the crack opens up. In this research, the amount of data for very high strength steel was found to be too small to permit definite conclusions. The question should be re-considered in the future as more data becomes available.

The Harries and Zeno (2012) and DCS (2018) models perform the best (the smallest COV and the biggest number of applicable points) for the MO-U, but not for the MO-P interface. For the MO-P interface, the proposed model (DCS model) is generally similar to that for the MO-U interface, but is made conservative for low f_y by setting the cohesion-like term to zero. This was done to reflect the physical condition that cohesion is unlikely to be present at an open crack. . For this reason, the proposed model (DCS model) is conservative and similar to the ACI and PCI provisions at low f_y . For the ACI, PCI and DCS models, the COVs of the R ratios for MO-P interfaces are 20.699%, 22.203% and 25.829% respectively.

The best model for MO-P interface was the Mattock 2001 of which main form was similar to the DCS model. The Mattock 2001 model's cohesion coefficient was 0.1 (similar term noted as A_1 in the DCS model) and friction coefficient was 0.8 (similar term noted as A_2 in the DCS model). These coefficients were close to the coefficients resulting in the absolute mathematical minimum sum of RMSD values (See Table 4.3.2.1). Hence, it makes sense that the Mattock (2001) model performed well.

The Mattock (2001) model performed well for MO and CJ-R interfaces but not for CJ-S interfaces (See Table 4.3.3.1 and Table 4.3.3.2). That is probably because the main form of Mattock (2001) model is similar to the DCS model but lacks a cohesion term for CJ-S interface. This results in overly conservative estimations. In the light of CJ-S interface data that has become available since 2001, the DCS model with a cohesion term performs better than Mattock (2001) model. This suggest that cohesion term for CJ-S interface is crucial and CJ-S interface should be modeled as a combination of cohesion and "shear friction".

Table 4.3.3.2: Performances of available models – Cold-joint interfaces (Ranked from top to bottom)

Interface performance	CJ-R				Interface performance	CJ-S			
	Average	Std.DEV	COV %	applicable points		Average	Std.DEV	COV %	applicable points
DCS (2018)	0.8023	0.2027	25.263	84	DCS (2018)	0.7868	0.3113	39.5673	64
Harries & Zeno (2012)	0.7339	0.1981	26.9868	84	Harries & Zeno (2012)	1.2607	0.5178	41.0668	64
EN 1992-1-1 (2004)	0.7252	0.2214	30.526	84	EN 1992-1-1 (2004)	0.7413	0.3282	44.271	64
Mattock (2001)	1.0134	0.3252	32.0922	84	CSA (2014)	0.5262	0.2792	53.0684	64
Shaikh (1978)	0.8619	0.2775	32.2001	84	Shaikh (1978)	1.2301	0.7927	64.4383	64
Mattock (1974, 1976)	1.0023	0.3313	33.0541	84	Mattock another update	1.8888	1.2268	64.9489	64
Mattock another update	1.0319	0.3648	35.3536	84	Mattock (1974, 1976)	1.8196	1.2034	66.133	64
CSA (2014)	0.5945	0.2161	36.3535	84	Mast (1958)	0.4633	0.3553	76.6816	64
Tsoukantas & Tassions (1989)	1.0963	0.5483	50.0158	84	Tsoukantas & Tassions (1989)	0.3089	0.2369	76.6816	64
Walraven (1987)	0.9602	0.4862	50.6377	84	Mattock (2001)	0.4062	0.324	79.7741	64
Raths (1977)	0.8348	0.4268	51.1273	84	ACI 318 Shear Friction	0.4065	0.3244	79.8079	64
Birkeland (1968)	0.7362	0.3764	51.1273	84	Walraven (1987)	1.2496	1.0079	80.6589	64
MC 90 (CEB-FIP, 1990)	1.0637	0.5591	52.5605	84	PCI 7th ed.	0.3647	0.3029	83.0572	64
PCI 7th ed.	0.6001	0.3191	53.1676	84	Kahn & Mitchell (2002)	2.9976	2.5521	85.1357	64
PCI 6th ed.	0.6001	0.3191	53.1676	84	Birkeland (1968)	0.9487	0.8464	89.2159	64
ACI 318 Shear Friction	0.4666	0.256	54.8561	84	Raths (1977)	1.0757	0.9597	89.2159	64
Mast (1958)	0.5355	0.3301	61.6489	84	MC 90 (CEB-FIP, 1990)	1.2657	1.182	93.3848	64
Kahn & Mitchell (2002)	1.4552	0.9215	63.3221	84	PCI 6th ed.	0.5976	0.6039	101.067	64
Lin & Chen (1989)	1.0277	0.1714	16.6763	69	AASHTO 7th	0.7413	0.2613	35.2474	43
AASHTO 7th	0.838	0.1704	20.3346	69	Lin & Chen (1989)	1.63	0.6337	38.876	43
Kono & Tanaka (2000)	0.7762	0.1294	16.6679	65	Kono & Tanaka (2000)	1.2481	0.449	35.9766	37
Vecchio & Collins (1986)	1.124	0.3517	31.2894	50	Vecchio & Collins (1986)	1.7475	0.2389	13.6711	36
Li et al. (1989)	1.2423	0.2833	22.8031	49	Gambarova & Karakoc (1983)	1.2717	0.3384	26.6106	36
Gambarova & Karakoc (1983)	0.8413	0.2602	30.9287	49	Li et al. (1989)	1.8158	0.5317	29.2827	36
Hamadi & Regan (1980)	0.7124	0.2963	41.5972	49	Hamadi & Regan (1980)	0.7581	0.3272	43.1575	36
Walraven & Reinhardt (1981)	0.9454	0.4991	52.7902	49	Walraven & Reinhardt (1981)	2.3886	1.2232	51.2114	36
Loov (1978)	N/A	N/A	N/A	0	Loov (1978)	N/A	N/A	N/A	0
Hsu & Mau (1988)	N/A	N/A	N/A	0	Hsu & Mau (1988)	N/A	N/A	N/A	0
Mansur & Vinagayam (2008)	N/A	N/A	N/A	0	Mansur & Vinagayam (2008)	N/A	N/A	N/A	0

As mentioned in Section 2.3, the PCI’s shear friction chapter prohibited the use of its effective shear friction method for CJ-S interfaces when transitioned from the 6th ed. to the 7th ed. The COV of the PCI 6th ed. was bigger than that of PCI 7th ed. for CJ-S interface. Also, the mean R ratio of the 6th ed. was closer to 1.0 while the 7th ed. was over conservative.

4.3.4 Comparison of the proposed model and Code Provisions

In this section, performances of the current ACI, PCI, and AASHTO LRFD code provisions and the proposed model (DCS model) are compared in detail (no safety factor is applied). These 4 design models perform their bests at different ranges of f'_c and ρf_y for each interface type. Hence, for all four design models, 3 types of plots of R ratio (ratio of calculated shear strength over test result) were produced for each interface (MO-U, MO-P, CJ-R, and CJ-S) to show:

1. Ln(R ratio) vs f'_c
2. The average plus and minus one standard deviation of R ratios for groups of ρf_y ranges.

3. Overall counts of R ratios in histogram forms with a bin width = 0.1.

MO-U interface:

Figure 4.3.4.1 shows how the four models perform with respect to f'_c . Since R ratio is the ratio calculated/measured strength, Ln(R) ratios smaller than 0.0 indicate conservative estimates and Ln(R) ratios above 0.0 indicate unsafe predictions.

Figure 4.3.4.2 shows the overall trend of the performance of each model with respect to variety of ranges of ρf_y . The center dots on each error bar marks indicate the average R ratios of that particular ρf_y range running half way between the adjacent error bar marks on both sides of the dot. The top and bottom of each error bar corresponds to average R ratio +/- one standard deviation of R ratio within the particular ρf_y range. The bigger the error bar mark, the bigger standard deviation in R ratio in the corresponding ρf_y range.

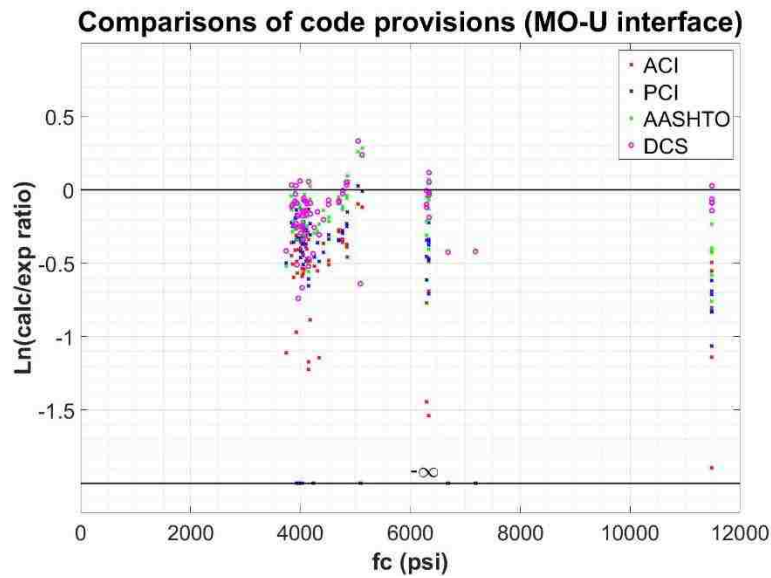


Figure 4.3.4.1: Ln(R) ratios vs. f'_c (MO-U interface)

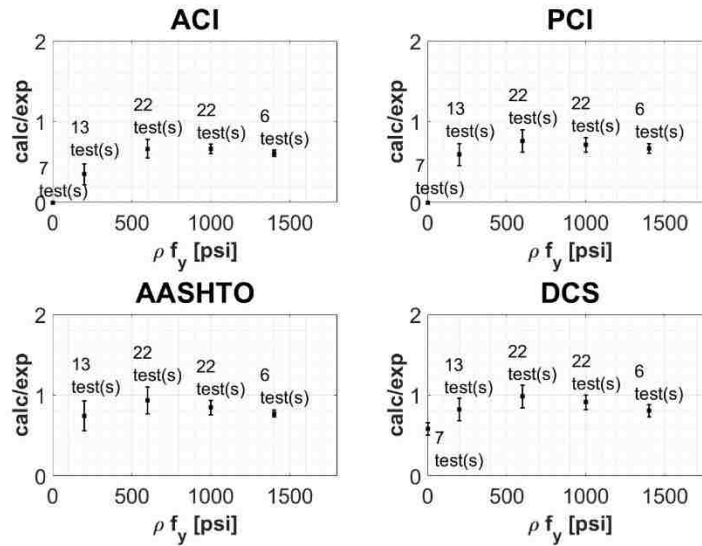


Figure 4.3.4.2: R ratios vs. ρf_y (MO-U interface)

For MO-U interface, the ACI and PCI provisions are conservative (See Figure 4.3.4.1) and over conservative at small ranges of ρf_y (See Figure 4.3.4.2). As can be seen in Figure 4.3.4.2, when no reinforcement is provided, the ACI and PCI's shear friction provisions estimate the shear strength to be zero and AASHTO do not allow for $\rho f_y < 50$ psi. This makes AASHTO's overall count of R ratios regarding data with $\rho f_y = 0$ to be zero and reduces overall count for lightly reinforced data to be less than actual. The R ratios of the AASHTO provision and the proposed DCS model are close to 1.0 on average. The proposed model conservatively estimates the shear strength when $\rho f_y = 0$.

Figure 4.3.4.3 shows that the ACI and PCI provisions are conservative for almost all test points. The zero R values in the ACI and PCI's histograms correspond to the estimations for MO-U data with reinforcement. The DCS model has several points with $R > 1$ but the majority of the data points have R values close to or less than 1. Also, it allows for estimation of shear strength of unreinforced MO-U interface unlike the AASHTO provision of which average is also close to 1.

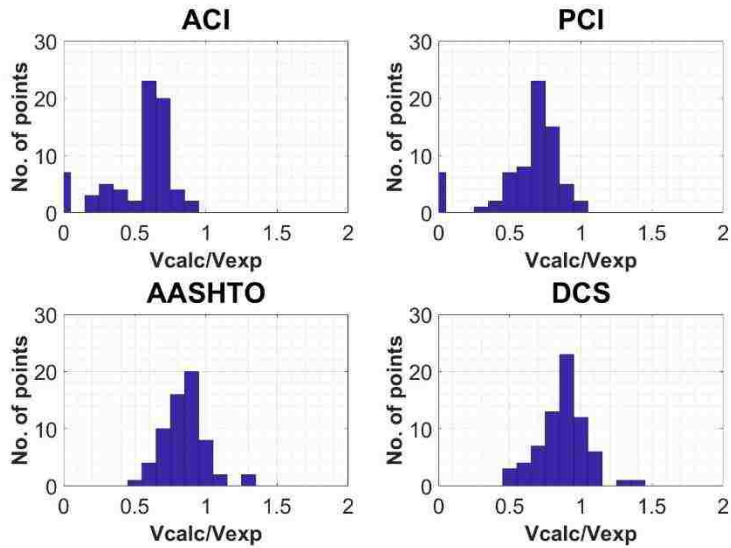


Figure 4.3.4.3: Bin counts of R ratios (MO-U interface)

MO-P interface:

Figure 4.3.4.4 shows that the AASHTO provision results in more numbers of unconservative estimates (i.e $\ln(R)>0.0$) than the rest of the models. The other 3 models mostly result in conservative estimations ($\ln(R)<0.0$).

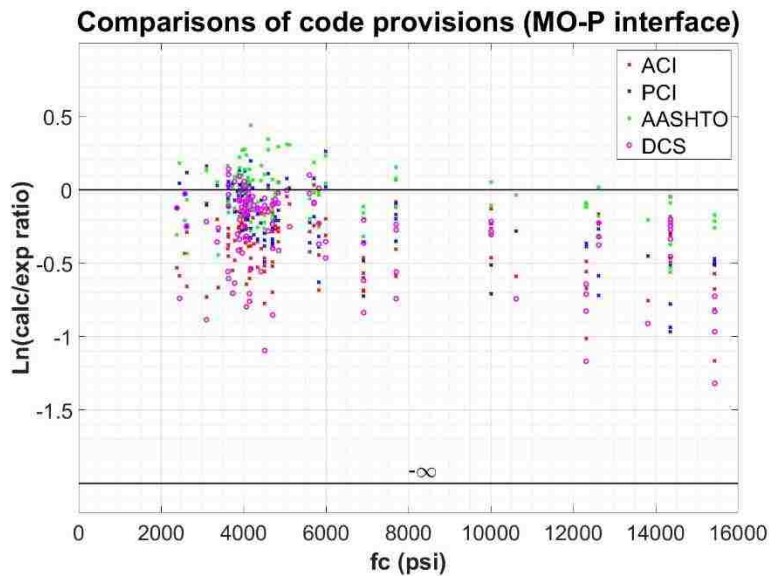


Figure 4.3.4.4: $\ln(R)$ ratios vs. f'_c (MO-P interface)

Figure 4.3.4.5 shows that the ACI provisions tend to underestimate shear strength of MO-P interface especially at small ranges of ρf_y . The DCS model also underestimates the shear strength at small ranges of reinforcement (especially when $\rho f_y < 400$ psi) but estimates slightly better than the ACI provision at

higher ranges of ρf_y . The AASHTO and PCI provisions have R values close to 1 on average at all ranges of ρf_y except for high ρf_y . This implies that all models perform well on average but each model works better in specific ranges of ρf_y rather than for all ranges of ρf_y . Figure 4.3.4.6 shows that R distribution of each model and the general shape of distribution of each model seemed reasonably good. The ACI model is conservative for all points considered.

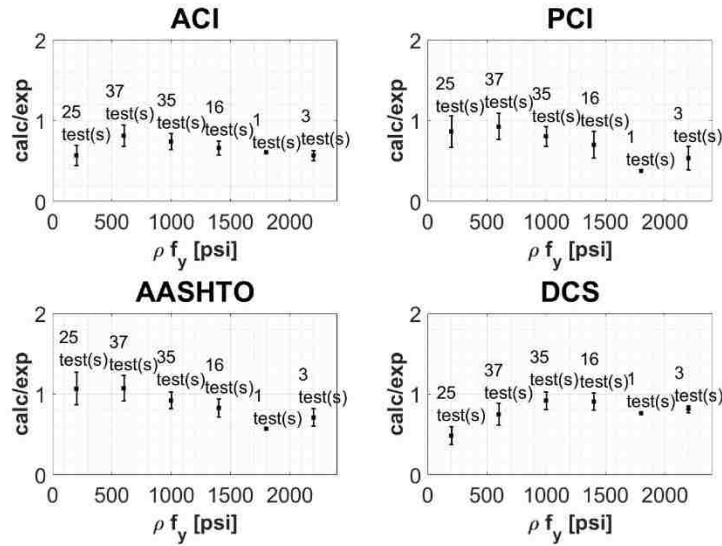


Figure 4.3.4.5: R ratios vs. ρf_y (MO-P interface)

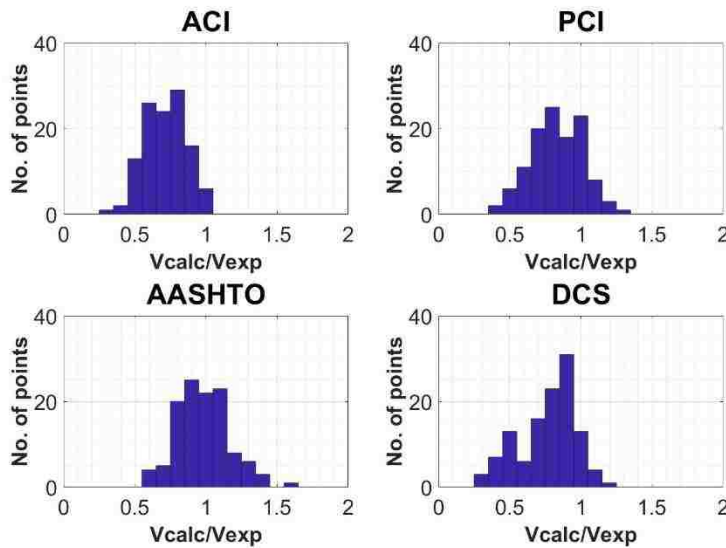


Figure 4.3.4.6: Bin counts of R ratios (MO-P interface)

CJ-R interface:

Figures 4.3.4.7 and 4.3.4.8 show that the ACI model seem to be little too conservative for CJ-R interface as all $\ln(R)$ ratios and R values are well below 0.0 and 1.0 respectively. The PCI model is also mostly on the conservative side. However, on average the PCI model's R value is closer to 1 than the ACI model due to effective shear friction method. The effective shear friction method helps estimate higher strength at small ranges of ρf_y than the regular shear friction method that the ACI model utilizes. However, they both assume that the strength of CJ-R interface with no reinforcement is zero. The AASHTO provision simply does not allow for $\rho f_y < 50$ psi as it was the case for MO-U interface discussion. Figure 4.3.4.8 shows that the DCS model results in R values close to 1 in overall and results in conservative estimate at $\rho f_y = 0$.

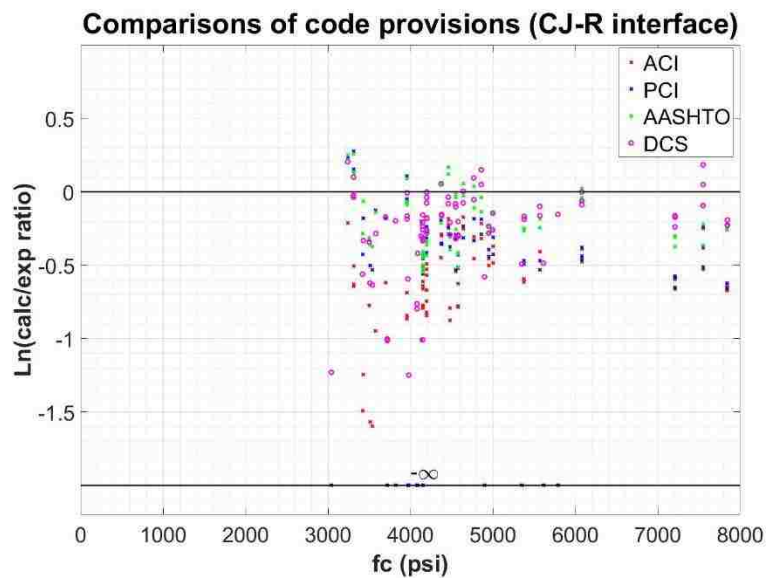


Figure 4.3.4.7: $\ln(R)$ ratios vs. f_c^1 (CJ-R interface)

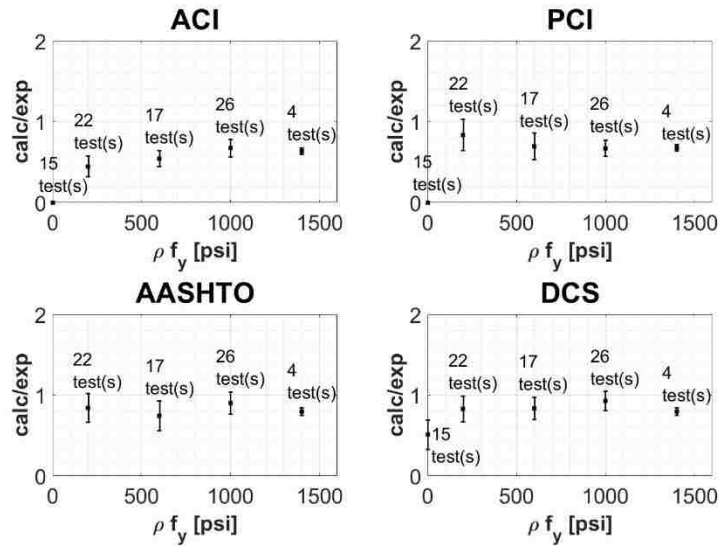


Figure 4.3.4.8: R ratios vs. ρf_y (CJ-R interface)

As shown Figure 4.3.4.9, the DCS model's overall shape of R value distribution is little bit better than the rest of the models as it allows for estimation of CJ-R interfaces with no reinforcement.

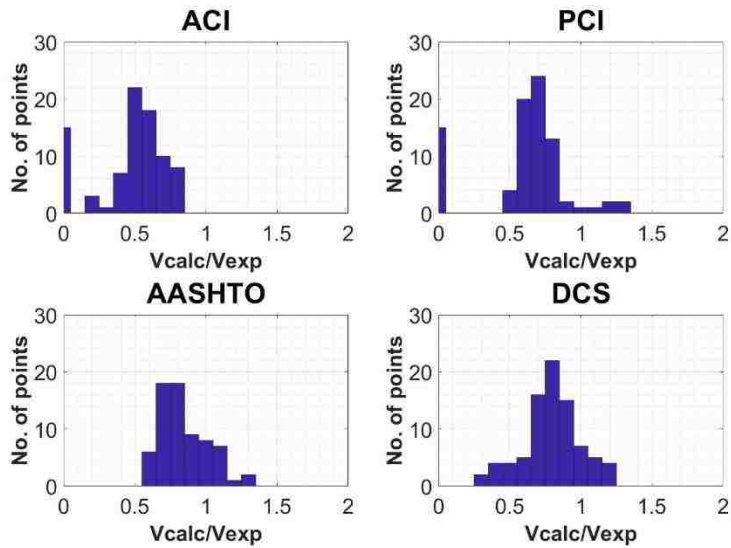


Figure 4.3.4.9: Bin counts of R ratios (CJ-R interface)

CJ-S interface:

Figure 4.3.4.10 shows that the ACI and PCI models are generally more conservative than the AASHTO model and the DCS model as they neglect cohesion hence underestimate the strength of interfaces with no shear reinforcement. However, the AASHTO model and the DCS model have more points with $\ln(R)$ close to 0.0 except for several points at $f'_c < 4000$ psi.

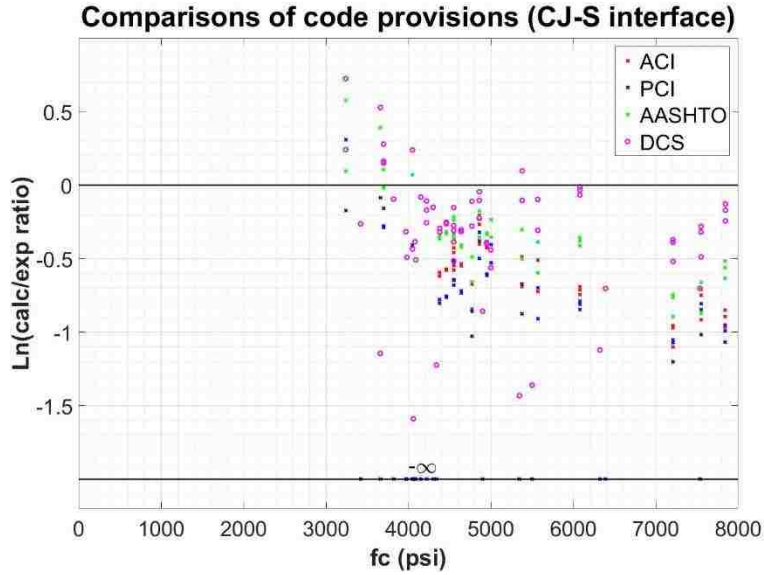


Figure 4.3.4.10: Ln(R) ratios vs. f'_c (CJ-S interface)

Figure 4.3.4.10 shows that the AASHTO and DCS models conservatively (and with bigger variations) estimate shear strengths of test points with $\rho f_y < 600$ psi. However, it is worth mentioning that at small ranges of ρf_y (not including $\rho f_y = 0$ data), there were only few tests with high variation in strength which were probably unavoidable due to the nature of CJ-S interfaces. Smooth interfaces are sensitive to how the interface was prepared and the definition of smooth interface varies between individual test programs. Hence, the error bars produced at smaller reinforcement range (not including $\rho f_y = 0$ data), should not be given big weight in determination of model performances. Also, the DCS model is the only one of the 4 models that estimates the strength of CJ-S interface with no shear reinforcement.

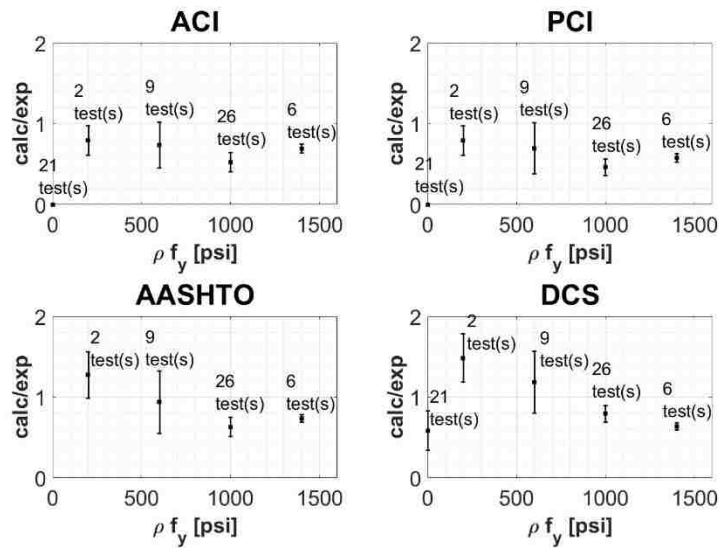


Figure 4.3.4.11: R ratios vs. ρf_y (CJ-S interface)

As shown in Figure 4.3.4.12, no single model has the perfect R value distribution but the DCS model has a reasonable distribution shape in overall.

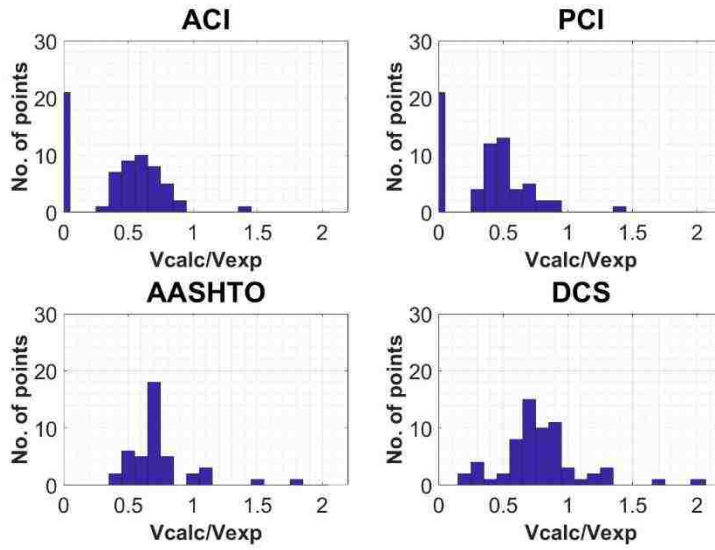


Figure 4.3.4.12: Bin counts of R ratios (CJ-S interface)

5. Analysis of Steel to Concrete Interface Data

5.1 Introduction

The database pertaining to steel-to-concrete interface tests comprised a total of 455 tests. Past research programs have identified a number of parameters that appear to be important with respect to the stress transfer capacity of steel-to-concrete interfaces. In this chapter, the parameters considered in the test programs are organized into two categories, one regarding the materials and configurations, another associated with loading procedures and failure modes.

Materials and configurations

Average contact pressure, ρf_u . In all shear friction code provisions, ρf_y is the most important parameter and the shear strength is proportional to this “clamping stress”. In “non-friction approaches”, the total area of the steel reinforcement multiplied by f_u is normally used to compute the shear capacity. The vast majority of researchers reported f_u values rather than f_y , hence ρf_u is used to determine the clamping stress in this study.

Concrete compressive strength, f'_c . Many researchers believe that higher concrete strength leads to higher shear capacity because of its higher resistance to “breaking off” and its higher bearing capacity.

Concrete density (normal or lightweight). Lightweight concrete is believed to possess a lower shear strength as it is more prone to cracking around the reinforcement, and its aggregates are characterized by lower toughness. Some researchers however, believe that this effect is minimal as long as f'_c is kept the same.

The three parameters mentioned above are most commonly perceived as the main influencing parameters in shear strength of interfaces. Other parameters are also believed to affect shear strength, but are either considered secondary or have received little experimental attention.

Surface type. The shear friction contribution to the strength of steel-to-concrete interfaces has been over the object of debates in the past. In an effort to separate the dowel contribution from the frictional component of the strength, some researchers conducted tests with greased (or with a sheet metal in between interfaces) and ungreased interfaces. However, greasing the interface did not produce any evident strength reduction. Thus, test data from both types of interface preparation were combined and analyzed together in this chapter.

Flange thickness. Flange thickness of the steel beam to which the studs are welded to, should have a thickness consistent with the diameter of the studs. Goble (1965) determined that the maximum d_s/t_f ratio should be 2.7 to avoid flange pull-out failure. This limit has been verified by other researchers and not many studies on beams with thin flanges are available in the literature.

Stud Spacing. It has been determined that adequate longitudinal and transverse spacing between studs should be provided in order to avoid premature concrete failure or excessive concrete damage.

Slab thickness and height of studs. Researchers believe that the slab thickness and the height of the studs should be sufficient to prevent longitudinal splitting failures in the slab and pry-out failures around the studs.

Loading procedures and failure modes

Combined loading in shear and tension. Applied tensile forces have been found to decrease the clamping stress across the interface hence reducing the shear capacity. However, this parameter was not considered in this study due to the small amount of available experimental data.

Failure modes. Due to the complex nature of steel-concrete composite structures, the types of failures that have been observed over the course of past research programs involve a variety of different mechanisms that need to be studied separately. Thus, in this chapter, the different failure types are grouped as a function of the failure modes reported in the literature by the various authors. These groups are:

1. Stud failure:
 - “Studs shearing” (with or without a mention of local concrete crack around the studs)
 - “Weld failure” (failure below weld collar or due to bad weld)
2. Concrete Failure:
 - “Concrete pry-out”
 - “Concrete cracks”
 - “Concrete failure”
 - “Stud yield/bent studs and concrete cracks”
 - “Premature failure”
3. Mixed Failure:
 - “Mixed” (e.g., 2 studs sheared and concrete around other 2 studs pried out, or stud sheared and concrete cracked significantly)
4. Pull-out:
 - “Pull-out” (Tension anchorage issue between studs and concrete)

Test data from specimens that failed in pull-out mode were not analyzed because they were considered of minor importance with respect to the performance of the types of pre-cast connections that represent the focus of this research work. The data corresponding to the rest of the failure types were analyzed independently and compared to each other.

5.2 Influence of Parameters

The test results pertaining to NW concrete and LW concrete were investigated separately. The majority of the observations reported refer to NW concrete data as the assembled database consisted mainly of NW concrete data. Also, data from tests with headless studs, reinforced with welded-wire fabric, and short studs that were intended to study pry-out failures were not included as considered beyond the scope of this research.

5.2.1 Combined Effects of Concrete Compressive Strength and Clamping Stress

The main influencing parameters were determined to be f'_c and ρf_u upon trial evaluations. To this end, 3D and contour plots similar to those utilized in Chapter 4 were produced to outline the overall trends.

Figure 5.2.1.1 shows the relationship between the interface shear strength, the concrete strength f'_c and ρf_u . Note that the results pertaining to specimens with greased and ungreased interfaces are grouped together, on account of the interface condition having no effect on the shear strength. The peak strength of the majority of the tests considered was lower than 1200 psi (but a few tests exceeded this values). The data suggest that both f'_c and ρf_u influence the interface shear strength and the observed failure mode (yet to different extents). More specifically, ρf_u appears to play a major role on the shear strength, while the influence of f'_c is mostly noted when high concrete strength (approximately $f'_c > 6$ ksi) is combined with high values of ρf_u (approximately $\rho f_u > 1200$ psi).

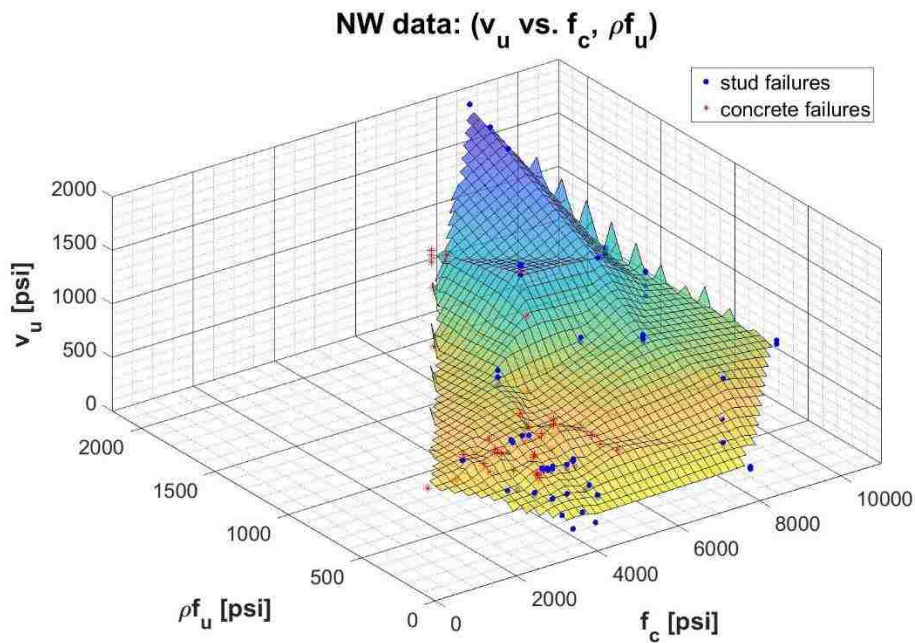


Figure 5.2.1.1: 3D shear strength plot for NW tests (Steel interface)

To emphasize how these two parameters affect the failure mode, the same data is shown in Figure 5.2.1.2 using a strength contour plot. Two “failure mode” zones can be identified, as a function of the different f'_c - ρf_u combinations. The data collected suggest that when f'_c is small ($f'_c < 6$ ksi), increasing ρf_u does not enhance the interface shear capacity, since the response is dominated by a concrete failure. Analogously, increasing the concrete strength while providing low values of ρf_u is not particularly beneficial as the response is governed by the failure of the steel studs. The experimental evidence suggests that it may be beneficial to increase both parameters simultaneously. However, not many high strength concrete ($f'_c > 6$ ksi) specimens with high ρf_u ($\rho f_u > 1200$ psi) values have been tested in the past, making it difficult to draw definitive conclusions.

The red line in Figure 5.2.1.2 attempts an approximate (and qualitative) division between the observable failure zones.

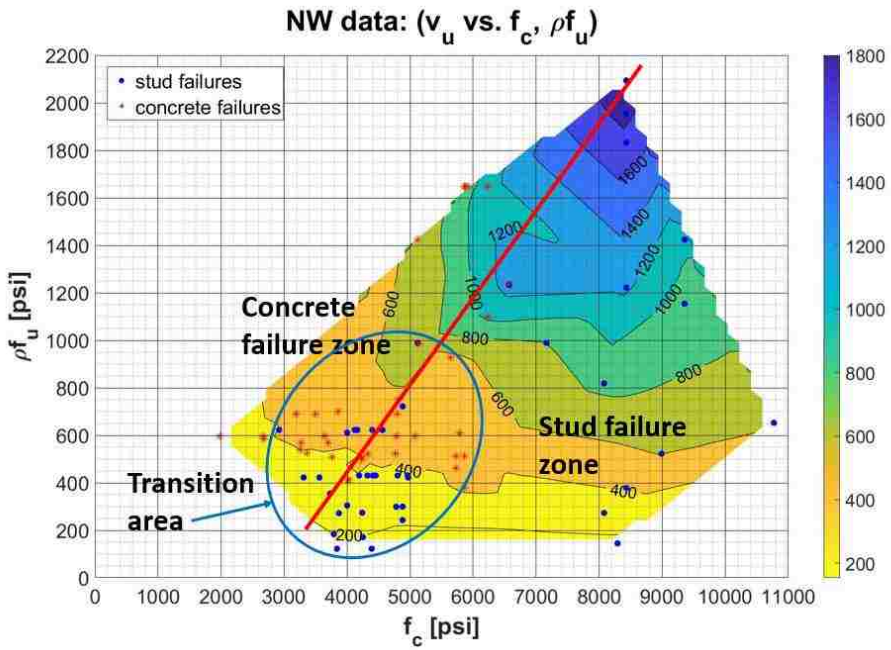


Figure 5.2.1.2: Shear strength contour plot for NW tests (Steel interface)

Figure 5.2.1.3 and Figure 5.2.1.4 summarize the available experimental results for lightweight concrete specimens. The trends observed for normal weight concrete specimens are confirmed and the comments provided apply to this case as well. However, the number of available lightweight concrete specimen test results available is somewhat limited, and only a small range of f'_c and ρf_u values has been covered in past research programs.

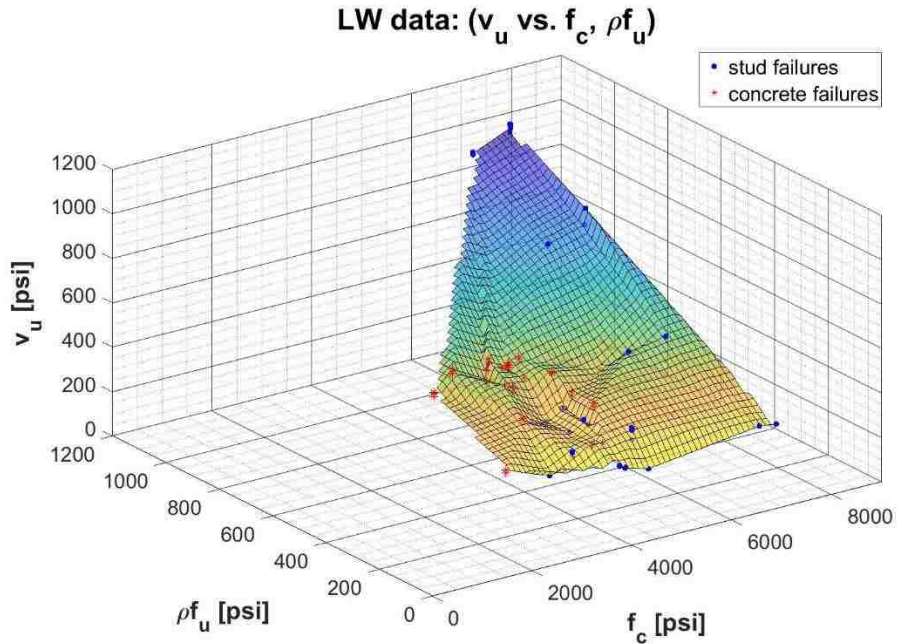


Figure 5.2.1.3: 3D shear strength plot for LW tests (Steel interface)

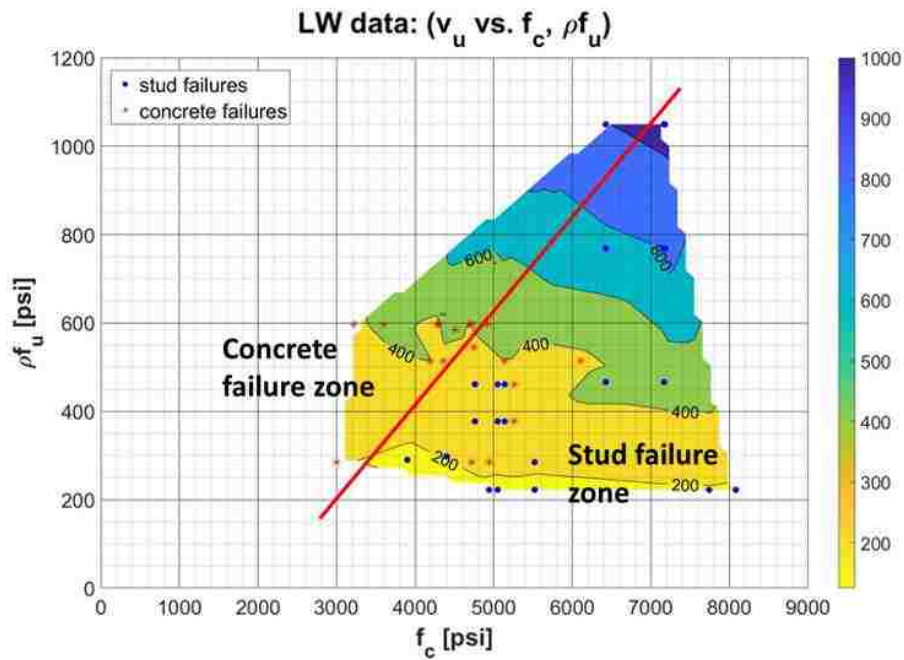


Figure 5.2.1.4: Shear strength contour plot for LW tests (Steel interface)

5.2.2 Effect of Tensile Strength of Shear Studs and Interface Preparations

From a thorough analysis of the experimental data available in the literature, it emerged that the steel stud ultimate stress, f_u , and the reinforcement ratio crossing the interface are the main parameters affecting the steel-concrete interface shear strength.

This is shown in Figures 5.2.2.1 and 5.2.2.2, for failure modes classified as “stud failure” and “concrete failure”, respectively. It should be noted that the shear strength of the specimens with different stud strength f_u , but similar values of f'_c and ρf_u , are not significantly different. This suggests that for normal strength concrete specimens (all results shown pertain to specimens with $f'_c < 6\text{ksi}$), the ultimate tensile strengths of the studs, f_u , has no significant effect as long as ρf_u is kept constant.

Another observation is that the shear strength does not seem to be significantly affected by the steel-concrete interface conditions. Note that some of the tests were performed on greased interfaces to decrease the interface friction, isolating the strength contribution provided by the steel studs. The expectations was that greased interfaces would be capable of transferring significantly less shear than their ungreased counterparts. However, the test results shown in Figures 5.2.2.1 and 5.2.2.2 outline that there is virtually no loss/gain in strength associated to the interface frictional properties. This suggests that frictional forces play a minor role with respect to the interface strength and that the majority of the applied shear is transferred by the steel studs.

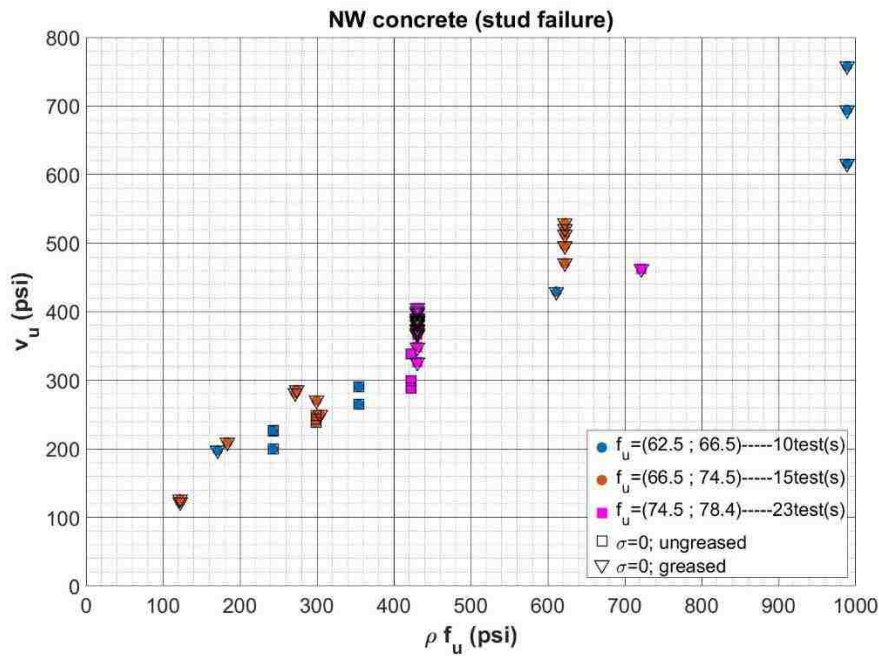


Figure 5.2.2.1: NW tests with $f'_c < 5.5$ ksi grouped by f_u (Steel interface)

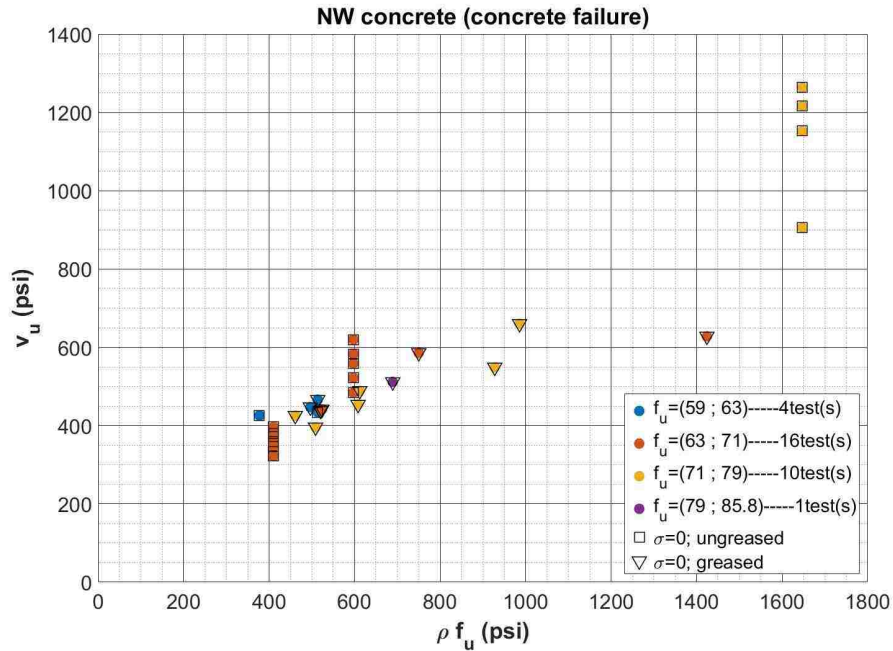


Figure 5.2.2.2: NW tests with $4 \text{ ksi} < f'_c < 6 \text{ ksi}$ grouped by f_u (Steel interface)

5.2.3 Effect of Concrete Type

Due to the limited amount of available data, the test results pertaining to SLW and ALW (sanded lightweight and all lightweight) concrete specimens with greased and ungreased interfaces were combined under the “LW concrete” label. Similarly, NW (normal weight) concrete specimens with ungreased and greased interface tests data were combined in a single group. However, stud failure and concrete failure mechanisms were examined separately.

To study the influence of the concrete type on the interface response, both NW and LW concrete with the same f'_c are necessary for comparison. Individual researchers did not provide such data; the alternative way to solve for concrete modification factor λ was to group data of similar f'_c . There were only certain ranges of f'_c with reasonable numbers of both NW and LW data points and these were chosen for comparison. The chosen ranges of f'_c were:

For concrete failures: $2.99 < f'_c < 4.93 \text{ ksi}$.

For stud failures: $4.39 < f'_c < 6.09 \text{ ksi}$.

Concrete Failures:

Figure 5.2.3.1 shows the interface shear strength as a function of ρf_u , for NW concrete specimens characterized by concrete compressive strength values within the range specified above. The solid lines represent the mean of the shear strengths; the dashed lines represent the mean plus or minus one standard deviation of the shear strength for data within each ρf_u range selected (separated with red circles). Figure 5.2.3.2 provides the same information for LW concrete specimens. It is possible to

extrapolate from Figure 5.2.3.1 and 5.2.3.2, that the ratio between the average shear strength, v_u , of LW and NW specimens ranges between 0.67-0.83 (See Table 5.2.3.1).

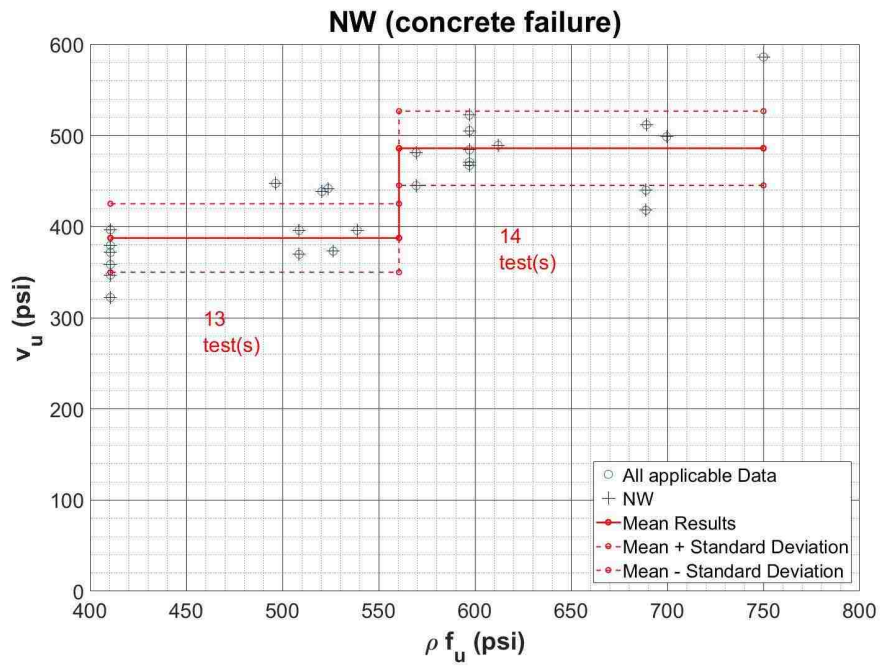


Figure 5.2.3.1: NW, concrete failure tests in the specified f'_c range

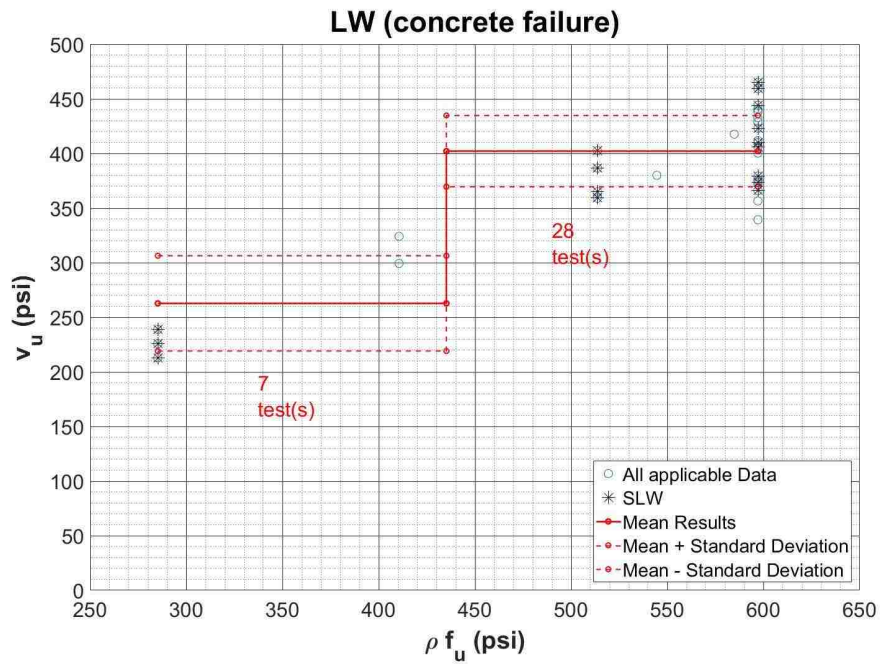


Figure 5.2.3.2: LW, concrete failure tests in the specified f'_c range

Table 5.2.3.1: Concrete failure tests— comparison between LW and NW concrete test results

Concrete failures	unit: [psi]		average
	400	600	
ρf_y	400	600	
$(\overline{v_{NW}}) \pm (\sigma_{NW})$	(388)+/-(38)	(486)+/-(41)	
$(\overline{v_{LW}}) \pm (\sigma_{LW})$	(263)+/-(44)	(402)+/-(33)	
$\lambda_{calc} = \frac{\text{average } v_{LW}}{\text{average } v_{NW}}$	0.68	0.89	0.79

Stud Failures:

The results summarized in Figures 5.2.3.3 and 5.2.3.4 suggest that LW concrete specimens are somewhat weaker than their NW concrete counterparts when similar ρf_u values are provided. Mean shear strength values for each concrete type at different reinforcement levels are shown in Table 5.2.3.2. The average strength ratio is between 0.7 and 0.83. It is worth remarking that both greased and ungreased data were combined to create this concrete type comparisons, which could affect the results.

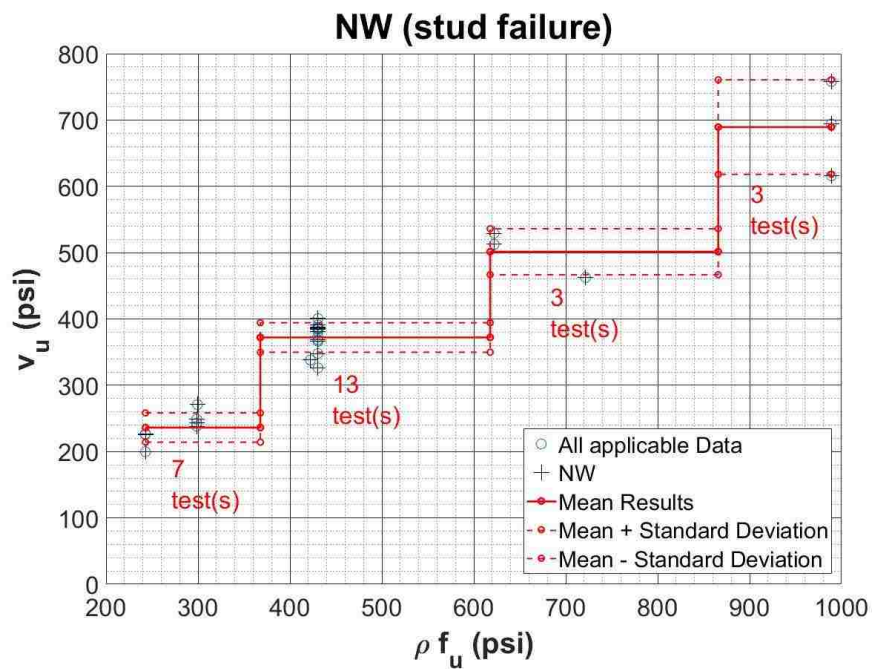


Figure 5.2.3.3: NW, stud failure tests in the specified f'_c range

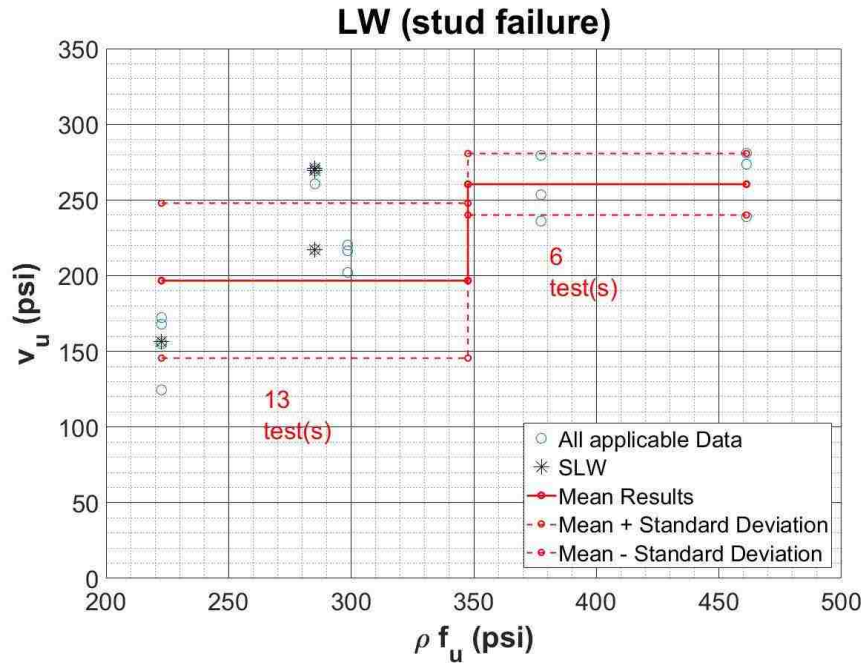


Figure 5.2.3.4: LW, stud failure tests in the specified f'_c range

Table 5.2.3.2: Stud failure tests— comparison between LW and NW concrete test results

Stud failures	unit: [psi]		average
	300	400	
$(\overline{v_{NW}}) \pm (\sigma_{NW})$	(236)+/-(22)	(372)+/-(22)	
$(\overline{v_{LW}}) \pm (\sigma_{LW})$	(197)+/-(51)	(260)+/-(20)	
$\lambda_{calc} = \frac{\text{average } v_{LW}}{\text{average } v_{NW}}$	0.83	0.70	0.77

5.2.4 Effect of Stud Spacing

Per AISC code provisions, the minimum center to center distance between shear studs in the direction parallel to the applied load should be 6 times the diameter of the stud. In the transverse direction, the minimum stud spacing should be at least 4 times the stud diameter. AISC provides no guidance about the likely decrease in strength of the connection, if smaller spacing is provided. It is assumed here that the limits are intended to inhibit concrete splitting failures. These spacing requirements are examined in this chapter, using the available test results pertaining to NW concrete specimens.

To minimize the impact of external variables, shear strengths normalized by ρf_u are examined with respect to stud spacing normalized by d_s . The results collected are summarized in Figures 5.2.4.1 and 5.2.4.2 to show the shear strengths of NW concrete specimens grouped as a function of f'_c . Figure 5.2.4.1 indicates that having ratios of longitudinal spacing over stud diameter smaller than 6 may result in a strength reduction. However, when the ratio increases, the spacing does not seem to affect the shear strength. No clear trends can be observed in Figure 5.2.4.2.

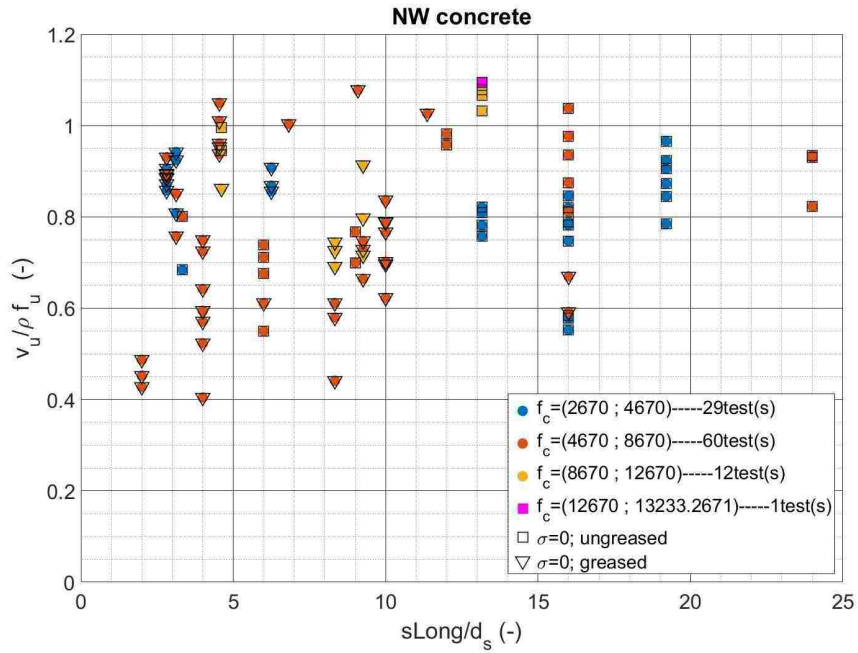


Figure 5.2.4.1: NW tests vs. ratios of longitudinal spacing over diameter of studs

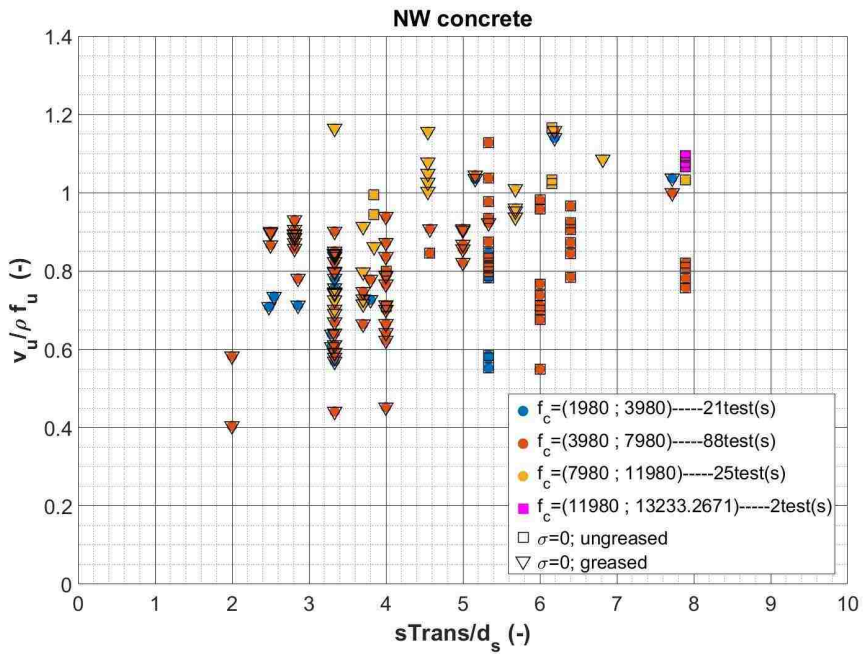


Figure 5.2.4.2: NW tests vs. ratios of transverse spacing over diameter of studs

5.2.5 Effects of Other Parameters

In addition to the five parameters (f'_c , ρf_w , f_u , longitudinal and transverse spacing, and concrete type) discussed in the previous sections (which are believed to be the primary factors influencing the interface

response), the importance of four more parameters was examined briefly. The additional parameter examined are:

- The diameter of the shear studs
- The thickness of the steel plate/flange (to which the studs are welded) relative to the diameter of the studs
- The thickness of the concrete slabs relative to longitudinal spacing of the studs
- The height of the studs relative to the stud diameter

The main observations can be summarized as follows:

1. The shear transfer strength does not appear to be significantly affected by the diameter of shear studs. The stud diameter values available in the database were between 0.37" and 1.25". Somewhat surprisingly, the few experimental results pertaining to specimens with $d_s > 1"$ showed that specimens with larger stud diameters failed at smaller loads than their companion specimens with smaller stud size. Few examples of the probable reasons for that are:
 - Insufficient anchorage due to stud head size compared to the diameter of the studs.
 - Grain sizes in the bigger studs differ from that of smaller studs due to cooling time required after welding. This affects steel strength and ductility.With these possible explanations in mind, the role played by the stud diameter on the shear strength should be studied more in depth as part of future studies.
2. The thickness of the steel plate to which the studs are welded does not seem to affect the shear strength as long as the ratio, d_s/t_f , is kept below the AISC Code Provision limit of 2.5. This limit stems from the research work by Goble (1968) in which a 2.7 limit was identified. The database analyzed in this research work contained data with d_s/t_f between 0.55 and 2.604 and the trends observed were in line with what is reported in the literature.
3. The maximum longitudinal stud spacing-slab thickness ratio is limited to 8 in the AISC Code Provisions. All the data analyzed in this work had smaller ratio than 8; consistently no remarkable or surprising trends were observed.
4. The AISC code currently limits the minimum height over diameter ratio to 4.0. The values of this ratio present in the database were between 3 and 9.09. In this context, no specific trends were observed. The only exceptions pertain to test results extracted from research programs intended to study pry-out failures (e.g. Anderson and Meinheit, 2005, in which short studs with $H_s < 2"$), which tended to have lower strength than the rest of the specimens analyzed.

5.3 Model comparisons

In this section, the performance of the main applicable code provisions and strength prediction models available in the literature is tested.

5.3.1 Performance Rankings of Available Models

The performance of the models considered in this section was analyzed analogously to what done in Section 4.3.3 for concrete to concrete interfaces. Predicted-to-measured shear strength ratios (indicated

with the letter “R”) are computed and statistically analyzed. The statistical measures pertaining to the computed R values (mean, standard deviation and coefficient of variation) and the total number of data points applicable to each model were summarized in Tables 5.3.1.1 through 5.3.1.3. Table 5.3.1.1 was produced using both NW and LW concrete data, while the other two tables were populated separately for NW and LW concrete data, respectively. Whenever the yield stress of shear studs was not reported, $f_y=60$ ksi was used to determine the predicted strength. Ultimate tensile strength of shear studs were set as measured tensile strength when reported; otherwise, taken as the nominal tensile strength of the studs.

The rankings are based on the following criteria:

- 1) The smallest coefficient of variation.
- 2) The smallest difference between mean R and 1.0.
- 3) The smallest standard deviation.

The models are ranked in the Tables 5.3.1.1 through 5.3.1.3 by COV, on the basis that if the predicted values were multiplied by a factor that would make R=1.0 in all cases, the standard deviation would increase by the same factor. Thus COV was chosen as the most critical measure of performance. This simple sorting approach was favored over more complex methods at this stage. Other sorting criteria, such as weighted average methods may also be considered and would possibly result in different outcomes. Tables 5.3.1.2 through 5.3.1.3 show that “shear friction” based models provided consistent (generally conservative) results for NW concrete specimens, while the rest of the models provided consistent results (with mean R values generally close to 1.0) for LW concrete.

*Table 5.3.1.1: Performances of available models – both NW and LW concretes
(Ranked from top to bottom)*

Concrete type performance	NW and LW combined			
	Average	Std.DEV	COV %	applicable points
CSA shear friction	0.5924	0.1332	22.4901	317
PCI 7ed. (2011) shear friction	0.6805	0.1578	23.1909	317
ACI (2014) shear friction	0.6805	0.1578	23.1957	317
AASHTO shear friction	0.7946	0.1907	24.0039	317
JSCE (2007)	1.0584	0.2599	24.5522	344
Oehlers & Johnson (1987)	1.2404	0.346	27.8986	344
Ollgaard Design (1971)	1.1648	0.3416	29.3279	396
Gobble (1968)	1.4759	0.4345	29.4387	396
Slutter&Driscoll (1965)	1.5563	0.4581	29.4387	396
EN (1994)	0.8785	0.259	29.4845	344
CSA (2010) and AASHTO(2014)	1.1708	0.3455	29.509	344
Ollgaard exact (1971)	1.1812	0.356	30.1415	396
Chinese Code (2003)	0.9351	0.287	30.692	344
AISC 14th ed.	0.9971	0.3067	30.7573	344
PCI 6th ed. Shear friction	1.1751	0.4571	38.9	317

Table 5.3.1.2: Performances of available models – NW concrete
(Ranked from top to bottom)

Concrete type performance	NW			applicable points
	Average	Std.DEV	COV %	
AASHTO shear friction	0.7511	0.1558	20.7436	221
CSA shear friction	0.6075	0.131	21.5568	221
ACI (2014) shear friction	0.6984	0.1526	21.8451	221
PCI 7ed. (2011) shear friction	0.6984	0.1526	21.8451	221
JSCE (2007)	1.0529	0.2883	27.3779	231
Oehlers & Johnson (1987)	1.2916	0.3921	30.3583	231
Ollgaard Design (1971)	1.1793	0.3842	32.5777	274
EN (1994)	0.9028	0.2963	32.8164	231
CSA (2010) and AASHTO(2014)	1.1978	0.3971	33.1486	231
Gobble (1968)	1.4421	0.4783	33.1664	274
Slutter&Driscoll (1965)	1.5206	0.5043	33.1664	274
Ollgaard exact (1971)	1.1915	0.4018	33.7201	274
Chinese Code (2003)	0.9306	0.3298	35.4433	231
AISC 14th ed.	0.9942	0.3532	35.5245	231
PCI 6th ed. Shear friction	1.1538	0.4175	36.1877	221

Table 5.3.1.3: Performances of available models – LW concrete
(Ranked from top to bottom)

Concrete type performance	LW			applicable points
	Average	Std.DEV	COV %	
Oehlers & Johnson (1987)	1.1355	0.1856	16.3475	113
CSA (2010) and AASHTO(2014)	1.1155	0.1929	17.2892	113
EN (1994)	0.8286	0.1464	17.6736	113
JSCE (2007)	1.0698	0.1897	17.733	113
AISC 14th ed.	1.0031	0.1784	17.7882	113
Chinese Code (2003)	0.9443	0.1694	17.9451	113
Ollgaard Design (1971)	1.1321	0.2153	19.0181	122
Ollgaard exact (1971)	1.1582	0.2211	19.0851	122
Gobble (1968)	1.5519	0.3029	19.5169	122
Slutter&Driscoll (1965)	1.6363	0.3194	19.5169	122
CSA shear friction	0.5575	0.1325	23.771	96
AASHTO shear friction	0.8948	0.2241	25.049	96
PCI 7ed. (2011) shear friction	0.6391	0.1696	25.4446	96
ACI (2014) shear friction	0.6392	0.1628	25.465	96
PCI 6th ed. Shear friction	1.2241	0.5365	43.8283	96

By comparing Table 5.3.1.2 and Table 5.3.1.3, the JSCE (Japanese design code) consistently performed well and had averages close to 1.0 for all concrete types. The unique thing about the JSCE code provisions is that the main form of the strength prediction has a stud height over diameter ratio term in it, while the majority of the other models only limit H_s/d_s ratios as an additional requirement.

The average R value for the AISC provisions is very close to 1.0, but with a greater scatter (COV).

The 6th edition and 7th edition of the PCI Design Handbook provisions performed significantly different from one another. The use of effective shear friction is no longer allowed in the 7th edition of PCI for steel interfaces. Table 5.3.1.2 and Table 5.3.1.3 show that the mean values of R for the 6th edition is greater than 1.0 (which corresponds to an unconservative estimate) with large scatter. More details will be discussed in section 5.3.2.

5.3.2 Detailed Performance of Code Provisions

The performance of the six North American code provisions tested in the previous section is discussed in more details in this chapter. The code provisions considered herein include the Shear friction provisions contained in the PCI (6th ed.), the PCI (7th ed.), the ACI 318-14, the AASHTO (2014), and the CSA (2014), and the provision for steel anchors contained in the AISC (14th ed.). Each code appears to have merits and flaws, showing either good or poor performance depending on the values of f'_c and ρf_u characterizing the specimen under consideration.

In Figure 5.3.2.1, the ratios of calculated/experimental strength values are plotted against $\ln f$, for the six code provisions. The ratio is plotted using a log scale so that ratios of two and one half appear on the plot to have the same error. The plot shows that the PCI 6th edition and the AISC 14th edition provisions tend to predict the shear strength of the majority of the tests with $f'_c < 6$ ksi somewhat unconservatively. All the other codes appear generally conservative, as their mean \ln° values are well below the $\ln(R)=0.0$ line.

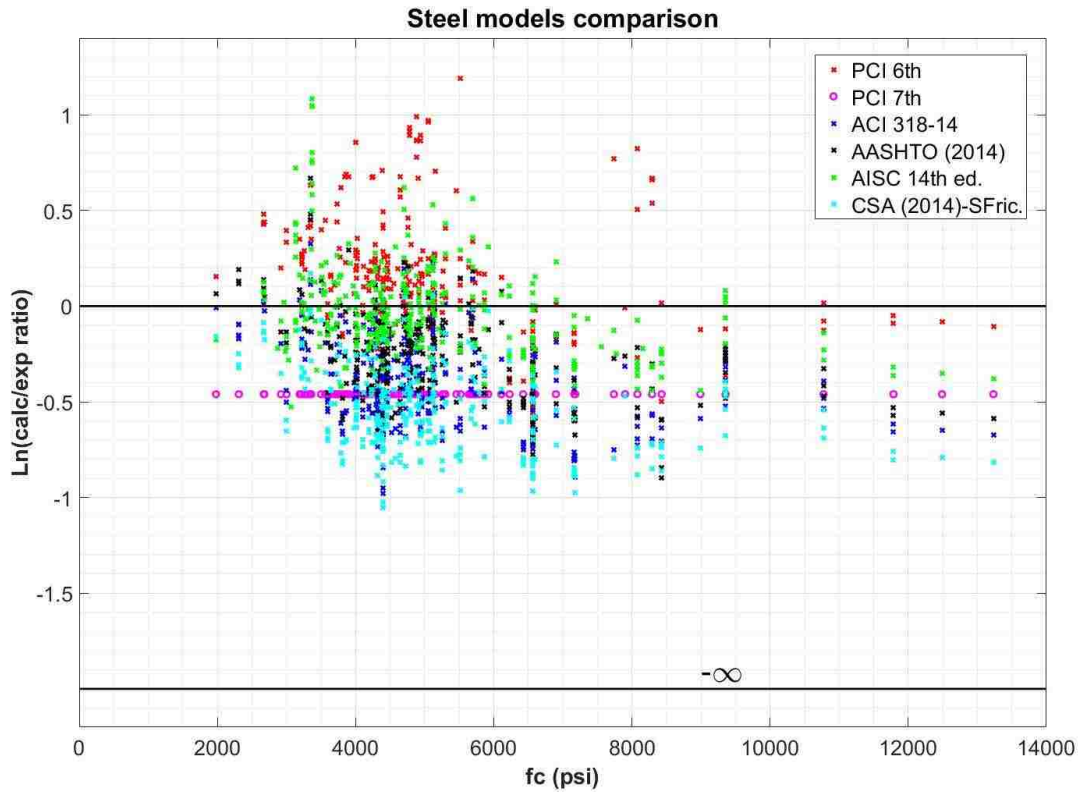


Figure 5.3.2.1: $\ln(R)$ ratios vs. f'_c (steel to concrete interfaces) —North American Code Provisions

Figure 5.3.2.2 shows the mean \pm one standard deviation of the R values for selected ρf_u ranges for all the code provisions considered and the JSCE code provisions (Section 5.3.1 showed JSCE perform well overall). It can be seen that the PCI 6th ed. provides unconservative strength predictions at approximately $\rho f_u < 800$ psi, while it becomes progressively more conservative as ρf_u increases in value. The average R values for the AASHTO provisions are consistently close to 1.0 compared to that of all other provisions, but the standard deviations are generally greater than the others. The AISC code provides R values that are on average close to 1.0 but it also provides significantly unconservative estimates in a number of occasions. The rest of the code provisions including PCI 7th ed., ACI 318-14, AASHTO (2014) and CSA (2014) are on the conservative sides at all ranges of ρf_u .

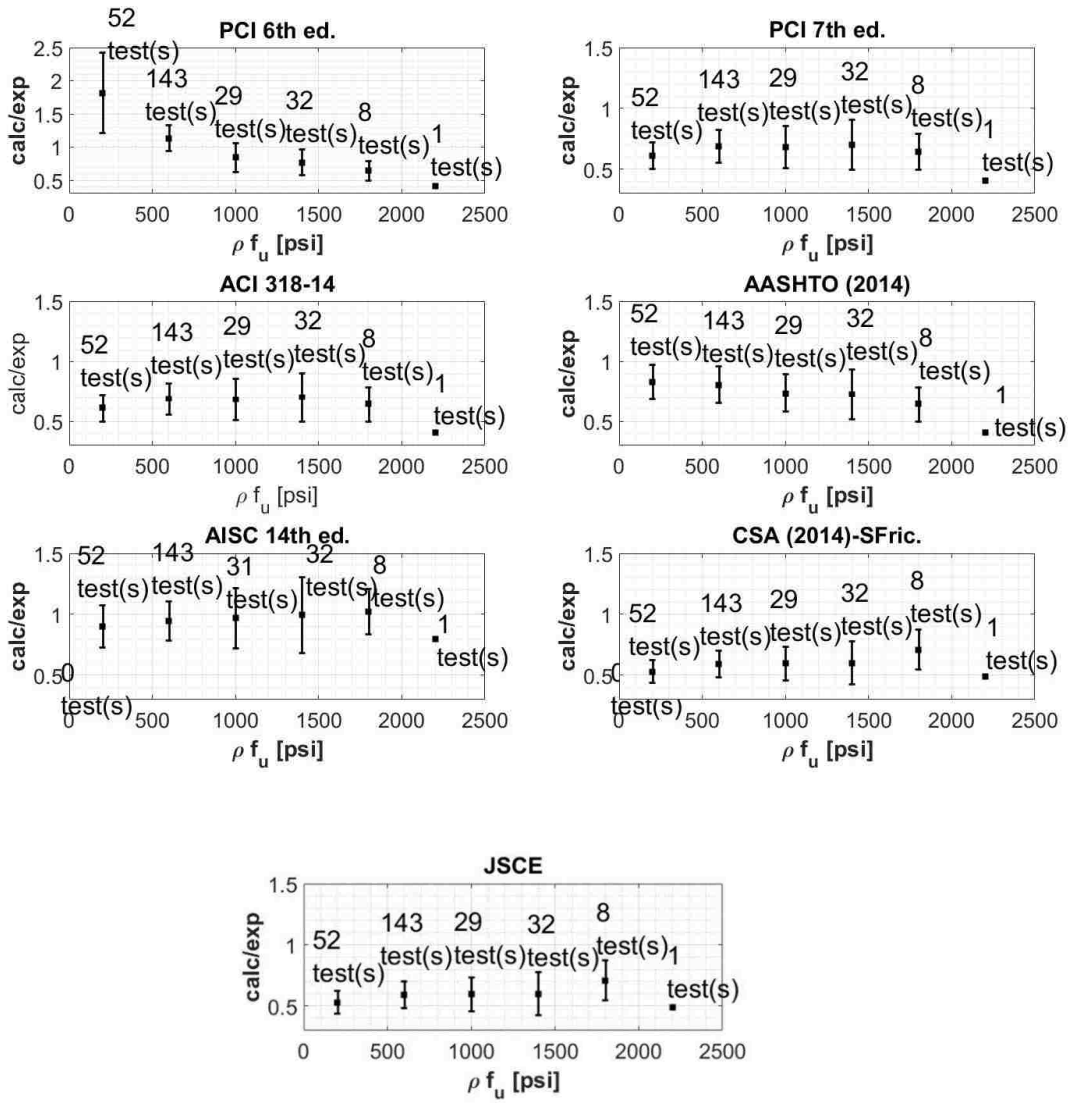


Figure 5.3.2.2: R ratios vs. ρf_u (steel to concrete interfaces)

Figure 5.3.2.3 provides another summary of the results of the analysis performed in this section. Here, the comparison between the performance of the 6th edition and the 7th edition of the PCI Design Handbook is notable. To this end, it is apparent that the 7th edition of PCI Design Handbook provides better and more conservative predictions than the 6th edition. It should be noted that while the 6th edition of the PCI Design Handbook allowed the use of an “effective friction coefficient”, the 7th edition no longer allows this option. This outcome suggests that the effective friction coefficient approach may not be a viable way of approaching the problem.

The JSCE provisions perform well on average and it indicates the value of a H_s/d_s ratio for the shear strength of shear connectors.

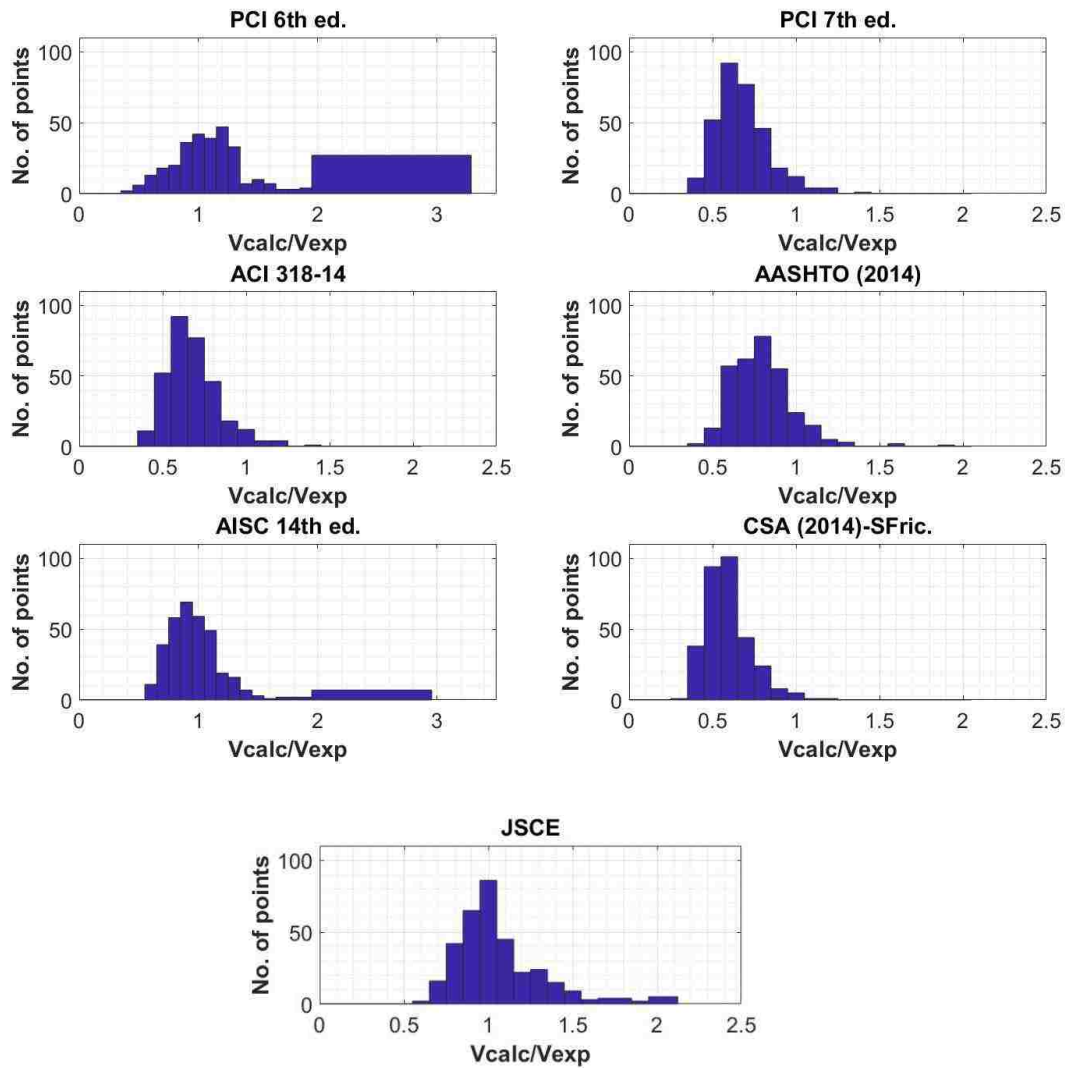


Figure 5.3.2.3: Bin counts of R ratios (steel to concrete interfaces)

6. Experimental Program

6.1 Introduction

As discussed in the previous sections, extensive research on stress transfer across interfaces has been conducted over the past 60 years. While concrete-to-concrete interfaces have been studied somewhat more thoroughly, the majority of the experiments dedicated to stress transfer across steel-to-concrete interfaces reported in the literature considered only “classic” solid slab test specimens. “Push-off” tests on solid slabs focus on “pure shear” rather than multiaxial stress states (e.g. shear and flexure). Thus, the characteristics of solid-slab tests cannot adequately represent some of the common applications of shear transfer across steel to concrete joints, which involve the simultaneous presence of shear and flexural forces to be transferred at the interface. These applications include (but are not limited to) steel

beam-to-concrete column or wall joints and steel column base connections (See Figure 6.1.1). These types of joints consist of embed plates/seats with welded headed studs or other types of fasteners.

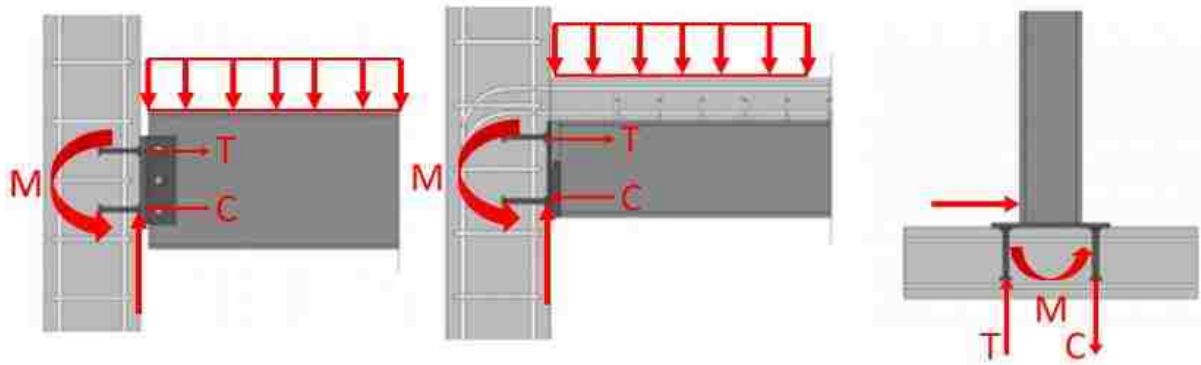


Figure 6.1.1: Example steel-to concrete joints (*Design of Steel-to-Concrete Joints Design Manual II*)

As shown in Figure 6.1.1, the applied loads generate combinations of shear and bending (which may be more or less significant, depending on the load eccentricity) that needs to be effectively transferred across the plate, to the adjacent structural element.

While there is general agreement that the simultaneous presence of shear and bending affects the behavior of the connections, with some notable exceptions (Kanvinde and Dierlein, 2011 and Lim et al., 2017), very few studies have looked at this phenomenon experimentally.

Thus, to provide some experimental evidence and to better understand the response of steel-to-concrete interfaces subjected to monotonic combinations of shear and bending, a test program was planned and conducted in the Structural Research Laboratory (SRL) at the University of Washington. The experimental program involved a total of five specimens, described in detail in later sections. The main variables considered were the M/V ratio and the stud distribution across the steel plate. All specimens were heavily instrumented: strain gauges were attached to the shear studs at various locations, to monitor flexural and axial strains in the studs and consequently calculate the stud forces; light-emitting diode (LED) targets were attached to both the plate and the loading post and tracked using an Optotrak HD system, to monitor plate displacements, rotations etc. in three dimensions; finally, two pairs of displacement sensors were used to monitor the horizontal displacement of the top and bottom of the loading post.

6.2 Specimen Design and Test setup

The test program aimed at studying the behavior of connections typical of precast beam-to-column/wall joints. In this type of connections, the load eccentricity (i.e. the distance between the point of application of the load and the interface along which the load is resisted) is relatively small; hence, a test setup was created to simulate this scenario (see Figure 6.2.2). More specifically, the H/L ratios considered in the experimental program (where H is the load eccentricity measured from the bottom

face of the embed plate and L is the distance between front row studs and the back edge of the embed plate) were 0.25, 0.5, and 0.92 (See Table 6.2.1). The fundamental properties of the specimens are summarized in Table 6.2.1.

Table 6.2.1: Test matrix

Test #	Specimen Name	Concrete block dimensions (in)	Embed plate dimensions (in)	d (in)	f_y (ksi)	f_u (ksi)	No. of front studs	No. of back studs	H (in.)	L (in.)	H/L
1	2-0-0.92	27 x 27 x 12	10 x 7 x 0.5	5/8	67.58	80.82	2	0	5.5	6	0.92
2	4-0-0.92						4	0	5.5	6	0.92
3	2-2-0.92						2	2	5.5	6	0.92
4	2-2-0.25						2	2	1.5	6	0.25
5	2-2-0.5						2	2	3	6	0.5

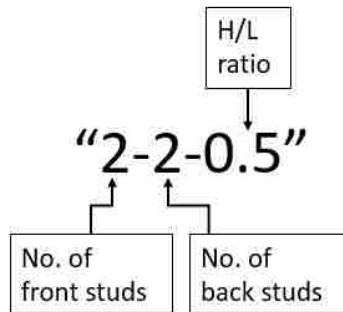


Figure 6.2.1: Specimen naming convention

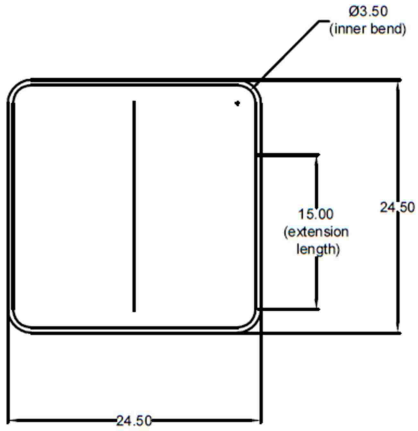
As reported in Table 6.2.1, all specimens consisted of 27"x27"x12" reinforced concrete blocks, with 10x7x 1/2" steel embed plates. The steel plates had two or four (the stud arrangement was varied throughout the test program as described later) 8" long-5/8" diameter headed studs welded to them. All specimens were cast on the same day, using a concrete mix with nominal specified compressive strength of 4,000 psi. A steel HSS welded to the steel plate served as the loading post. More details on the specimens, fabrication process and test setup can be found in later sections of this chapter.



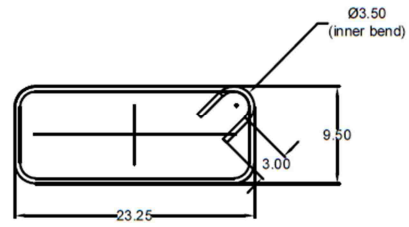
Figure 6.2.2: A typical specimen

6.2.1 Reinforced Concrete Blocks

The reinforced concrete blocks were designed to ensure that no premature failure of the blocks would occur. Five types of reinforcing bars were used to fabricate the reinforcement cages of the concrete blocks. The steel bars were purchased from Addison Construction Supply. All the longitudinal and transverse (horizontally placed) reinforcement bars were deformed Grade 60 #4 bars. The U bars for shear reinforcement were Grade 60 #3 bars (See Figure 6.2.1.1 for dimensions). Figure 6.2.1.2 shows the spacing details for an assembled reinforcement cage.

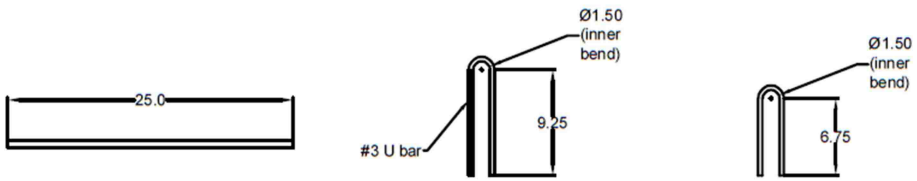


Type A:
Hoops with
parallel ends
(#4 bar)



Type B:
Hoops with 135°
bent ends (#4 bar)

Figure 6.2.1.1.a: Reinforcement types



Type C:
Straight bar (#4
bar)

Type D:
U bar (#3 bar)

Type E:
U bar (#3 bar)

Figure 6.2.1.1.b: Reinforcement types cont.

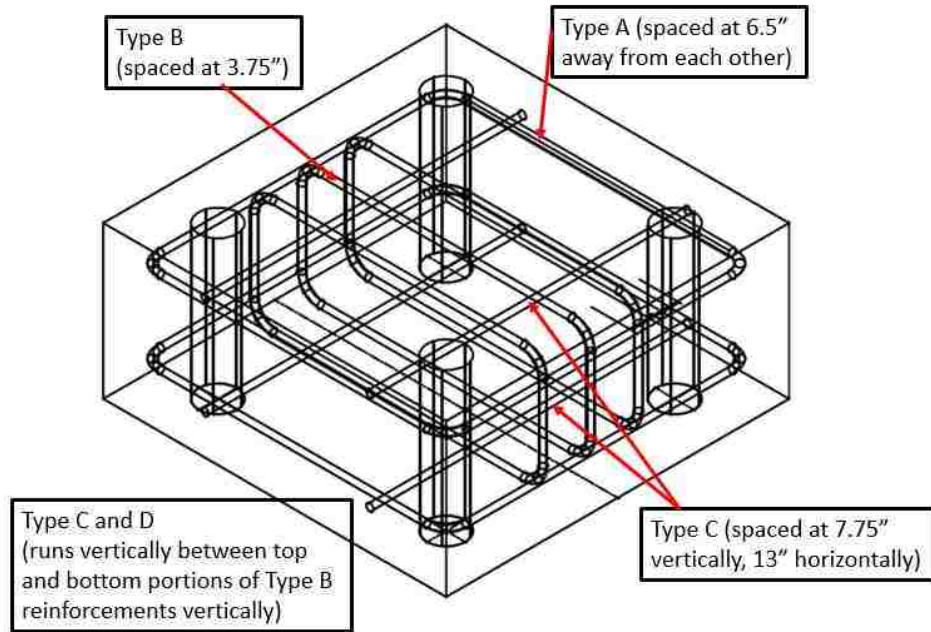


Figure 6.2.1.2: Spacing details of reinforcement cage

Shear reinforcements were placed with respect to the embed plate and the other reinforcements in the concrete block as shown in Figure 6.2.1.3. The final assembled reinforcing cages looked as shown in Figure 6.2.1.4.

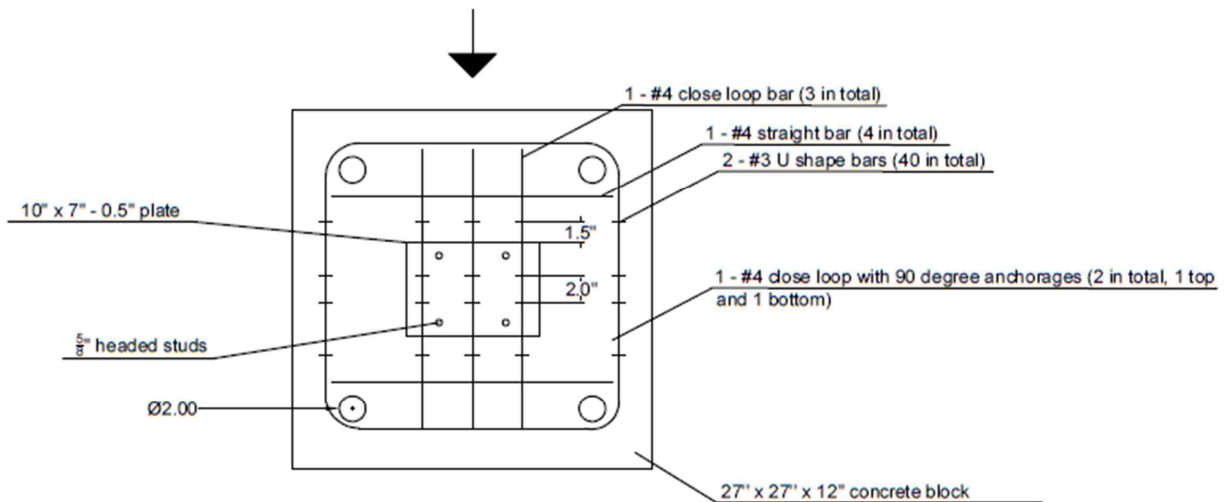


Figure 6.2.1.3: Spacing details shear reinforcement



Figure 6.2.1.4: Reinforcement cage side by side views

Besides the reinforcement cages, 4 pieces of steel pipes (SCH 40, inner $\phi 2''$, wall $t=0.154''$) per specimen were used to create the necessary holes to accommodate the threaded rods that were used to connect the specimens to the strong floor (See Figure 6.2.1.5). These pipes also served as reinforcements for the concrete around them, preventing a premature failure around the locations of holes.

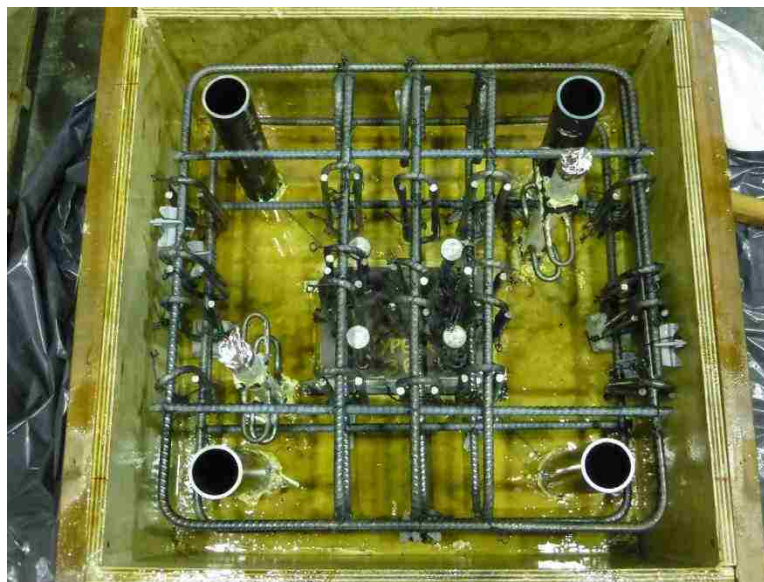


Figure 6.2.1.5: Reinforcement cage and steel pipes in place

6.2.2 Formwork

Custom formworks were built using 2"x4" and 2"x2" lumbers and 0.75" thick plywood. The inner dimensions of each formwork was 27"x27"x12". Each wall of the formwork and the bottom piece were built separately and bolted together to allow for ease of disassembling after casting. The notched 2"x4" pieces were glued to the other components of the same wall before being bolt together with them. The bottom plywood sheet was bolted to three 2"x4" lumbers. The space provided in between the bottom lumbers would allow for transportation using forklift. An example of assembled formwork is shown in Figure 6.2.2.1.



Figure 6.2.2.1: Assembled formwork

Later in the manufacturing process, 2 holes on the bottom and one hole on a side wall were drilled. The reasons for these holes will be discussed in Section 6.2.4 and 6.2.5. The inner surface of the completed formworks was varnished with two coats of polyurethane and all gaps and edges were sealed with acrylic latex caulk.

6.2.3 Placement of embed plates

The embed plates were designed to go in the center of the formwork such that the 7" long direction of the plates would be in the longitudinal direction (parallel to the applied load). To eliminate the bearing contribution of the concrete around the plate, 0.5" thick and 0.75" wide foam strips (11" or longer) were glued to the bottom of the formwork where the back side of the embed plate would go. To secure the embed plates in place, small angles were bent and bolted down to the formwork (See Figure 6.2.3.1). All edges were sealed with acrylic caulk (See Figure 6.2.3.2). Then, the strain gauge wires were taped around the studs to avoid the wires getting in the way of rebar cages.

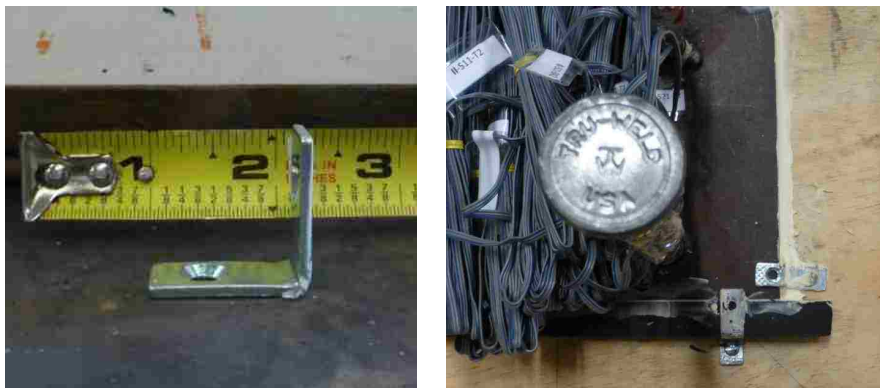


Figure 6.2.3.1: Embed plate securement



Figure 6.2.3.2: Embed plate placement

6.2.4 Lifting system

A lifting system other than the 2"x4" lumbers on the bottom of formwork was necessary to lift the specimens after disassembling the formwork. Since the specimens were cast upside down, simple lifting loops would not have been ideal. Thus, two rods (ϕ 7/8") were placed symmetrically near the top and bottom of the concrete block (2 rods and 4 inserts per specimen) and were later used to flip the concrete blocks and to move them to the testing rig (See Figure 6.2.4.1).



Figure 6.2.4.1: Lifting rods and their coil inserts

Two $\phi 1$ " holes were drilled symmetrically for the rods to go through the bottom plywood of the formwork. The bottom inserts were secured to the plywood by tightening bolts and nuts from the other side of the plywood. $\phi 1$ " PVC pipes were placed in between the coil inserts and above the top insert to protect the rod from the concrete. The gaps between the coil inserts and the PVC pipes as well as the plywood were sealed with acrylic caulk. The top PVC pipes were partially dipped in the concrete to allow for the top inserts to be close to the tip of the lifting Eye Rods that would be inserted later. Hence, the dipped portion of the PVC pipes was also covered in wax to prevent them from sticking to the concrete permanently. Finally, the top of the PVC pipes were wrapped with foil tapes to keep the concrete out of the pipes.

6.2.5 Reinforcement and pipes

Before putting the reinforcing cages in, the strain gauge bundles were released and were extended through the hole in the side wall of the formwork. The hole was then sealed with self-hardening clay (See Figure 6.2.5.1).



Figure 6.2.5.1: Strain gauge wires going out of the formwork

The dimensions of the reinforcing bars and the steel pipes were briefly discussed in Section 6.2.1. The steel pipes were located 4.5" away from the closest two edges of the formwork. The pipes were inserted in a tight circle surrounded by 4 nails. The bottom of the pipes were sealed with acrylic caulk. After all the pipes were sealed, the formwork was greased in preparation to install the rebar cage.

To provide proper clearances, 1.5" concrete rebar chairs as well as 1.25" plastic rebar chairs were placed on the bottom of each rebar cage. 1" plastic rebar chairs were attached to the sides of the rebar cages. The rebar cages were then placed in the formwork. Finally, to prevent the steel pipes from wobbling, small frames with 4 plywood plugs (with similar diameter as the ID of the pipes) were screwed down to the top edges of the formworks (See Figures 6.2.5.2 and 6.2.5.3).



Figure 6.2.5.2: Frame with plugs for the steel pipes



Figure 6.2.5.3: Rebar cage and steel pipes secured in place

Once all the cage components were in place in the formwork, the loose strain gauge wires were zip tied to the nearest reinforcing bars all the way to the tiny hole in the side wall (See Figure 6.2.5.4).



Figure 6.2.5.4: Strain gauge wires secured to the nearest rebar

The wires coming out of the formworks were bundled together and were sealed in plastic bags. The plastic bags were attached to the sides of the formworks (See Figure 6.2.5.5).



Figure 6.2.5.5: Strain gauge wires protected for casting process

6.2.6 Concrete casting, surface preparation

The day before casting, the formwork was greased while making sure that there was no oil on any steel component including rebar cages, embed plates, and the steel pipes. Any grease dropped on the steel components was cleaned thoroughly before casting. On March 16th, 2018, the specimens were cast. To keep the disturbance to the strain gauges minimal, the concrete was shoveled into the formwork from wheel barrows instead of casting directly from the concrete truck. Also, all the concrete in the surrounding of the shear studs and strain gauges wires was vibrated with extra care.



Figure 6.2.6.1: Casting day

After an hour of casting, the top frame with plugs were removed. The top surfaces of the specimens were scraped and floated to ensure even and smooth finish. After floating, curved end edger was used to finish the edges of the specimens. Also, the rods in the lifting systems were twisted around to make sure they were not stuck with concrete.

Curing methods of concrete cylinders and specimens

Concrete cylinders (4"x8") were cast and removed from the plastic molds within 24 hours after casting; then, they were sulfur capped and stored in a moisture cure room until being tested. However, the test specimens were not stored in the moisture cure room but simply covered with wet burlaps and then with saran wraps as shown in Figure 6.2.6.2. The burlap covers were rewetted every other day for the first 7 days.



Figure 6.2.6.2: Moisture curing set up for test specimens

6.3 Materials

6.3.1 Concrete mixture

All specimens were made from same batch of concrete mixture and were cast on 03/16/2018. The mixture was prepared and delivered to the structural engineering laboratory by the Salmon Bay Sand and Gravel Co.

Standard mixture design:

6 ½ sacks (meets the Seattle IBC) of cement per cubic yard of concrete with ¾" Pea gravel as the coarse aggregate. 4" slump was expected but the actual slump during casting was 5.5" (See Figure 6.3.1.1).



Figure 6.3.1.1: Slump test result

The specified compressive strength was 4000psi. However, the actual compressive strengths on test days and at different ages (days) were tested in accordance with ASTM 39 standard for compressive strength (See Table 6.3.1.1). Companion cylinders for Specimens 2-2-0.25 and 4-0-0.92 were not tested but the compressive strength was extrapolated using the 7, 14, 28, 34, 40, and 45 day strengths (See Figure 6.3.1.3). All test cylinders were standard moisture cured 4"x8" cylinders. A FORNEY—400 kips compressing testing machine was used to test the cylinders. The loading rate was kept between 21,111 lbs/min and 31,666 lbs/min (See Figure 6.3.1.2 for cylinder test set up).



Figure 6.3.1.2: Compressive strength test set up

Table 6.3.1.1: Compressive strengths of concrete at different ages

Test #	Specimen name	f'_c at test day (test date and age indicated in parenthesis)	f'_c at 7 days (03/23/2018)	f'_c at 14 days (03/30/2018)	f'_c at 28 days (04/13/2018)
1	2-0-0.92	Average: 7589 psi (04/19/2018=34 days)	Cylinder 1: 5366 psi Cylinder 2: 5761 psi Average: 5563 psi	Cylinder 1: 6160 psi Cylinder 2: 6291 psi Average : 6226 psi	Cylinder 1: 7118 psi Cylinder 2: 6877 psi Average : 6998 psi
2	4-0-0.92	Extrapolated: 7545 psi (04/23/2018=38 days)			
3	2-2-0.92	Average: 7627 psi (04/25/2018=40 days)			
4	2-2-0.25	Extrapolated: 7667 psi (04/27/2018=42 days)			
5	2-2-0.5	Average: 7749 psi (04/30/2018=45 days)			

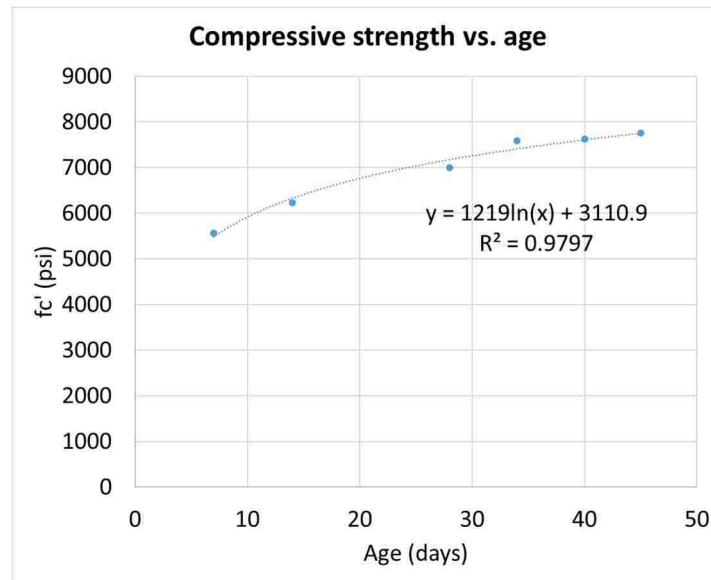


Figure 6.3.1.3: Compressive strength trend with time

6.3.2 Embed plates

Properties provided by the manufacturer:

The stud arrangements for the embed plates will be discussed in Section 6.4.2. All studs were welded in accordance to the AWS D1.1 (American Welding Society). The 0.5" thick steel plates were of Grade A36. The mechanical and chemical properties of the base plates are summarized in Table 6.3.2.1.

Table 6.3.2.1: Properties of embed plates

Yield-1 [psi]	Tensile-1 [psi]	Elong. % in 8"							
42,200	61,000	28.8							
Yield-2 [psi]	Tensile-2 [psi]	Elong. % in 8"							
44,700	62,800	29.1							
Heat No.	C	Mn	P	S	Si	Cu	Ni	Cr	Mo
7508293	0.07%	0.87%	0.1%	0%	0.29%	0.24%	0.07%	0.09%	0.03%
Al (tot)	V	Nb	Ti	N	Ca	B	Sn	Ceq	Pcm
0.027%	0.006%	0.002%	0.004%		0.0042%	0.0002%	0.01%	0.26%	0.15%

The ϕ 5/8" studs were purchased from "Tru-Weld USA" (5/8x8—3/16 B/W). The geometrical properties of the studs were as shown in Figure 6.3.2.1 (Note that L is length before welding. Length after welding is 3/16" shorter):



Figure 6.3.2.1: Dimensions of shear studs (taken from a catalog of "Tru-Weld")

The studs were made of low carbon steel Grade C1015 in accordance to the ASTM A108. The specified mechanical and chemical properties of the shear studs are reported in Table 6.3.2.2. Note that the stud strength obtained from tensile tests performed in the structural engineering laboratory at the University of Washington differed from the manufacturer specified values.

Table 6.3.2.2: Properties of shear studs (provided by the manufacturer)

Yield [psi]	Tensile [psi]	Elong. % in 2"					
52,784	69,619	39.1					
Heat No.	C	Mn	P	S	Ni	Cr	CEV %
20313250	0.16%	0.58%	0.008%	0.001%	0.04%	0.07%	0.306%

Tensile Test Results (Conducted at SRL at UW)

Three stud samples were tested in the SRL at UW, to obtain the actual stress-strain relationships characterizing their tensile response. To allow for better grip in the machine, the stud heads were cut off. The total length of the shank was 7-5/8" as shown in Figure 6.3.3.2.



Figure 6.3.2.2: Sample stud shanks

To ensure stress concentration hence failure at mid length of the shank, the diameter of the shank was reduced from 0.621" down to 0.6" (See Figure 6.3.2.3). This process was achieved using Systig Lathe machine. All dimension measurements are summarized in Table 6.3.2.3.



Figure 6.3.2.3: Machined stud shanks for tensile tests

Table 6.3.2.3: Diameters of the sample stud shanks at different lengths

Sample No.	Wide end diameter (in)	Mid-length diameter (in) OD: outer diameter ID: machined inner diameter	Narrow end diameter (in)
1.	0.623	OD: 0.621, ID: 0.6	0.618
2.	0.623	OD: 0.621, ID: 0.6	0.617
3.	0.624	OD: 0.621, ID: 0.6	0.616

The tensile test was conducted using an MTS 110 kip machine with MTS 647 hydraulic wedge grips (See Figure 6.3.2.4). The grip stress was 3000 psi. The gauge length was taken as the entire length of the shank rather than distance between the out most wedge grip teeth of top and bottom grips (See Table 6.3.2.4 for initial distance between top and bottom grips). The deformation was measured with the MTS machine's LVDT. The readings were taken until the samples fractured at the intended location.

Table 6.3.2.4: Gauge length information for stud tests

Sample No.	Initial distance between top and bottom grips (in.)	Gauge length (in.)
1.	2.2	7-5/8
2.	2.2	7-5/8
3.	2.12	7-5/8



Figure 6.3.2.4.a: Test set up for tensile strength of studs



Figure 6.3.2.4.a: Test set up for tensile strength of studs (close-ups)

As the tensile load increased, each sample necked and eventually fractured at the stress concentration zone. Figure 6.3.2.5 shows typical necking and fractured stud shanks.



Figure 6.3.2.5: Stud shank test (necking and fracture photos)

Stress strain relationships of the stud tests:

As mentioned previously in this section, the entire length of stud shank (7-5/8") was used for gauge length in the strain calculations to account for the deformation of the gripped portions of the studs. Figure 6.3.2.6 shows the stress strain relationship of the studs in tension. Sample 1's loading was put on hold once during the test and was then continued. The spike in Sample 1's curve around 0.03 strain does not illustrate the fracture but simply the pause in loading. As shown in Figure 6.3.2.6, the average

ultimate strength was 80.82 ksi and the yielding strength determined by the 0.2% offset method was 67.58 ksi.

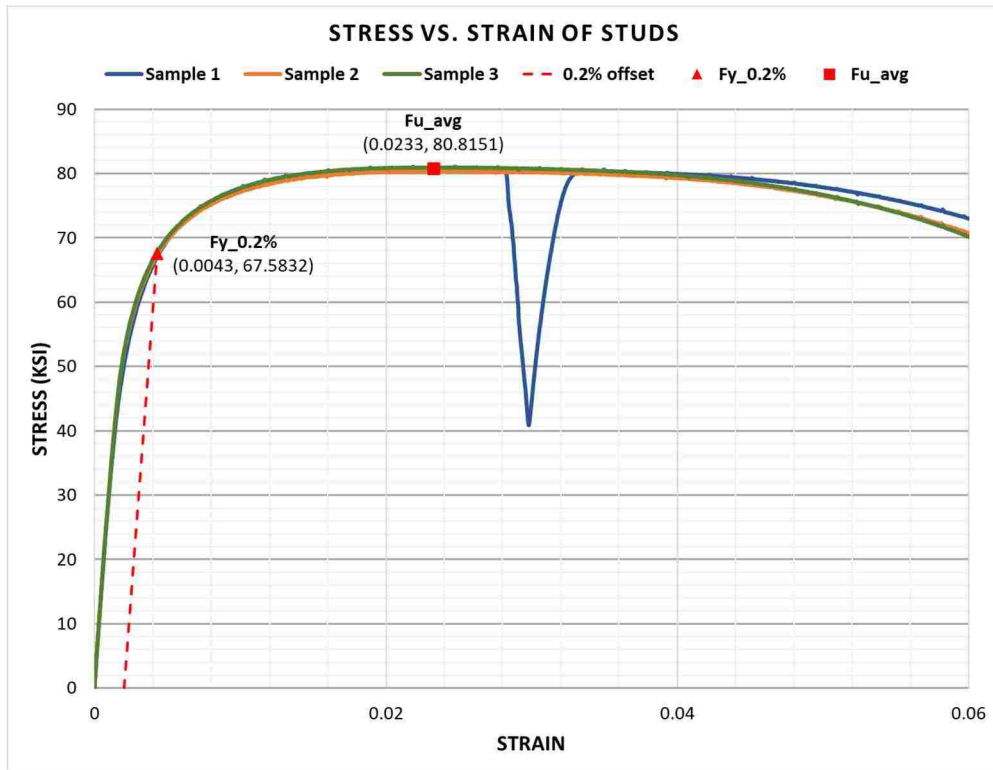


Figure 6.3.2.6: Stress-strain relationship of shear stud shanks in tension.

6.4 Test Setup and Instrumentation

6.4.1 Test Setup

All specimens were designed so that shear and bending forces could be generated across the plate-to-concrete interface. This was achieved by applying a monotonic “line load” to the HSS loading post until failure (See Figure 6.4.1.1).

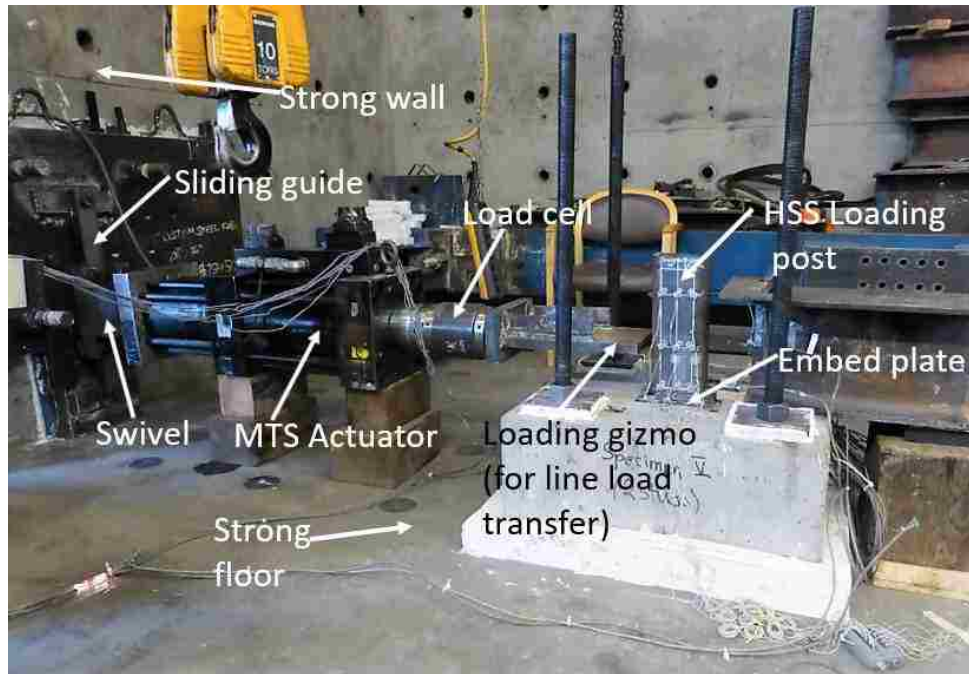


Figure 6.4.1.1: Load transfer system

The loading posts were fabricated using five HSS tubes welded to the embed plates. The load demand on the HSS was conservatively determined assuming that the total tensile strengths of the 4 shear studs would control failure. Evidently, the specimen with 2 shear studs would have less demand than the other four specimens. As a result, the sizes of the tubes were chosen to handle a minimum load of either 55kips (for the two-stud specimen) or 110 kips (for all other specimens):

- 6"x6" HSS tubes with wall thickness of 0.5" for specimens with 4 studs. These tubes were Grade A500-B. All 6"x6" HSS tubes were 15" long (Figure 6.4.1.2.a).
- 5"x5" HSS tube with wall thickness of 0.375" was used for the specimen with 2 studs. The exact Grade of this particular tube was unknown but it is believed to be Grade A500. The 5"x5" tube was 13.5" long (Figure 6.4.1.2.b).



Figure 6.4.1.2.a: 6"x6 HSS tubes for 4-stud specimens



Figure 6.4.1.2.b: 5"x5" HSS tube for 2-stud specimen

Specimen failure was defined as the moment when the applied load started to drop after the peak monotonic load had been reached. An MTS 110-kips hydraulic actuator was used to induce the desired loading conditions. The actuator was placed on top of timber blocks and connected through a swivel to a strong reaction wall (See Figure 6.4.1.1).

A special connection was designed to allow the connection between the swivel and the strong wall. To this end, the back side swivel of the actuator was bolted to four 1" thick steel spacers which in turn were connected to a 1" thick plate (See Figure 6.4.1.3.a). Concurrently, a "sliding guide" was welded to a 4" thick steel plate bolted to the strong wall, to allow a secure connection between the actuator and the wall, while still allowing the actuator to slide vertically (Figure 6.4.1.3.b).

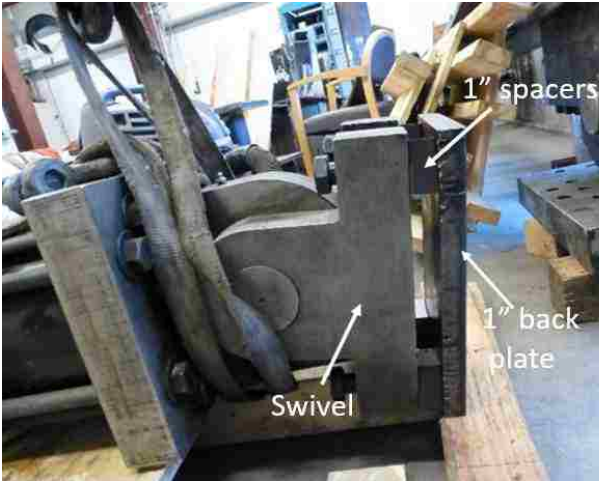


Figure 6.4.1.3.a: Back side swivel being checked for component fitting (bolts were tightened in place later)

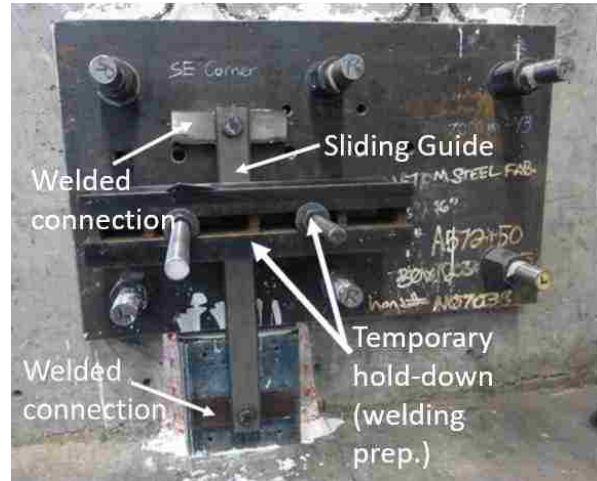


Figure 6.4.1.3.b: The guide held-down for welding preparation (the horizontal hold-downs were removed after welding)

This custom design was implemented to enable the actuator to work at any desired elevation (See Figure 6.4.1.4.a). Heavy duty C-clamps were also used to vertically restrain the movement of actuator along the guide (See Figure 6.4.1.4.b).



Figure 6.4.1.4.a: Actuator sitting on timber pieces



Figure 6.4.1.4.b: Back of the actuator

A special gizmo was fabricated and connected to the front end of the actuator (See Figure 6.4.1.5) to transfer the loads from the actuator to the loading post. This gizmo consisted of an 8.5" wide, 1" thick steel plate, welded to a 1.5" thick steel plate which was bolted to the actuator rod. This system allows for the applied load to be evenly distributed across the width of the HSS loading post, while allowing for desirably low load eccentricity to be achieved.



Figure 6.4.1.5: Assembled gizmo

The peak strength (i.e. the maximum sustainable horizontal force) of the strongest specimen was estimated at 110 kips. Thus, this load was used to find the flexural and shear capacity needed for the gizmo. The buckling capacity of the horizontal plate was also checked. As a result of the calculations, the following size of plates were chosen:

- 5" x 9.5" ($t_p=1.5$ ") vertical plate with a ϕ 2" hole in the center (centered 2" from the bottom edge of the plate in the 5" direction). This plate was designed to be connected to the actuator system through ϕ 2" —12TPI threaded rod (4-7/8" long) and were tightened with a nut. The nut was 2" tall and the distance between the across corners was 3.5" .
- 8.5" wide, 13.5" long ($t_p=1$ ") horizontal plate was welded to the vertical plate 2" away from the bottom of the vertical plate. To allow for the nut to fit and for possible adjusting later on, the horizontal plate had a 4.5" wide, 3" long notch where it met the nut. To provide additional stiffness, two 2" tall, 9" long ($t_p=0.5$ ") stiffener plates were welded to the vertical and horizontal plates symmetrically.

Prior to testing, all specimens were pre-stressed to the strong floor using ϕ 1.5" threaded rods, as shown in Figure 6.4.1.6.



Figure 6.4.1.6.a: Concrete block in place



Figure 6.4.1.6.b: Pre-stressing set up

6.4.2 Specimen Instrumentation

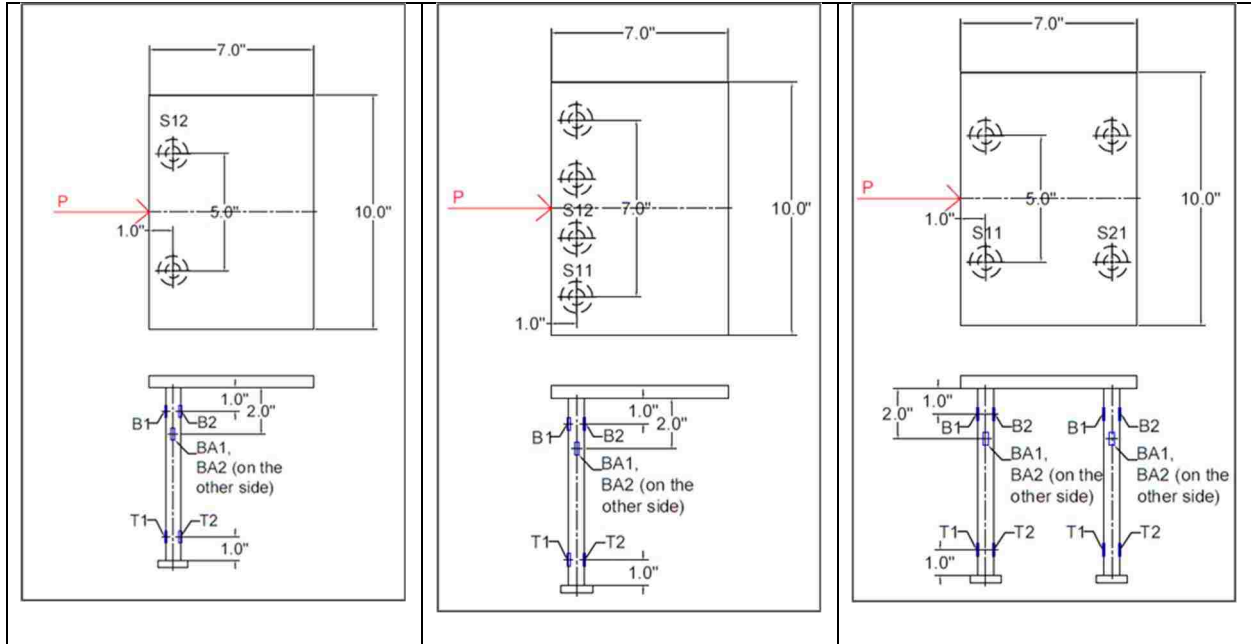
To fully document the behavior exhibited by the test specimens, a detailed instrumentation scheme was used to acquire specimen local and global displacements, reactions, stud strains and applied loads.

Strain Gauges

See Table 6.4.2.1 for stud instrumentation scheme for all tests. The studs labeled in the drawings in Table 6.4.2.1 were instrumented with strain gauges with 5mm gauge lengths.

Table 6.4.2.1: Stud instrumentation scheme

Specimen 2-0-0.92	Specimen 4-0-0.92	Specimen 2-2-0.92 Specimen 2-2-0.25 Specimen 2-2-0.50
-------------------	-------------------	---



The surfaces of the selected studs were abraded with finely gritted sandpapers and cleaned with acid and base. Once the surface was ready, the strain gauges were put in place using M-LINE PCT-2A cellophane tape and a glue. The strain gauges were then coated with M-Coat D. Detailed instruction ("*Strain Gauge Installations with M-Bond and AE-10 Adhesive Systems*") from Micro Measurements (MM) were followed step by step. (See Figure 6.4.2.1)



Figure 6.4.2.1: Installed Strain gauges (before and after M-Coat application)

Beyond the installation guidelines from MM, more protection over the M-Coat was necessary to minimize impacts from the concrete around the studs. The strain gauges were covered with wax and then wrapped with foil tape. The base of the strain gauge wires were wiggled and taped to the studs to

prevent the wires from being accidentally pulled away during manufacturing and testing (See Figure 6.4.2.2). The other ends of the strain gauge wires were labeled neatly and protected with tapes.

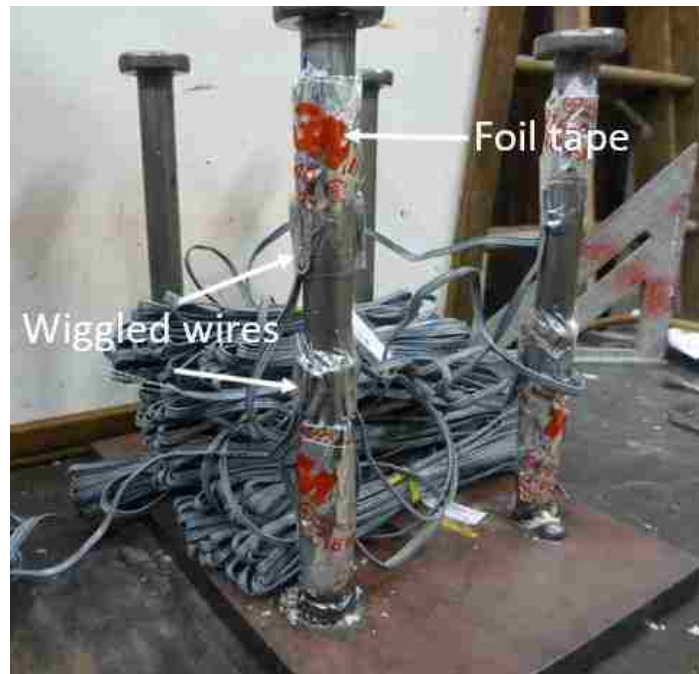


Figure 6.4.2.2: Typical completely protected strain gauges

LVDTs

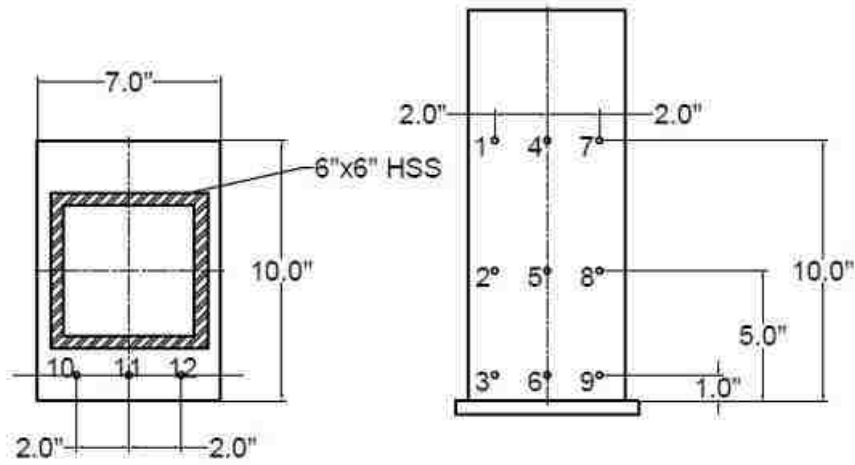
Two pairs of LVDTs were used to continuously monitor the top and bottom horizontal displacements of the HSS loading post. These LVDTs were connected to the side of the HSS and supported by a purposely fabricated steel frame (See Figure 6.4.2.3). They were placed at 1" and 10" away from the embed plate and were spaced 3" or 4" away from one another in the direction transverse to the direction of the applied load (i.e. the transverse direction), depending on the size of the HSS tube. More specifically, for the 5"x5" tube, used only for Specimen 2-0-0.92, the horizontal LVDT spacing was 3", while a 4" spacing was used for the rest of the specimens.



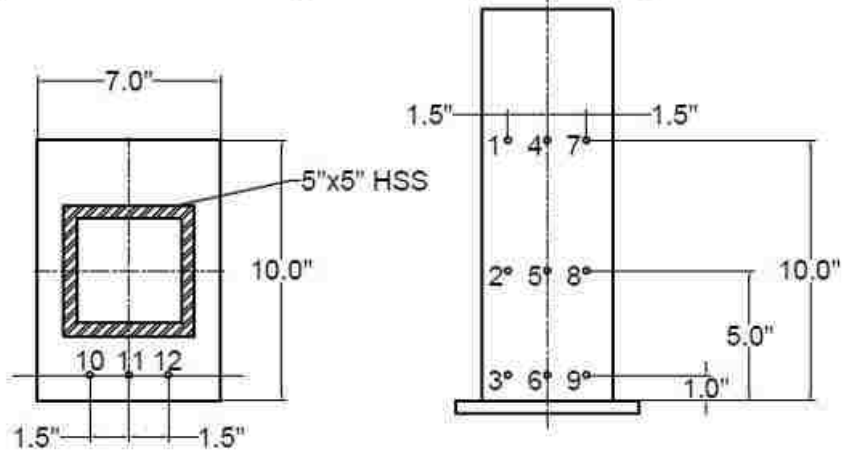
Figure 6.4.2.3: Close up of displacement sensors and the tip of actuator gizmo

LED Targets (Optotrack)

As shown in Figure 6.4.2.4, in addition to the 4 LVDTs, the surface of the HSS and the surface of the embed plate were instrumented with LED targets. These targets were attached to the specimen using two sided tape 1", 5", and 10" away from the embed plate in the vertical direction. The 3 sensors placed on the embed plate were in line with the sensors on the HSS tube. The sensors on the embed plates were placed 1" away from the side edge of the plate. The horizontal spacing between the sensors was 1.5" and 2" for the 5"x5" and the 6"x6" tubes, respectively. The horizontal distance between the outermost LED targets at the same height was 3" and 4" for the 5"x5" and the 6"x6" tubes, respectively.



(Specimens "4-0-0.92", "2-2-0.92", "2-2-0.25", and "2-2-0.50")



(Specimen "2-0-0.92" only)

Figure 6.4.2.4: Locations of Optotrak sensors

The complete test setup is shown in Figure 6.4.2.5.



Figure 6.4.2.5: Complete test set up

6.5 Test Results

All five specimens were subjected to displacement controlled monotonic lateral loading as shown in Figure 6.5.1. The loading rate was 0.1"/min and the unloading was completed in 9.3 seconds from failure. Each specimen's loading was paused at different load stages to observe the specimen status closely, depending on several factors. These factors included the expected failure load, the appearance of the first cracks in the concrete etc.



Figure 6.5.1: Monotonic loading direction

The Optotrak system’s data collection frequency was set to 4 Hz and the rest of the instruments were configured to collect data every 0.25 seconds. The order of the tests was as follows:

Table 6.5.1: Brief test descriptions and dates

Test #	Specimen name	Description of the specimen	Test date:
1.	2-0-0.92	2 studs, loaded at 5.5” eccentricity	04/19/2018
2.	4-0-0.92	4 studs in one row, loaded at 5.5” eccentricity	04/23/2018
3.	2-2-0.92	4 studs distributed in two rows, loaded at 5.5” eccentricity	04/25/2018
4.	2-2-0.25	4 studs distributed in two rows, loaded at 1.5” eccentricity	04/27/2018
5.	2-2-0.50	4 studs distributed in two rows, loaded at 3” eccentricity	04/30/2018

6.5.1 Specimen “2-0-0.92”

Specimen 2-0-0.92 was one of the three specimens subjected to horizontal load applied at a distance of 5.5” from the bottom of the embed plate. This was the largest value of load eccentricity considered in the experimental program, and a mixed response, significantly affected by the induced moment, was expected. The specimen was loaded non-stop until the first planned routine stop—25 kips as there was

no concrete cracks or sign of distress. At 25 kips, no visible slip or cracks were observed (See Figure 6.5.1.1.).



Figure 6.5.1.1: Specimen 2-0-0.92 at P=25 kips

After thorough examination, the load was increased until the next planned stop—35 kips. The embed plates did not show visible slip until the load reached 34 or 35 kips (See Figure 6.5.1.2). No cracks were observed at 35 kips and the loading was further increased.



Figure 6.5.1.2.a: Specimen 2-0-0.92 at P=35kips



Figure 6.5.1.2.a: Close-up of Specimen 2-0-0.92 at P=35kips

Once the applied load passed 36 kips, the load increase rate started to slow down, while the strain in the studs kept increasing until failure occurred at 39.21 kips. Cracks formed in the concrete near the West

and East sides of the embed plate. Soon after the failure point, the embed plate hit the concrete behind it, resulting in concrete cracks in the back (near South edge, See Figure 6.5.1.3). The studs made noise as they fractured to failure.



(Top view)

(West side)

(East side)

Figure 6.5.1.3: Crack patterns near embed plates after failure (Specimen 2-0-0.92)

After unloading, photographs of the front edge uplift and of the slip of the embed plate were taken (See Figure 6.5.1.4). The residual slip after failure was little over 1/2", which almost corresponded to the maximum space (3/4") that was provided behind the plate. It can be seen in Figure 6.5.1.4 that the plate uplift was approximately 3/8" at the very tip of the plate.

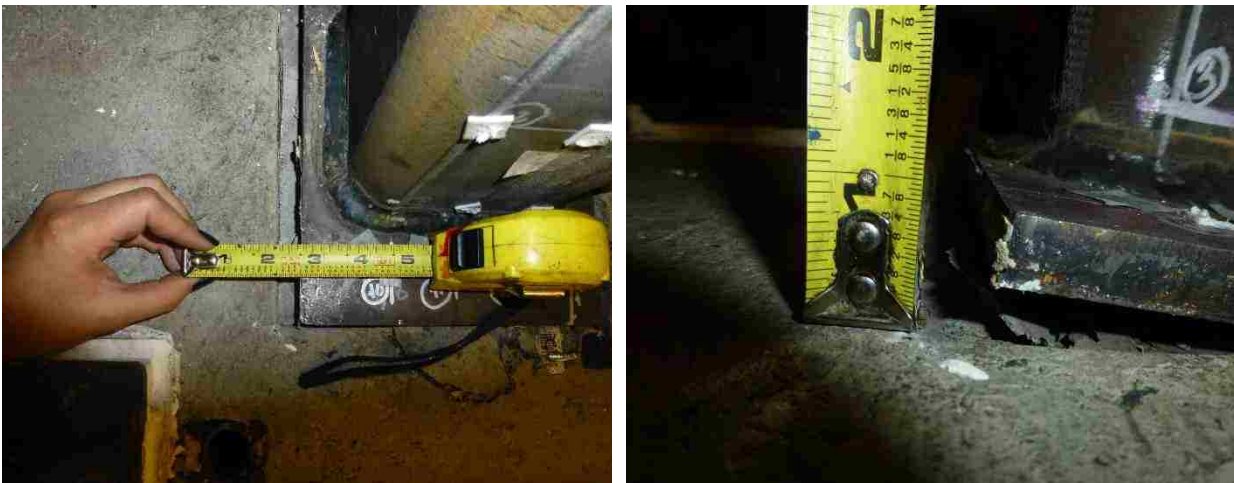


Figure 6.5.1.4: Specimen 2-0-0.92's slip and separation after unloading

Specimen 2-0-0.92 was the only specimen whose studs fractured completely. The fracture occurred approximately 1" from the embed plate (See Figure 6.5.1.5). The concrete surrounding the studs cracked all around at the surface level but no significant spalling could be observed.



Figure 6.5.1.5: Specimen 2-0-0.92's sheared studs and local concrete crack profile

The strains in the shear studs were collected during the test. Figure 6.5.1.6 shows the applied shear load vs. the strain readings provided by strain gauges. Stud S12 was instrumented for this specimen. Strain gauge B2 was lost as the specimen started to pick up a load, and provided no useful readings. The readings were thus excluded from Figure 6.5.1.6. Also, strain gauge B1 was damaged when the loading approached the ultimate condition. However, strain gauge B1 worked until the load reached approximately 36 kips.

Figure 6.5.1.6 shows that the readings from strain gauge B1 were significantly larger than any other readings (about 5 times bigger than other gauge readings at ultimate condition and all ultimate readings were within the order of 10^{-3} and 10^{-2}). This implies that the flexural strain near the base plate was significant while the flexural strain in the tip of the stud was relatively small.

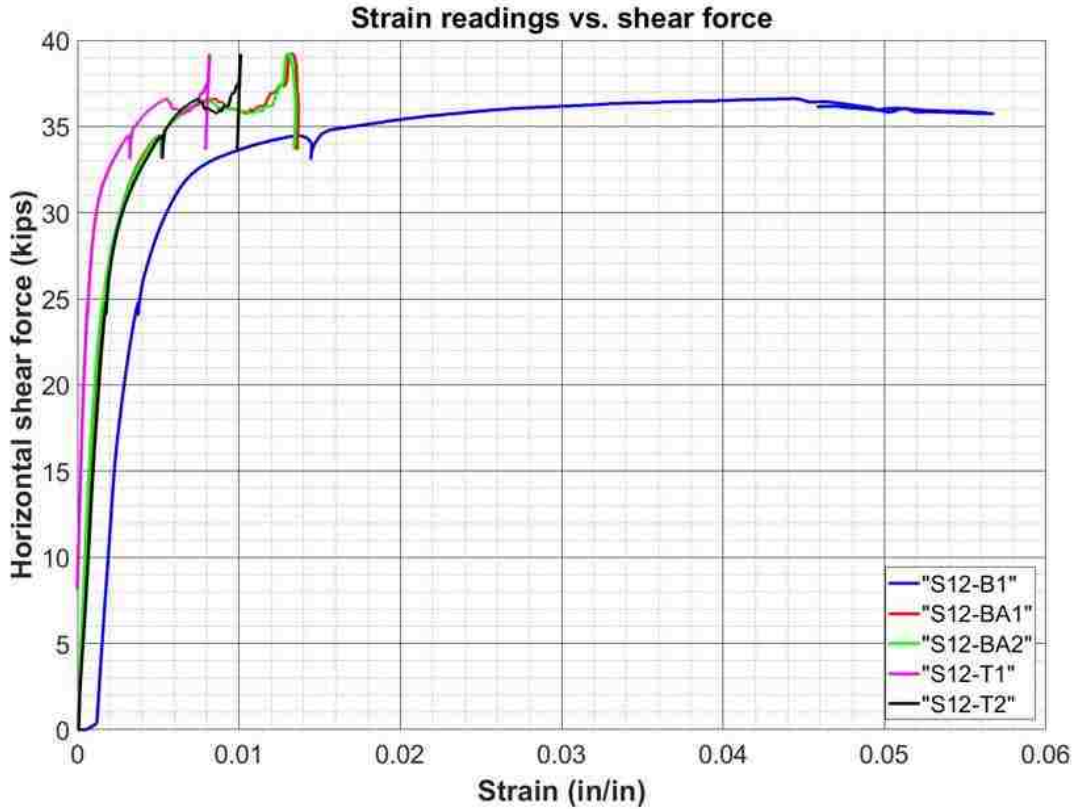


Figure 6.5.1.6: Shear force vs strains in a stud (Specimen 2-0-0.92)

The average horizontal displacement of the plate (i.e. in the x-direction) was obtained from LED targets 10, 11, and 12 which were attached to the base plate surface. As shown in Figure 6.5.1.7, the slip of the base plate was 0.51" at the ultimate condition.

Similarly, the displacements of the same three sensors in the y-direction provide information pertaining to the separation at the interface between the steel plate the concrete block. Figure 6.5.1.8 shows that the target 10 (the North most target sensor) had upward movement of 0.195" while the other two remained smaller than that at ultimate condition. Target 12 (the South most target sensor) had a displacement of 0.04" at ultimate condition. Figure 6.5.1.8 also indicates that all three targets moved downwards initially as the plate started to pick up compression from the loading and then eventually the whole plate was lifted upwards.

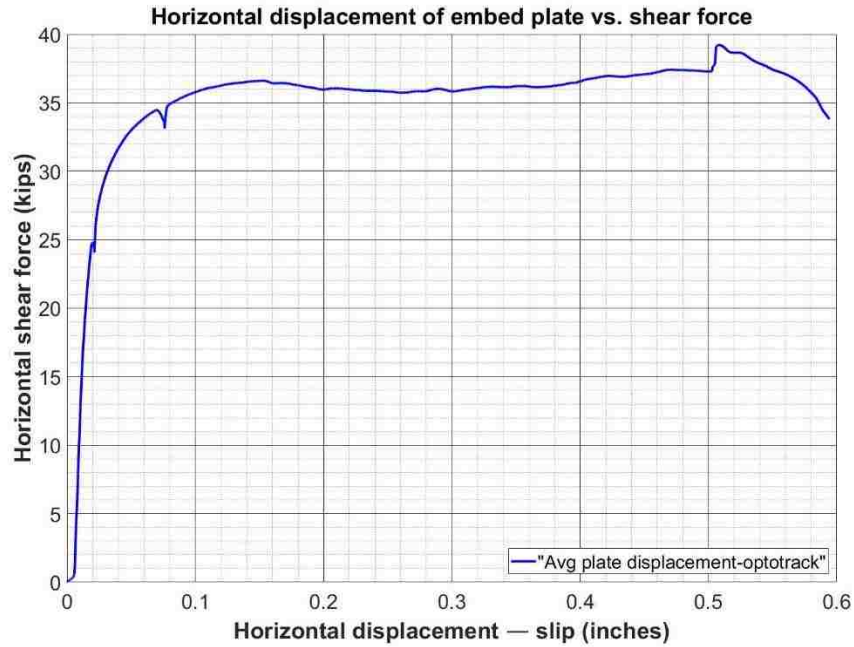


Figure 6.5.1.7: Shear force vs. slip (Specimen 2-0-0.92)

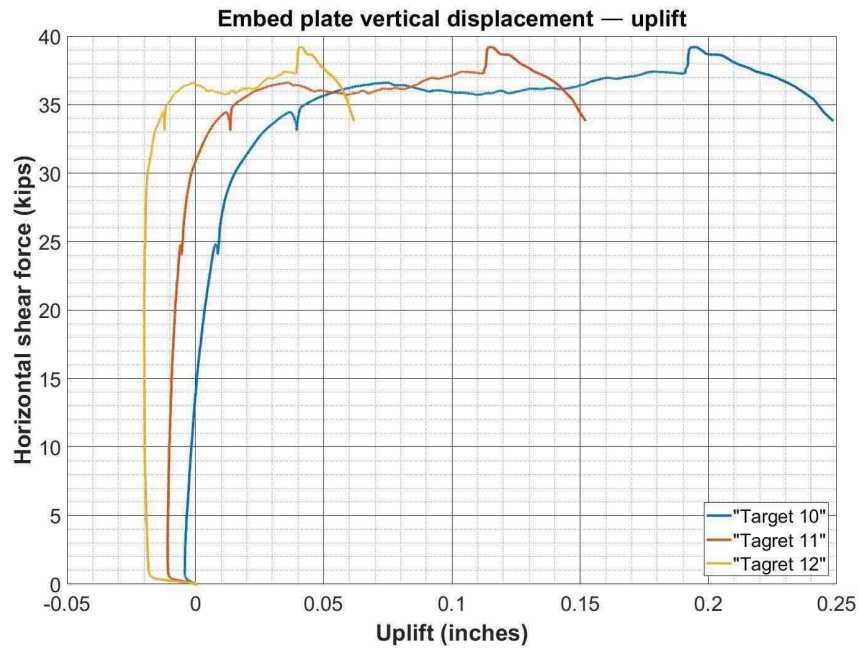


Figure 6.5.1.8: Shear force vs. uplift (Specimen 2-0-0.92)

In addition to horizontal slip, substantial rotation of the plate was observed as a result of the significant load eccentricity, which induced nontrivial base moment. The rotation of the base plate was calculated from x and y displacements of the Optotrak sensors placed on the plate. Also, the base rotation was estimated using the displacements measured by the top and bottom potentiometric devices and the

vertical distance between them. The results from the two types of devices matched reasonably well (See Figure 6.5.1.9). Obviously, the y components of the potentiometric measuring device readings cannot be distinguished as the rotation increases. Thus, the rotation at the ultimate condition, which was about 0.054 radians measured by the Optotrak system is believed to be more accurate. Similarly, all the other Optotrak measurements were verified using the LVDTs, and the match was always good.

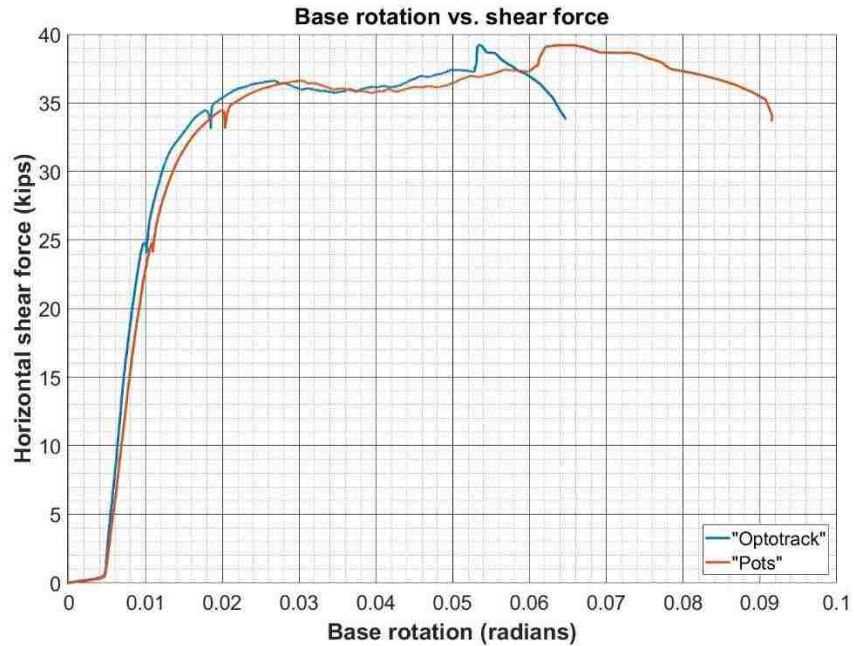


Figure 6.5.1.9: Shear force vs. base rotation (Specimen 2-0-0.92)

6.5.2 Specimen “4-0-0.92”

Specimen 4-0-0.92 was the second of the three specimens subjected to horizontal load applied at a distance of 5.5” from the bottom of the embed plate. Again, a mixed response, significantly affected by the induced moment, was expected. However, specimen 4-0-0.92 was expected to be significantly stronger than Specimen 2-0-0.92, on account of the greater number of studs resisting the applied load (a row of 4 studs located on the tensile side of the plate instead of 2). Specimen 4-0-0.92 was loaded non-stop until the first planned hold—35 kips – as there was no visible cracks or slowdown in the increase of load. The next planned load holding was at 50 kips and up to that load stage, nothing notable happened other than a little bit of rotation of the loading post (See Figure 6.5.2.1). At 50 kips, no cracks were observable near the embed plate.



Figure 6.5.2.1.a: Specimen 4-0-0.92 at P=50kips



Figure 6.5.2.1.b: Close up of Specimen 4-0-0.92 at P=50kips

Around 60 kips, the load increase rate started to slow down and the load was put on hold for observation. At this point, the embed plate had undergone noticeable horizontal slip (see Figure 6.5.2.2), but there was still no cracks around the embed plate.

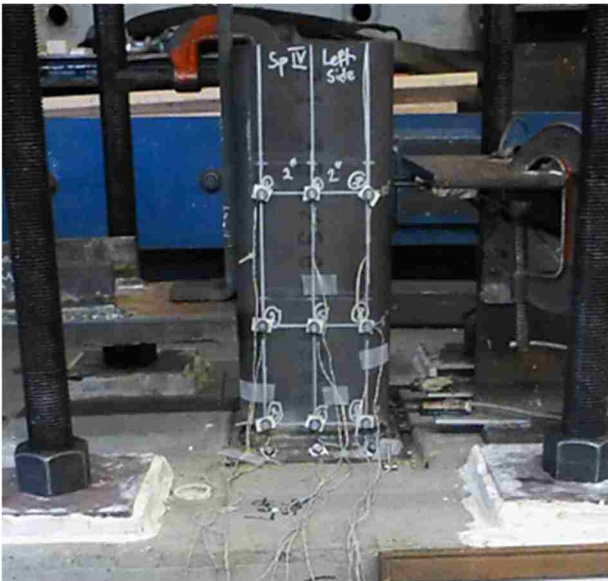


Figure 6.5.2.2.a: Specimen 4-0-0.92 at P=60kips



Figure 6.5.2.2.b: Close up of Specimen 4-0-0.92 at P=60kips

The next load hold was at 70 kips where the shear studs started to make noises and the slip further increased. Furthermore, significant plate uplift and rotation could be observed. No cracks in the concrete could be detected. Shortly after the last planned load hold, the specimen failed at 76.8 kips. Small cracks in the concrete near the South edge on the East side and near the North edge on the West

side of the embed plate were observed. This suggests that when the studs fractured, some out-of-plane rotation of the embed plate occurred (See Figure 6.5.2.3).



Figure 6.5.2.3: Crack patterns near embed plates after failure (Specimen 4-0-0.92)

At failure, the base plate slid and was noticeably rotated (in-plane) as shown in Figure 6.5.2.4.



Figure 6.5.2.4: Specimen 4-0-0.92 at failure

The studs did not completely fracture at failure. Some cracks in the concrete near the studs were photographed through the gap between the concrete block and the base plate (See Figure 6.5.2.5). The surrounding concrete appeared to be cracked in between the studs.



Figure 6.5.2.5: Concrete profile around the studs after failure (Specimen 4-0-0.92)

For this specimen, Stud S11 and S12 were instrumented with strain gauges. These two studs were the 2 studs on the left half of the embed plate. During testing, strain gauges S11-B2, T1, S12-B1 and B2 were damaged. Hence, the readings from those strain gauges were excluded from the applied load vs. strain plot (Figure 6.5.2.6). Similarly to Specimen 2-0-0.92, the strain in strain gauge S11-B1 was the greatest, while the strains in S11-T1 and T2 were relatively small (17×10^{-3} vs. 7×10^{-3} ultimate strain). This implies that the flexural strains in the stud near the base of the plate were relatively large compared to the flexural strains near the stud tips.

Also, the base plate slid across the provided gap until it hit the concrete. The plot of applied force vs. average slip of the base plate shows that the ultimate slip was 0.56" (See Figure 6.5.2.7). This means that the ultimate load was reached before the plate reached the South edge of the provided concrete gap.

As shown in Figure 6.5.2.8, the vertical displacements of target 11 (the sensor placed on the plate at mid-length) and target 12 (the South most target on the plate) indicated that the embed plate started rotating from the very beginning of the test, with this side of the plate going into compression. The y-displacement of target 12 remained negative throughout the whole test (at least until $P=70$ kips and beyond 70 kips the readings were disrupted) indicating that the back end of the plate was in compression while the other areas of the plate separated from the concrete. However, target 10 (the North most sensor on the base plate) started separating from the concrete as soon as the load was applied to the loading post. The vertical displacement of target 10 at ultimate load was about 0.2".

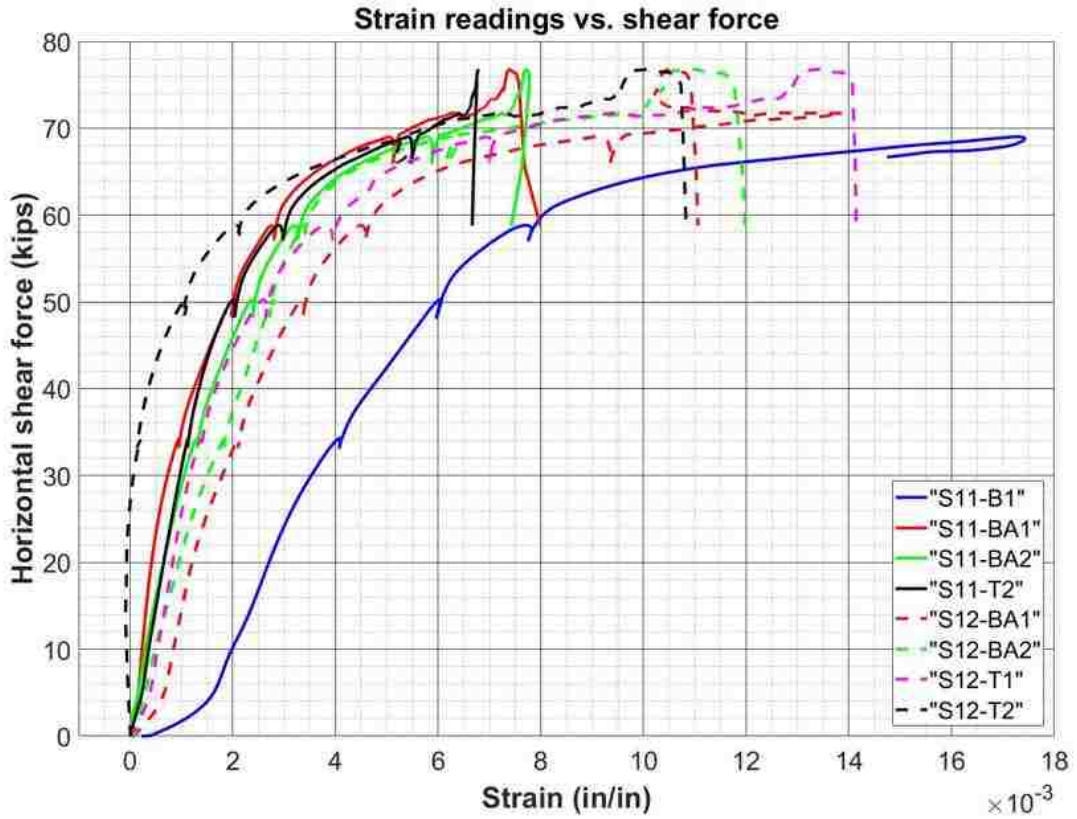


Figure 6.5.2.6: Shear force vs strains in the studs (Specimen 4-0-0.92)

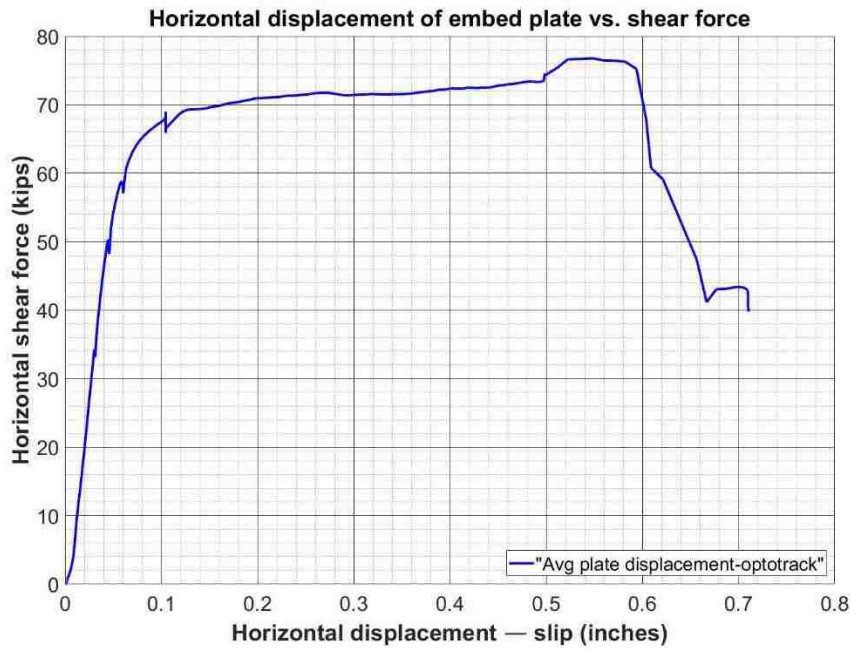


Figure 6.5.2.7: Shear force vs. slip (Specimen4-0-0.92)

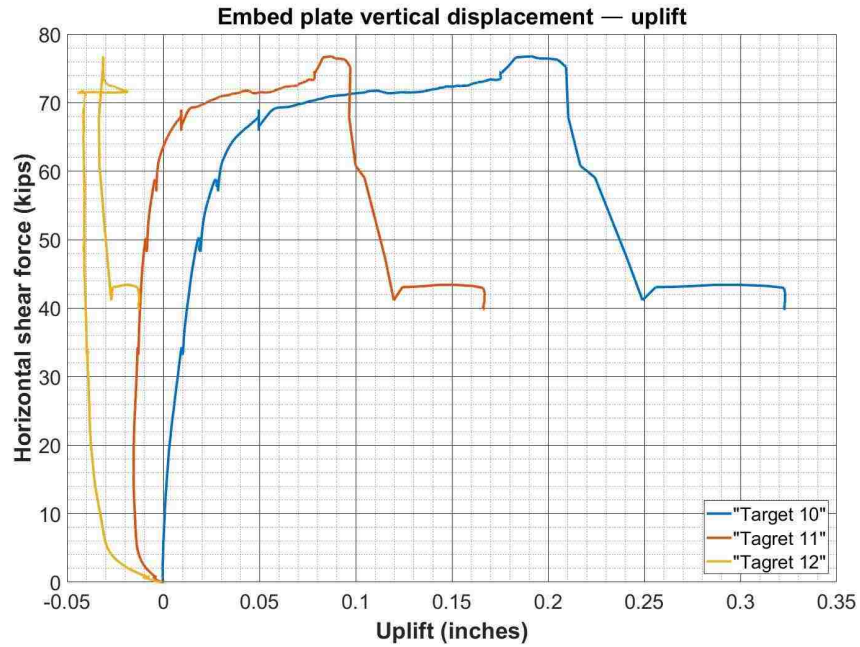


Figure 6.5.2.8: Shear force vs. uplift (Specimen 4-0-0.92)

The base rotation was as described in Section 6.5.1 and the applied force vs. base rotation plot indicates that the ultimate rotation was about 0.058 radians (See Figure 6.5.2.9).

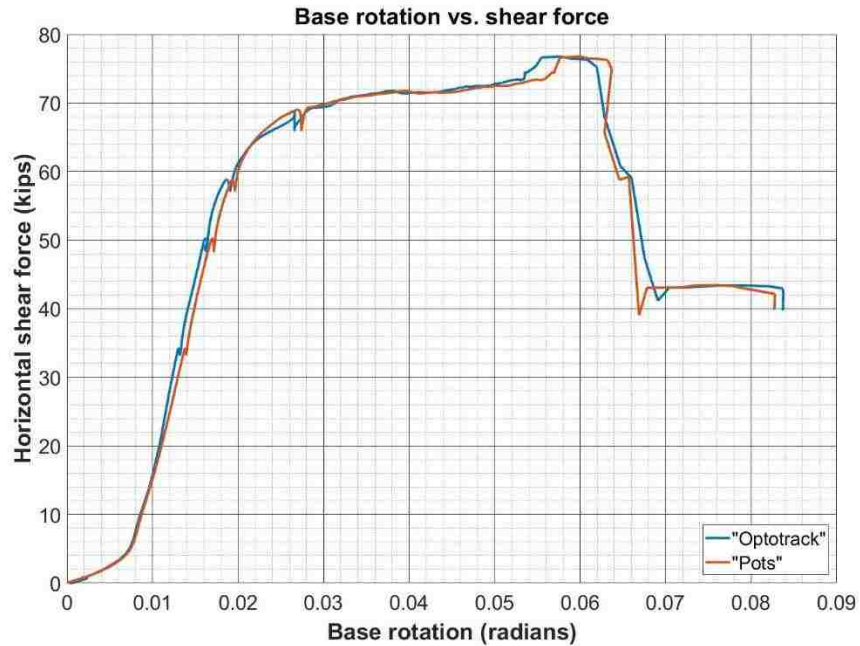


Figure 6.5.2.9: Shear force vs. base rotation (Specimen 4-0-0.92)

6.5.3 Specimen “2-2-0.92”

Specimen 2-2-0.92 was the third and last specimen subjected to horizontal load applied at a distance of 5.5” from the bottom of the embed plate. However, the plate had a different (more traditional) stud arrangements with two rows of two studs resisting the applied load. Again, a mixed response, affected by the induced moment, was expected. In terms of strength, specimen 2-2-0.92 was expected to be comparable to Specimen 2-0-0.92, as it was believed that the capacity would be controlled by the studs on the tensile side of the plate.

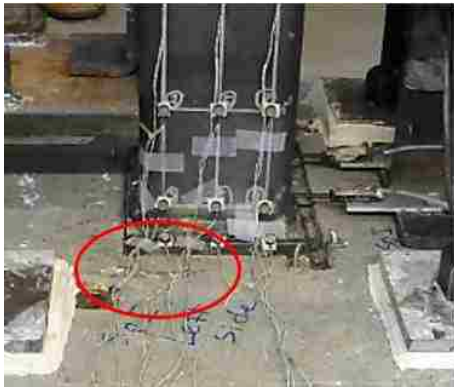


Figure 6.5.3.1: Specimen 2-2-0.92 before testing (West side)

It should be noted that Specimen 2-2-0.92 had a thin piece of concrete (approximately 1/4” thick) ready to be chipped off on the surface level near the West side of the embed plate before loading (See Figure 6.5.3.1). The specimen was initially loaded to 25 kips. At this point, no visible cracks could be observed but minor uplift of the plate was detected (See Figure 6.5.3.2.a). The next load hold was at 35 kips and the shear studs started to make some noises, suggesting that they were approaching failure. The plate-concrete separation increased a little bit more but no significant slip was observed (See Figure 6.5.3.2.b).



Figure 6.5.3.2.a: Specimen 2-2-0.92 at P=25 kips (East side)



Figure 6.5.3.2.b: Specimen 2-2-0.92 at P=35 kips (East side)

At about 38 kips, the studs made significant noise, so the loading was put on hold for observation. The plate-concrete separation had further increased with respect to the previous load stage and horizontal

slip was noticeable upon inspection. Further damage to the initially cracked concrete area was observed (See Figure 6.5.3.3).



(West side)



(East side)

Figure 6.5.3.3: Specimen 2-2-0.92 at P=38 kips

Shortly after P=38 kips load hold, the specimen failed at P=38.68 kips. While the load was decreasing, there was another very loud noise at around 33 kips. As shown in figure 6.5.3.4, the piece of concrete layer on the West side broke off, while there was no observable damage on the East side of the specimen at failure.



(West side)



(East side)

Figure 6.5.3.4: Specimen 2-2-0.92 after failure

It was not possible to detect whether (and at what location) the tensile studs had fully fractured as the specimen was held together by the studs on the compression side. The crack pattern in the concrete surrounding the studs was photographed through the gap between the plate and concrete (See Figure 6.5.3.5). Significant cracking and spalling was observed mostly in the tensile studs region, while no crack propagation in the compressive stud area was detected.



Figure 6.5.3.5: Concrete profile around the studs after failure (Specimen 2-2-0.92)

Strain readings from strain gauges S11-B2, BA1 and T1 were lost. Figure 6.5.3.6 shows the readings of the strain gauges that were not damaged during the test. The S21-B2 readings stayed negative in the order of 10^{-3} . S21-B1 stayed positive and bigger than S21-BA1 and BA2 readings at all times (in the order of 10×10^{-3} vs. 4×10^{-3} ultimate strains). S21-T1 and T2 were small at all times (2×10^{-3} ultimate

strains). This suggests that the base of the studs on the compression side of the plate underwent significant local bending, while their tips underwent only minor tension.

As shown in Figure 6.5.3.6, the S11-B1, BA2, and T2 readings were close to one another and significantly larger than the strains of the S21 stud, at all times. This suggests that the entire length of the front studs underwent mostly tension and carried the majority of the load applied.

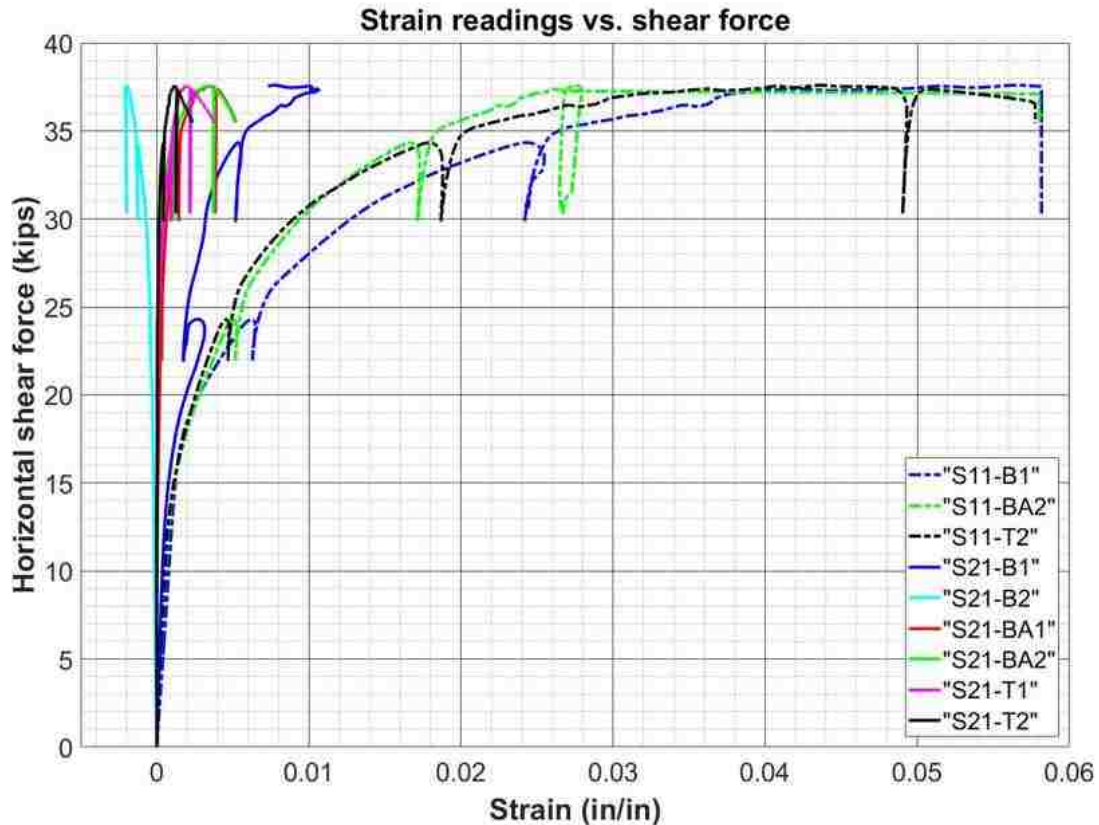


Figure 6.5.3.6: Shear force vs strains in the studs (Specimen 2-2-0.92)

The plate slip and uplift for this specimen at ultimate condition were 0.19" and 0.36" respectively (See Figure 6.5.3.7 and Figure 6.5.3.8).

The base plate did not slip much compared to the specimens with a single row of studs in the tension zone (Specimens 2-0-0.92 and 4-0-0.92). This suggests that adding a row of studs on the compression side of the plate has at least the effect of limiting the horizontal displacement of the embed plate. However, the plate opening, hence the base rotation, was bigger than that of Specimens 2-0-0.92 and 4-0-0.92. The ultimate base rotation for this specimen was about 0.070 radians (See Figure 6.5.3.9).

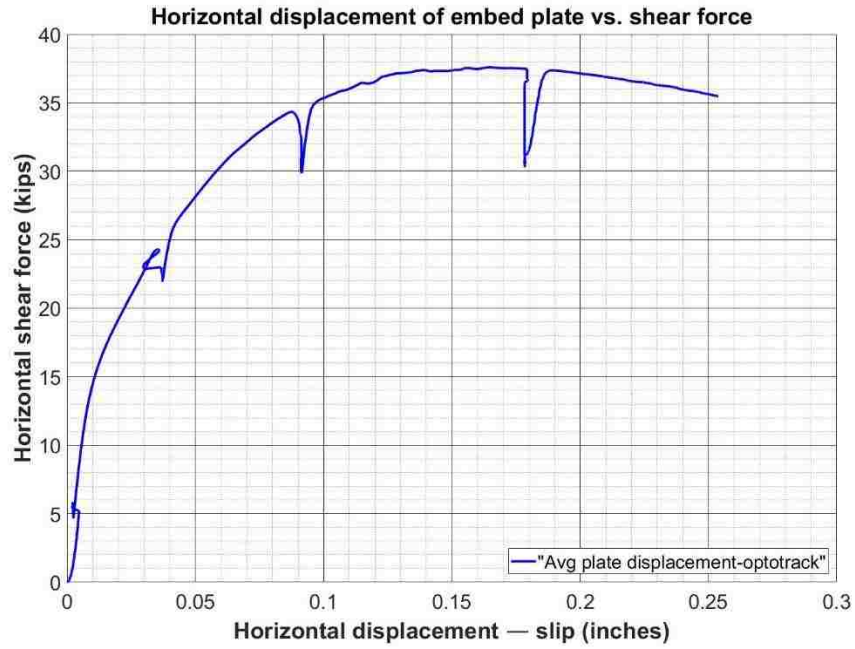


Figure 6.5.3.7: Shear force vs. slip (Specimen 2-2-0.92)

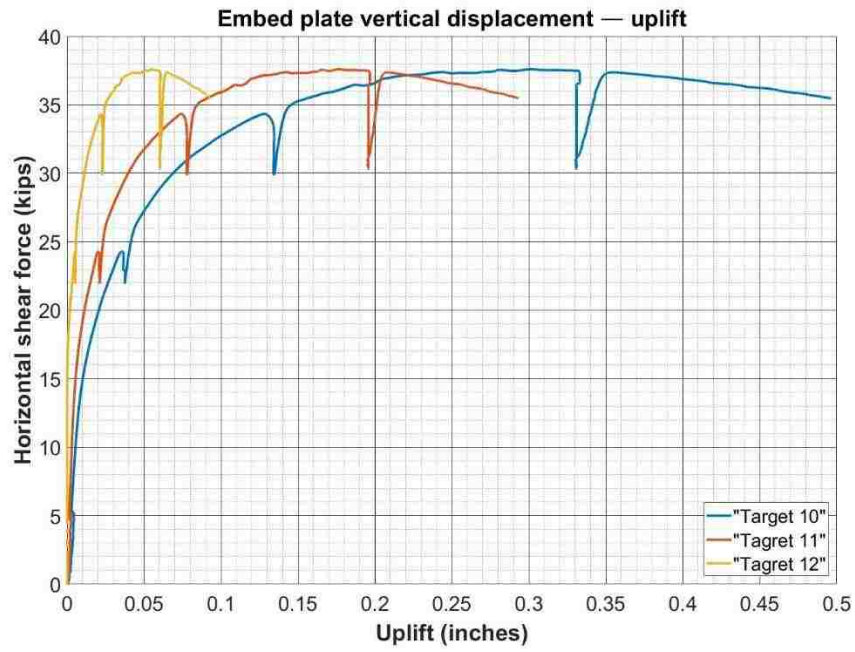


Figure 6.5.3.8: Shear force vs. uplift (Specimen 2-2-0.92)

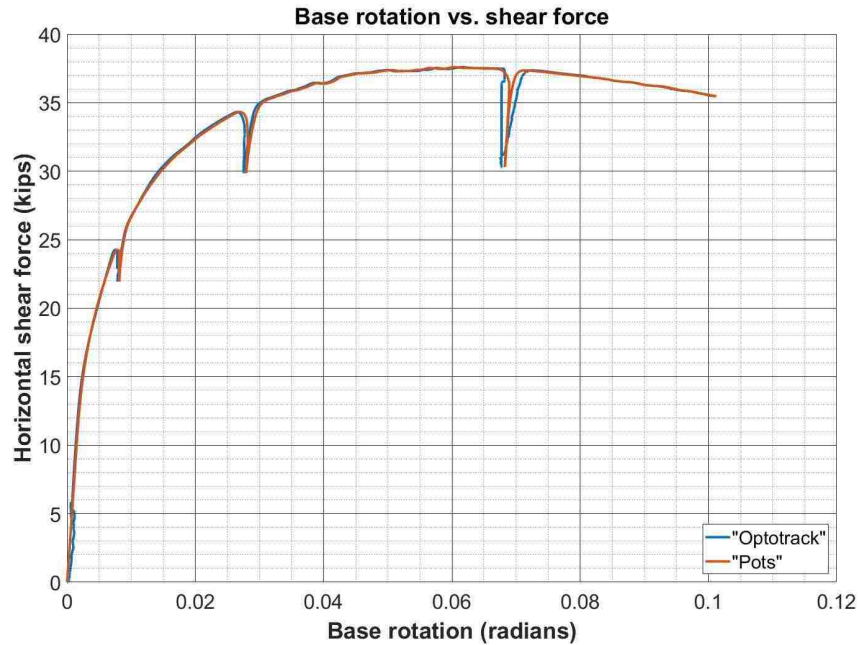
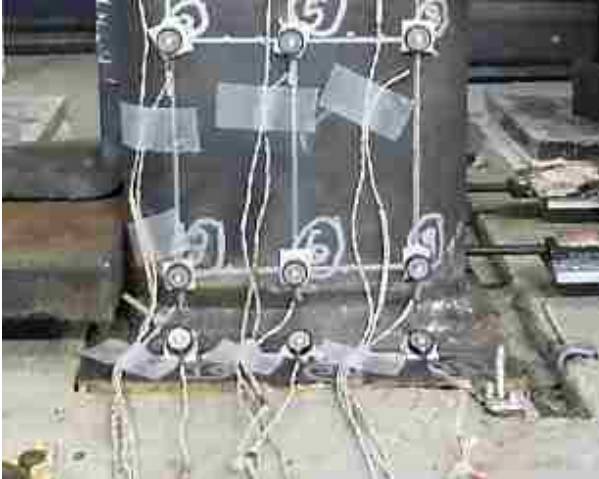


Figure 6.5.3.9: Shear force vs. base rotation (Specimen 2-2-0.92)

6.5.4 Specimen “2-2-0.25”

Specimen 2-2-0.25 was nominally identical to Specimen 2-2-0.92. However, the load eccentricity was reduced from 5.5” to 1.5”. This eccentricity corresponds to an H/L ratio of about 0.25, which represents a reasonable lower bound for real precast connections. Because the load eccentricity was significantly reduced with respect to the previous tests, it was expected that the response of Specimen 2-2-0.25 would be shear-dominated. Load stages were taken at P=25, 40, 50, 60, 70 and 76 kips before failure. Until P=60 kips, no slip, uplift, or concrete cracking was noticeable. The increase in load started to slow down around P=67 kips so the load was hold at 70 kips. During the specimen examination at P=70 kips, the base plate appeared to have experienced some minor horizontal slipping (See Figure 6.5.4.1 for comparison between P=60 and 70 kips).



(Close up: P=60 kips)



(Close up: P=70 kips)

Figure 6.5.4.1: Comparison between P=60 and 70 kips holds (Specimen 2-2-0.25)

The loading was resumed after the hold at P=70 kips. At P=76 kips, the shear studs made loud noise so the load was put on hold once more. The additional 6 kips resulted in the slip to be more noticeable than it was at P=70 kips. Then, the load was continued until P=80 kips. During this examination the slip was 0.21". No cracks in the concrete were observed (See Figure 6.5.4.2).



(The loading post HSS)



(Close up of the slip)

Figure 6.5.4.2: Specimen 2-2-0.25 at P=80 kips

Shortly after P=80 kips hold, the specimen failed at P=84.15 kips. After failure, light concrete cracks were observed on the East side of the embed plate (See Figure 6.5.4.3). The plate rotation was visually observed to be small.



Figure 6.5.4.3: Specimen 2-2-0.25 after failure

The plate slip and separation photographs are shown in Figure 6.5.4.4. The slip shown to be around $3/8$ " while the separation was about $1/8$ ". Due to this small separation, the concrete profile around studs could not be visually observed.



Figure 6.5.4.4: Photographs of slip and crack width after failure (Specimen 2-2-0.25)

Figure 6.5.4.5 shows the strain gauge readings for Studs 11 and 21 against the applied shear load. Strain gauges S11-B2, S21-B2 and BA2 were damaged during testing. Overall, the flexural strain gauges at the base of each stud (strain gauge B1) had the biggest strain readings (0.035 and 0.012 strains for tensile and compression zone studs at failure respectively) compared to the rest of the strain gauges on the same stud. This suggests that the base of the studs underwent significant bending but did not experience much axial strains. Also, T1 and T2 readings were 6 to 7 times smaller than BA1 and BA2 readings. This suggests that the tip of the studs were curved slightly but the shear load mainly impacted

the base of the studs locally. However, the tension zone stud faced more deflection than the stud in the compression zone since the S11-B1 readings were bigger than S21-B1 readings.

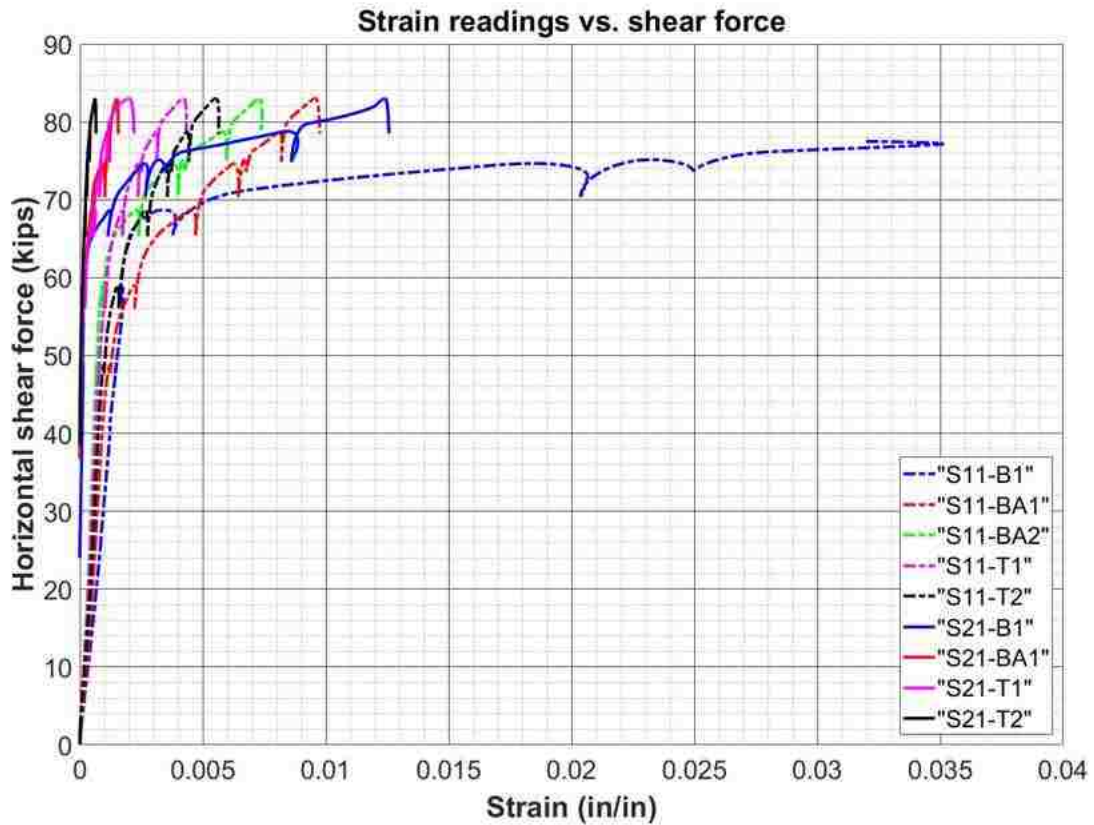


Figure 6.5.4.5: Shear force vs strains in the studs (Specimen 2-2-0.25)

The slip and uplift details are shown in Figure 6.5.4.6 and Figure 6.5.4.7. The horizontal slip at ultimate condition was 0.32" as shown in Figure 6.5.4.6.

Figure 6.5.4.7 indicates that the all three targets on the plate moved upwards and that the plate underwent some minor rotation in addition to horizontal slip. The displacement of the North most target (Target 10) in the y-direction reached 0.11" at the ultimate condition.

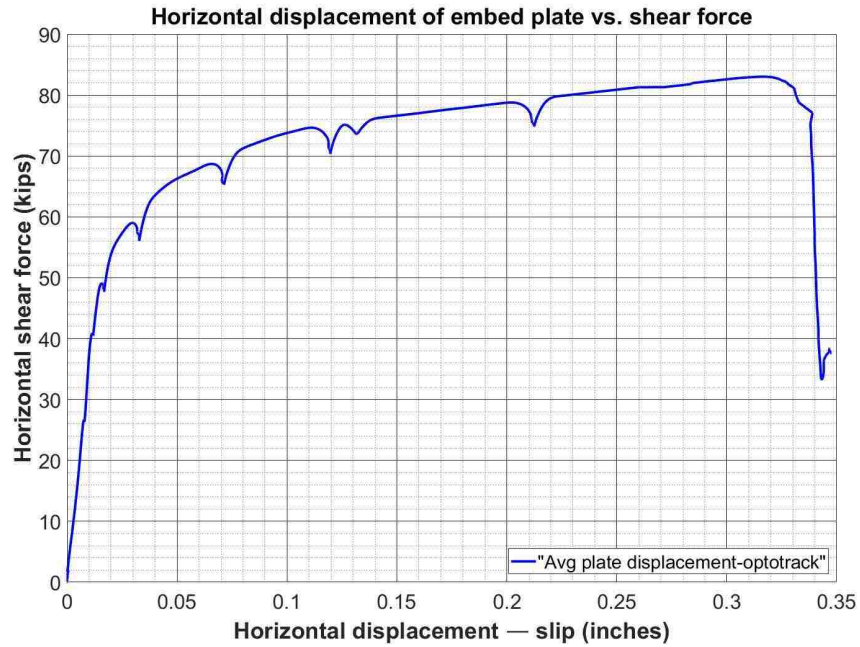


Figure 6.5.4.6: Shear force vs. slip (Specimen 2-2-0.25)

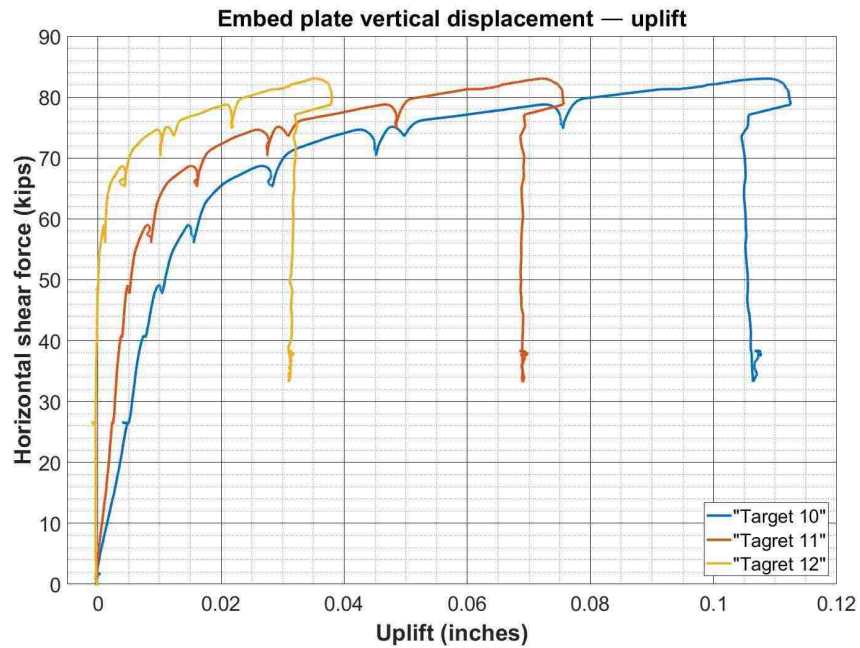


Figure 6.5.4.7: Shear force vs. uplift (Specimen 2-2-0.25)

The base rotation plot for this specimen (Figure 6.5.4.6) shows that the ultimate rotation was only 0.019 radians. This is consistent with the expectation that the response of this specimen would be “shear-dominated”.

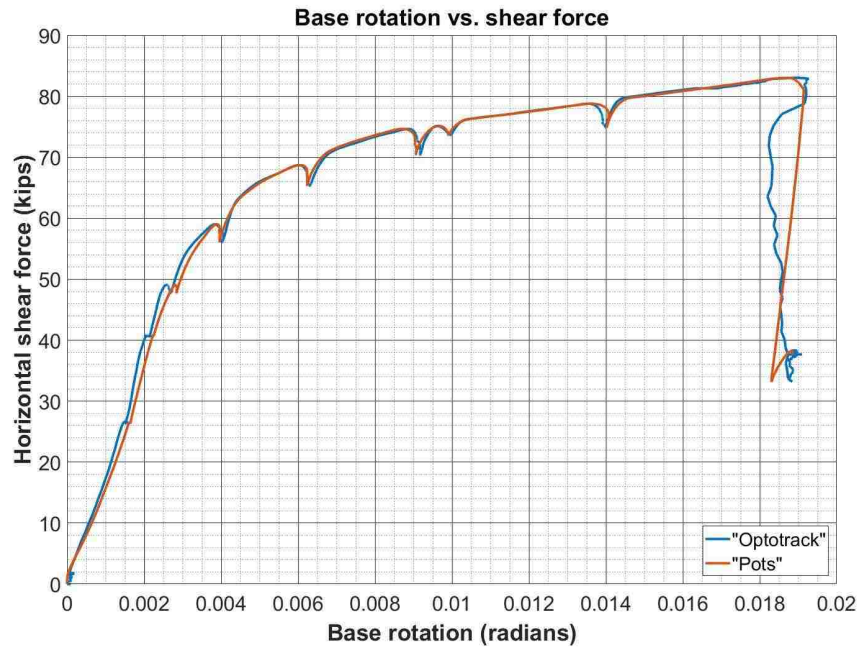


Figure 6.5.4.6: Shear force vs. base rotation (Specimen 2-2-0.25)

6.5.5 Specimen "2-2-0.50"

Specimen 2-2-0.50 was nominally identical to Specimens 2-2-0.92 and 2-2-0.25, and was the third specimen within the group intended to study the effects of load eccentricity. Thus, the load eccentricity was increased from 1.5" to 3". This eccentricity corresponds to an H/L ratio of about 0.5, which represents a reasonable intermediate value for real precast connections. For this specimen, failure was expected to occur around P=65 kips. Load stages were planned at P=35, 45, 55, 60 kips and after failure. The first load stages (at P=35, 45 and 55 kips) did not reveal anything remarkable. Only minor horizontal plate slip could be detected. The first cracks in the concrete were observed near the North end of the plate on the West side at P=55 kips (See Figure 6.5.5.1).



(West side)



(Close up of the base plate on the West side)

Figure 6.5.5.1: Specimen 2-2-0.50 at P=55 kips

More light cracks formed on the West side of the base plate at P=60 kips and became more significant as the applied load approached P=65 kips (See Figure 6.5.5.2). Also, the studs made noise at P=62 kips and the load increase slowed down.



Figure 6.5.5.2.a: Concrete crack pattern at P=60 kips
(Specimen 2-2-0.50)



Figure 6.5.5.2.b: Concrete crack pattern at P=65 kips
(Specimen 2-2-0.50)

After the load stage at P=65 kips, the specimen was loaded until failure. In the meantime, there was more noise coming from the studs at P=67 kips. Once the load reached P=83 kips, the loading rate

decreased and the specimen failed at $P=83.86$ kips. Figure 6.5.5.3 shows the rotation of the HSS tube and the crack patterns around the embed plate.



(West side view)



(Top view)

Figure 6.5.5.3: Specimen 2-2-0.50 after failure

The separation of the plate from the concrete is shown in Figure 6.5.5.4. The embed plate did not completely come off the concrete block. The cracks appeared to run across the row of studs in the tension zone, as well as locally right behind the studs.



Figure 6.5.5.4: Concrete profile around the studs after failure (Specimen 2-2-0.50)

Studs 11 and 21 were instrumented with strain gauges but the strain gauges B2 of both studs were damaged during testing. Figure 6.5.5.5 shows the strain gauge readings for Specimen 2-2-0.50. The strain gauge S11-B1 stopped working past $P=70$ kips. Similarly to Specimen 2-2-0.25's behavior, the

flexural strains (in the order of 10^{-2} at failure) near the stud tips were at least 2 times smaller compared to the flexural strains near the base of the studs.

However, unlike Specimen 2-2-0.25's T1 and T2 strain gauge readings, for Specimen 2-2-0.50 the readings from strain gauges T1 and T2 had similar readings to strain gauges BA1 and BA2 (i.e. the axial strain gauges). This suggests that even though the tip of the studs underwent a minor extent of bending, they experienced substantial axial tensile strain along their length. Similarly to the other specimens with 2 rows of 2 studs (Specimens 2-2-0.92 and 2-2-0.25), the tensile zone studs had bigger strains than the studs in the compression zone (strains in the order of 10^{-2} at failure).

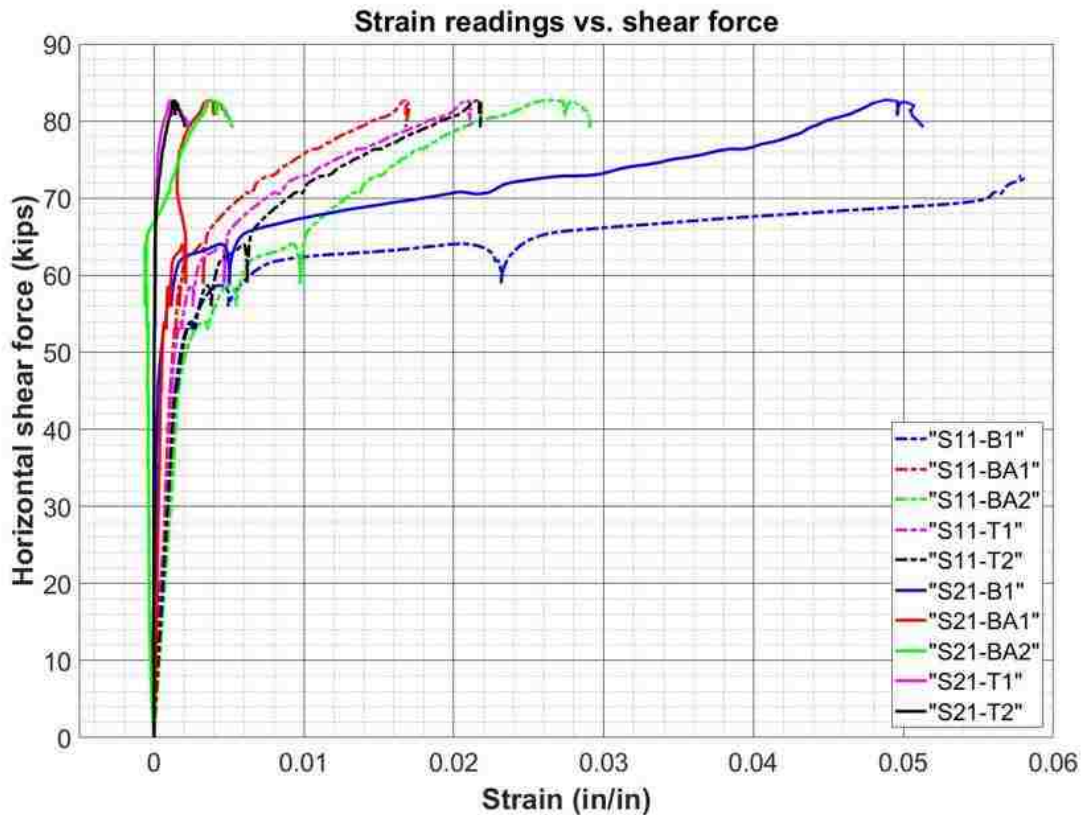


Figure 6.5.5.5: Shear force vs strains in the studs (Specimen 2-2-0.50)

The plate slip and uplift were also larger for this specimen than they were for the companion Specimen 2-2-0.25. As shown in Figure 6.5.5.6, the ultimate slip was 0.46" (in contrast with 0.32" for Specimen 2-2-0.25). As shown in Figure 6.5.5.7, the peak uplift (computed from target 10) was 0.32" (in contrast with 0.14" for Specimen 2-2-0.25).

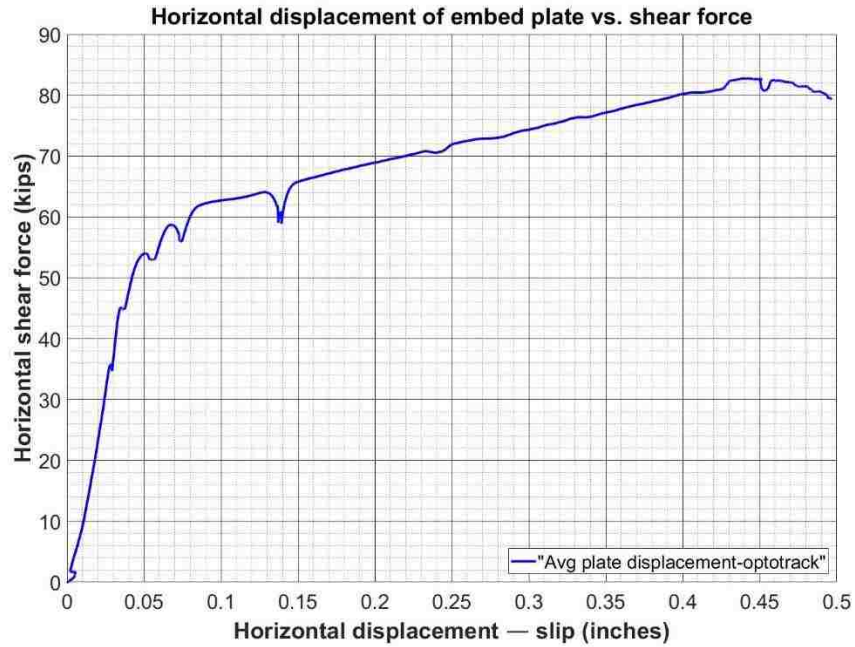


Figure 6.5.5.6: Shear force vs. slip (Specimen 2-2-0.50)

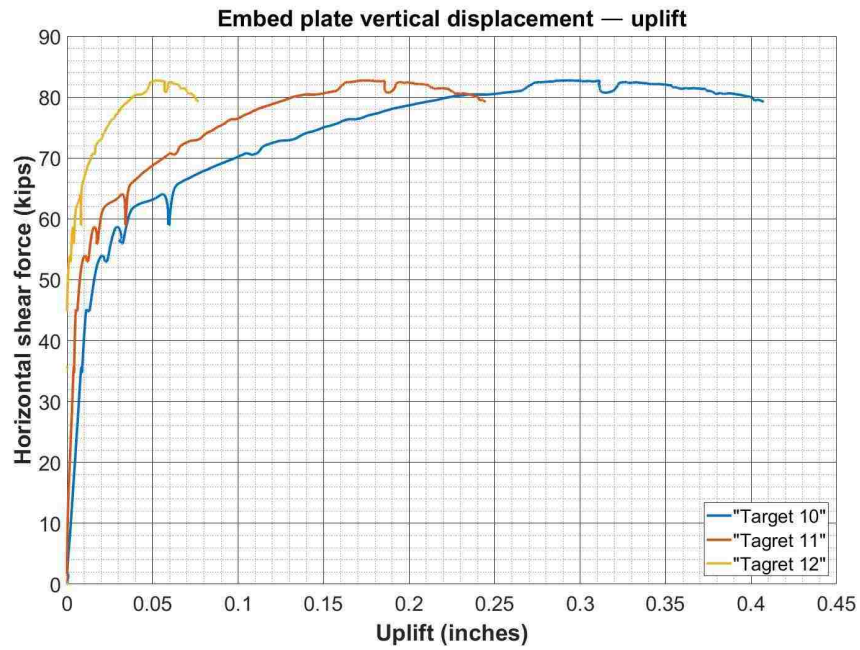


Figure 6.5.5.7: Shear force vs. crack width—uplift (Specimen 2-2-0.50)

At failure, as shown in Figure 6.5.5.8, the base plate rotation was about 0.067 radians.

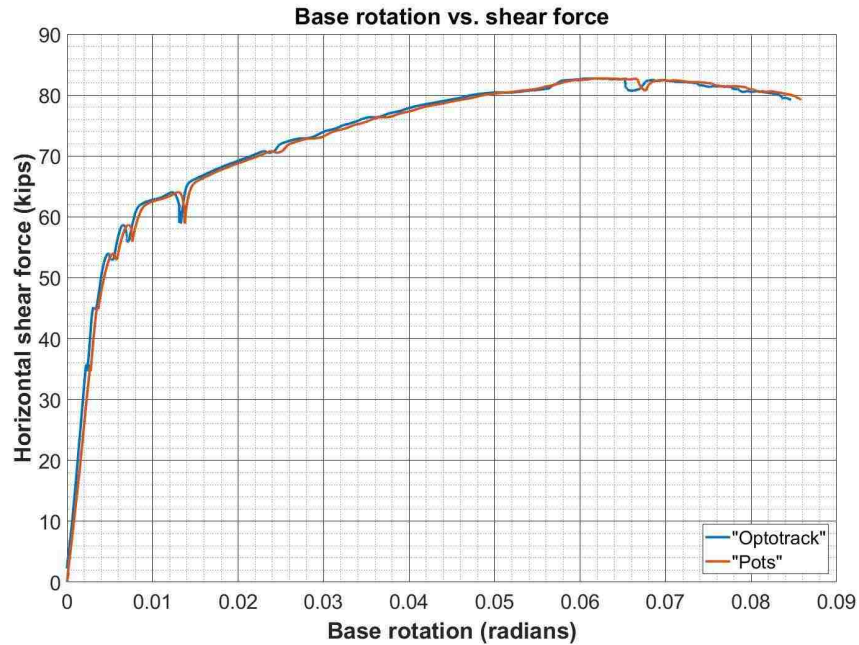


Figure 6.5.5.8: Shear force vs. base rotation (Specimen 2-2-0.50)

6.5.6 Summary of Test Results

All five test results are summarized in Table 6.5.6.1. The common notations used are:

H = eccentricity of load (from the bottom of the base plate)

L = distance between front row studs (tension zone studs) to the back edge of the embed plate

P_u = ultimate load

s_u = slip at ultimate condition

w_u = uplift at ultimate condition (vertical movement at LED Target 10 as described in Section 6.4.2)

α_u = base rotation at ultimate condition

Table 6.5.6.1: Summary of test results

Specimen	H/L	P_u (kips)	s_u (inches)	w_u (inches)	α_u (radians)
2-0-0.92	0.92	39.21	0.51	0.195	0.054
4-0-0.92	0.92	76.80	0.56	0.2	0.058
2-2-0.92	0.92	38.68	0.19	0.36	0.070
2-2-0.25	0.25	84.15	0.32	0.11	0.019
2-2-0.50	0.50	83.86	0.46	0.32	0.067

Figure 6.5.6.1 shows the comparison between load-slip relationships of all five tests.

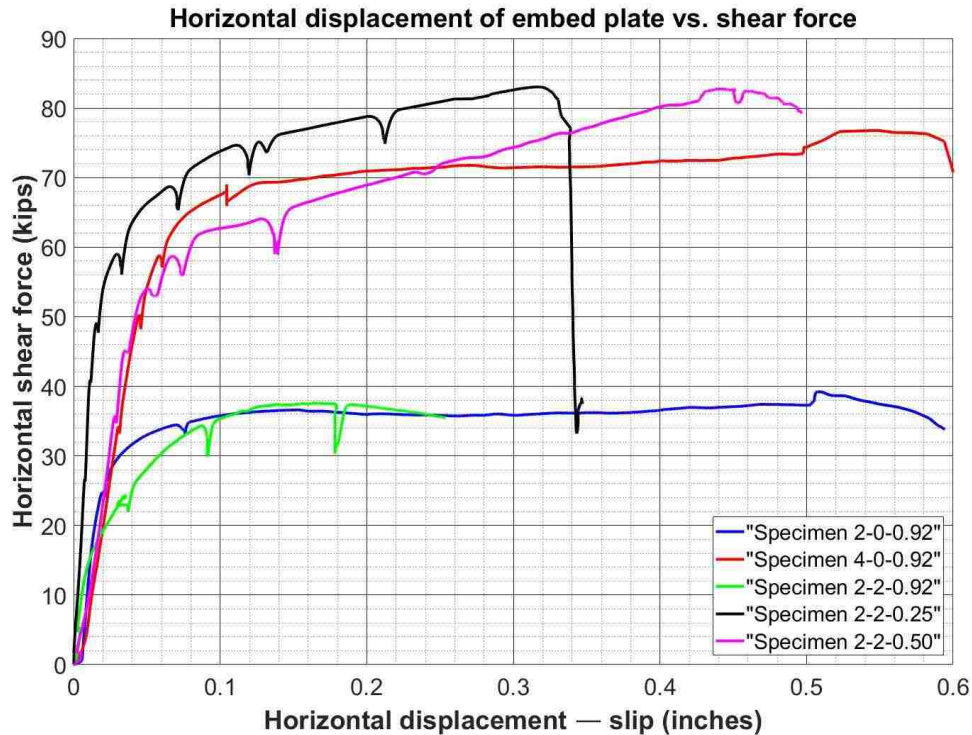


Figure 6.5.6.1: Load vs. slip relationship of all specimens

Based on the results summarized in Table 6.5.6.1 and Figure 6.5.6.1, the following preliminary conclusions can be drawn:

By comparing the results of Specimens 2-0-0.92, 4-0-0.92, and 2-2-0.92:

1. At large H/L (in this case H/L=0.92), the behavior is strongly affected by bending, and the connection capacity is determined largely by the tension strength of the “tension” studs. Doubling the number of the tension studs doubles the connection capacity. Adding studs in the compression zone does not add strength, but it does reduce the slip at failure.

By comparing the results of Specimens 2-2-0.92, 2-2-0.25, and 2-2-0.50:

2. For smaller eccentricities (H/L = 0.5 and H/L = 0.25) the behavior is dominated by shear and the shear strength is most closely related to the total number of studs.
3. At small H/L, little increase in load eccentricity (H/L=0.25 to H/L=0.50) does not linearly decrease the shear strength.

In Figure 6.5.6.2, the results of all five tests are shown with respect to their H/L ratios along with their stud arrangement schemes. The vertical black line in Figure 6.5.6.2, represents the theoretical boundary between sliding failures (shear and flexure mixed failures) and pure rotation failures. This boundary was determined based on the following calculations:

$V > \mu * C$ (<i>mixed sliding failure</i>) $V \leq \mu * C$ (<i>rotation failure</i>)	$V = \mu * C$ (boundary)
--	--------------------------

Where:

V=applied shear load

μ = coefficient of shear friction

C=compressive normal load on shear interface

From moment equilibrium:

$$M = C * L = V * H$$

$$C * L = \mu * C * H \text{ (at the failure mode boundary)}$$

$$\frac{H}{L} = \mu \text{ (at the failure mode boundary)}$$

Where:

M = Moment due to the shear load applied at an eccentricity

L = distance between the tension studs and the back edge of the embed plate (Simplified moment arm for the tensile force in the studs and the center of compressive force under the embed plate)

H = load eccentricity

The maximum axial tension force at the failure mode transition boundary:

$$T = A_s f_y$$

From force equilibrium:

$$V = \mu * C = \mu * A_s f_y \text{ (at the failure mode boundary)}$$

Beyond the failure mode transition boundary (in pure rotation zone of H/L):

$$V = C * \frac{L}{H} = A_s f_y * \frac{L}{H}$$

Using the above two equations, one point at the boundary and two points in the pure rotation failure zone (assuming 2 studs were available in the tension zone) were estimated and plotted in Figure 6.5.6.2 along with the test program results. It should be noted that the curve connecting the points is not a “fitted” curve, but it is rather intended to provide a visual representation of the trend.

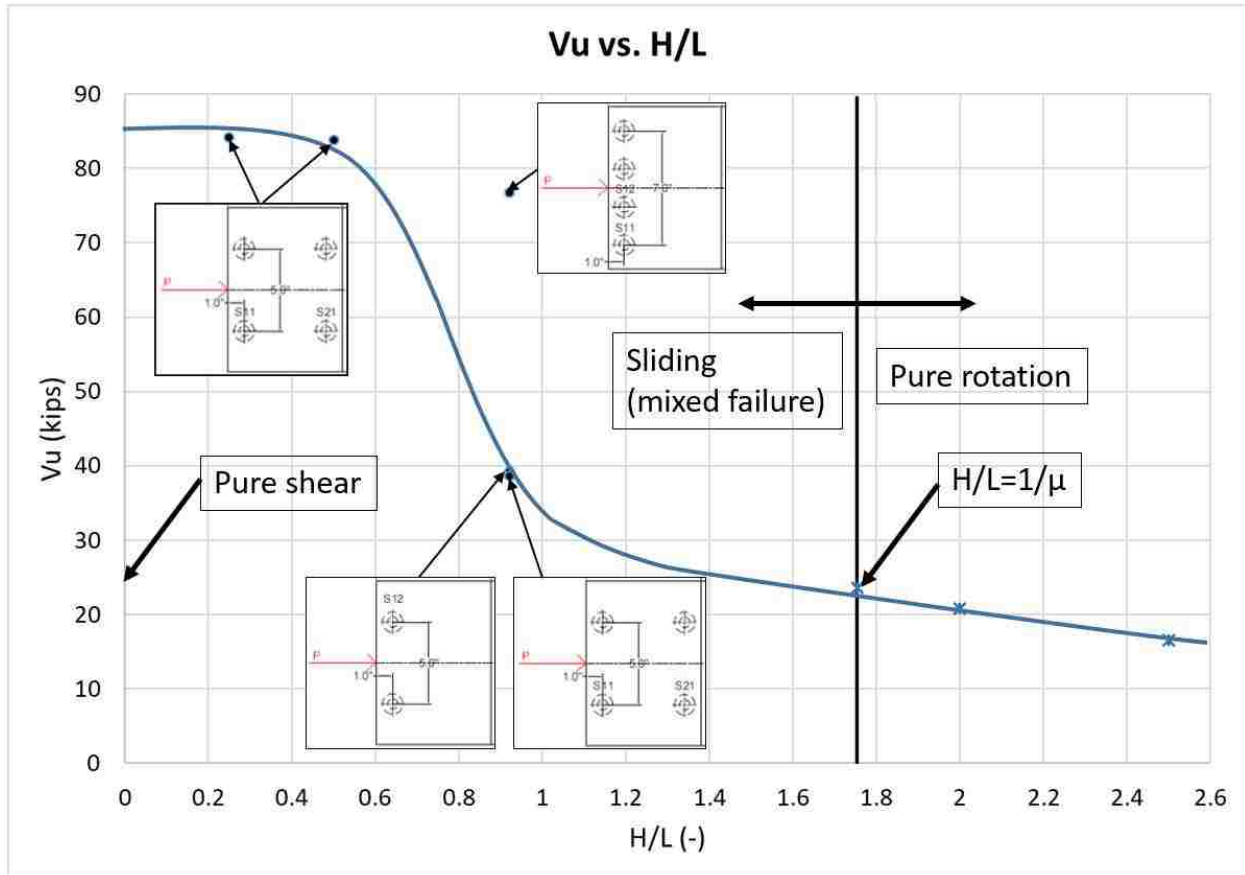


Figure 6.5.6.2: Schematics of failure mode analysis with respect to load eccentricity

6.6. Discussion of Results

This section provides a brief discussion of the interpretation of the experimental results discussed in the previous sections. In particular, a closer look at the mechanisms resisting the applied loads is taken and possible physical explanations for the responses observed are provided using global equilibrium, compatibility and stress-strain relationships for the materials involved. It should be noted that the reported discussion is intended to provide a qualitative rather than quantitative interpretation of the results, and that the conclusions drawn are of preliminary nature.

In general, it is reasonable to assume that the applied shear loads were partly resisted by frictional forces at the plate-concrete interface and partly resisted through dowel (and potentially other actions) by the studs. At the same time, the induced moment was carried by the couple of forces proportional to the tensile force that developed in the studs.

Thus, the experimental results were interpreted in a general sense adopting two approaches which were then compared to one another to verify their consistency:

1. Find/assume the Tension-Compression lever arm (distance between studs in tension and the required reaction) and use global equilibrium to calculate the forces in all the other components.
2. Use the strain gauge readings to calculate the forces in the shear studs and use global equilibrium to calculate the forces in all the other components.

Method 1:

The applied shear force, P , induces a moment demand, M_{demand} and shear demand, V_{demand} , at the plate-concrete interface that can be calculated as follows:

$$M_{demand} = P * H$$

$$V_{demand} = P$$

The applied moment, M_{demand} , needs to be resisted by a couple of forces as shown in Figure 6.6.1.a. In this context, the front studs provide the main contribution undergoing significant tension, while the back studs play a minor role, undergoing little to no axial tension. However, their contribution was incorporated in the calculations when deemed appropriate. The system is statically indeterminate without an additional assumption. The assumption in the calculation of axial forces in the studs was that their relative contribution would be proportional to the plate opening measured at the respective stud locations (See Figure 6.6.1.b). The forces were calculated by satisfying global translational and rotational equilibrium.

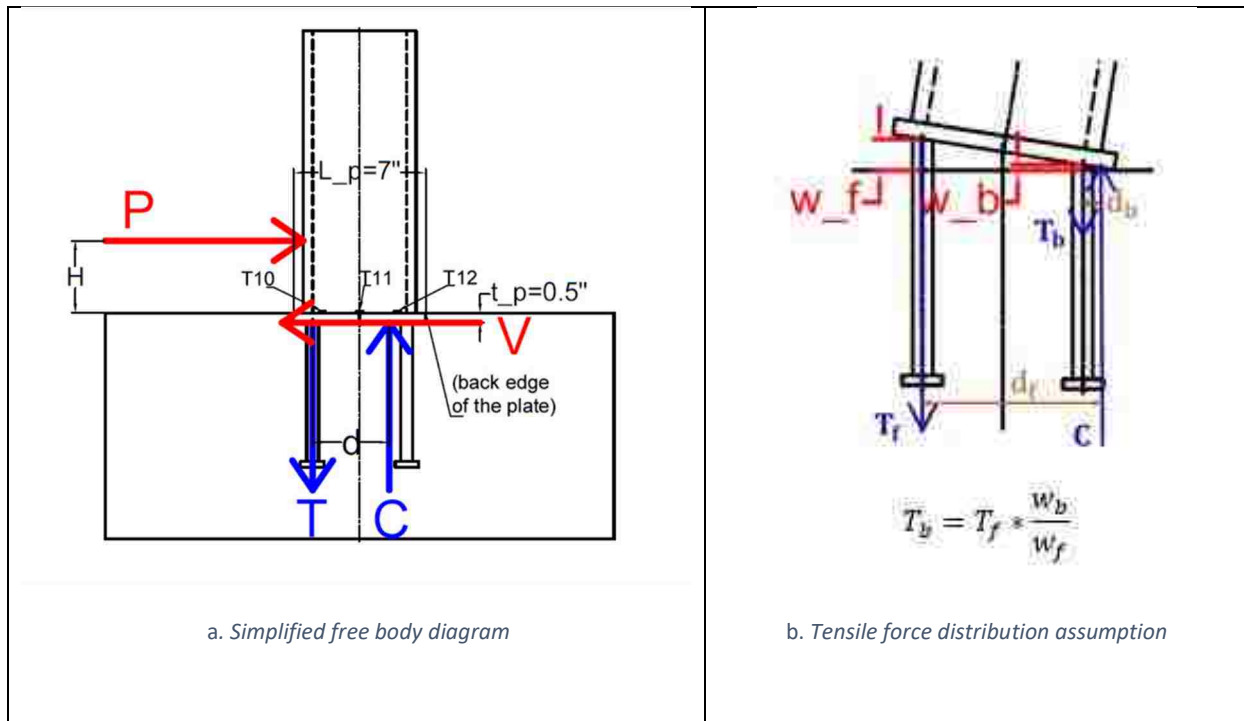


Figure 6.6.1: Free body diagram of Method 1

The plate was assumed to rotate as a rigid body and the center was taken as the origin. From targets 10, 11, and 12, the rotation and vertical displacement of the origin could be found at each load stage. The back of the plate experienced negative vertical displacements (i.e. downwards) which can be expressed with a fitted smooth curve. The fitted curve was substituted with a triangular shape with the same “zero vertical displacement” location along x-direction. The center of compression was assumed to act at the center of the triangle, as shown in Figure 6.6.2. The lever arm, d (or d_f and d_b , if both rows of studs are considered as shown in Figure 6.6.1.b), for the resisting moment was the distance between the studs in tension and the center of compression.

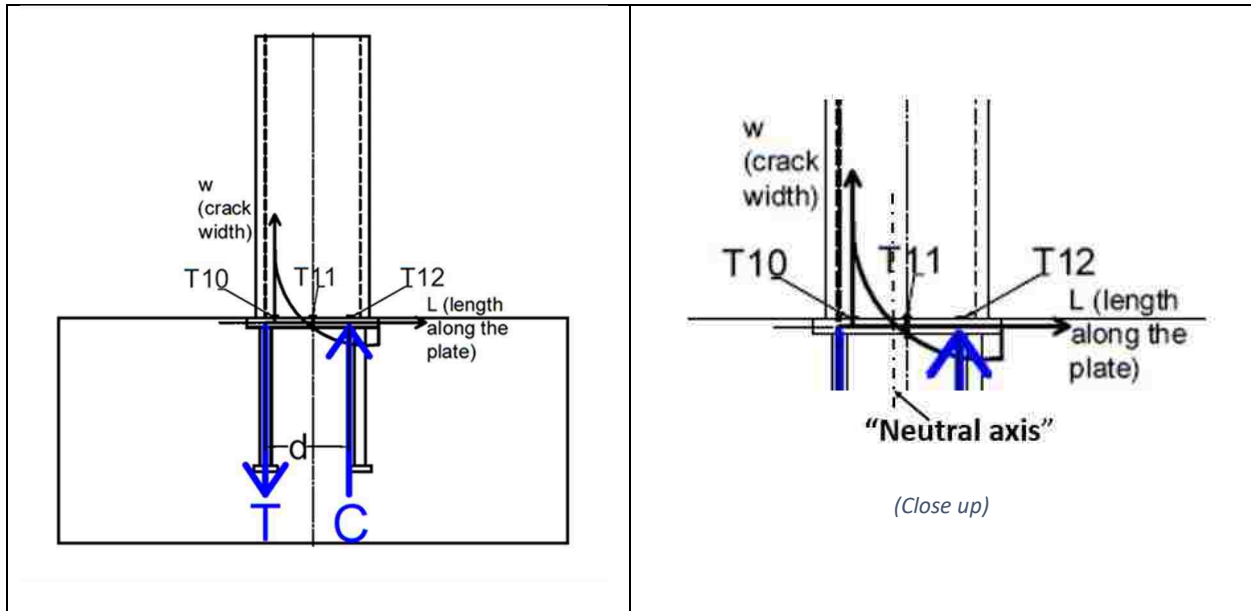


Figure 6.6.2: Exaggerated crack width profile along the base plate

After solving for the lever arm of the couple of forces (T and C), the tension force in the front studs and the compressive reaction were calculated as follows:

$$T_{total} = M_{demand}/d$$

$$C = T_{total}$$

To estimate the “friction” component of the shear resistance, a friction coefficient $\mu=0.57$ was used in accordance with Rabbat and Russell (1985). The frictional component of the strength is activated as soon as some displacement occurs, and can be approximated as:

$$V_{friction} = \mu * C$$

Unlike frictional strength, dowel action is a nonlinear stiffness quantity. All the shear resistance coming from the studs (e.g. including kinking and dowel action combined) is lumped in a single component, V_{dowel} . The shear resistance of the studs can be calculated as follows:

$$V_{dowel} = V_{demand} - V_{friction}$$

Method 2:

The second method uses the average readings of BA1 and BA2 strain gauges (strain gauges intended to measure axial strains) of both rows of studs to solve for the axial force in the studs. Axial stresses ($f_{axial,f}$) in the studs were obtained from the stress-strain relationship of tensile strength test results conducted on sample studs. In general:

$$T = f_{axial,f}(\varepsilon_{axial,f}) * A_{studs,f} + f_{axial,b}(\varepsilon_{axial,b}) * A_{studs,b}$$

However, the normal force is not necessarily equal to the axial tension force in the studs due to the angle they create while deforming. This angle could not be measured during the tests. To estimate the normal force, the average stud inclination angle, α , (the average angle between stud axes and the horizontal surface), was estimated. In Figure 6.6.3 the inclination angle of the front row studs is shown. The similar inclination angle of the back row studs is not shown in Figure 6.6.3 and the α value used in the force calculation is average of those two angles.

The angle, α , was calculated to provide the most accurate match (on average) between the normal force estimates obtained from method 1 and method 2. In other words, the angle α was solved using an optimization method where the sum of the differences between the normal force approximated by method 1 and method 2 (using the particular α) at all loading stages was minimized. When both rows of studs were considered, an average stud inclination was estimated and used in method 2 (rather than finding different inclinations for each rows of studs). It is worth noting that the following can lead to discrepancy in strength estimations when α is used in calculations; hence, caution is advised:

- The inclination angle along the studs is not uniform and different rows of studs may not be characterized by the same α value.
- The general stud bending profile is complex and can be even more complicated if kinking occurs. Then, the strain measured may only be suitable for local stress in the stud rather than the overall average axial strain.

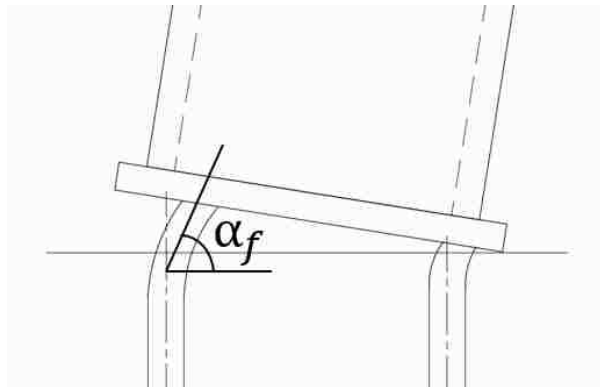


Figure 6.6.3: Stud deformation scheme

The total normal force provided by the studs in tension was then calculated as:

$$N = T * \sin(\alpha)$$

Using the same friction coefficient used in Method 1, the “friction” force and the “dowel” component were estimated as follows:

$$C = N$$

$$V_{friction} = \mu * C$$

$$V_{dowel} = V_{demand} - V_{friction}$$

6.6.1 Specimen 2-0-0.92

Specimen 2-0-0.92 had a single row of 2 studs and was subjected to a horizontal load with an eccentricity of 5.5”. As discussed in section 6.5.1, the embed plate experienced a mixed response characterized by simultaneous rotation and horizontal sliding. In this context, to provide rotational equilibrium, a normal force proportional to the tensile force developed in the studs must be present. This normal force, estimated as described in section 6.6 (i.e. satisfying global equilibrium and estimating a reasonable lever from the measured plate displacements), is outlined in Figure 6.6.1.1 as a function of the plate horizontal displacement.

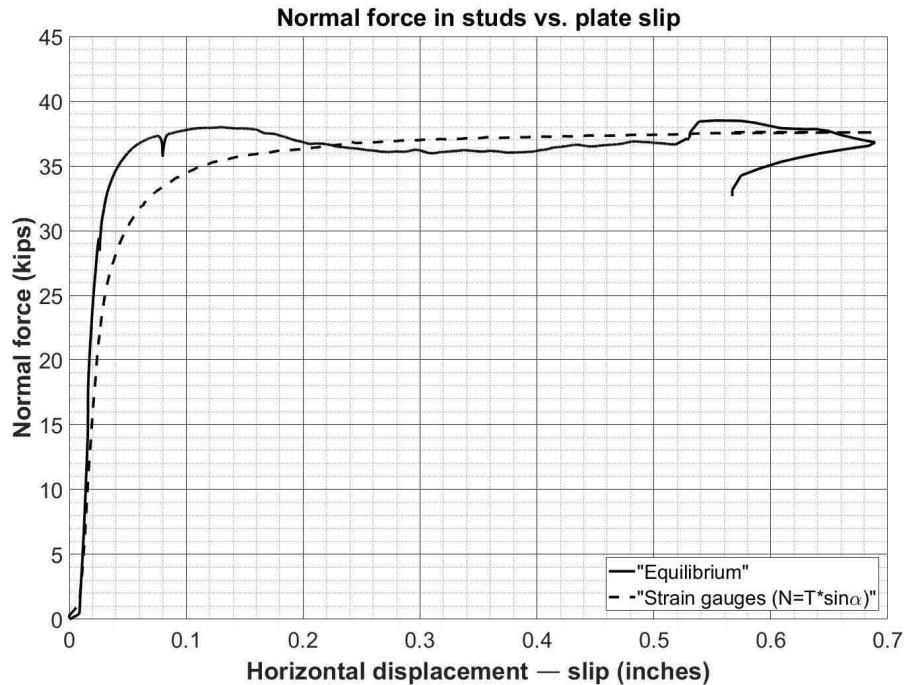


Figure 6.6.1.1: Normal force vs. slip (Specimen 2-0-0.92)

The normal force obtained from the strain gauge readings is also shown in Figure 6.6.1. The normal force is calculated as the vertical component of the tensile force developed in the studs. The stud angle that provides the best agreement between the results of the two approaches adopted was estimated to be 0.89 radians.

The normal force developed by the studs in tension needs to be balanced by a compressive force that develops at the contact point between the steel plate and the underlying concrete. This compressive force, multiplied by the friction coefficient between concrete and steel (assumed as 0.57, in line with the recommendations of Rabbat and Russell, 1985) provides part of the interface shear strength, in the form of a frictional force V_μ . The magnitude of this frictional force is outlined in Figure 6.6.1.2, as a function of the horizontal plate displacement. It can be seen in Figure 6.6.1.2 that the strength provided through friction is significantly lower than the applied load. Thus, part of the strength must be provided by the studs through “dowel” (and possibly kinking and shearing) action. This strength component, referred to as V_d , is also outlined in Figure 6.6.1.2, as a function of the plate displacement.

It can be seen that for this specimen, the frictional strength contribution was greater than the dowel contribution (assuming $\mu=0.57$). For instance, at failure ($P = 39.2$ kips), it is estimated that approximately 22 kips (about 56% of the total load) were carried through friction while 17 kips (about 44% of the total load) were carried by the studs. This outcome is consistent with the experimental observations and with the fact that, due to the nontrivial load eccentricity, the tension-compression couple induced at the interface was significant and so was the resulting resisting frictional force.

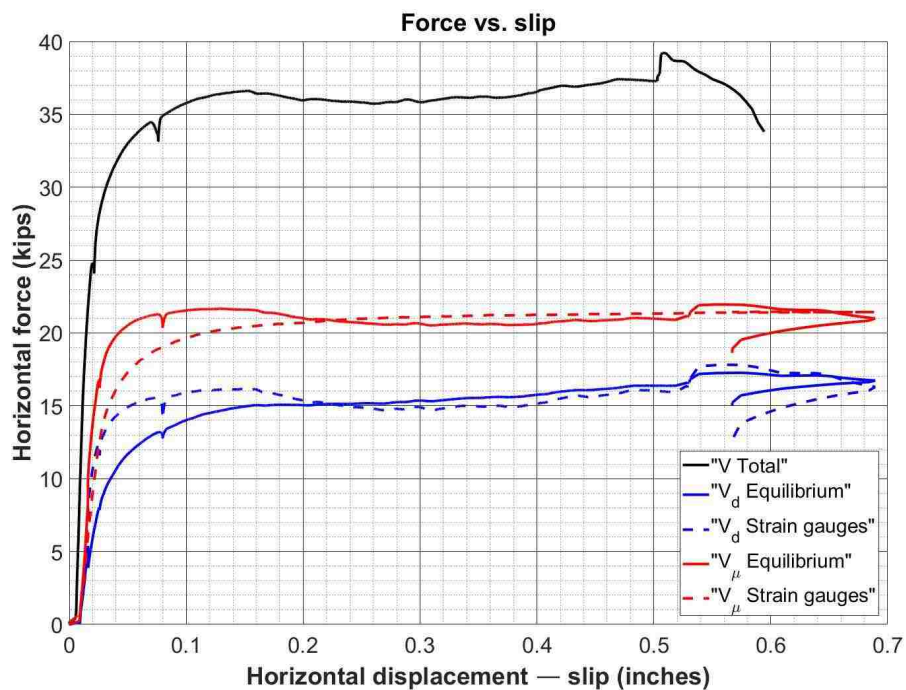


Figure 6.6.1.2: Resisting forces vs. slip (Specimen 2-0-0.92)

6.6.2 Specimen 4-0-0.92

Specimen 4-0-0.92 had a single row of 4 studs and was subjected to a horizontal load with an eccentricity of 5.5". Thus, this specimen was nominally identical to Specimen 2-0-0.92, except for the number of studs located on the tension side of the embed plate. Similarly to Specimen 2-0-0.92, the embed plate of Specimen 4-0-0.92, experienced a mixed response characterized by simultaneous

rotation and horizontal sliding. The mechanics involved is that described for Specimen 2-0-0.92. The normal force arising on the tension side of the plate to balance the induced rotation was computed using the two approaches described earlier. This tensile normal force is depicted in Figure 6.6.2.1, as a function of the horizontal plate slip. It can be seen that this force was two times greater than the force obtained for Specimen 2-0-0.92, on account of the doubled amount of stud area provided.

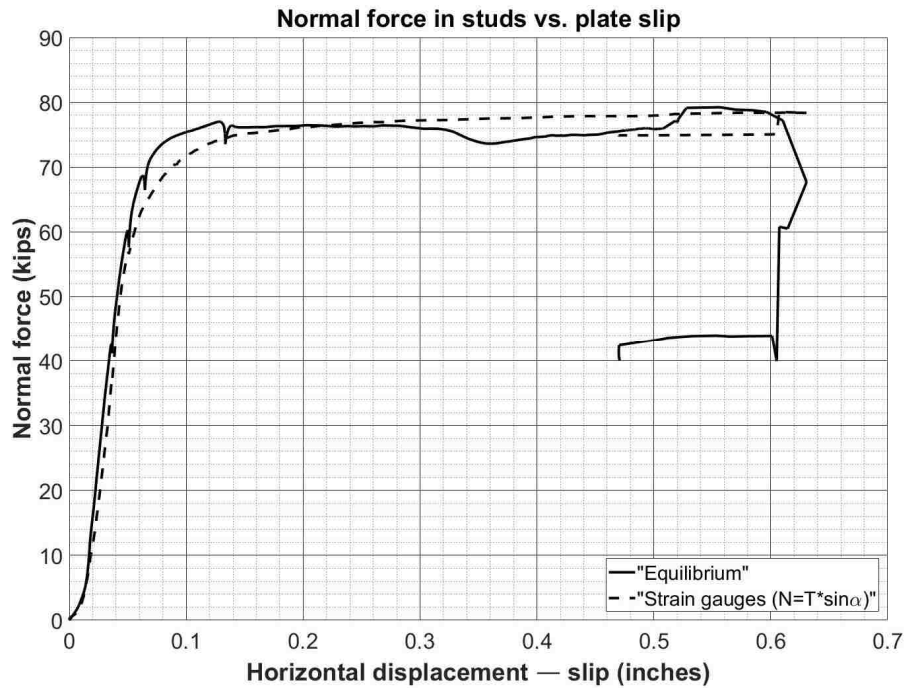


Figure 6.6.2.1: Normal force vs. slip (Specimen 4-0-0.92)

For this case, the stud angle that provides the best agreement between the results of the two approaches adopted was estimated to be approximately 1.03 radians (fairly close to the 0.89 radians angle estimated for Specimen 2-0-0.92).

The normal force developed by the studs in tension was again used to compute the compressive force that develops at the contact point between the steel plate and the underlying concrete. This compressive force was then used to estimate the frictional component of the shear strength V_μ (computed as $C \cdot \mu$, where $\mu = 0.57$). The magnitude of this frictional force is outlined in Figure 6.2.2.2, as a function of the plate horizontal displacement. It can be seen in Figure 6.2.2.2 that the strength provided through friction is not sufficient to resist the applied load. To this end, it was discussed that part of the strength is provided by the studs through “dowel” action. This strength component, V_d , is also outlined in Figure 6.2.2.2, as a function of the plate displacement.

Consistently with what obtained for Specimen 2-0-0.92, the frictional strength contribution was greater than the dowel contribution. At failure ($P = 76.8$ kips) it is estimated that approximately 45 kips (about 58% of the total load) were carried through friction while 32 kips (about 42% of the total load) were carried by the studs. This strength distribution is essentially identical to that estimated for Specimen 2-0-

0.92. This outcome is also consistent with the experimental observations and with the fact that significant compression (and in turn shear-friction) is induced at the interface because of the eccentric load.

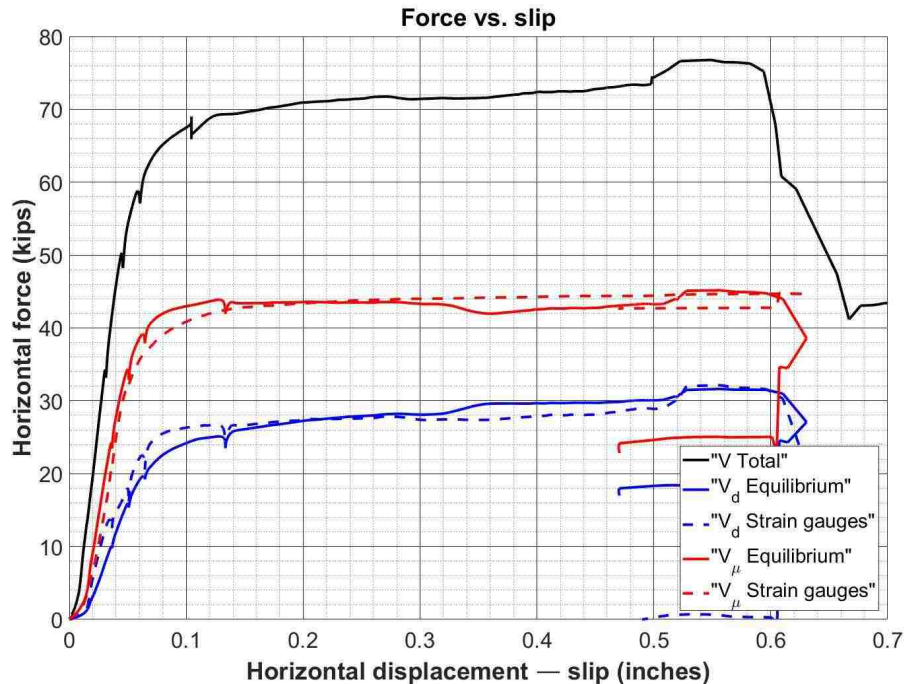


Figure 6.6.2.2: Resisting forces vs. slip (Specimen 4-0-0.92)

6.6.3 Specimen 2-2-0.92

Specimen 2-2-0.92 had a more traditional stud arrangement, involving two rows of 2 studs (spaced at 5", center-to-center) and was subjected to a horizontal load with an eccentricity of 5.5". This specimen was subjected to the same loading conditions as Specimens 2-0-0.92 and 4-0-0.92, but had a different stud arrangement. Similarly to Specimen 2-0-0.92, the embed plate of Specimen 2-2-0.92, experienced a mixed response characterized by simultaneous rotation and horizontal sliding. However, the measured plate displacements were significantly smaller than in the previous two cases. The plate slip at failure was approximately 0.25 in., in contrast with the approximately 0.6 in. measured for Specimens 2-0-0.92 and 4-0-0.92.

The mechanics involved is somewhat different and more complex than that described for the previous two specimens. More specifically, the presence of an additional row of studs makes it more difficult to estimate the normal forces induced by the two rows of studs simply from equilibrium (the problem becomes statically undetermined, with 3 unknowns and only 2 equations). The strain gauges revealed that the back row of studs developed some tensile strains towards the end of the tests. Thus a combination of strain gauge readings, measured plate displacements and equilibrium considerations were used to determine the best course of action. Overall, the calculations showed that accounting for

the second row of studs to determine the total normal compressive force at the interface made a very small difference.

This normal force is depicted in Figure 6.6.3.1, as a function of the horizontal plate slip. It can be seen that the peak value of this force was essentially identical to that computed for Specimen 2-0-0.92. This is consistent with the idea that the normal force that develops at the interface is mostly proportional to the tensile force that develops in the front row of studs, while the back row provides little contribution in this sense.

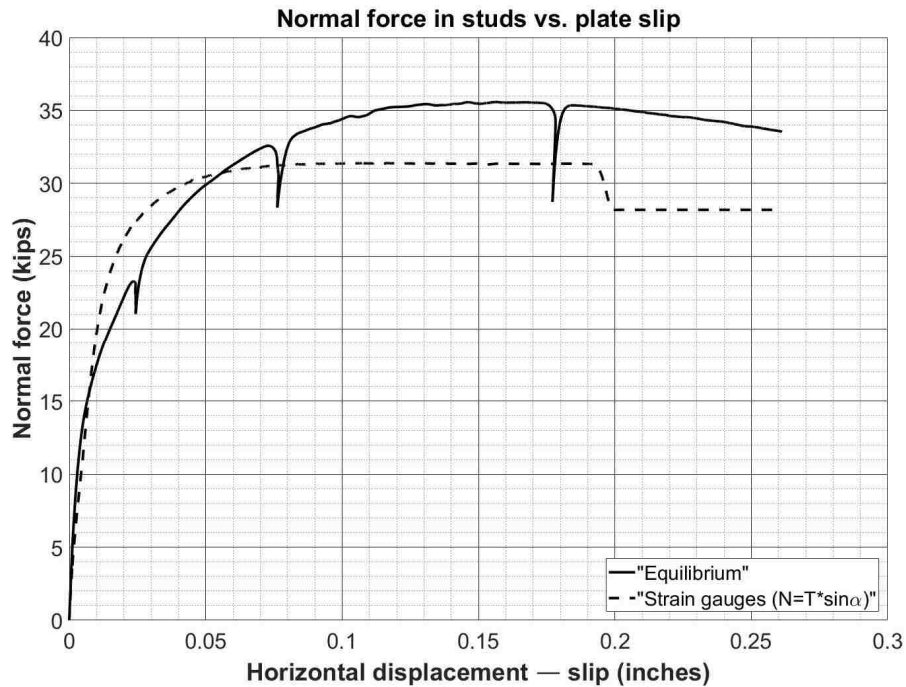


Figure 6.6.3.1: Normal force vs. slip (Specimen 2-2-0.92)

The stud angle (average for both rows of studs) that provides the best agreement between the results of the two approaches adopted was approximately 0.69 radians (significantly lower than in the other two cases). This is consistent with the smaller slip values measured for this test.

The shear-friction V_{μ} , and the “dowel” shear V_d (computed as discussed earlier) are shown in Figure 6.6.3.3, along with the total applied load, as a function of the embed plate displacement. It can be seen that the frictional strength contribution is still greater than the dowel contribution, and the strength distribution between the two resisting mechanism is essentially identical to what estimated for Specimen 2-0-0.92 (the two specimens have also virtually identical strength). At peak load ($P = 38$ kips) it is estimated that approximately 21 kips (about 55% of the total load) were carried through friction while 17 kips (about 45% of the total load) were carried by the studs is shear. This outcome suggests that when there is significant load eccentricity, the presence of a back row of studs limits the horizontal plate displacements but does not provide any additional strength, which is still governed by the capacity of the front studs.

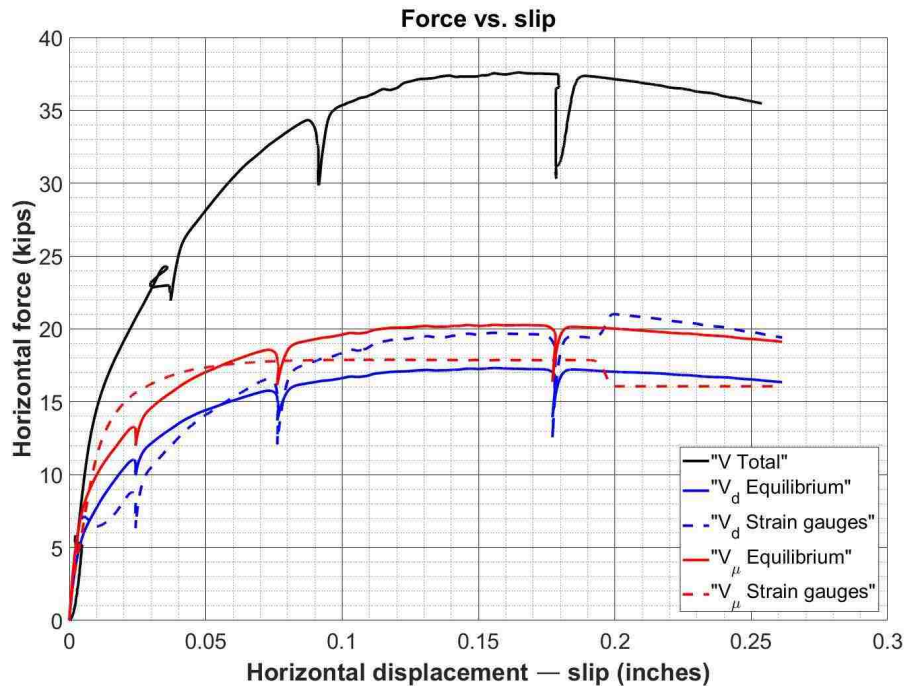


Figure 6.6.3.2: Resisting forces vs. slip (Specimen 2-2-0.92)

6.6.4 Specimen 2-2-0.25

Specimen 2-2-0.25 was nominally identical to Specimen 2-2-0.92, with the same stud arrangement involving two rows of 2 studs (spaced at 5", center-to-center). However, the load eccentricity in this case was reduced from 5.5" to 1.5". While the embed plate, still experienced a mixed response characterized by simultaneous rotation and horizontal sliding, the amount of rotation observed with respect to the horizontal displacement was significantly smaller than in the previous cases (at failure, the measured plate rotation was about 0.019 radians, in contrast with the 0.070 radians measured for Specimen 2-2-0.92). The failure load and horizontal slip (84.15 kips and 0.35 in, respectively) were also greater than for Specimen 2-2-0.92 (38 kips and 0.25 in, respectively).

The analysis of the mechanics involved in the response of this specimen was conducted analogously to what done for Specimen 2-2-0.92, using a combination of strain gauge readings, measured plate displacements and equilibrium considerations were used to determine the best course of action. Overall, the calculations showed that accounting for the tension in the second row of studs to determine the total normal compressive force at the interface made a very small difference. However, in contrast with what observed for Specimen 2-2-0.92, the second row of studs made a significant difference with respect to the overall shear strength (which increased by a factor of more than 2.0).

The estimated normal force is depicted in Figure 6.6.4.1, as a function of the horizontal plate slip. It can be seen that the peak value of this force was lower than the normal force estimated for Specimen 2-2-0.92 (approximately 60%). This is consistent with the test observations and with the idea that the response of this specimen was shear-dominated, on account of the low load eccentricity.

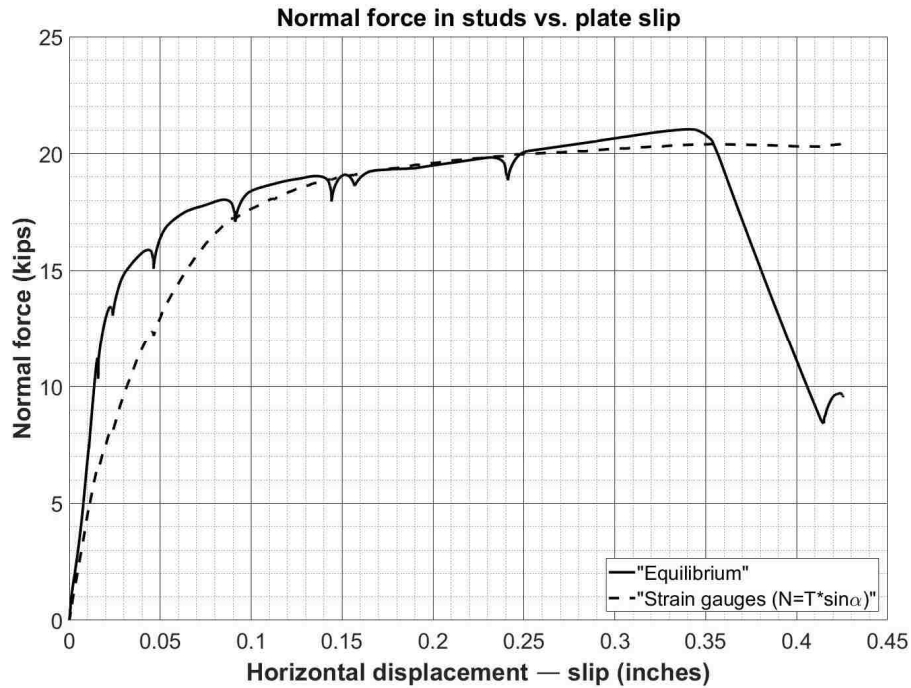


Figure 6.6.4.1: Normal force vs. slip (Specimen 2-2-0.25)

The stud angle (average for both rows of studs) that provides the best agreement between the results of the two approaches adopted was estimated to be approximately 0.45 radians (significantly lower than in all other cases).

The shear-friction V_{μ} , and the “dowel” shear V_d computed for this experiment are shown in Figure 6.6.4.3, along with the total applied load, as a function of the embed plate displacement. It can be seen that the trend is significantly different from what observed for Specimen 2-2-0.92 (and the other specimens), with the frictional strength contributing for only 13% of the applied load and the studs providing approximately 87% for the total strength. This outcome is consistent with the expectations and suggests that, as the load eccentricity is reduced, the overall response shifts from a mixed mode in which flexure is potentially as (or more) relevant as shear, to a mode dominated by shear. In this context, the back row of studs provides a significant strength contribution.

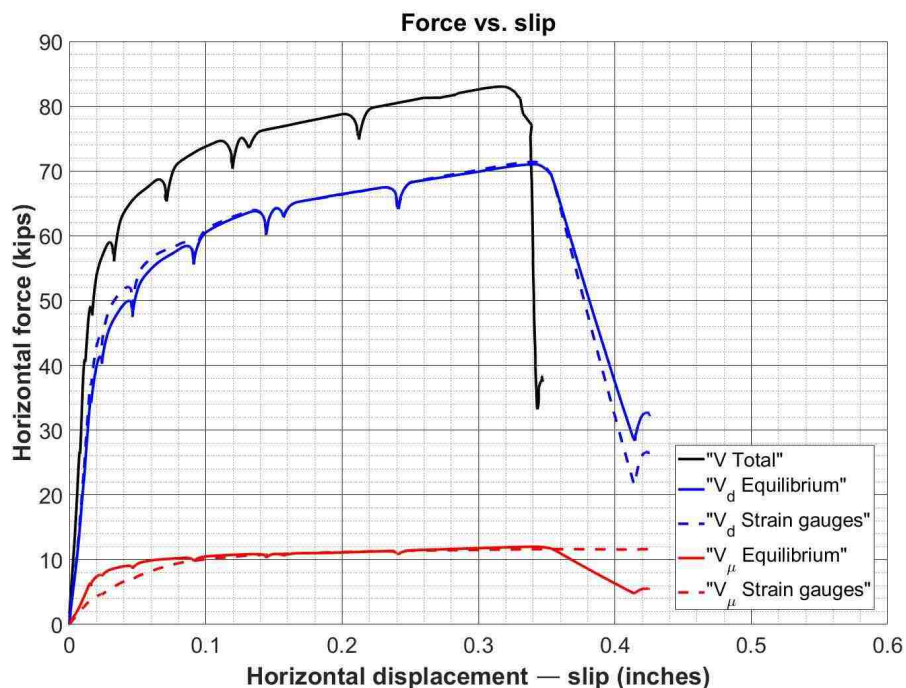


Figure 6.6.4.2: Resisting forces vs. slip (Specimen 2-2-0.25)

6.6.5 Specimen 2-2-0.50

Specimen 2-2-0.50 was nominally identical to Specimens 2-2-0.92 and 2-2-0.25, with the same stud arrangement involving two rows of 2 studs (spaced at 5", center-to-center). However, the load eccentricity in this case was set at 3". Somewhat surprisingly, the overall response and peak strength (83.86 kips) were similar to those of Specimen 2-2-0.25. A lower strength was expected, on account of the higher load eccentricity. However, the embed plate underwent greater slip and rotation, with values equal to 0.45 in and 0.067 radians recorded at peak load.

The analysis of the mechanics involved in the response of this specimen was conducted analogously to what done for Specimens 2-2-0.92 and 2-2-0.25. Consistently with what observed previously, the calculations showed that accounting for the second row of studs to determine the total normal compressive force at the interface made a small difference compared to normal force calculations ignoring the tension in the back row studs. However, in line with what observed for Specimen 2-2-0.25, the second row of studs made a significant difference with respect to the overall shear strength (which increased by a factor of more than 2.0 compared to Specimen 2-2-0.92).

The estimated normal force is depicted in Figure 6.6.5.1, as a function of the horizontal plate slip. It can be seen that at large displacements, the estimates computed from the strain gauge readings do not correspond to the estimates obtained from equilibrium (when constant α is used in force calculations for all load stages). The strain gauge readings provide a normal force that is greater than that estimated for Specimen 2-2-0.25, but similar to that computed for Specimen 2-2-0.92. In contrast, pure equilibrium considerations suggest that, in this case, the peak normal force greater than that estimated for

Specimens 2-2-0.92 and 2-2-0.25. At this stage there is no certainty as to which of the two estimates is more accurate. Either way, this outcome is consistent with the significant plate rotation recorded, which results in large axial (tensile) deformation of the studs. However, the results suggest that while this specimen experienced a mixed response, the behavior was still shear-dominated and both the front and back rows of studs were engaged in shear (similarly to what observed for Specimen 2-2-0.25).

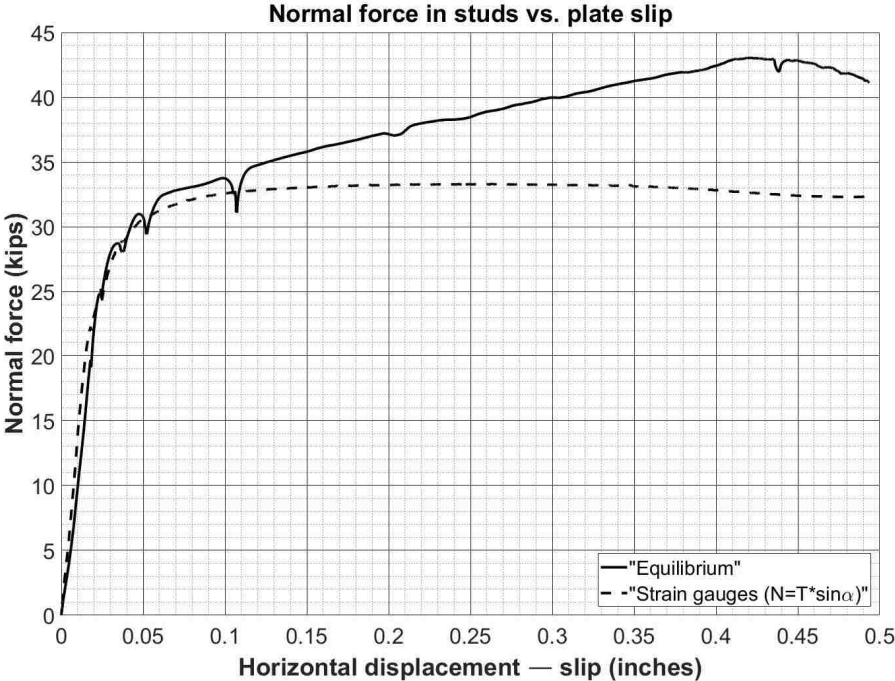


Figure 6.6.5.1: Normal force vs. slip (Specimen 2-2-0.50)

The stud angle (average for both rows of studs) that provides the best agreement between the results of the two approaches adopted was estimated to be approximately 0.73 radians.

The shear-friction V_{μ} , and the “dowel” shear V_d computed for this experiment are shown in Figure 6.6.5.3, along with the total applied load, as a function of the embed plate displacement. It can be seen that the trend is similar to what observed for Specimen 2-2-0.25, with a slightly higher frictional strength contribution (approximately 29% of the applied load) and a slightly lower contribution coming from the studs in shear (approximately 71% for the total strength). While the overall strength is higher than expected, this trend is consistent with the expectations and suggests that, with an intermediate value of load eccentricity, the overall response is still shear-dominated, but the shear-friction contribution becomes somewhat more significant. Again, the back row of studs provides a significant strength contribution in shear transfer.

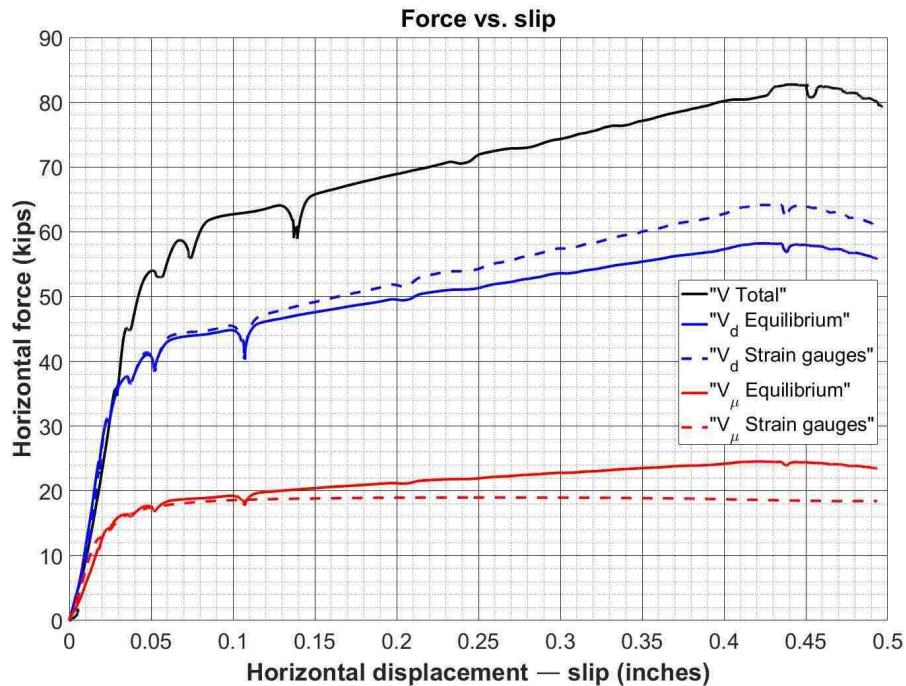


Figure 6.6.5.2: Resisting forces vs. slip (Specimen 2-2-0.50)

7. Summary, Conclusions and Recommendations

7.1 Summary

This research work focused on interface stress transfer problems that can arise in all kinds of structures but are particularly frequent in those that make heavy use of precast elements. Regions such as (but not limited to) interfaces between precast elements and cast-in-place parts, connections between precast elements and cast in place concrete and connections between structural steel and structural concrete members need to be able to safely transfer large shear forces and can potentially be subjected to more complex states involving shear and bending stresses.

To this end, a number of models have been proposed over the years. Some of these models (or simplified versions of them) have been implemented into modern code provisions. These provisions differ (sometimes significantly) from one another and, on occasions, recommend somewhat contradictory design approaches. For instance, ACI 318 contains separate provisions for shear friction (with steel crossing the crack) and interface shear transfer (without such steel), and there is a significant discontinuity between the two sets, even though they both address the same fundamental behavior.

In this context, the first objective of this research work was to explore whether a unified interface design approach could be developed, rectifying the differences between current code recommendations. Instrumental in accomplishing this objective was the formulation and critical analysis of an extensive database that gathered all the relevant experimental results available in the literature. The results pertaining to both concrete-to-concrete and steel-to-concrete interfaces were collected and examined.

The performance of the main available models and codes was tested against the experimental evidence. The results for concrete-to-concrete and concrete-to-steel were assembled and evaluated separately, because the types of test that have been conducted on the two differ significantly.

Most of the existing concrete-to-concrete interface models were able to predict accurately the strength of a subset of the available test data, (typically the one against which they were calibrated) but fared less well in predicting a broader range of the data. However, the model proposed by Mattock (2001) for concrete-to-concrete interfaces provided relatively accurate predictions across all the data. Thus, a new model, built on the framework of Mattock's, was formulated in light of the much larger number of experimental results available today.

While several of the steel-to-concrete interface models analyzed showed fairly accurate performances, none appeared to be consistently and significantly better than the others. Overall, the information available in the literature was deemed insufficient to justify the formulation of a new design model, so no new model was developed. It should be noted that the great majority of the tests were conducted by pushing a steel beam off a concrete block, when the two were connected by welded studs.

However, the analysis of the available experimental data pertaining to steel-to-concrete interfaces led to the identification of a series of gaps in the literature. One significant gap that was identified is that virtually no tests have been performed considering interfaces subjected to combined shear and flexural load. It should be noted that most of the common applications of shear transfer across steel to concrete joints (e.g. steel beam-to-concrete column or wall joints) involve the simultaneous presence of shear and flexural forces to be transferred at the interface.

Motivated by this, an experimental program involving five specimens was conducted, using as the main variables the M/V ratio and the stud distribution across the steel plate. These experiments provided valuable experimental evidence as well as some insight into the mechanics involved, allowing for some preliminary considerations for the formulation of a rational behavior model.

7.2 Conclusions

This section presents the main conclusions from the research program. For clarity, findings from the different topics treated are presented separately.

With respect to concrete-to-concrete interfaces, the following conclusions can be drawn:

1. Analysis of the test data shows that shear resistance consists of a cohesion component and a friction component. This finding is consistent with the existence in ACI318-14 of both interface shear transfer and shear friction (respectively without and with transverse steel) and with the provisions of the AASHTO LRFD Specifications.
2. When there is no reinforcement crossing the interface, both uncracked monolithic and cold-joint interfaces possess some cohesive strength, which appears to increase with the concrete compressive strength. This cohesive strength is greater for the uncracked monolithic interfaces

than it is for cold-joints. It shows more scatter than the friction component of shear strength, particularly for cold joints made with a smooth surface.

3. The interface shear strength increases with the concrete compressive strength. However, once the concrete compressive strength reaches a certain value (approximately $f'_c=11$ ksi), further increasing the concrete compressive strength does not result in any higher shear strength.
4. The use of lightweight concrete results in lower shear strength than for normal weight concrete of the same compressive strength, but the data available in the literature show no clear distinction between results for “sanded lightweight” and “all lightweight” concrete.
5. The friction force is directly related to ρf_y , and this holds true for steels up to and including 80 grade. For higher strength steels, the data are too sparse to permit a conclusion.
6. The shear friction coefficient (μ) for intentionally roughened cold-joint interfaces should not be less than that of pre-cracked monolithic interfaces.
7. The effective coefficient of friction presented in the PCI handbook is unduly complicated to use and provides strength predictions that are less good than those of Mattock’s model or the model proposed here.
8. Both the 6th and 7th editions of the PCI Design Handbook lead to conservative estimations for smooth cold-joint interface strengths on average. However, the variation in accuracy of both editions are significant.

With respect to steel-to-concrete interfaces, the following conclusions can be drawn:

1. The shear strength of an interface can be predicted based on the combination of concrete compressive strength (f'_c) and ultimate clamping stress (ρf_u).
2. f_u rather than f_y is an appropriate measure of stud material strength because the stress-strain curve of a stud has no clear yield point but a relatively long plateau at ultimate strength.
3. For a given ρf_u , the ultimate tensile strength, f_u , of the stud material has no noticeable effect on the interface shear strength.
4. The use of lightweight concrete can decrease the shear transfer strength, but the difference between “sand lightweight” and “all lightweight” concrete is difficult to quantify.
5. The “effective friction method” that was available in the PCI 6th tends to provide inaccurate estimates of the interface strength. More specifically, it tends to provide unconservative estimates at small ρf_u values and overly conservative estimates at higher ρf_u .
6. The main differences in performance between the shear friction approach (e.g. in ACI 318) and the dowel action approach (e.g. in AISC) are:
 - a. “Shear friction” provisions generally result in overly conservative predictions with lower scatter in the results. The conservatism could be corrected by changing the friction coefficient used.
 - b. “Dowel action” models generally provide accurate “average” strength predictions but the scatter in the results tends to be quite large, particularly when f'_c is smaller than approximately 6 ksi.

With respect to the experimental program used to investigate the effects of combined shear and moment loading, the following preliminary conclusions can be drawn:

1. When the load eccentricity is significant (e.g. $H/L \geq 0.92$), the strength of the connection is controlled by bending, and can be computed from the strength of the studs at the tension face. The shear strength is provided largely by friction. Any additional shear strength needed is provided by dowel action, the majority of which occur in the studs at the compression end of the connection.
2. When the load eccentricity is smaller (e.g. the tests at $H/L = 0.25$ and $H/L = 0.50$ in this study), the strength of the connection is controlled by shear. The shear strength is provided mostly by shear in the studs and little by friction between the steel plate and the concrete. The studs near the tension face carry the tension force needed to resist the moment and some shear as well. Determining the distribution of shear force between the two sets of studs (i.e. at the tension and compression faces) was not possible within the scope of the test program. The strength of the two relative specimens tested was approximately the same, suggesting that a small eccentricity has little effect on the shear strength.

7.3 Recommendations for Design Equations

1. The updated version of Mattock's model proposed here should be adopted for design of concrete-to-concrete interfaces. It contains a cohesion term and uses values for the friction coefficient and upper bound strength that were calibrated against a larger dataset than has been used in any previous model development.
2. The use of μ_{eff} , available in the PCI Design Handbook, is not recommended, particularly for smooth cold-joints and steel-to-concrete interfaces. It is more complicated to use, and gives less accurate results, than the model proposed here.
3. For steel-to-concrete interfaces modeled using the shear friction approach, higher friction coefficients are justified. The AISC code method, based on a dowel action model, provides reasonable average estimates of the interface strength, but there is potential to implement improved provisions, particularly when $f'_c < 6$ ksi.

7.4 Recommendations for Future Work

1. Numerous parameters appear to influence the strength in sliding shear at an interface. The focus of this study was to examine concrete-to-concrete and steel-to-concrete interfaces subjected primarily to shear loads. Test data from experiments with specimens subjected to both shear forces and moments, or with inclined reinforcement crossing the interface, should be incorporated in the database in the future.
2. A deeper analysis of the parameters that were deemed "secondary" with respect to the interface strength (such as bar size, spacing, dependency of friction coefficient on concrete strength) should be performed. More reliable design models may need to incorporate some of these parameters. To this end, it is necessary to collect, and if necessary to generate, more experimental evidence because many of those parameters were disregarded in this study simply because insufficient evidence was available in the literature.
3. In particular, more experiments considering steel-to-concrete interfaces subjected to combined moments and shear forces should be performed as part of future studies, considering a wider range of load eccentricity, stud distribution, stud size, number or stud rows etc. This experimental evidence is necessary to formulate a rational design model. The results of such an

experimental program, combined with the evidence already available in the literature, would provide a basis for improving existing design models.

References

- AASHTO (2014). "AASHTO LRFD Bridge Design Specifications," Seventh edition, American Association of State Highway and Transportation Officials (AASHTO), Washington, DC.
- ACI Committee 318 (2014). "Building Code Requirements for Structural Concrete and Commentary (ACI 318R-14)," Farmington Hills, MI: American Concrete Institute.
- American Institute of Steel Construction, "Manual of Steel Construction". 13th Edition. Chicago: AISC, 2005.
- Anderson, A. R., "Composite Designs in Precast and Cast-in-Place Concrete," *Progressive Architecture*, Vol. 41, No. 9, September 1960, pp. 172-179.
- Anderson, Neal S., and Meinheit Donald F. (2005). "Connections in Precast Concrete Construction," *PCI Journal*, Vol. 50, No. 2, pp. 90-112.
- ASTM C39/C39M-18 Standard Test Method for Compressive Strength of Cylindrical Concrete Specimens, ASTM International, West Conshohocken, PA, 2018.
- Baldwin, J. W., (1965). "Bond of Reinforcement in Lightweight Aggregate Concrete," *Preliminary Report*, University of Missouri, Mar., 10.
- Barbosa, Andre R, et al. "Effect of High-Strength Reinforcement Steel on Shear Friction Behavior." *Journal of Bridge Engineering*, vol. 22, no. 8, 2017, pp.
- Birkeland, H.W. (1969), Class Notes for Course on "Precast and Prestressed Concrete," University of British Columbia, Spring 1968.
- Birkeland, P.W. and Birkeland, H.W. (1966). "Connections in Precast Concrete Construction," *ACI Journal, Proceedings*, Vol. 63, No. 3, pp. 345-368.
- Buttry, K. E. (1965). "Behavior of Stud Shear Connectors in Lightweight and Normal-Weight Concrete." MS Thesis, University of Missouri, Columbia, MO.
- CEB-FIP Model Code 1990. "Model code for concrete structures". In: Comité Euro-international du Béton. Secretariat permanent. Case Postale 88, CH-1015 Lausanne, Switzerland; 1990.
- Cederwall K. and An L. (1996). "Push-out Tests on Studs in High Strength and normal strength concrete", *Journal of Constructional Steel Research*, 36(1), 15-29.
- Chapman, J. C., and Balakrishnan, S. (1964). "Experiments on composite beams." *Struct. Eng.*, 42(11), 369-383.
- Chinn, J. (1965). "Pushout Tests on Lightweight Composite Slabs." *Engineering Journal*, AISC, 2(4), 129-134.
- Crane, Charles, and Kahn, Lawrence F. "Shear and Shear Friction of Ultra-High Performance Concrete Bridge Girders." *Shear and Shear Friction of Ultra-High Performance Concrete Bridge Girders*, 2010, pp. ProQuest Dissertations and Theses.

- CSA. (2014). *Design of Concrete Structures (A23.3-04)*. Toronto, Canada: Canadian Standards Association.
- Concrete Technology Associates (1974). Composite Systems without Roughness. Technical Bulletin 74-B6.
- Concrete Technology Associates (1976). Composite Systems without Ties. Technical Bulletin 76- B4.
- Dallam, L. N., "Bibliography of Composite Concrete-Steel Beams," Missouri Cooperative Highway Research Program Report, 68-5, 1968.
- Davies, C. (1967). "Small-Scale Push-Out Tests on Welded Stud Shear Connectors." *Concrete*, September, 311-316.
- Eurocode 2. "Design of concrete structures", *Part 1.1: General rules and rules for buildings*. In: Comité Européen de Normalisation. Avenue Marnix 17, B-1000 Brussels, Belgium; 2004 [with corrigendum of 16th January 2008].
- Eurocode 4, (1997). "Design of composite steel and concrete structures", *Part 2 :composite bridges (ENV 1994-2), CEN*
- Gambarova, P, and C Karakoc. "New Approach to the Analysis of the Confinement Role in Regularly Cracked Concrete Elements." Transactions of the International Conference on Structural Mechanics in Reactor Technology, 1983, pp. Transactions of the International Conference on Structural Mechanics in Reactor Technology, 1983.
- GB 50017-2013: "Code for Design of Steel Structures."* Department of Standards and Norms, Ministry of Housing and Urban-Rural Development of the People's Republic of China, 2013.
- Goble, G. G. (1968). "Shear Strength of Thin Flange Composite Specimens." *Engineering Journal*, AISC, 5(2), 62-65.
- Handbook of Steel Construction*. 11th ed., Canadian Institute of Steel Construction, 2010.
- Hanson, N.W., (1960). "Precast-Prestressed Concrete Bridges 2: Horizontal Shear Connections," *PCA – Journal of the Research and Development Division*, Vol. 2, No. 2, pp. 38-58.
- Harries, Kent A., Zeno, and Shahrooz. (2012). "Toward an Improved Understanding of Shear-Friction Behavior," *ACI Structural Journal*, Vol. 109, No. 6, pp. 835-844.
- Hawkins, N. M., (1973). " The Strength of Stud Shear Connectors," *Civil Engineering Transactions*, The Institution of Engineers. Australia.
- Hawkins, N. M., and Mitchell D. (1984). "Seismic Response of Composite Shear Connections." *J. Struct. Engrg.*, ASCE, 110(9), 2120-2136.
- Hofbeck, J. A.; Ibrahim, I. O.; and Mattock, A. H. (1969). "Shear Transfer in Reinforced Concrete," *ACI Journal, Proceedings*, V. 66, No. 2, pp. 119-128.
- Hoff, G.C. (1992). "High Strength Lightweight Aggregate Concrete for Arctic Applications--Part 3: Structural Parameters," *American Concrete Institute Special Publication*, SP-136, pp. 175-246.

- Hsu, Thomas T.C., S.T. Mau, and Bin Chen. (1987). "Theory of Shear Transfer Strength of Reinforced Concrete," *ACI Structural Journal*, Vol. 84, No. 2, pp. 149-160.
- Japan Society of Civil Engineers, (2010). *Standard Specifications for Concrete Structures 2007 Design*.
- Jayas, B. S., and Hosain, M. U. (1988). "Behavior of Headed Studs in Composite Beams: Push-Out Tests." *Can. J. Civ. Eng.*, 15(2), 240-253.
- Kahn, L.F. and A.D. Mitchell. (2002). "Shear-friction Tests with High-Strength Concrete," *ACI Structural Journal*, Vol. 99, No. 1, pp. 98-103.
- Kanvinde, Amit M., and Gregory G. Deierlein. "Recent Research on Column Base Connections." *Modern Steel Construction*, AISC, 2011.
- Kono, Susumu, et al. "Interface Shear Transfer for High Strength Concrete and High Strength Shear Friction Reinforcement." *High Performance Materials in Bridges*, 2001, pp. 319–328.
- Lin I. J, Chen Y. L." Shear transfer across a crack in reinforced high strength concrete". In: *Proceedings 2nd east Asia–Pacific conference on structural engineering & construction*, Chiang Mai, Thailand, January, 1989. p. 505–10.
- Loov, R.E. and A.K. Patnaik. (1994). "Horizontal Shear Strength of Composite Beams with a Rough Interface," *PCI Journal*, Vol. 39, No. 1, pp. 48-58.
- Lyons, J. C., Easterling, W. S. and Murray, T. M. (1994). "Strength of Welded Shear Studs." Report No. CE/VPI-ST 94/07. Virginia Polytechnic Institute and State University, Blacksburg, VA.
- Mainstone, R.J. and Menzies, J.B. (1967). "Shear connectors in steel-concrete composite beams for bridges. Part 1: Static and fatigue tests on push-out specimens", *Concrete*, London, Vol. 1, pp 291–302.
- Mansur, M.T., T. Vinayagam, and Kiang-Hwee Tan. (2008). "Shear Transfer Across a Crack in Reinforced High-Strength Concrete," *ASCE Journal of Materials in Civil Engineering*, Vol. 20, No. 4, pp. 294-302.
- Mast, R.F. (1968). "Auxiliary Reinforcement in Concrete Connections," *ASCE Journal of the Structural Division Proceedings*, Vol. 94, No. ST6, pp. 1485-1504.
- Mattock, A.H. (1974). "Shear Transfer in Concrete Having Reinforcement at an Angle to the Shear Plane," American Concrete Institute Publication SP-42, *Shear in Reinforced Concrete*, pp. 17-42.
- Mattock, A. H., W. K. Li, and T. C. Wang. (1976). "Shear Transfer in Lightweight Reinforced Concrete." *PCI Journal*, Vol. 21, No. 1, pp. 20-39.
- Mattock, A.H. (1976). "Shear Transfer Under Monotonic Loading Across and Interface Between Concretes Cast at Different Times," *University of Washington Department of Civil Engineering Report SM 76-3*.
- Mattock, A.H. (2001). "Shear-friction and High-Strength Concrete," *ACI Structural Journal*, Vol. 98, No. 1, pp. 50-59.

- Mattock, A. H., Johal, L, and Chow, C. H. (1975). "Shear transfer in reinforced concrete with moment or tension acting across the shear plane." *PCI Journal*, Vol. 20, No. 4, pp. 76-93.
- Mattock, A.H. and N.M. Hawkins. (1972). "Shear Transfer in Reinforced Concrete – Recent Research," *PCI Journal*, Vol. 17, No. 2, pp. 55-75.
- Menzies, John B. (1971). "@P 1 17 and shear connectors in steel-concrete composite beams made with normal-density or lightweight concrete." *The Structural Engineer*, 49(3), 137-154.
- Nagle, T.J. and D.A. Kuchma. (2007). "Nontraditional Limitations on the Shear Capacity of Prestressed Concrete Girders," *University of Illinois at Urbana-Champaign NSEL Report-003*.
- Oehlers, D. J (1980). "Stud Shear Connectors for Composite Beams", PhD Thesis, University of Warwick.
- Oehlers, D. J., and Johnson, R. P. (1987). "The Strength of Stud Shear Connections in Composite Beams." *The Structural Engineer*, 65(2), 44-48.
- Okada J., Yoda T., Lebet J.-P. (2004). "A study of the grouped arrangements of stud connections on shear strength behavior", *Journal of Structural Mechanics and Earthquake Engineering*, Vol. 23, No. 776/I-68, 81-95.
- Ollgaard, J. G., Slutter, R. G., and Fisher, J. W. (1971). "Shear Strength of Stud Connectors in Lightweight and Normal-Weight Concrete." *Engineering Journal*, AISC, 8(2), 55-64.
- Pallares L., Hajjar J.F. (2010). "Headed steel stud anchors in composite structures", Part I: Shear, *Journal of constructional steel research*, 66, 198-212.
- Pincheira, Jose A., et al. "Tests on Double Tee Flange Connectors Subjected to Monotonic and Cyclic Loading." *PCI Journal*, vol. 43, no. 3, 1998, pp. 82–96.
- Precast/Prestressed Concrete Institute (2004). *PCI Design Handbook: Precast and Prestressed Concrete Institute*. 6th ed. Chicago: Precast/Prestressed Concrete Institute.
- Precast/Prestressed Concrete Institute (2010). *PCI Design Handbook: Precast and Prestressed Concrete Institute*. 7th ed. Chicago: Precast/Prestressed Concrete Institute.
- Rabbat, B., & Russell, H. (1985). Friction Coefficient of Steel on Concrete or Grout. *Journal of Structural Engineering*, 111(3), 505-515.
- Rahal, Khaldoun, and Abdul-Lateef Al-Khaleefi. "Shear-Friction Behavior of Recycled and Natural Aggregate Concrete-An Experimental Investigation." *ACI Structural Journal*, vol. 112, no. 6, 2015, pp. 725–733.
- Rambo-Roddenberry M. (2002). "Behavior and strength of welded stud shear connectors", PhD Thesis, Virginia Polytechnic Institute and State University.

- Raths, C. H. (1977). "Reader Comments: Design Proposals for Reinforced Concrete Corbels." *PCI Journal*, Vol. 21, No. 3, pp 93–98.
- Sagasetta, J, and Vollum, RI. "Influence of Aggregate Fracture on Shear Transfer through Cracks in Reinforced Concrete." *Magazine of Concrete Research*, vol. 63, no. 2, 2011, pp. 119–137.
- Scott, Jana. (2010) "Interface Shear Strength in Lightweight Concrete Bridge Girders." MS Thesis. Virginia Polytechnic Institute.
- Shaikh, Fattah A. (1978). "Proposed Revisions to Shear-friction Provisions." *PCI Journal*, Vol. 23, No. 2, pp. 12-21.
- Shim C.S., Lee P.G., Yoon T.Y. (2004). "Static behavior of large stud shear connectors," *Engineering Structures*, 26(12), 1853-1860.
- Slutter, R. G., and Driscoll, G. C. (1965). "Flexural Strength of Steel-Concrete Composite Beams." *J. Struct. Div.* 91 (2) 71-99.
- Sneed, L. H., and D. M. Shaw. 2013. "Lightweight Concrete Modification Factor for Shear Friction." Report NUTC R276/R317. Rolla, MO: Center for Transportation Infrastructure and Safety/NUTC Program, Missouri University of Science and Technology.
- Sneed, Lesley H., et al. "Interface Shear Transfer of Lightweight-Aggregate Concretes with Different Lightweight Aggregates ." *PCI Journal*, vol. 61, no. 2, 2016, pp. 38–55.
- Shaw, D. and Sneed, L. (2014). "Interface Shear Transfer of Lightweight Aggregate Concretes Cast at Different Times," *PCI Journal*, V. 59, No. 3, pp. 130-144.
- Shoup, Thomas E., and Singleton Robert C. "Headed Concrete Anchors." *Journal of the American Concrete Institute.*, Sept. 1963.
- Spremic, Milan., Markovic, Zlatko., and Veljkovic, Milan. (2013). "Push-Out Experiments of Headed Shear Studs in Group Arrangements." *Advanced Steel Construction*, V.9, No. 2, pp139-160.
- Steele, D. H., "The Use of Nelson Studs with Lightweight Aggregate Concrete in Composite Construction," MS Thesis, University of Colorado, Boulder, CO, October 1967, 143 pp.
- Su Qingtian, and Mark A. Bradford. (2014). "Static Behaviour of Multi-Row Stud Shear Connectors in High- Strength Concrete." *Steel and Composite Structures*, V.17, No. 6. pp.967-980.
- Tanner, John A. (2008). "Calculating Shear-friction Using Effective Coefficient of Friction." *PCI Journal*, Vol. 53, No. 3, pp. 114-20.
- Tsoukantas SG, Tassios TP. Shear resistance of connections between reinforced concrete linear precast elements. *ACI Structural Journal* 1989;86(3):242–9.

- Vecchio FJ, Collins MP. The modified compression-field theory for reinforced concrete elements subjected to shear. *Journal of American Concrete Institute*. 1986;83(2):219–31.
- Viest, I. M., Siess, C. P., Appleton, J. H. and Newmark, N. M. "Studies of Slab and Beam Highway Bridges": Part IV—Full Scale Tests of Channel Shear Connectors and Composite T-Beams. *Univ. of Illinois Engg. Expt. Station Bulletin No. 405*, 1952.
- Viest, I. M. (1956). "Investigation of Stud Shear Connectors for Composite Concrete and Steel T-Beams." *J. of the American Concrete Institute*, 27, 875-891.
- W., Frenay J. *Shear Transfer across a Single Crack in Reinforced Concrete under Sustained Loading. Part I: Experiments*. Delft University of Technology, Faculty Civil Engineering and Geosciences, 1985.
- Walraven, J.C. and Reinhardt, H.W., "Theory and Experiments on the Mechanical Behaviour of Cracks in Plain and Reinforced Concrete Subjected to Shear Loading", *Heron*, Vol. 26 (1981) No. 1A, pp. 1-68.
- Walraven, J. C.; Frenay, J.; and Pruijssers, A. (1987). "Influence of Concrete Strength and Load History on the Shear-friction Capacity of Concrete Members," *PCI Journal*, Vol. 32, No. 1, pp. 66-84.
- Walraven, J. and Stroband, J. (1994). "Shear-friction in High-Strength Concrete," *American Concrete Institute Special Publication*, SP-42, pp. 311-330.
- Woo-Young Lim, Dongkeun Lee, Young-Chan You. "Exposed column-base plate strong-axis connections for small-size steel construction", *Journal of Constructional Steel Research*, Volume 137, 2017, Pages 286-296, ISSN 0143-974X, <https://doi.org/10.1016/j.jcsr.2017.06.018>.
- Xu C., Sugiura K., Wu C., Su Q. (2012). "Parametrical static analysis on group studs with typical push-out tests", *Journal of constructional steel research*, 72, 84-96.
- Xue D., Liu Y., Yu Z., He J. (2012). "Static behavior of multi-stud shear connectors for steel-concrete composite bridge", *Journal of Constructional Steel Research*, 74, 1–7.
- Yi Liu, Ammar Alkhatib. (2013). "Experimental study of static behaviour of stud shear connectors" *Canadian Journal of Civil Engineering*, Vol.40. No.9, pp.909-9016.
- Zhao, G., "Tragverhalten von randfernen Kopfbolzenverankerungen bei Betonbruch (Load-Carrying Behavior of Headed Stud Anchors in Concrete Breakout Away From an Edge)," Report 1994/1, Institut für Werkstoffe im Bauwesen, Universität of Stuttgart, Stuttgart, Germany, 1994, 197 pp. [in German].
- Zia, P. (1961). "Torsional Strength of Prestressed Concrete Members," *ACI Journal*, Vol. 57, No. 10, pp. 1337-1360.

Appendix A: Concrete-to-concrete interface database

Types of test	Author1	Author2	year	ID	orig. spec. ID	concrete type	interface type	surface preparation	strip diameter, d _s	bars at angle, α	ρ	f _y or f _{yk}	pfr	f' _c	External Normal stress, σ	surface strength, σ _{tr} or σ _{cr}	additional info (crack opening and slip)							additional info (aggregate and rebars)	
																	initial residual crack width	crack width at ultimate load	slip at ultimate load	strain in steel at ultimate load	load kept constant while strain increased or any unusual	ultimate load reached or not	if stopped before reaching ultimate load, the max slip	if stopped before reaching ult. load, the max width	bumps on rebars
vertical push-off	Mattek	U	1976	1	A0	SW	NO	U	0.375	90	0.00	0.00	0.0	42300	0.0	500.0	unavailable	[n]	unavailable	N/A	1.0	N/A	N/A	1.0	0.375
vertical push-off	Mattek	U	1976	2	A1	SW	NO	U	0.375	90	4.40	4770	2100	37400	0.0	758.0	N/A	0.015	0.022	unavailable	1.0	N/A	N/A	1.0	0.375
vertical push-off	Mattek	U	1976	3	A2	SW	NO	U	0.375	90	8.81	53.60	4720	40950	0.0	914.0	N/A	0.012	unavailable	unavailable	1.0	N/A	N/A	1.0	0.375
vertical push-off	Mattek	U	1976	4	A3	SW	NO	U	0.375	90	13.20	53.20	7020	39100	0.0	1020.0	N/A	0.009	0.015	unavailable	1.0	N/A	N/A	1.0	0.375
vertical push-off	Mattek	U	1976	5	A4	SW	NO	U	0.375	90	17.60	50.90	8960	41000	0.0	1100.0	N/A	0.019	0.019	unavailable	1.0	N/A	N/A	1.0	0.375
vertical push-off	Mattek	U	1976	6	A5	SW	NO	U	0.375	90	22.00	51.90	11200	39600	0.0	1190.0	N/A	0.014	0.010	unavailable	1.0	N/A	N/A	1.0	0.375
vertical push-off	Mattek	U	1976	7	A6	SW	NO	U	0.375	90	26.41	51.80	13860	42900	0.0	1340.0	N/A	0.011	unavailable	unavailable	1.0	N/A	N/A	1.0	0.375
vertical push-off	Mattek	U	1976	8	B1	SW	NO	P	0.375	90	4.40	49.86	3180	37400	0.0	450.0	0.009	0.005	0.008	unavailable	1.0	N/A	N/A	1.0	0.375
vertical push-off	Mattek	U	1976	9	B2	SW	NO	P	0.375	90	8.80	50.90	4480	33600	0.0	652.0	0.009	0.010	0.024	unavailable	1.0	N/A	N/A	1.0	0.375
vertical push-off	Mattek	U	1976	10	B3	SW	NO	P	0.375	90	13.20	50.90	6720	39100	0.0	840.0	0.009	0.008	0.016	unavailable	1.0	N/A	N/A	1.0	0.375
vertical push-off	Mattek	U	1976	11	B4	SW	NO	P	0.375	90	17.60	49.10	8640	41000	0.0	940.0	0.009	0.007	0.021	unavailable	1.0	N/A	N/A	1.0	0.375
vertical push-off	Mattek	U	1976	12	B5	SW	NO	P	0.375	90	22.00	50.50	11110	39600	0.0	1000.0	0.009	0.009	0.019	unavailable	1.0	N/A	N/A	1.0	0.375
vertical push-off	Mattek	U	1976	13	B6	SW	NO	P	0.375	90	26.41	51.80	13860	42900	0.0	1154.0	0.009	0.013	0.021	unavailable	1.0	N/A	N/A	1.0	0.375
vertical push-off	Mattek	U	1976	14	C1	SW	NO	P	0.375	90	4.40	49.60	2180	23300	0.0	364.0	0.009	0.008	0.013	unavailable	1.0	N/A	N/A	1.0	0.375
vertical push-off	Mattek	U	1976	15	C2	SW	NO	P	0.375	90	8.81	53.60	4720	23300	0.0	514.0	0.009	0.012	0.022	unavailable	1.0	N/A	N/A	1.0	0.375
vertical push-off	Mattek	U	1976	16	C3	SW	NO	P	0.375	90	13.20	50.90	6720	20000	0.0	526.0	0.009	0.016	0.032	unavailable	1.0	N/A	N/A	1.0	0.375
vertical push-off	Mattek	U	1976	17	C4	SW	NO	P	0.375	90	17.61	52.30	9210	20900	0.0	560.0	0.009	0.015	0.029	unavailable	1.0	N/A	N/A	1.0	0.375
vertical push-off	Mattek	U	1976	18	C5	SW	NO	P	0.375	90	22.00	52.30	11700	23300	0.0	640.0	0.009	0.016	0.033	unavailable	1.0	N/A	N/A	1.0	0.375
vertical push-off	Mattek	U	1976	19	C6	SW	NO	P	0.375	90	26.39	49.60	13900	23300	0.0	740.0	0.009	0.019	unavailable	1.0	N/A	N/A	1.0	0.375	
vertical push-off	Mattek	U	1976	20	D1	SW	NO	P	0.375	90	4.40	51.80	2280	39950	0.0	370.0	0.009	0.006	0.016	unavailable	1.0	N/A	N/A	1.0	0.375
vertical push-off	Mattek	U	1976	21	D2	SW	NO	P	0.375	90	8.80	52.30	4600	39950	0.0	668.0	0.009	0.004	0.013	unavailable	1.0	N/A	N/A	1.0	0.375
vertical push-off	Mattek	U	1976	22	D3	SW	NO	P	0.375	90	13.19	52.30	6900	39950	0.0	772.0	0.009	0.007	0.020	unavailable	1.0	N/A	N/A	1.0	0.375
vertical push-off	Mattek	U	1976	23	D4	SW	NO	P	0.375	90	17.59	52.30	9200	57100	0.0	1022.0	0.009	0.006	0.015	unavailable	1.0	N/A	N/A	1.0	0.375
vertical push-off	Mattek	U	1976	24	D5	SW	NO	P	0.375	90	22.01	52.30	11510	56000	0.0	1082.0	0.009	0.010	0.020	unavailable	1.0	N/A	N/A	1.0	0.375
vertical push-off	Mattek	U	1976	25	D6	SW	NO	P	0.375	90	26.41	51.80	13860	56000	0.0	1220.0	0.010	0.011	0.018	unavailable	1.0	N/A	N/A	1.0	0.375
vertical push-off	Mattek	U	1976	26	E0	AW	NO	U	0.375	90	0.00	0.00	0.0	39600	0.0	560.0	unavailable	unavailable	N/A	1.0	N/A	N/A	1.0	0.375	
vertical push-off	Mattek	U	1976	27	E1	AW	NO	U	0.375	90	4.40	52.30	2300	41500	0.0	780.0	N/A	0.010	0.020	unavailable	1.0	N/A	N/A	1.0	0.375
vertical push-off	Mattek	U	1976	28	E2	AW	NO	U	0.375	90	8.80	52.30	4600	40300	0.0	872.0	N/A	0.009	0.011	unavailable	1.0	N/A	N/A	1.0	0.375
vertical push-off	Mattek	U	1976	29	E3	AW	NO	U	0.375	90	13.19	52.30	6900	40300	0.0	960.0	N/A	0.010	0.010	unavailable	1.0	N/A	N/A	1.0	0.375
vertical push-off	Mattek	U	1976	30	E4	AW	NO	U	0.375	90	17.59	52.30	9360	40300	0.0	1150.0	N/A	0.011	0.009	unavailable	1.0	N/A	N/A	1.0	0.375
vertical push-off	Mattek	U	1976	31	E5	AW	NO	U	0.375	90	22.00	50.90	11110	41500	0.0	1260.0	N/A	0.009	0.015	unavailable	1.0	N/A	N/A	1.0	0.375
vertical push-off	Mattek	U	1976	32	E6	AW	NO	U	0.375	90	26.41	52.30	13810	40900	0.0	1350.0	N/A	0.007	0.007	unavailable	1.0	N/A	N/A	1.0	0.375
vertical push-off	Mattek	U	1976	33	F1	AW	NO	P	0.375	90	4.40	52.30	2340	41500	0.0	450.0	0.009	0.004	0.012	unavailable	1.0	N/A	N/A	1.0	0.375
vertical push-off	Mattek	U	1976	34	F2	AW	NO	P	0.375	90	8.80	52.30	4600	40300	0.0	530.0	0.009	0.009	unavailable	1.0	N/A	N/A	1.0	0.375	
vertical push-off	Mattek	U	1976	35	F2A	AW	NO	P	0.375	90	8.80	50.90	4480	39700	0.0	620.0	0.009	0.006	0.016	unavailable	1.0	N/A	N/A	1.0	0.375
vertical push-off	Mattek	U	1976	36	F3	AW	NO	P	0.375	90	13.19	52.30	6900	40650	0.0	734.0	0.009	0.007	0.025	unavailable	1.0	N/A	N/A	1.0	0.375
vertical push-off	Mattek	U	1976	37	F3A	AW	NO	P	0.375	90	13.19	51.40	6780	39700	0.0	700.0	0.009	0.009	unavailable	1.0	N/A	N/A	1.0	0.375	
vertical push-off	Mattek	U	1976	38	F4	AW	NO	P	0.375	90	17.58	50.90	8950	40400	0.0	870.0	0.009	0.009	0.025	unavailable	1.0	N/A	N/A	1.0	0.375
vertical push-off	Mattek	U	1976	39	F5	AW	NO	P	0.375	90	22.01	51.80	11400	41500	0.0	920.0	0.009	0.013	0.030	unavailable	1.0	N/A	N/A	1.0	0.375
vertical push-off	Mattek	U	1976	40	F6	AW	NO	P	0.375	90	26.39	52.30	10400	40900	0.0	980.0	0.009	0.010	0.021	unavailable	1.0	N/A	N/A	1.0	0.375
vertical push-off	Mattek	U	1976	41	G0	AW	NO	U	0.375	90	0.00	0.00	0.0	40300	0.0	530.0	N/A	unavailable	N/A	1.0	N/A	N/A	1.0	0.500	
vertical push-off	Mattek	U	1976	42	G1	AW	NO	U	0.375	90	4.40	52.30	2300	41950	0.0	820.0	N/A	0.004	0.021	unavailable	1.0	N/A	N/A	1.0	0.500
vertical push-off	Mattek	U	1976	43	G2	AW	NO	U	0.375	90	8.79	50.90	4440	38800	0.0	846.0	N/A	0.022	0.014	unavailable	1.0	N/A	N/A	1.0	0.500
vertical push-off	Mattek	U	1976	44	G3	AW	NO	U	0.375	90	13.20	51.80	6840	41000	0.0	1060.0	N/A	0.018	0.013	unavailable	1.0	N/A	N/A	1.0	0.500
vertical push-off	Mattek	U	1976	45	G4	AW	NO	U	0.375	90	17.59	52.30	9360	44200	0.0	1190.0	N/A	0.012	0.017	unavailable	1.0	N/A	N/A	1.0	0.500
vertical push-off	Mattek	U	1976	46	G5	AW	NO	U	0.375	90	22.01	51.80	11400	40050	0.0	1140.0	N/A	0.014	0.010	unavailable	1.0	N/A	N/A	1.0	0.500
vertical push-off	Mattek	U	1976	47	G6	AW	NO	U	0.375	90	26.41	51.80	13860	40050	0.0	1190.0	N/A	0.014	0.012	unavailable	1.0	N/A	N/A	1.0	0.500
vertical push-off	Mattek	U	1976	48	H1	AW	NO	P	0.375	90	4.40	49.80	2190	41450	0.0	400.0	0.009	0.002	0.019	unavailable	1.0	N/A	N/A	1.0	0.500
vertical push-off	Mattek	U	1976	49	H2	AW	NO	P	0.375	90	8.80	51.80	4560	38800	0.0	620.0	0.009	0.007	0.019	unavailable	1.0	N/A	N/A	1.0	0.500
vertical push-off	Mattek	U	1976	50	H3	AW	NO	P	0.375	90	13.20	51.80	6840	41200	0.0	866.0									

additional info (crack opening and slip)													additional info (aggregate and rebars)													
Type of test	Author1	Author2	year	ID	orig. spec. ID	concrete type	interface type	surface preparation	strip diameter ds	bars at angle, α	ρ	fy or fu	fy	f'c	External Normal compressive stress, σ	surface strength, σ _{tr} or τ	initial residual crack width	crack width at ultimate load	slip at ultimate load	strain in steel at ultimate load	load kept constant while strain increased? Or any unusual	ultimate load reached or not	if stopped before reaching ult. load, the max slip	if stopped before reaching ult. load, the max width	bumps on rebars (yes=0, no=1)	max coarse aggregate size (feet or slow size where 5% or less retained)
									[in]	[°]		[ksi]	[ksi]	[ksi]	[psi]	[psi]	[in]	[in]	[in]	[in]	[in]	[yes=1 no=0]	[in]	[in]	[yes=0, no=1]	[in]
vertical push-off	Mattcock	Li	1976	51	H4	AW	MO	P	0.375	90	17.81	51.80	912.0	41.80	0.0	940.0	0.009	0.010	0.021	unavailable	unavailable	1.0	N/A	N/A	1.0	0.500
vertical push-off	Mattcock	Li	1976	52	H5	AW	MO	P	0.375	90	22.00	50.50	1111.0	39.50	0.0	950.0	0.009	0.021	0.025	unavailable	unavailable	1.0	N/A	N/A	1.0	0.500
vertical push-off	Mattcock	Li	1976	53	H6	AW	MO	P	0.375	90	26.41	49.80	1315.0	40.00	0.0	1040.0	0.009	0.010	0.018	unavailable	unavailable	1.0	N/A	N/A	1.0	0.500
vertical push-off	Mattcock	Li	1976	54	M0	NW	MO	U	0.375	90	0.00	0.00	0.0	39.50	0.0	950.0	0.000	N/A	unavailable	N/A	N/A	1.0	N/A	N/A	1.0	0.750
vertical push-off	Mattcock	Li	1976	55	M1	NW	MO	U	0.375	90	4.40	50.90	224.0	41.80	0.0	760.0	N/A	0.013	0.012	unavailable	unavailable	1.0	N/A	N/A	1.0	0.750
vertical push-off	Mattcock	Li	1976	56	M2	NW	MO	U	0.375	90	8.80	52.70	464.0	39.00	0.0	980.0	N/A	0.020	0.014	unavailable	unavailable	1.0	N/A	N/A	1.0	0.750
vertical push-off	Mattcock	Li	1976	57	M3	NW	MO	U	0.375	90	13.19	52.30	690.0	39.50	0.0	1100.0	N/A	0.016	0.014	unavailable	unavailable	1.0	N/A	N/A	1.0	0.750
vertical push-off	Mattcock	Li	1976	58	M4	NW	MO	U	0.375	90	17.60	50.90	886.0	41.80	0.0	1140.0	N/A	0.022	0.014	unavailable	unavailable	1.0	N/A	N/A	1.0	0.750
vertical push-off	Mattcock	Li	1976	59	M5	NW	MO	U	0.375	90	22.01	52.70	1160.0	39.50	0.0	1280.0	N/A	0.027	0.020	unavailable	unavailable	1.0	N/A	N/A	1.0	0.750
vertical push-off	Mattcock	Li	1976	60	M6	NW	MO	U	0.375	90	26.41	52.70	1392.0	41.80	0.0	1320.0	N/A	0.027	0.020	unavailable	unavailable	1.0	N/A	N/A	1.0	0.750
vertical push-off	Mattcock	Li	1976	61	N1	NW	MO	P	0.375	90	4.40	50.90	224.0	41.80	0.0	460.0	0.009	0.008	0.027	unavailable	unavailable	1.0	N/A	N/A	1.0	0.750
vertical push-off	Mattcock	Li	1976	62	N2	NW	MO	P	0.375	90	8.80	52.70	464.0	39.00	0.0	780.0	0.009	0.009	0.025	unavailable	unavailable	1.0	N/A	N/A	1.0	0.750
vertical push-off	Mattcock	Li	1976	63	N3	NW	MO	P	0.375	90	13.19	52.30	690.0	39.50	0.0	960.0	0.009	0.011	0.019	unavailable	unavailable	1.0	N/A	N/A	1.0	0.750
vertical push-off	Mattcock	Li	1976	64	N4	NW	MO	P	0.375	90	17.60	50.90	886.0	41.80	0.0	1150.0	0.009	0.011	0.020	unavailable	unavailable	1.0	N/A	N/A	1.0	0.750
vertical push-off	Mattcock	Li	1976	65	N5	NW	MO	P	0.375	90	22.00	50.90	1120.0	39.50	0.0	1175.0	0.009	0.021	0.024	unavailable	unavailable	1.0	N/A	N/A	1.0	0.750
vertical push-off	Mattcock	Li	1976	66	N6	NW	MO	P	0.375	90	26.40	50.00	1320.0	41.80	0.0	1190.0	0.009	0.019	0.026	unavailable	unavailable	1.0	N/A	N/A	1.0	0.750
vertical push-off	Sneed	Krc	2016	67	H-MO-U-13-1	NW	MO	U	0.375	90	13.00	72.20	938.6	48.80	0.0	1380.0	N/A	0.047	0.057	2721.000	no	1.0	N/A	N/A	1.0	0.750
vertical push-off	Sneed	Krc	2016	68	H-MO-U-13-2	NW	MO	U	0.375	90	13.00	72.20	938.6	48.80	0.0	1257.0	N/A	0.024	0.027	2268.000	yes	1.0	N/A	N/A	1.0	0.750
vertical push-off	Sneed	Krc	2016	69	H-MO-P-13-1	NW	MO	P	0.375	90	13.00	72.20	938.6	48.80	0.0	1294.0	unavailable	0.011	0.020	unavailable	unavailable	1.0	N/A	N/A	1.0	0.750
vertical push-off	Sneed	Krc	2016	70	H-MO-P-13-2	NW	MO	P	0.375	90	13.00	72.20	938.6	48.80	0.0	1151.0	unavailable	0.021	0.044	4239.000	no	1.0	N/A	N/A	1.0	0.750
vertical push-off	Sneed	Krc	2016	71	S-MO-U-13-1	SLW	MO	U	0.375	90	13.00	72.20	938.6	47.00	0.0	1170.0	N/A	0.011	0.018	2022.000	no	1.0	N/A	N/A	1.0	0.750
vertical push-off	Sneed	Krc	2016	72	S-MO-U-13-2	SLW	MO	U	0.375	90	13.00	72.20	938.6	47.00	0.0	1143.0	N/A	0.024	0.031	2809.000	no	1.0	N/A	N/A	1.0	0.750
vertical push-off	Sneed	Krc	2016	73	S-MO-P-13-1	SLW	MO	P	0.375	90	13.00	72.20	938.6	47.00	0.0	1022.0	unavailable	0.008	0.014	1659.000	no	1.0	N/A	N/A	1.0	0.750
vertical push-off	Sneed	Krc	2016	74	S-MO-P-13-2	SLW	MO	P	0.375	90	13.00	72.20	938.6	47.00	0.0	1046.0	unavailable	0.019	0.043	3000.000	yes	1.0	N/A	N/A	1.0	0.750
vertical push-off	Sneed	Krc	2016	75	A5H-MO-U-13-1	AW	MO	U	0.375	90	13.00	72.20	938.6	47.00	0.0	1051.0	N/A	0.009	0.017	1483.000	no	1.0	N/A	N/A	1.0	0.750
vertical push-off	Sneed	Krc	2016	76	A5H-MO-U-13-2	AW	MO	U	0.375	90	13.00	72.20	938.6	47.00	0.0	1052.0	N/A	0.022	0.059	2616.000	no	1.0	N/A	N/A	1.0	0.750
vertical push-off	Sneed	Krc	2016	77	A5H-MO-P-13-1	AW	MO	P	0.375	90	13.00	72.20	938.6	47.00	0.0	932.0	N/A	0.009	0.037	unavailable	unavailable	1.0	N/A	N/A	1.0	0.750
vertical push-off	Sneed	Krc	2016	78	A5H-MO-P-13-2	AW	MO	P	0.375	90	13.00	72.20	938.6	47.00	0.0	1064.0	N/A	0.013	0.048	3855.000	yes	1.0	N/A	N/A	1.0	0.750
vertical push-off	Sneed	Krc	2016	79	S-C-R-R-9-1	SLW	C	R	0.375	90	9.00	72.20	649.8	53.80	0.0	1000.0	N/A	0.007	0.008	2048.000	no	1.0	N/A	N/A	1.0	0.750
vertical push-off	Sneed	Krc	2016	80	S-C-R-R-9-2	SLW	C	R	0.375	90	9.00	72.20	649.8	53.80	0.0	1000.0	N/A	0.005	0.007	1856.000	no	1.0	N/A	N/A	1.0	0.750
vertical push-off	Sneed	Krc	2016	81	S5L-C-5-9-1	SLW	C	S	0.375	90	9.00	72.20	649.8	53.80	0.0	940.0	N/A	0.008	0.021	2816.000	no	1.0	N/A	N/A	1.0	0.750
vertical push-off	Sneed	Krc	2016	82	S5L-C-5-9-2	SLW	C	S	0.375	90	9.00	72.20	649.8	53.80	0.0	960.0	N/A	0.006	0.013	2448.000	no	1.0	N/A	N/A	1.0	0.750
vertical push-off	Sneed	Krc	2016	83	S5L-C-R-13-1	SLW	C	R	0.375	90	13.00	72.20	938.6	57.00	0.0	1776.0	N/A	0.009	0.013	1776.000	no	1.0	N/A	N/A	1.0	0.750
vertical push-off	Sneed	Krc	2016	84	S5L-C-R-13-2	SLW	C	R	0.375	90	13.00	72.20	938.6	57.00	0.0	1199.0	N/A	0.009	0.012	1439.000	no	1.0	N/A	N/A	1.0	0.750
vertical push-off	Sneed	Krc	2016	85	S5L-C-5-13-1	SLW	C	S	0.375	90	13.00	72.20	938.6	57.00	0.0	796.0	N/A	0.007	0.017	1638.000	no	1.0	N/A	N/A	1.0	0.750
vertical push-off	Sneed	Krc	2016	86	S5L-C-5-13-2	SLW	C	S	0.375	90	13.00	72.20	938.6	57.00	0.0	965.0	N/A	0.008	0.015	2523.000	yes	1.0	N/A	N/A	1.0	0.750
vertical push-off	Sneed	Krc	2016	87	S5L-C-R-17-1	SLW	C	R	0.375	90	17.00	72.20	1227.4	49.50	0.0	1260.0	N/A	0.008	0.012	997.000	no	1.0	N/A	N/A	1.0	0.750
vertical push-off	Sneed	Krc	2016	88	S5L-C-R-17-2	SLW	C	R	0.375	90	17.00	72.20	1227.4	49.50	0.0	1300.0	N/A	0.007	0.009	1303.000	no	1.0	N/A	N/A	1.0	0.750
vertical push-off	Sneed	Krc	2016	89	S5L-C-5-17-1	SLW	C	S	0.375	90	17.00	72.20	1227.4	49.50	0.0	960.0	N/A	0.008	0.018	note	note	1.0	N/A	N/A	1.0	0.750
vertical push-off	Sneed	Krc	2016	90	S5L-C-5-17-2	SLW	C	S	0.375	90	17.00	72.20	1227.4	49.50	0.0	950.0	N/A	0.006	0.015	note	note	1.0	N/A	N/A	1.0	0.750
vertical push-off	Sneed	Krc	2016	91	S5L-C-R-22-1	SLW	C	R	0.375	90	22.00	72.20	1588.4	50.00	0.0	1300.0	N/A	0.006	0.007	unavailable	unavailable	1.0	N/A	N/A	1.0	0.750
vertical push-off	Sneed	Krc	2016	92	S5L-C-R-22-2	SLW	C	R	0.375	90	22.00	72.20	1588.4	50.00	0.0	1160.0	N/A	0.007	0.004	1249.000	no	1.0	N/A	N/A	1.0	0.750
vertical push-off	Sneed	Krc	2016	93	S5L-C-5-22-1	SLW	C	S	0.375	90	22.00	72.20	1588.4	50.00	0.0	1000.0	N/A	0.006	0.012	2180.000	no	1.0	N/A	N/A	1.0	0.750
vertical push-off	Sneed	Krc	2016	94	S5L-C-5-22-2	SLW	C	S	0.375	90	22.00	72.20	1588.4	50.00	0.0	1140.0	N/A	0.006	0.011	1662.000	no	1.0	N/A	N/A	1.0	0.750
vertical push-off	Sneed	Krc	2016	95	S5L-C-R-9-1	SLW	C	R	0.375	90	9.00	72.20	649.8	47.00	0.0	750.0	N/A	0.006	0.011	1652.000	no	1.0	N/A	N/A	1.0	0.750
vertical push-off	Sneed	Krc	2016	96	S5L-C-R-9-2	SLW	C	R	0.375	90	9.00	72.20	649.8	47.00	0.0	870.0	N/A	0.005	0.009	1652.000	no	1.0	N/A	N/A	1.0	0.750
vertical push-off	Sneed	Krc	2016	97	S5L-C-5-9-1	SLW	C	S	0.375	90	9.00	72.20	649.8	47.00	0.0	650.0	N/A	0.006	0.013	2326.000	no	1.0	N/A	N/A	1.0	0.750
vertical push-off	Sneed	Krc	2016	98	S5L-C-5-9-2	SLW	C	S	0.375	90	9.00	72.20	649.8	47.00	0.0	770.0	N/A	0.005	0.009	1813.000	no	1.0	N/A	N/A	1.0	0.750
vertical push-off	Sneed	Krc	2016	99	S5L-C-R-13-1	SLW	C	R	0.375	90	13.00	72.20	938.6	46.40	0.0	1026.0	N/A	0.006	0.006	1548.000	no	1.0	N/A	N/A	1.0	0.750
vertical push-off	Sneed	Krc	2016	100	S5L-C-R-13-2	SLW	C	R	0.375	90	13.00	72.20	938.6	46.40	0.0	947.0	N/A	0.005	0.014	339.000	no	1.0	N/A	N/A	1.0	0.750

additional info (crack opening and slip)														additional info (aggregate and rebars)														
Type of test	Author1	Author2	Year	ID	orig. spec. ID	concrete type	interface type	surface preparation	strip diameter	bars at angle, α	ρ	f _y or f _u	ρ _{fy}	f _c	Ext. Normal compression stress, σ	Surface strength, σ _r or τ	initial residual crack width	crack width at ultimate load	slip at ultimate load	strain in steel at ultimate load	load kept constant while strain increased? Or any annual	ultimate load reached or not	if stopped before reaching ult. load, the max slip	if stopped before reaching ult. load, the max width	bumps on rebars	max coarse aggregate size (feet or slow size where 5% or less retained)		
									in	°	[10 ⁻³]	ksi	ksi	ksi	ksi	psi	in	in	in	in	in	in	in	in	in	in	in	
vertical push-off	Sneed	Krc	2016	101	5-CI-C5-13-1	SW	C	S	0.375	90	13.00	72.20	988.6	4640.0	0.0	828.0	N/A	0.006	0.04	0.04	1548000	no	1.0	N/A	N/A	N/A	1.0	0.375
vertical push-off	Sneed	Krc	2016	102	5-CI-C5-13-2	SW	C	S	0.375	90	13.00	72.20	988.6	4640.0	0.0	870.0	N/A	0.008	0.07	0.07	1484000	no	1.0	N/A	N/A	N/A	1.0	0.375
vertical push-off	Sneed	Krc	2016	103	5-CI-C5-17-1	SW	C	S	0.375	90	17.00	72.20	1277.4	4550.0	0.0	817.0	N/A	0.005	0.03	0.03	1747000	no	1.0	N/A	N/A	N/A	1.0	0.375
vertical push-off	Sneed	Krc	2016	104	5-CI-C5-17-2	SW	C	S	0.375	90	17.00	72.20	1277.4	4550.0	0.0	990.0	N/A	0.006	0.02	0.02	1747000	no	1.0	N/A	N/A	N/A	1.0	0.375
vertical push-off	Sneed	Krc	2016	105	A-S-C-R-13-1	AW	C	R	0.375	90	13.00	72.20	988.6	4380.0	0.0	940.0	N/A	0.006	0.04	0.04	1435000	no	1.0	N/A	N/A	N/A	1.0	0.375
vertical push-off	Sneed	Krc	2016	106	A-S-C-R-13-2	AW	C	R	0.375	90	13.00	72.20	988.6	4380.0	0.0	948.0	N/A	0.004	0.005	0.005	1193000	no	1.0	N/A	N/A	N/A	1.0	0.375
vertical push-off	Sneed	Krc	2016	107	A-S-C-S-13-1	AW	C	S	0.375	90	13.00	72.20	988.6	4380.0	0.0	764.0	N/A	0.006	0.020	0.020	2148000	yes	1.0	N/A	N/A	N/A	1.0	0.375
vertical push-off	Sneed	Krc	2016	108	A-S-C-S-13-2	AW	C	S	0.375	90	13.00	72.20	988.6	4380.0	0.0	782.0	N/A	0.007	0.020	0.020	1470000	no	1.0	N/A	N/A	N/A	1.0	0.375
vertical push-off	Sneed	Krc	2016	109	A-CI-CR-13-1	AW	C	R	0.375	90	13.00	72.20	988.6	4460.0	0.0	865.0	N/A	note	note	note	2940000	no	1.0	N/A	N/A	N/A	1.0	0.375
vertical push-off	Sneed	Krc	2016	110	A-CI-CR-13-2	AW	C	R	0.375	90	13.00	72.20	988.6	4460.0	0.0	880.0	N/A	0.006	0.02	0.02	1075000	no	1.0	N/A	N/A	N/A	1.0	0.375
vertical push-off	Sneed	Krc	2016	111	A-CI-C5-13-1	AW	C	S	0.375	90	13.00	72.20	988.6	4460.0	0.0	747.0	N/A	0.005	0.009	0.009	878000	no	1.0	N/A	N/A	N/A	1.0	0.375
vertical push-off	Sneed	Krc	2016	112	A-CI-C5-13-2	AW	C	S	0.375	90	13.00	72.20	988.6	4460.0	0.0	754.0	N/A	0.005	0.016	0.016	394000	note	1.0	N/A	N/A	N/A	1.0	0.375
vertical push-off	Mattcock	Johal	1975	113	ETC	NW	MO	P	0.375	90	10.48	51.80	543.0	3850.0	0.0	881.0	0.010	0.237	0.032	unavailable	unavailable	1.0	N/A	N/A	N/A	1.0	0.750	
vertical push-off	Mattcock	Johal	1975	114	ETC	NW	MO	P	0.375	90	10.48	51.80	546.0	4230.0	-10.0	929.0	0.010	0.244	0.032	unavailable	unavailable	1.0	N/A	N/A	N/A	1.0	0.750	
vertical push-off	Mattcock	Johal	1975	115	ETC	NW	MO	P	0.375	90	10.47	52.70	582.0	3960.0	-13.0	714.0	0.010	0.231	0.017	unavailable	unavailable	1.0	N/A	N/A	N/A	1.0	0.750	
vertical push-off	Mattcock	Johal	1975	116	FAC	NW	MO	P	0.375	90	10.48	50.50	529.0	3820.0	-20.0	673.0	0.010	0.406	0.016	unavailable	unavailable	1.0	N/A	N/A	N/A	1.0	0.750	
vertical push-off	Mattcock	Johal	1975	117	FSC	NW	MO	P	0.375	90	10.48	53.30	548.0	4020.0	-30.0	572.0	0.010	0.409	0.038	unavailable	unavailable	1.0	N/A	N/A	N/A	1.0	0.750	
vertical push-off	Mattcock	Johal	1975	118	ETC	NW	MO	P	0.375	90	10.47	50.90	533.0	3965.0	-40.0	396.0	0.010	0.095	0.025	unavailable	unavailable	1.0	N/A	N/A	N/A	1.0	0.750	
vertical push-off	Mattcock	Johal	1975	119	ETU	NW	MO	U	0.375	90	10.47	52.70	582.0	4060.0	0.0	1089.0	0.010	0.220	0.019	unavailable	unavailable	1.0	N/A	N/A	N/A	1.0	0.750	
vertical push-off	Mattcock	Johal	1975	120	EAU	NW	MO	U	0.375	90	10.47	49.10	534.0	3860.0	-20.0	946.0	0.010	0.250	0.009	unavailable	unavailable	1.0	N/A	N/A	N/A	1.0	0.750	
vertical push-off	Mattcock	Johal	1975	121	ESU	NW	MO	U	0.375	90	10.47	50.80	532.0	4120.0	-40.0	607.0	0.010	0.166	0.004	unavailable	unavailable	1.0	N/A	N/A	N/A	1.0	0.750	
vertical push-off	Mattcock	Johal	1975	122	FAC	NW	MO	P	0.375	90	15.71	50.10	787.0	4270.0	0.0	988.0	0.010	0.216	0.017	unavailable	unavailable	1.0	N/A	N/A	N/A	1.0	0.750	
vertical push-off	Mattcock	Johal	1975	123	RFC	NW	MO	P	0.375	90	15.71	51.30	806.0	3890.0	-20.0	839.0	0.010	0.226	0.017	unavailable	unavailable	1.0	N/A	N/A	N/A	1.0	0.750	
vertical push-off	Mattcock	Johal	1975	124	FIU	NW	MO	U	0.375	90	15.71	51.70	822.0	4150.0	-40.0	804.0	0.010	0.221	0.009	unavailable	unavailable	1.0	N/A	N/A	N/A	1.0	0.750	
vertical push-off	Mattcock	Johal	1975	125	FUI	NW	MO	U	0.375	90	15.71	52.20	820.0	4035.0	0.0	1369.0	0.010	0.010	0.010	unavailable	unavailable	1.0	N/A	N/A	N/A	1.0	0.750	
vertical push-off	Mattcock	Johal	1975	126	F4U	NW	MO	U	0.375	90	15.71	53.20	886.0	4735.0	-30.0	1143.0	0.010	0.010	0.010	unavailable	unavailable	1.0	N/A	N/A	N/A	1.0	0.750	
vertical push-off	Mattcock	Johal	1975	127	F6U	NW	MO	U	0.375	90	15.71	51.00	801.0	4245.0	-40.0	1065.0	0.010	0.008	0.025	unavailable	unavailable	1.0	N/A	N/A	N/A	1.0	1.000	
vertical push-off	Miller	Harris	2011	128	P615-3-A	NW	C	R	0.375	90	4.11	67.30	276.9	5800.0	0.0	700.0	N/A	0.008	0.025	0.028	238000	no	1.0	N/A	N/A	1.0	1.000	
vertical push-off	Miller	Harris	2011	129	P615-3-B	NW	C	R	0.375	90	4.04	67.30	272.2	5800.0	0.0	690.0	N/A	0.007	0.027	0.027	465000	no	1.0	N/A	N/A	1.0	1.000	
vertical push-off	Miller	Harris	2011	130	P615-4-A	NW	C	R	0.300	90	7.27	61.50	447.3	3800.0	0.0	690.0	N/A	0.009	0.037	0.037	515000	no	1.0	N/A	N/A	1.0	1.000	
vertical push-off	Miller	Harris	2011	131	P615-4-B	NW	C	R	0.300	90	7.38	61.50	454.2	3800.0	0.0	790.0	N/A	0.008	0.038	0.038	410000	no	1.0	N/A	N/A	1.0	1.000	
vertical push-off	Miller	Harris	2011	132	P1035-3-A	NW	C	R	0.375	90	4.19	126.00	544.8	5800.0	0.0	570.0	N/A	0.007	0.027	0.027	222000	yes	1.0	N/A	N/A	1.0	1.000	
vertical push-off	Miller	Harris	2011	133	P1035-3-B	NW	C	R	0.375	90	4.19	126.00	517.5	5800.0	0.0	650.0	N/A	0.008	0.031	0.031	527000	yes	1.0	N/A	N/A	1.0	1.000	
vertical push-off	Miller	Harris	2011	134	P1035-4-A	NW	C	R	0.300	90	7.38	140.00	1033.8	5800.0	0.0	840.0	N/A	0.008	0.032	0.032	529000	yes	1.0	N/A	N/A	1.0	1.000	
vertical push-off	Miller	Harris	2011	135	P1035-4-B	NW	C	R	0.300	90	7.47	131.30	986.5	5800.0	0.0	710.0	N/A	0.010	0.041	0.041	579000	yes	1.0	N/A	N/A	1.0	1.000	
vertical push-off	Grane	N/A	2000	136	UH-F-0-A	NW	C	R	0.375	90	0.00	0.00	0.0	12000.0	0.0	526.4	N/A	unavailable	0.02	N/A	no	N/A	N/A	N/A	N/A	1.0	0.750	
vertical push-off	Grane	N/A	2000	137	UH-F-0-B	NW	C	R	0.375	90	0.00	0.00	0.0	12000.0	0.0	535.6	N/A	unavailable	0.03	N/A	N/A	N/A	N/A	N/A	N/A	1.0	0.750	
vertical push-off	Grane	N/A	2000	138	UH-F-2-A	NW	C	R	0.375	90	5.00	73.50	367.5	12000.0	0.0	1011.5	N/A	unavailable	0.05	unavailable	unavailable	1.0	N/A	N/A	N/A	1.0	0.750	
vertical push-off	Grane	N/A	2000	139	UH-F-2-B	NW	C	R	0.375	90	5.00	73.50	367.5	12000.0	0.0	1344.8	N/A	unavailable	0.016	unavailable	unavailable	1.0	N/A	N/A	N/A	1.0	0.750	
vertical push-off	Grane	N/A	2000	140	UH-F-2-C	NW	C	R	0.375	90	5.00	73.50	367.5	12000.0	0.0	954.0	N/A	unavailable	0.016	unavailable	unavailable	1.0	N/A	N/A	N/A	1.0	0.750	
vertical push-off	Grane	N/A	2000	141	UH-S-0-A	NW	C	S	0.375	90	0.00	0.00	0.0	12000.0	0.0	32.3	N/A	unavailable	0.005	N/A	no	N/A	N/A	N/A	N/A	1.0	0.750	
vertical push-off	Grane	N/A	2000	142	UH-S-0-B	NW	C	S	0.375	90	0.00	0.00	0.0	12000.0	0.0	30.5	N/A	unavailable	0.001	N/A	no	N/A	N/A	N/A	N/A	1.0	0.750	
vertical push-off	Grane	N/A	2000	143	UH-S-0-C	NW	C	S	0.375	90	0.00	0.00	0.0	12000.0	0.0	46.6	N/A	unavailable	0.001	N/A	no	N/A	N/A	N/A	N/A	1.0	0.750	
vertical push-off	Grane	N/A	2000	144	UH-S-1-A	NW	C	S	0.375	90	3.50	73.50	183.8	12200.0	0.0	68.8	N/A	unavailable	0.025	unavailable	unavailable	1.0	N/A	N/A	N/A	1.0	0.750	
vertical push-off	Grane	N/A	2000	145	UH-S-1-B	NW	C	S	0.375	90	2.50	73.50	183.8	12200.0	0.0	75.3	N/A	unavailable	0.025	unavailable	note	1.0	N/A	N/A	N/A	1.0	0.750	
vertical push-off	Grane	N/A	2000	146	UH-S-1-C	NW	C	S	0.375	90	2.50	73.50	183.8	12200.0	0.0	69.6	N/A	unavailable	0.025	unavailable	note	1.0	N/A	N/A	N/A	1.0	0.750	
vertical push-off	Grane	N/A	2000	147	UH-S-2-A	NW	C	S	0.375	90	5.00	73.50	367.5	12200.0	0.0	126.7	N/A	unavailable	0.014	unavailable	unavailable	1.0	N/A	N/A	N/A	1.0	0.750	
vertical push-off	Grane	N/A	2000	148	UH-S-2-B	NW	C	S	0.375	90	5.00	73.50	367.5	12200.0	0.0	104.2	N/A	unavailable	0.011	unavailable	unavailable	1.0	N/A	N/A	N/A	1.0	0.750	
vertical push-off	Grane	N/A	2000	149	UH-S-2-C	NW	C	S	0.375	90	5.00	73.50	367.5	12200.0	0.0	107.1	N/A	unavailable	0.173	unavailable	unavailable	1.0	N/A	N/A	N/A	1.0	0.750	
vertical push-off	Grane	N/A	2000	150	UH-S-3-A	NW	C	S	0.375	90	7.50	73.50	581.3	12200.0	0.0	144.8	N/A	unavailable	0.046	unavailable	note	1.0	N/A	N/A	N/A	1.0	0.750	

Type of test	Author1	Author2	year	ID	orig. spec. ID	concrete type	interface type	surface preparation	strip diameter ds	bars at angle α	p	fy or fu	dly	fc'	External Normal compression stress, σ	surface strength, σc or τ	initial residual crack width	crack width at ultimate load	slip at ultimate load	strain in steel at ultimate load	load kept constant while strain increased or any unusual	ultimate load reached or not	if stopped before reaching ult. load, the max slip	if stopped before reaching ult. load, the max slip	additional info (aggregate and rebars)					
																									max coarse aggregate size (mm) or size (inches) where 5% or less retained	if formed, no reinforcement				
vertical push-off	Grane	N/A	2000	151	UH-S3-B	NW	Cj	S	0.375	90.0	7.50	79.50	551.3	12200.0	0.0	109.7	N/A	unavailable	0.026	unavailable	note	1.0	N/A	N/A	1.0	0.750				
vertical push-off	Grane	N/A	2000	152	UH-S3-C	NW	Cj	R	0.375	90.0	7.50	79.50	551.3	12200.0	0.0	157.2	N/A	unavailable	0.023	unavailable	unavailable	1.0	N/A	N/A	1.0	0.750				
vertical push-off	Grane	N/A	2000	153	UH-S3-A	NW	Cj	S	0.375	90.0	0.00	0.00	0.00	0.00	379.3	N/A	unavailable	0.002	N/A	N/A	1.0	N/A	N/A	1.0	0.750					
vertical push-off	Grane	N/A	2000	154	UH-S3-B	NW	Cj	R	0.375	90.0	0.00	0.00	0.00	0.00	310.3	N/A	unavailable	0.001	N/A	N/A	1.0	N/A	N/A	1.0	0.750					
vertical push-off	Grane	N/A	2000	155	UH-S3-C	NW	Cj	R	0.375	90.0	0.00	0.00	0.00	0.00	413.8	N/A	unavailable	0.002	N/A	N/A	1.0	N/A	N/A	1.0	0.750					
vertical push-off	Mansur	Vinayagam	2008	156	AN-2	NW	MO	P	0.394	90.0	8.89	76.87	683.1	8380.5	0.0	1186.4	0.004	0.024	0.001	unavailable	unavailable	1.0	N/A	N/A	0.0	0.787				
vertical push-off	Mansur	Vinayagam	2008	157	AN-4	NW	MO	P	0.394	90.0	17.77	76.87	1366.3	8380.5	0.0	1475.0	0.006	0.000	0.125	unavailable	unavailable	1.0	N/A	N/A	0.0	0.787				
vertical push-off	Mansur	Vinayagam	2008	158	AN-6	NW	MO	P	0.394	90.0	26.66	76.87	2049.4	8380.5	0.0	1873.9	0.004	0.009	0.197	unavailable	unavailable	1.0	N/A	N/A	0.0	0.787				
vertical push-off	Mansur	Vinayagam	2008	159	AN-2	NW	MO	P	0.394	90.0	8.89	76.87	683.1	10070.6	0.0	1067.8	0.011	0.019	0.066	unavailable	unavailable	1.0	N/A	N/A	0.0	0.787				
vertical push-off	Mansur	Vinayagam	2008	160	AN-3	NW	MO	P	0.394	90.0	13.34	76.87	1025.4	10070.6	0.0	1667.9	0.003	0.046	0.105	unavailable	unavailable	1.0	N/A	N/A	0.0	0.787				
vertical push-off	Mansur	Vinayagam	2008	161	AN-4	NW	MO	P	0.394	90.0	17.77	76.87	1366.3	10070.6	0.0	2049.9	0.008	0.057	0.138	unavailable	unavailable	1.0	N/A	N/A	0.0	0.787				
vertical push-off	Mansur	Vinayagam	2008	162	AN-2	NW	MO	P	0.394	90.0	8.89	76.87	683.1	12618.3	0.0	1128.4	0.007	0.044	0.057	unavailable	unavailable	1.0	N/A	N/A	0.0	0.787				
vertical push-off	Mansur	Vinayagam	2008	163	AN-3	NW	MO	P	0.394	90.0	13.34	76.87	1025.4	12618.3	0.0	1792.7	0.013	0.049	0.094	unavailable	unavailable	1.0	N/A	N/A	0.0	0.787				
vertical push-off	Mansur	Vinayagam	2008	164	AN-4	NW	MO	P	0.394	90.0	17.77	76.87	1366.3	12618.3	0.0	2052.2	0.005	0.056	0.112	unavailable	unavailable	1.0	N/A	N/A	0.0	0.787				
vertical push-off	Mansur	Vinayagam	2008	165	B1-4	NW	MO	P	0.315	90.0	8.90	43.51	387.3	10616.8	0.0	976.1	0.009	0.088	0.329	unavailable	unavailable	1.0	N/A	N/A	0.0	0.787				
vertical push-off	Mansur	Vinayagam	2008	166	B2-2	NW	MO	P	0.315	90.0	4.47	43.51	194.4	12313.7	0.0	748.0	0.009	0.075	0.273	unavailable	unavailable	1.0	N/A	N/A	0.0	0.787				
vertical push-off	Mansur	Vinayagam	2008	167	B2-4	NW	MO	P	0.315	90.0	8.90	43.51	387.3	12313.7	0.0	1061.7	0.007	0.102	0.325	unavailable	unavailable	1.0	N/A	N/A	0.0	0.787				
vertical push-off	Mansur	Vinayagam	2008	168	B2-5	NW	MO	P	0.315	90.0	11.20	43.51	487.3	12313.7	0.0	1199.8	0.005	0.133	0.402	unavailable	unavailable	1.0	N/A	N/A	0.0	0.787				
vertical push-off	Mansur	Vinayagam	2008	169	B2-6	NW	MO	P	0.315	90.0	13.40	43.51	583.1	12313.7	0.0	1330.0	0.005	0.149	0.438	unavailable	unavailable	1.0	N/A	N/A	0.0	0.787				
vertical push-off	Mansur	Vinayagam	2008	170	B3-4	NW	MO	P	0.315	90.0	8.90	43.51	387.3	13807.6	0.0	1159.0	0.005	0.141	0.366	unavailable	unavailable	1.0	N/A	N/A	0.0	0.787				
vertical push-off	Mansur	Vinayagam	2008	171	B4-2	NW	MO	P	0.315	90.0	4.47	43.51	194.4	15432.0	0.0	871.7	0.007	0.133	0.355	unavailable	unavailable	1.0	N/A	N/A	0.0	0.787				
vertical push-off	Mansur	Vinayagam	2008	172	B4-4	NW	MO	P	0.315	90.0	8.90	43.51	387.3	15432.0	0.0	1222.7	0.005	0.144	0.341	unavailable	unavailable	1.0	N/A	N/A	0.0	0.787				
vertical push-off	Mansur	Vinayagam	2008	173	B4-5	NW	MO	P	0.315	90.0	11.20	43.51	487.3	15432.0	0.0	1340.2	0.005	0.188	0.450	unavailable	unavailable	1.0	N/A	N/A	0.0	0.787				
vertical push-off	Mansur	Vinayagam	2008	174	B4-6	NW	MO	P	0.315	90.0	13.40	43.51	583.1	15432.0	0.0	1444.6	0.004	0.218	0.500	unavailable	unavailable	1.0	N/A	N/A	0.0	0.787				
vertical push-off	Mattcock	Hawkins	1972	175	7.100	NW	MO	U	0.375	90.0	7.76	49.50	384.0	4850.0	0.0	851.0	N/A	unavailable	unavailable	unavailable	1.0	N/A	N/A	1.0	note					
Vertical push-off	Mattcock	Hawkins	1972	176	7.200	NW	MO	U	0.375	90.0	11.64	49.50	576.0	5120.0	0.0	906.0	N/A	unavailable	unavailable	unavailable	1.0	N/A	N/A	1.0	note					
Vertical push-off	Mattcock	Hawkins	1972	177	7.300	NW	MO	U	0.375	90.0	15.52	49.50	768.0	5950.0	0.0	974.0	N/A	unavailable	unavailable	unavailable	1.0	N/A	N/A	1.0	note					
Vertical push-off	Mattcock	Hawkins	1972	178	8.100	NW	MO	P	0.375	90.0	7.76	49.50	384.0	4850.0	0.0	897.0	unavailable	unavailable	unavailable	unavailable	1.0	N/A	N/A	1.0	note					
Vertical push-off	Mattcock	Hawkins	1972	179	8.200	NW	MO	P	0.375	90.0	11.64	49.50	576.0	5120.0	0.0	888.0	unavailable	unavailable	unavailable	unavailable	1.0	N/A	N/A	1.0	note					
Vertical push-off	Mattcock	Hawkins	1972	180	8.300	NW	MO	P	0.375	90.0	15.52	49.50	768.0	5950.0	0.0	925.0	unavailable	unavailable	unavailable	unavailable	1.0	N/A	N/A	1.0	note					
Vertical push-off	Mattcock	Hawkins	1972	181	9.100	NW	MO	U	0.375	90.0	15.27	52.40	800.0	5500.0	2460.0	2460.0	N/A	unavailable	unavailable	unavailable	unavailable	1.0	N/A	N/A	1.0	note				
Vertical push-off	Mattcock	Hawkins	1972	182	9.200	NW	MO	U	0.375	90.0	18.31	52.20	956.0	5500.0	1480.0	2560.0	N/A	unavailable	unavailable	unavailable	unavailable	1.0	N/A	N/A	1.0	note				
Vertical push-off	Mattcock	Hawkins	1972	183	9.300	NW	MO	U	0.375	90.0	18.66	52.30	976.0	3940.0	406.0	1515.0	N/A	unavailable	unavailable	unavailable	unavailable	1.0	N/A	N/A	1.0	note				
Vertical push-off	Mattcock	Hawkins	1972	184	9.400	NW	MO	U	0.375	90.0	18.34	52.70	985.0	3940.0	0.0	1389.0	N/A	unavailable	unavailable	unavailable	unavailable	1.0	N/A	N/A	1.0	note				
Vertical push-off	Mattcock	Hawkins	1972	185	9.500	NW	MO	U	0.375	90.0	12.72	51.00	621.0	6440.0	1655.0	2370.0	N/A	unavailable	unavailable	unavailable	unavailable	1.0	N/A	N/A	1.0	note				
Vertical push-off	Mattcock	Hawkins	1972	186	9.600	NW	MO	U	0.375	90.0	6.13	51.00	312.0	6440.0	1655.0	2720.0	N/A	unavailable	unavailable	unavailable	unavailable	1.0	N/A	N/A	1.0	note				
Vertical push-off	Mattcock	Hawkins	1972	187	10.500	NW	MO	P	0.375	90.0	15.28	52.70	805.0	4830.0	2265.0	2465.0	unavailable	unavailable	unavailable	unavailable	unavailable	1.0	N/A	N/A	1.0	note				
Vertical push-off	Mattcock	Hawkins	1972	188	10.600	NW	MO	P	0.375	90.0	18.35	52.00	954.0	4830.0	1250.0	2165.0	unavailable	unavailable	unavailable	unavailable	unavailable	1.0	N/A	N/A	1.0	note				
Vertical push-off	Mattcock	Hawkins	1972	189	10.700	NW	MO	P	0.375	90.0	18.36	52.40	962.0	4070.0	387.0	1445.0	unavailable	unavailable	unavailable	unavailable	unavailable	1.0	N/A	N/A	1.0	note				
Vertical push-off	Mattcock	Hawkins	1972	190	10.800	NW	MO	P	0.375	90.0	18.34	53.70	985.0	4020.0	0.0	1115.0	unavailable	unavailable	unavailable	unavailable	unavailable	1.0	N/A	N/A	1.0	note				
Vertical push-off	Mattcock	Hawkins	1972	191	10.900	NW	MO	P	0.375	90.0	12.72	51.00	621.0	3800.0	1490.0	2590.0	unavailable	unavailable	unavailable	unavailable	unavailable	1.0	N/A	N/A	1.0	note				
Vertical push-off	Mattcock	Hawkins	1972	192	10.100	NW	MO	P	0.375	90.0	6.10	51.00	312.0	3800.0	813.0	1410.0	unavailable	unavailable	unavailable	unavailable	unavailable	1.0	N/A	N/A	1.0	note				
Vertical push-off	Mattcock	Hawkins	1972	193	11.000	NW	MO	P	0.375	90.0	6.40	69.91	321.6	13445.0	0.0	748.4	0.012	0.012	0.012	unavailable	unavailable	unavailable	1.0	N/A	N/A	1.0	note			
Vertical push-off	Nagle	Kuchma	2007	194	631.2.13.25	NW	MO	P	0.512	90.0	2.29	69.91	180.8	13445.0	0.0	395.7	0.008	0.008	0.008	unavailable	unavailable	unavailable	unavailable	unavailable	unavailable	unavailable	unavailable	unavailable	unavailable	unavailable
Vertical push-off	Nagle	Kuchma	2007	195	631.2.13.25	NW	MO	P	0.512	90.0	2.29	69.91	180.8	13445.0	0.0	704.9	0.005	0.005	0.005	unavailable	unavailable	unavailable	unavailable	unavailable	unavailable	unavailable	unavailable	unavailable	unavailable	unavailable
Vertical push-off	Nagle	Kuchma	2007	196	631.2.13.25																									

Type of test		Author1	Author2	year	ID	orig. spec. ID	concrete type	interface type	surface preparation	strip diameter	bars at angle, α	ρ	fy or fu	f_c	External Normal compressive stress, σ	surface strength, σ_{cr} or τ	initial residual crack width	crack width at ultimate load	slip at ultimate load	strain in steel at ultimate load	load kept constant while strain increased? Or any unusual	ultimate load reached or not	if stopped before reaching ult. load, the max slip	if stopped before reaching ult. load, the max width	bumps on rebars	max coarse aggregate size (feet or slow size where 5% or less retained)							
vertical push-off	push-off with bars crossing the interface at an angle	Nagle	Kuchma	2007	201	631-4-13-25	NW	MO	P	0.532	90	4.60	67.73	311.6	16592.3	0.0	765.8	0.006	unavailable	unavailable	unavailable	unavailable	unavailable	unavailable	unavailable	unavailable	unavailable	unavailable	unavailable				
		Sneed	Kuchma	2007	202	631h-4-13-35	NW	MO	P	0.512	90	6.30	67.73	426.7	16592.3	0.0	958.7	0.009	unavailable	unavailable	unavailable	unavailable	unavailable	unavailable	unavailable	unavailable	unavailable	unavailable	unavailable	unavailable			
		Nagle	Kuchma	2007	203	631-4-13-35	NW	MO	P	0.532	90	4.20	67.73	284.5	16592.3	0.0	788.2	0.028	unavailable	unavailable	unavailable	unavailable	unavailable	unavailable	unavailable	unavailable	unavailable	unavailable	unavailable	unavailable	unavailable		
		Nagle	Kuchma	2007	204	631h-4-10-25	NW	MO	P	0.630	90	14.20	64.54	916.5	16592.3	0.0	1672.3	0.005	unavailable	unavailable	unavailable	unavailable	unavailable	unavailable	unavailable	unavailable	unavailable	unavailable	unavailable	unavailable	unavailable		
		Nagle	Kuchma	2007	205	631h-4-10-25	NW	MO	P	0.394	90	1.50	76.43	114.7	17491.5	0.0	310.4	0.022	unavailable	unavailable	unavailable	unavailable	unavailable	unavailable	unavailable	unavailable	unavailable	unavailable	unavailable	unavailable	unavailable	unavailable	
		Nagle	Kuchma	2007	206	631h-4-10-35	NW	MO	P	0.394	90	4.40	76.43	107.0	17491.5	0.0	288.6	0.034	unavailable	unavailable	unavailable	unavailable	unavailable	unavailable	unavailable	unavailable	unavailable	unavailable	unavailable	unavailable	unavailable	unavailable	unavailable
		Nagle	Kuchma	2007	207	631h-4-16-25	NW	MO	P	0.630	90	7.20	64.69	465.7	13488.5	0.0	1193.7	0.007	unavailable	unavailable	unavailable	unavailable	unavailable	unavailable	unavailable	unavailable	unavailable	unavailable	unavailable	unavailable	unavailable	unavailable	
		Nagle	Kuchma	2007	208	631h-4-16-35	NW	MO	P	0.630	90	6.50	64.69	430.5	13488.5	0.0	945.6	0.007	unavailable	unavailable	unavailable	unavailable	unavailable	unavailable	unavailable	unavailable	unavailable	unavailable	unavailable	unavailable	unavailable	unavailable	unavailable
		Sneed	Shaw	2013	209	N584	NW	CJ	R	0.375	90	13.33	66.23	882.8	4860.0	0.0	1193.1	N/A	0.007	0.03	210.000	no	1.0	N/A	N/A	1.0	N/A	1.0	0.500	0.500			
		Sneed	Shaw	2013	210	N585	NW	CJ	R	0.375	90	13.33	66.23	882.8	4860.0	0.0	1079.6	N/A	0.007	0.02	1505.000	no	1.0	N/A	N/A	1.0	N/A	1.0	0.500	0.500			
		Sneed	Shaw	2013	211	N586	NW	CJ	R	0.375	90	13.33	66.23	882.8	4860.0	0.0	1079.6	N/A	0.007	0.02	1505.000	no	1.0	N/A	N/A	1.0	N/A	1.0	0.500	0.500			
		Sneed	Shaw	2013	212	N584	NW	CJ	S	0.375	90	13.33	66.23	882.8	4860.0	0.0	860.0	0.0	907.9	0.006	0.03	1936.900	no	1.0	N/A	N/A	1.0	0.500	0.500				
		Sneed	Shaw	2013	213	N585	NW	CJ	S	0.375	90	13.33	66.23	882.8	4860.0	0.0	790.6	0.0	808.8	0.002	0.01	4354.400	no	1.0	N/A	N/A	1.0	0.500	0.500				
		Sneed	Shaw	2013	214	N586	NW	CJ	S	0.375	90	13.33	66.23	882.8	4860.0	0.0	791.0	0.0	808.8	0.002	0.01	4106.600	no	1.0	N/A	N/A	1.0	0.500	0.500				
		Sneed	Shaw	2013	215	S581	SLW	CJ	R	0.375	90	13.33	66.23	882.8	4550.0	0.0	1039.0	N/A	0.007	0.010	1743.000	no	1.0	N/A	N/A	1.0	N/A	1.0	0.500	0.500			
		Sneed	Shaw	2013	216	S582	SLW	CJ	R	0.375	90	13.33	66.23	882.8	4550.0	0.0	1038.1	N/A	0.008	0.014	1743.000	no	1.0	N/A	N/A	1.0	N/A	1.0	0.500	0.500			
		Sneed	Shaw	2013	217	S583	SLW	CJ	R	0.375	90	13.33	66.23	882.8	4550.0	0.0	1291.0	N/A	0.007	0.022	2492.000	no	1.0	N/A	N/A	1.0	N/A	1.0	0.500	0.500			
		Sneed	Shaw	2013	218	S581	SLW	CJ	S	0.375	90	13.33	66.23	882.8	4550.0	0.0	778.4	0.0	808.8	0.006	0.019	3956.000	yes	1.0	N/A	N/A	1.0	0.500	0.500				
		Sneed	Shaw	2013	219	S582	SLW	CJ	S	0.375	90	13.33	66.23	882.8	4550.0	0.0	889.1	N/A	0.003	0.016	2125.000	no	1.0	N/A	N/A	1.0	N/A	1.0	0.500	0.500			
		Sneed	Shaw	2013	220	S583	SLW	CJ	S	0.375	90	13.33	66.23	882.8	4550.0	0.0	803.9	N/A	0.007	0.021	2416.000	no	1.0	N/A	N/A	1.0	N/A	1.0	0.500	0.500			
		Sneed	Shaw	2013	221	A581	ALW	CJ	R	0.375	90	13.33	66.23	882.8	6080.0	0.0	978.6	0.0	803.9	0.005	0.010	2942.000	no	1.0	N/A	N/A	1.0	0.500	0.500				
		Sneed	Shaw	2013	222	A582	ALW	CJ	R	0.375	90	13.33	66.23	882.8	6080.0	0.0	1066.7	N/A	0.005	0.011	1921.900	no	1.0	N/A	N/A	1.0	N/A	1.0	0.500	0.500			
		Sneed	Shaw	2013	223	A583	ALW	CJ	R	0.375	90	13.33	66.23	882.8	6080.0	0.0	1038.6	N/A	0.004	0.013	4354.400	no	1.0	N/A	N/A	1.0	N/A	1.0	0.500	0.500			
		Sneed	Shaw	2013	224	A581	ALW	CJ	S	0.375	90	13.33	66.23	882.8	6080.0	0.0	837.8	N/A	0.006	0.021	4000.000	yes	1.0	N/A	N/A	1.0	N/A	1.0	0.500	0.500			
		Sneed	Shaw	2013	225	A582	ALW	CJ	S	0.375	90	13.33	66.23	882.8	6080.0	0.0	807.7	N/A	0.005	0.023	unavailable	unavailable	unavailable	unavailable	unavailable	unavailable	unavailable	unavailable	unavailable	unavailable	unavailable	unavailable	
		Sneed	Shaw	2013	226	A583	ALW	CJ	S	0.375	90	13.33	66.23	882.8	6080.0	0.0	792.9	N/A	0.007	0.032	1936.900	no	1.0	N/A	N/A	1.0	N/A	1.0	0.500	0.500			
		Sneed	Shaw	2013	227	N881	NW	CJ	R	0.375	90	13.33	66.23	882.8	7500.0	0.0	1495.8	N/A	0.008	0.030	2394.000	no	1.0	N/A	N/A	1.0	N/A	1.0	0.500	0.500			
		Sneed	Shaw	2013	228	N882	NW	CJ	R	0.375	90	13.33	66.23	882.8	7500.0	0.0	1133.1	N/A	0.005	0.008	1788.000	no	1.0	N/A	N/A	1.0	N/A	1.0	0.500	0.500			
		Sneed	Shaw	2013	229	N883	NW	CJ	R	0.375	90	13.33	66.23	882.8	7500.0	0.0	1295.8	N/A	0.005	0.007	2758.000	no	1.0	N/A	N/A	1.0	N/A	1.0	0.500	0.500			
		Sneed	Shaw	2013	230	N881	NW	CJ	S	0.375	90	13.33	66.23	882.8	7500.0	0.0	1334.6	N/A	0.006	0.007	2136.000	no	1.0	N/A	N/A	1.0	N/A	1.0	0.500	0.500			
		Sneed	Shaw	2013	231	N882	NW	CJ	S	0.375	90	13.33	66.23	882.8	7500.0	0.0	1076.9	N/A	0.005	0.010	2288.000	no	1.0	N/A	N/A	1.0	N/A	1.0	0.500	0.500			
		Sneed	Shaw	2013	232	N883	NW	CJ	S	0.375	90	13.33	66.23	882.8	7500.0	0.0	1117.8	N/A	0.006	0.001	2167.000	no	1.0	N/A	N/A	1.0	N/A	1.0	0.500	0.500			
		Sneed	Shaw	2013	233	S881	SLW	CJ	R	0.375	90	13.33	66.23	882.8	7210.0	0.0	1455.5	N/A	0.006	0.007	1754.000	no	1.0	N/A	N/A	1.0	N/A	1.0	0.500	0.500			
		Sneed	Shaw	2013	234	S882	SLW	CJ	R	0.375	90	13.33	66.23	882.8	7210.0	0.0	1361.2	N/A	0.006	0.010	1754.000	no	1.0	N/A	N/A	1.0	N/A	1.0	0.500	0.500			
		Sneed	Shaw	2013	235	S883	SLW	CJ	R	0.375	90	13.33	66.23	882.8	7210.0	0.0	1348.0	N/A	0.005	0.006	1944.000	no	1.0	N/A	N/A	1.0	N/A	1.0	0.500	0.500			
		Sneed	Shaw	2013	236	S881	SLW	CJ	S	0.375	90	13.33	66.23	882.8	7210.0	0.0	1354.0	N/A	0.006	0.007	2398.000	no	1.0	N/A	N/A	1.0	N/A	1.0	0.500	0.500			
		Sneed	Shaw	2013	237	S882	SLW	CJ	S	0.375	90	13.33	66.23	882.8	7210.0	0.0	1169.3	N/A	0.003	0.005	1564.000	no	1.0	N/A	N/A	1.0	N/A	1.0	0.500	0.500			
		Sneed	Shaw	2013	238	S883	SLW	CJ	S	0.375	90	13.33	66.23	882.8	7210.0	0.0	1189.2	N/A	0.007	0.018	511.700	no	1.0	N/A	N/A	1.0	N/A	1.0	0.500	0.500			
		Sneed	Shaw	2013	239	A881	ALW	CJ	R	0.375	90	13.33	66.23	882.8	7845.0	0.0	1248.0	N/A	0.003	0.009	unavailable	unavailable	unavailable	unavailable	unavailable	unavailable	unavailable	unavailable	unavailable	unavailable	unavailable		
		Sneed	Shaw	2013	240	A882	ALW	CJ	R	0.375	90	13.33	66.23	882.8	7845.0	0.0	1291.6	N/A	0.007	0.008	unavailable	unavailable	unavailable	unavailable	unavailable	unavailable	unavailable	unavailable	unavailable	unavailable	unavailable	unavailable	
Sneed	Shaw	2013	241	A883	ALW	CJ	R	0.375	90	13.33	66.23	882.8	7845.0	0.0	931.1	N/A	0.004	0.011	unavailable	unavailable	unavailable	unavailable	unavailable	unavailable	unavailable	unavailable	unavailable	unavailable	unavailable	unavailable			
Sneed	Shaw	2013	242	A881	ALW	CJ	S	0.375	90	13.33	66.23	882.8	7845.0	0.0	970.4	N/A	0.006	0.012	unavailable	unavailable	unavailable	unavailable	unavailable	unavailable	unavailable	unavailable	unavailable	unavailable	unavailable	unavailable			
Sneed	Shaw	2013	243	A882	ALW	CJ	S	0.375	90	13.33	66.23	882.8	7845.0	0.0	1045.3	N/A	0.004	0.012	unavailable	unavailable	unavailable	unavailable	unavailable	unavailable	unavailable	unavailable	unavailable	unavailable	unavailable	unavailable			
Sneed	Shaw	2013	244	A883	ALW	CJ	S	0.375	90	13.33	6																						

		additional info (crack opening and slip)												additional info (aggregate and rebars)													
Type of test	Author1	Author2	year	ID	orig. spec. ID	concrete type	interface type	surface preparation	strip diameter ds	bars at angle, α	ρ	f _y or f _u	f _y	f _c	External Normal compressive stress, σ	surface strength, σ or τ	initial residual crack width	crack width at ultimate load	slip at ultimate load	strain in steel at ultimate load	load kept constant while strain increased? Or any unusual	ultimate load reached or not	if stopped before reaching ult. load, the max slip	if stopped before reaching ult. load, the max width	bumps on rebars (yes=1, no=0)	max coarse aggregate size (feet or slow size where 5% or less retained)	
Vertical push-off	Holbeck	Mattok	1989	251	1.4A	NW	MO	U	0.375	90	18.00	50.70	92.6	45100	0.0	1360.0	N/A	N/A	unavailable	unavailable	unavailable	unavailable	1.0	N/A	N/A	1.0	0.875
Vertical push-off	Holbeck	Mattok	1989	252	1.4B	NW	MO	U	0.375	90	18.00	48.00	86.0	3855.0	0.0	1380.0	N/A	N/A	0.04	unavailable	unavailable	unavailable	1.0	N/A	N/A	1.0	0.875
Vertical push-off	Holbeck	Mattok	1989	253	1.5A	NW	MO	U	0.375	90	22.00	50.70	115.4	4510.0	0.0	1400.0	N/A	N/A	unavailable	unavailable	unavailable	unavailable	1.0	N/A	N/A	1.0	0.875
Vertical push-off	Holbeck	Mattok	1989	254	1.5B	NW	MO	U	0.375	90	22.00	48.00	105.0	4065.0	0.0	1384.0	N/A	N/A	0.00	unavailable	unavailable	unavailable	1.0	N/A	N/A	1.0	0.875
Vertical push-off	Holbeck	Mattok	1989	255	1.6A	NW	MO	U	0.375	90	26.00	50.70	131.8	4310.0	0.0	1432.0	N/A	N/A	unavailable	unavailable	unavailable	unavailable	1.0	N/A	N/A	1.0	0.875
Vertical push-off	Holbeck	Mattok	1989	256	1.6B	NW	MO	U	0.375	90	26.00	48.00	124.8	4050.0	0.0	1420.0	N/A	N/A	0.09	unavailable	unavailable	unavailable	1.0	N/A	N/A	1.0	0.875
Vertical push-off	Kahn	Mitchell	2002	257	SF-4-1-U	NW	MO	U	0.375	90	4.00	69.50	78.0	685.0	0.0	96.0	N/A	unavailable	0.62	unavailable	unavailable	unavailable	1.0	N/A	N/A	1.0	0.750
Vertical push-off	Kahn	Mitchell	2002	258	SF-4-2-U	NW	MO	U	0.375	90	7.00	69.50	486.5	685.0	0.0	1335.0	N/A	unavailable	0.86	unavailable	unavailable	unavailable	1.0	N/A	N/A	1.0	0.750
Vertical push-off	Kahn	Mitchell	2002	259	SF-4-3-U	NW	MO	U	0.375	90	11.00	69.50	794.5	685.0	0.0	1431.0	N/A	unavailable	0.81	unavailable	unavailable	unavailable	1.0	N/A	N/A	1.0	0.750
Vertical push-off	Kahn	Mitchell	2002	260	SF-7-1-U	NW	MO	U	0.375	90	4.00	83.00	32.0	1174.0	0.0	1459.0	N/A	unavailable	0.08	unavailable	unavailable	unavailable	1.0	N/A	N/A	1.0	0.750
Vertical push-off	Kahn	Mitchell	2002	261	SF-7-2-U	NW	MO	U	0.375	90	7.00	83.00	58.0	1241.0	0.0	1569.0	N/A	unavailable	0.08	unavailable	unavailable	unavailable	1.0	N/A	N/A	1.0	0.750
Vertical push-off	Kahn	Mitchell	2002	262	SF-7-3-U	NW	MO	U	0.375	90	11.00	83.00	91.0	1310.0	0.0	2307.0	N/A	unavailable	0.68	unavailable	unavailable	unavailable	1.0	N/A	N/A	1.0	0.750
Vertical push-off	Kahn	Mitchell	2002	263	SF-7-4-U	NW	MO	U	0.375	90	15.00	83.00	124.0	1271.0	0.0	2485.0	N/A	unavailable	0.76	unavailable	unavailable	unavailable	1.0	N/A	N/A	1.0	0.750
Vertical push-off	Kahn	Mitchell	2002	264	SF-10-1-Ua	NW	MO	U	0.375	90	4.00	83.00	32.0	1263.0	0.0	1668.0	N/A	unavailable	0.03	unavailable	unavailable	unavailable	1.0	N/A	N/A	1.0	0.750
Vertical push-off	Kahn	Mitchell	2002	265	SF-10-1-Ub	NW	MO	U	0.375	90	4.00	83.00	32.0	1431.0	0.0	1374.0	N/A	unavailable	0.08	unavailable	unavailable	unavailable	1.0	N/A	N/A	1.0	0.750
Vertical push-off	Kahn	Mitchell	2002	266	SF-10-2-Ua	NW	MO	U	0.375	90	7.00	83.00	58.0	1471.0	0.0	2178.0	N/A	unavailable	0.02	unavailable	unavailable	unavailable	1.0	N/A	N/A	1.0	0.750
Vertical push-off	Kahn	Mitchell	2002	267	SF-10-2-Ub	NW	MO	U	0.375	90	7.00	83.00	58.0	1484.0	0.0	2089.0	N/A	unavailable	0.07	unavailable	unavailable	unavailable	1.0	N/A	N/A	1.0	0.750
Vertical push-off	Kahn	Mitchell	2002	268	SF-10-3-Ua	NW	MO	U	0.375	90	11.00	83.00	91.0	1617.0	0.0	2414.0	N/A	unavailable	0.05	unavailable	unavailable	unavailable	1.0	N/A	N/A	1.0	0.750
Vertical push-off	Kahn	Mitchell	2002	269	SF-10-3-Ub	NW	MO	U	0.375	90	11.00	83.00	91.0	1394.0	0.0	2465.0	N/A	unavailable	0.85	unavailable	unavailable	unavailable	1.0	N/A	N/A	1.0	0.750
Vertical push-off	Kahn	Mitchell	2002	270	SF-10-4-Ua	NW	MO	U	0.375	90	15.00	83.00	124.0	1548.0	0.0	2620.0	N/A	unavailable	0.79	unavailable	unavailable	unavailable	1.0	N/A	N/A	1.0	0.750
Vertical push-off	Kahn	Mitchell	2002	271	SF-10-4-Ub	NW	MO	U	0.375	90	15.00	83.00	124.0	1647.0	0.0	2667.0	N/A	unavailable	0.00	unavailable	unavailable	unavailable	1.0	N/A	N/A	1.0	0.750
Vertical push-off	Kahn	Mitchell	2002	272	SF-14-1-U	NW	MO	U	0.375	90	4.00	83.00	32.0	1797.0	0.0	1383.0	N/A	unavailable	0.40	unavailable	unavailable	unavailable	1.0	N/A	N/A	1.0	0.750
Vertical push-off	Kahn	Mitchell	2002	273	SF-14-2-U	NW	MO	U	0.375	90	7.00	83.00	58.0	1782.0	0.0	1808.0	N/A	unavailable	0.62	unavailable	unavailable	unavailable	1.0	N/A	N/A	1.0	0.750
Vertical push-off	Kahn	Mitchell	2002	274	SF-14-3-U	NW	MO	U	0.375	90	11.00	83.00	91.0	1625.0	0.0	2437.0	N/A	unavailable	0.65	unavailable	unavailable	unavailable	1.0	N/A	N/A	1.0	0.750
Vertical push-off	Kahn	Mitchell	2002	275	SF-14-4-U	NW	MO	U	0.375	90	15.00	83.00	124.0	1659.0	0.0	2620.0	N/A	unavailable	0.89	unavailable	unavailable	unavailable	1.0	N/A	N/A	1.0	0.750
Vertical push-off	Holbeck	Mattok	1989	276	2.100	NW	MO	P	0.375	90	4.00	50.70	202.8	3100.0	0.0	590.0	unavailable	unavailable	0.08	unavailable	unavailable	unavailable	1.0	N/A	N/A	1.0	0.875
Vertical push-off	Holbeck	Mattok	1989	277	2.200	NW	MO	P	0.375	90	5.00	50.70	456.3	3100.0	0.0	680.0	unavailable	unavailable	0.41	unavailable	unavailable	unavailable	1.0	N/A	N/A	1.0	0.875
Vertical push-off	Holbeck	Mattok	1989	278	2.300	NW	MO	P	0.375	90	13.00	50.70	691.1	3900.0	0.0	840.0	unavailable	unavailable	0.09	unavailable	unavailable	unavailable	1.0	N/A	N/A	1.0	0.875
Vertical push-off	Holbeck	Mattok	1989	279	2.400	NW	MO	P	0.375	90	18.00	50.70	912.6	3900.0	0.0	1000.0	unavailable	unavailable	0.07	unavailable	unavailable	unavailable	1.0	N/A	N/A	1.0	0.875
Vertical push-off	Holbeck	Mattok	1989	280	2.500	NW	MO	P	0.375	90	22.00	50.70	1115.4	4180.0	0.0	1300.0	unavailable	unavailable	0.02	unavailable	unavailable	unavailable	1.0	N/A	N/A	1.0	0.875
Vertical push-off	Holbeck	Mattok	1989	281	2.600	NW	MO	P	0.375	90	26.00	50.70	1318.2	4180.0	0.0	1385.0	unavailable	unavailable	0.03	unavailable	unavailable	unavailable	1.0	N/A	N/A	1.0	0.875
Vertical push-off	Holbeck	Mattok	1989	282	3.300	NW	MO	P	0.375	90	3.00	50.70	456.3	3100.0	0.0	680.0	unavailable	unavailable	unavailable	unavailable	unavailable	unavailable	1.0	N/A	N/A	1.0	0.875
Vertical push-off	Holbeck	Mattok	1989	283	3.400	NW	MO	P	0.375	90	16.00	47.20	755.2	4040.0	0.0	1028.0	unavailable	unavailable	unavailable	unavailable	unavailable	unavailable	1.0	N/A	N/A	1.0	0.875
Vertical push-off	Holbeck	Mattok	1989	284	3.500	NW	MO	P	0.375	90	25.00	42.40	1060.0	4040.0	0.0	1153.0	unavailable	unavailable	unavailable	unavailable	unavailable	unavailable	1.0	N/A	N/A	1.0	0.875
Vertical push-off	Holbeck	Mattok	1989	285	4.100	NW	MO	P	0.375	90	4.00	66.10	284.4	4070.0	0.0	704.0	unavailable	unavailable	unavailable	unavailable	unavailable	unavailable	1.0	N/A	N/A	1.0	0.875
Vertical push-off	Holbeck	Mattok	1989	286	4.200	NW	MO	P	0.375	90	5.00	66.10	594.9	4070.0	0.0	980.0	unavailable	unavailable	unavailable	unavailable	unavailable	unavailable	1.0	N/A	N/A	1.0	0.875
Vertical push-off	Holbeck	Mattok	1989	287	4.300	NW	MO	P	0.375	90	13.00	66.10	893.3	4340.0	0.0	1380.0	unavailable	unavailable	unavailable	unavailable	unavailable	unavailable	1.0	N/A	N/A	1.0	0.875
Vertical push-off	Holbeck	Mattok	1989	288	4.400	NW	MO	P	0.375	90	18.00	66.10	1189.8	4340.0	0.0	1400.0	unavailable	unavailable	unavailable	unavailable	unavailable	unavailable	1.0	N/A	N/A	1.0	0.875
Vertical push-off	Holbeck	Mattok	1989	289	4.500	NW	MO	P	0.375	90	22.00	66.10	1454.2	4340.0	0.0	1320.0	unavailable	unavailable	unavailable	unavailable	unavailable	unavailable	1.0	N/A	N/A	1.0	0.875
Vertical push-off	Holbeck	Mattok	1989	290	5.100	NW	MO	P	0.375	90	4.00	50.70	202.8	2450.0	0.0	510.0	unavailable	unavailable	unavailable	unavailable	unavailable	unavailable	1.0	N/A	N/A	1.0	0.875
Vertical push-off	Holbeck	Mattok	1989	291	5.200	NW	MO	P	0.375	90	3.00	50.70	456.3	2650.0	0.0	700.0	unavailable	unavailable	unavailable	unavailable	unavailable	unavailable	1.0	N/A	N/A	1.0	0.875
Vertical push-off	Holbeck	Mattok	1989	292	5.300	NW	MO	P	0.375	90	13.00	50.70	691.1	2380.0	0.0	800.0	unavailable	unavailable	unavailable	unavailable	unavailable	unavailable	1.0	N/A	N/A	1.0	0.875
Vertical push-off	Holbeck	Mattok	1989	293	5.400	NW	MO	P	0.375	90	18.00	50.70	912.6	2580.0	0.0	795.0	unavailable	unavailable	unavailable	unavailable	unavailable	unavailable	1.0	N/A	N/A	1.0	0.875
Vertical push-off	Holbeck	Mattok	1989	294	5.500	NW	MO	P	0.375	90	22.00	50.70	1115.4	2620.0	0.0	1020.0	unavailable	unavailable	unavailable	unavailable	unavailable	unavailable	1.0	N/A	N/A	1.0	0.875
Vertical push-off	Kahn	Mitchell	2002	295	SF-4-1-C	NW	MO	P	0.375	90	4.00	69.50	78.0	685.0	0.0	583.0	unavailable	unavailable	unavailable	unavailable	unavailable	unavailable	1.0	N/A	N/A	1.0	0.750
Vertical push-off	Kahn	Mitchell	2002	296	SF-4-2-C	NW	MO	P	0.375	90	7.00	69.50	486.5	685.0	0.0	528.0	unavailable	unavailable	0.86	unavailable	unavailable	unavailable	1.0	N/A	N/A	1.0	0.750
Vertical push-off	Kahn	Mitchell	2002	297	SF-4-3-C	NW	MO	P	0.375	90	11.00	69.50	764.5	685.0	0.0	1186.0	unavailable	unavailable	0.86	unavailable	unavailable	unavailable	1.0	N/A	N/A	1.0	0.750
Vertical push-off	Kahn	Mitchell	2002	298	SF-7-1-C	NW	MO	P	0.375	90	4.00	83.00	32.0	1174.0	0.0	695.0	unavailable	unavailable	unavailable	unavailable	unavailable	unavailable	1.0	N/A	N/A	1.0	0.750
Vertical push-off	Kahn	Mitchell	2002	299	SF-7-3-C	NW	MO	P	0.375	90	11.00	83.00	91.0	1310.0	0.0	1192.0	unavailable	unavailable	0.81	unavailable	unavailable	unavailable	1.0	N/A	N/A	1.0	0.750
Vertical push-off	Kahn	Mitchell	2002	300	SF-10-1-Cb	NW	MO	P	0.375	90	4.00	83.00	32.0	1431.0	0.0	500.0	unavailable	unavailable	0.08	unavailable	unavailable	unavailable	1.0	N/A	N/A	1.0	0.750

Type of test	Author1	Author2	year	ID	orig. spec. ID	concrete type	interface type	surface preparation	strip diameter ds	p	fy or fu	fy	fc'	External Normal stress, σ	surface strength, σ_c or σ_t	initial residual crack width	crack width at ultimate load	slip at ultimate load	strain in steel at ultimate load	load kept constant while strain increased? Or any annual	ultimate load reached or not	if stopped before reaching ult. load, the max slip	if stopped before reaching ult. load, the max width	additional info (aggregate and rebars)	
																								bumps on rebars	max coarse aggregate size (feet or slow size where 5% or less retained)
Vertical push-off	Kahn	Mitchell	2002	301	SF-10-2-C-a	NW	MO	P	0.375	90	7.00	82.00	58.0	14676.0	0.0	846.0	unavailable	unavailable	note	unavailable	1.0	N/A	N/A	1.0	0.750
Vertical push-off	Kahn	Mitchell	2002	302	SF-10-2-C-b	NW	MO	P	0.375	90	7.00	83.00	58.0	14864.0	0.0	802.0	unavailable	unavailable	note	unavailable	1.0	N/A	N/A	1.0	0.750
Vertical push-off	Kahn	Mitchell	2002	303	SF-10-3-C-a	NW	MO	P	0.375	90	11.00	89.00	93.0	16170.0	0.0	1079.0	unavailable	unavailable	0.099	unavailable	1.0	N/A	N/A	1.0	0.750
Vertical push-off	Kahn	Mitchell	2002	304	SF-10-4-C-a	NW	MO	P	0.375	90	15.00	83.00	1245.0	15468.0	0.0	1236.0	unavailable	unavailable	note	unavailable	1.0	N/A	N/A	1.0	0.750
Vertical push-off	Kahn	Mitchell	2002	305	SF-10-4-C-b	NW	MO	P	0.375	90	15.00	83.00	1245.0	16476.0	0.0	1271.0	unavailable	unavailable	0.059	unavailable	1.0	N/A	N/A	1.0	0.750
Vertical push-off	Kahn	Mitchell	2002	306	SF-14-1-C	NW	MO	P	0.375	90	4.00	83.00	32.0	16015.0	0.0	415.0	unavailable	unavailable	note	unavailable	1.0	N/A	N/A	1.0	0.750
Vertical push-off	Kahn	Mitchell	2002	307	SF-14-2-C	NW	MO	P	0.375	90	7.00	83.00	58.0	15466.0	0.0	670.0	unavailable	unavailable	note	unavailable	1.0	N/A	N/A	1.0	0.750
Vertical push-off	Kahn	Mitchell	2002	308	SF-14-3-C	NW	MO	P	0.375	90	11.00	83.00	83.0	15321.0	0.0	935.0	unavailable	unavailable	note	unavailable	1.0	N/A	N/A	1.0	0.750
Vertical push-off	Hoff	N/A	1993	309	1LWC1	SLW	MO	P	0.375	90	5.24	53.60	280.8	8496.0	0.0	262.0	0.010	unavailable	0.147	unavailable	note	N/A	N/A	1.0	0.750
Vertical push-off	Hoff	N/A	1993	310	2LWC1	SLW	MO	P	0.375	90	5.24	53.60	280.8	8510.0	0.0	395.0	0.013	unavailable	0.038	unavailable	note	N/A	N/A	1.0	0.750
Vertical push-off	Hoff	N/A	1993	311	3LWC1	SLW	MO	P	0.375	90	5.24	53.60	280.8	8290.0	0.0	413.0	0.011	unavailable	0.033	unavailable	1.0	N/A	N/A	1.0	0.750
Vertical push-off	Hoff	N/A	1993	312	4LWC1	SLW	MO	P	0.300	90	9.52	68.00	647.6	8390.0	0.0	761.0	0.010	unavailable	0.020	unavailable	1.0	N/A	N/A	1.0	0.750
Vertical push-off	Hoff	N/A	1993	313	5LWC1	SLW	MO	P	0.300	90	9.52	68.00	647.6	8510.0	0.0	680.0	0.012	unavailable	0.018	unavailable	1.0	N/A	N/A	1.0	0.750
Vertical push-off	Hoff	N/A	1993	314	6LWC1	SLW	MO	P	0.500	90	9.52	68.00	647.6	8290.0	0.0	727.0	0.012	unavailable	0.015	unavailable	1.0	N/A	N/A	1.0	0.750
Vertical push-off	Hoff	N/A	1993	315	1LWC2	SLW	MO	P	0.375	90	5.24	53.60	280.8	8760.0	0.0	489.0	0.008	unavailable	0.009	unavailable	1.0	N/A	N/A	1.0	0.750
Vertical push-off	Hoff	N/A	1993	316	2LWC2	SLW	MO	P	0.375	90	5.24	53.60	280.8	8760.0	0.0	335.0	0.011	unavailable	0.029	unavailable	1.0	N/A	N/A	1.0	0.750
Vertical push-off	Hoff	N/A	1993	317	3LWC2	SLW	MO	P	0.375	90	5.24	53.60	280.8	8790.0	0.0	299.0	0.010	unavailable	0.017	unavailable	note	N/A	N/A	1.0	0.750
Vertical push-off	Hoff	N/A	1993	318	4LWC2	SLW	MO	P	0.300	90	9.52	68.00	647.6	9210.0	0.0	739.0	0.010	unavailable	0.018	unavailable	1.0	N/A	N/A	1.0	0.750
Vertical push-off	Hoff	N/A	1993	319	5LWC2	SLW	MO	P	0.500	90	9.52	68.50	652.4	8760.0	0.0	692.0	0.010	unavailable	0.027	unavailable	1.0	N/A	N/A	1.0	0.750
Vertical push-off	Hoff	N/A	1993	320	6LWC2	SLW	MO	P	0.375	90	9.52	68.50	652.4	8730.0	0.0	680.0	0.011	unavailable	0.029	unavailable	1.0	N/A	N/A	1.0	0.750
Vertical push-off	Hoff	N/A	1993	321	1HSWC	SLW	MO	P	0.300	90	5.24	72.10	377.7	10310.0	0.0	668.0	0.009	unavailable	0.066	unavailable	1.0	N/A	N/A	1.0	0.750
Vertical push-off	Hoff	N/A	1993	322	2HSWC	SLW	MO	P	0.375	90	5.24	72.10	377.7	10910.0	0.0	548.0	0.008	unavailable	0.026	unavailable	1.0	N/A	N/A	1.0	0.750
Vertical push-off	Hoff	N/A	1993	323	3HSWC	SLW	MO	P	0.375	90	5.24	72.10	377.7	11010.0	0.0	585.0	0.010	unavailable	0.006	unavailable	1.0	N/A	N/A	1.0	0.750
Vertical push-off	Hoff	N/A	1993	324	4HSWC	SLW	MO	P	0.500	90	9.52	66.80	686.2	10310.0	0.0	870.0	0.011	unavailable	0.010	unavailable	1.0	N/A	N/A	1.0	0.750
Vertical push-off	Hoff	N/A	1993	325	5HSWC	SLW	MO	P	0.500	90	9.52	66.80	686.2	10810.0	0.0	870.0	0.011	unavailable	0.009	unavailable	1.0	N/A	N/A	1.0	0.750
Vertical push-off	Hoff	N/A	1993	326	6HSWC	SLW	MO	P	0.500	90	9.52	66.80	686.2	11010.0	0.0	884.0	0.009	unavailable	0.025	unavailable	1.0	N/A	N/A	1.0	0.750
Vertical push-off	Kahn	Mitchell	2002	327	SF-7-3-C	NW	CJ	R	0.375	90	4.00	83.00	32.0	11744.0	0.0	300.0	N/A	unavailable	unavailable	unavailable	1.0	N/A	N/A	1.0	0.750
Vertical push-off	Kahn	Mitchell	2002	328	SF-7-2-C	NW	CJ	R	0.375	90	7.00	83.00	58.0	11744.0	0.0	1368.0	N/A	unavailable	0.028	unavailable	1.0	N/A	N/A	1.0	0.750
Vertical push-off	Kahn	Mitchell	2002	329	SF-7-3-C	NW	CJ	R	0.375	90	11.00	83.00	93.0	12471.0	0.0	1838.0	N/A	unavailable	0.024	unavailable	1.0	N/A	N/A	1.0	0.750
Vertical push-off	Kahn	Mitchell	2002	330	SF-7-4-C	NW	CJ	R	0.375	90	15.00	83.00	1245.0	12471.0	0.0	2211.0	N/A	unavailable	0.062	unavailable	1.0	N/A	N/A	1.0	0.750
Vertical push-off	Kahn	Mitchell	2002	331	SF-10-3-C	NW	CJ	R	0.375	90	11.00	83.00	93.0	12953.0	0.0	1899.0	N/A	unavailable	0.070	unavailable	1.0	N/A	N/A	1.0	0.750
Vertical push-off	Kahn	Mitchell	2002	332	SF-14-1-C	NW	CJ	R	0.375	90	4.00	83.00	32.0	14756.0	0.0	2101.0	N/A	unavailable	0.061	unavailable	1.0	N/A	N/A	1.0	0.750
Vertical push-off	Kahn	Mitchell	2002	333	SF-14-2-C	NW	CJ	R	0.375	90	7.00	83.00	58.0	14756.0	0.0	1515.0	N/A	unavailable	0.052	unavailable	1.0	N/A	N/A	1.0	0.750
Vertical push-off	Kahn	Mitchell	2002	334	SF-14-3-C	NW	CJ	R	0.375	90	11.00	83.00	93.0	15318.0	0.0	2245.0	N/A	unavailable	0.074	unavailable	1.0	N/A	N/A	1.0	0.750
Vertical push-off	Kahn	Mitchell	2002	335	SF-14-4-C	NW	CJ	R	0.375	90	15.00	83.00	1245.0	15318.0	0.0	2552.0	N/A	unavailable	2.328	unavailable	1.0	N/A	N/A	1.0	0.750
Vertical push-off	Kahn	Mitchell	2002	336	SF-10-1-C	NW	CJ	S	0.375	90	4.00	83.00	32.0	14356.0	0.0	529.0	N/A	unavailable	0.009	unavailable	1.0	N/A	N/A	1.0	0.750
Vertical push-off	Kahn	Mitchell	2002	337	SF-10-3-C	NW	CJ	S	0.375	90	7.00	83.00	58.0	12053.0	0.0	822.0	N/A	unavailable	0.010	unavailable	1.0	N/A	N/A	1.0	0.750
Vertical push-off	Kahn	Mitchell	2002	338	SF-10-2-C	NW	CJ	S	0.375	90	11.00	83.00	93.0	14358.0	0.0	914.0	0.002	0.008	0.012	unavailable	1.0	N/A	N/A	1.0	0.630
Vertical push-off	Walraven	Stroband	1994	339	10.000	NW	MO	P	0.315	90	5.60	86.30	967.0	14358.0	0.0	1624.0	0.002	0.002	0.013	unavailable	1.0	N/A	N/A	1.0	0.630
Vertical push-off	Walraven	Stroband	1994	340	12.000	NW	MO	P	0.315	90	11.20	86.30	1450.0	14358.0	0.0	2175.0	0.002	0.009	0.012	unavailable	1.0	N/A	N/A	1.0	0.630
Vertical push-off	Walraven	Stroband	1994	341	13.000	NW	MO	P	0.315	90	16.80	86.30	1924.0	14358.0	0.0	2625.0	0.002	0.011	0.012	unavailable	1.0	N/A	N/A	1.0	0.630
Vertical push-off	Walraven	Stroband	1994	342	14.000	NW	MO	P	0.472	90	22.30	86.30	1087.0	14358.0	0.0	1595.0	0.002	0.008	0.012	unavailable	1.0	N/A	N/A	1.0	0.630
Vertical push-off	Walraven	Stroband	1994	343	15.000	NW	MO	P	0.472	90	25.30	86.30	2166.0	14358.0	0.0	2353.0	0.002	0.008	0.012	unavailable	1.0	N/A	N/A	1.0	0.630
Vertical push-off	Walraven	Reinhardt	1981	345	11026T	NW	MO	P	0.315	90	5.60	62.86	352.0	4416.0	0.0	737.0	0.001	0.016	0.015	unavailable	1.0	N/A	N/A	1.0	0.630
Vertical push-off	Walraven	Reinhardt	1981	346	11026B.000	NW	MO	P	0.315	90	5.60	62.86	352.0	3785.0	0.0	795.0	0.001	0.016	0.016	unavailable	1.0	N/A	N/A	1.0	0.630
Vertical push-off	Walraven	Reinhardt	1981	347	11026B	NW	MO	P	0.315	90	16.80	62.86	352.0	3624.0	0.0	737.0	0.004	0.016	0.016	unavailable	1.0	N/A	N/A	1.0	0.630
Vertical push-off	Walraven	Reinhardt	1981	348	11026B.000	NW	MO	P	0.315	90	16.80	62.92	1057.0	3785.0	0.0	1072.0	0.000	0.014	0.013	unavailable	1.0	N/A	N/A	1.0	0.630
Vertical push-off	Walraven	Reinhardt	1981	349	110716.000	NW	MO	P	0.236	90	11.00	73.55	809.0	3908.0	0.0	1043.0	0.001	unavailable	unavailable	unavailable	1.0	N/A	N/A	1.0	0.630
Vertical push-off	Walraven	Reinhardt	1981	350	210204.000	NW	MO	P	0.157	90	1.40	110.00	154.0	4512.0	0.0	467.0	0.003	unavailable	unavailable	unavailable	1.0	N/A	N/A	1.0	0.630

additional info (crack opening and slip)											additional info (aggregate and rebars)																
Type of test	Author1	Author2	ID	orig. spec. ID	concrete type	interface type	surface preparation	strip diameter	bars at angle, α	p	f _y or f _u	ρ _{fy}	f _{c'}	External Normal compressive stress, σ	surface strength, σ _t or τ	initial residual crack width	crack width at ultimate load	slip at ultimate load	strain in steel at ultimate load	load kept constant while strain increased? Or any unusual	ultimate load reached or not	if stopped before reaching ult. load, the max slip	if stopped before reaching ult. load, the max width	bumps on rebars (see or size where 5% or less retained)	max coarse aggregate size where 5% or less retained		
vertical push-off	Walraven	Reinhardt	1981	351	210608.000	NW	MO	P	0.315	90	16.80	62.92	1057.0	4512.0	0.0	1410.0	0.000	unavailable	unavailable	unavailable	unavailable	unavailable	unavailable	if (f _{crack} > 2, pain=0, no reinforcement)	1.0	0.630	
vertical push-off	Walraven	Reinhardt	1981	352	210216.000	NW	MO	P	0.630	90	22.30	65.83	1468.0	4512.0	0.0	1342.0	0.001	unavailable	unavailable	unavailable	unavailable	unavailable	unavailable	unavailable	if (f _{crack} > 2, pain=0, no reinforcement)	1.0	0.630
vertical push-off	Walraven	Reinhardt	1981	353	210316.000	NW	MO	P	0.630	90	33.50	65.67	2200.0	4512.0	0.0	1466.0	0.001	unavailable	unavailable	unavailable	unavailable	unavailable	unavailable	unavailable	if (f _{crack} > 2, pain=0, no reinforcement)	1.0	0.630
vertical push-off	Walraven	Reinhardt	1981	354	120208.000	NW	MO	P	0.315	90	5.60	62.86	352.0	3637.0	0.0	1730.0	0.002	unavailable	unavailable	unavailable	unavailable	unavailable	unavailable	unavailable	if (f _{crack} > 2, pain=0, no reinforcement)	1.0	0.630
vertical push-off	Walraven	Reinhardt	1981	355	120408.000	NW	MO	P	0.315	90	11.20	62.95	705.0	3637.0	0.0	947.0	0.002	unavailable	unavailable	unavailable	unavailable	unavailable	unavailable	unavailable	if (f _{crack} > 2, pain=0, no reinforcement)	1.0	0.630
vertical push-off	Walraven	Reinhardt	1981	356	120608.000	NW	MO	P	0.315	90	16.80	62.92	1410.0	3637.0	0.0	983.0	0.000	unavailable	unavailable	unavailable	unavailable	unavailable	unavailable	unavailable	if (f _{crack} > 2, pain=0, no reinforcement)	1.0	0.630
vertical push-off	Walraven	Reinhardt	1981	357	120808.000	NW	MO	P	0.315	90	22.30	63.23	1410.0	3637.0	0.0	1060.0	0.000	unavailable	unavailable	unavailable	unavailable	unavailable	unavailable	unavailable	if (f _{crack} > 2, pain=0, no reinforcement)	1.0	0.630
vertical push-off	Walraven	Reinhardt	1981	358	120706.000	NW	MO	P	0.236	90	11.00	75.55	890.0	3637.0	0.0	1000.0	0.001	unavailable	unavailable	unavailable	unavailable	unavailable	unavailable	unavailable	if (f _{crack} > 2, pain=0, no reinforcement)	1.0	0.630
vertical push-off	Walraven	Reinhardt	1981	359	230216.000	NW	MO	P	0.630	90	22.30	62.83	1468.0	3637.0	0.0	947.0	0.001	unavailable	unavailable	unavailable	unavailable	unavailable	unavailable	unavailable	if (f _{crack} > 2, pain=0, no reinforcement)	1.0	0.630
vertical push-off	Walraven	Reinhardt	1981	360	230208.000	NW	MO	P	0.315	90	5.60	62.86	352.0	6916.0	0.0	975.0	0.002	0.009	0.010	0.010	unavailable	unavailable	unavailable	unavailable	if (f _{crack} > 2, pain=0, no reinforcement)	1.0	0.630
vertical push-off	Walraven	Reinhardt	1981	361	230408.000	NW	MO	P	0.315	90	11.20	63.04	706.0	6916.0	0.0	1571.0	0.001	0.005	0.014	0.014	unavailable	unavailable	unavailable	unavailable	if (f _{crack} > 2, pain=0, no reinforcement)	1.0	0.630
vertical push-off	Walraven	Reinhardt	1981	362	230608.000	NW	MO	P	0.315	90	16.80	62.92	1057.0	6916.0	0.0	1822.0	0.001	0.007	0.015	0.015	unavailable	unavailable	unavailable	unavailable	if (f _{crack} > 2, pain=0, no reinforcement)	1.0	0.630
vertical push-off	Walraven	Reinhardt	1981	363	230808.000	NW	MO	P	0.315	90	22.30	63.23	1410.0	6916.0	0.0	2058.0	0.001	0.007	0.015	0.015	unavailable	unavailable	unavailable	unavailable	if (f _{crack} > 2, pain=0, no reinforcement)	1.0	0.630
vertical push-off	Walraven	Reinhardt	1981	364	250208.000	NW	MO	P	0.315	90	5.60	62.86	352.0	4789.0	0.0	951.0	0.000	unavailable	unavailable	unavailable	unavailable	unavailable	unavailable	unavailable	if (f _{crack} > 2, pain=0, no reinforcement)	1.0	1.260
vertical push-off	Walraven	Reinhardt	1981	365	250408.000	NW	MO	P	0.315	90	11.20	62.95	705.0	4789.0	0.0	1400.0	0.000	unavailable	unavailable	unavailable	unavailable	unavailable	unavailable	unavailable	if (f _{crack} > 2, pain=0, no reinforcement)	1.0	1.260
vertical push-off	Walraven	Reinhardt	1981	366	250608.000	NW	MO	P	0.315	90	16.80	62.92	1057.0	4789.0	0.0	1400.0	0.000	unavailable	unavailable	unavailable	unavailable	unavailable	unavailable	unavailable	if (f _{crack} > 2, pain=0, no reinforcement)	1.0	1.260
vertical push-off	Walraven	Reinhardt	1981	367	250808.000	NW	MO	P	0.315	90	22.30	63.23	1410.0	4789.0	0.0	1443.0	0.000	unavailable	unavailable	unavailable	unavailable	unavailable	unavailable	unavailable	if (f _{crack} > 2, pain=0, no reinforcement)	1.0	1.260
vertical push-off	Freny	N/A	1985	368	210000.000	NW	MO	P	0.315	90	11.20	66.72	747.0	6720.0	0.0	1617.0	0.006	0.020	0.017	0.017	unavailable	unavailable	unavailable	unavailable	if (f _{crack} > 2, pain=0, no reinforcement)	1.0	0.630
vertical push-off	Freny	N/A	1985	369	310000.000	NW	MO	P	0.315	90	11.19	79.77	893.0	6720.0	0.0	2150.0	0.006	0.025	0.018	0.018	unavailable	unavailable	unavailable	unavailable	if (f _{crack} > 2, pain=0, no reinforcement)	1.0	0.630
vertical push-off	Freny	N/A	1985	370	410000.000	NW	MO	P	0.315	90	11.19	79.77	893.0	6720.0	0.0	1961.0	0.008	0.022	0.018	0.018	unavailable	unavailable	unavailable	unavailable	if (f _{crack} > 2, pain=0, no reinforcement)	1.0	0.630
vertical push-off	Freny	N/A	1985	371	510000.000	NW	MO	P	0.315	90	11.19	79.77	893.0	6720.0	0.0	1489.0	0.009	0.026	0.015	0.015	unavailable	unavailable	unavailable	unavailable	if (f _{crack} > 2, pain=0, no reinforcement)	1.0	0.630
vertical push-off	Freny	N/A	1985	372	610000.000	NW	MO	P	0.315	90	11.19	79.77	893.0	7051.0	0.0	2142.0	0.008	0.022	0.019	0.019	unavailable	unavailable	unavailable	unavailable	if (f _{crack} > 2, pain=0, no reinforcement)	1.0	0.630
vertical push-off	Freny	N/A	1985	373	710000.000	NW	MO	P	0.315	90	16.80	66.72	1121.0	8044.0	0.0	2036.0	0.004	0.032	0.021	0.021	unavailable	unavailable	unavailable	unavailable	if (f _{crack} > 2, pain=0, no reinforcement)	1.0	0.630
vertical push-off	Freny	N/A	1985	374	101000.000	NW	MO	P	0.315	90	16.80	66.72	1121.0	7567.0	0.0	1856.0	0.007	0.020	0.014	0.014	unavailable	unavailable	unavailable	unavailable	if (f _{crack} > 2, pain=0, no reinforcement)	1.0	0.630
vertical push-off	Freny	N/A	1985	375	111000.000	NW	MO	P	0.315	90	16.80	66.72	1121.0	7567.0	0.0	1856.0	0.006	0.025	0.024	0.024	unavailable	unavailable	unavailable	unavailable	if (f _{crack} > 2, pain=0, no reinforcement)	1.0	0.630
vertical push-off	Freny	N/A	1985	376	121000.000	NW	MO	P	0.315	90	22.40	79.77	1787.0	7568.0	0.0	2676.0	0.006	0.027	0.019	0.019	unavailable	unavailable	unavailable	unavailable	if (f _{crack} > 2, pain=0, no reinforcement)	1.0	0.630
vertical push-off	Freny	N/A	1985	377	131000.000	NW	MO	P	0.315	90	11.20	66.72	747.0	9433.0	0.0	1688.0	0.006	0.024	0.011	0.011	unavailable	unavailable	unavailable	unavailable	if (f _{crack} > 2, pain=0, no reinforcement)	1.0	0.630
vertical push-off	Freny	N/A	1985	378	141000.000	NW	MO	P	0.315	90	11.20	66.72	747.0	9433.0	0.0	1777.0	0.006	0.024	0.011	0.011	unavailable	unavailable	unavailable	unavailable	if (f _{crack} > 2, pain=0, no reinforcement)	1.0	0.630
vertical push-off	Freny	N/A	1985	379	151000.000	NW	MO	P	0.315	90	11.19	79.77	893.0	9902.0	0.0	2384.0	0.007	0.038	0.012	0.012	unavailable	unavailable	unavailable	unavailable	if (f _{crack} > 2, pain=0, no reinforcement)	1.0	0.630
vertical push-off	Freny	N/A	1985	380	161000.000	NW	MO	P	0.315	90	11.19	79.77	893.0	9882.0	0.0	1774.0	0.009	0.034	0.012	0.012	unavailable	unavailable	unavailable	unavailable	if (f _{crack} > 2, pain=0, no reinforcement)	1.0	0.630
vertical push-off	Freny	N/A	1985	381	171000.000	NW	MO	P	0.315	90	11.20	66.72	747.0	9144.0	0.0	1753.0	0.007	0.027	0.013	0.013	unavailable	unavailable	unavailable	unavailable	if (f _{crack} > 2, pain=0, no reinforcement)	1.0	0.630
vertical push-off	Freny	N/A	1985	382	191000.000	NW	MO	P	0.315	90	11.20	66.72	747.0	9144.0	0.0	1561.0	0.021	0.036	0.040	0.040	unavailable	unavailable	unavailable	unavailable	if (f _{crack} > 2, pain=0, no reinforcement)	1.0	0.630
vertical push-off	Freny	N/A	1985	383	201000.000	NW	MO	P	0.315	90	16.80	66.72	1121.0	9882.0	0.0	2371.0	0.003	0.020	0.012	0.012	unavailable	unavailable	unavailable	unavailable	if (f _{crack} > 2, pain=0, no reinforcement)	1.0	0.630
vertical push-off	Freny	N/A	1985	384	211000.000	NW	MO	P	0.315	90	16.80	66.72	1121.0	9882.0	0.0	2330.0	0.003	0.020	0.010	0.010	unavailable	unavailable	unavailable	unavailable	if (f _{crack} > 2, pain=0, no reinforcement)	1.0	0.630
vertical push-off	Freny	N/A	1985	385	221000.000	NW	MO	P	0.315	90	16.80	66.72	1121.0	9225.0	0.0	2273.0	0.005	0.022	0.012	0.012	unavailable	unavailable	unavailable	unavailable	if (f _{crack} > 2, pain=0, no reinforcement)	1.0	0.630
vertical push-off	Freny	N/A	1985	386	231000.000	NW	MO	P	0.315	90	16.80	66.72	1121.0	9225.0	0.0	2181.0	0.006	0.038	0.029	0.029	unavailable	unavailable	unavailable	unavailable	if (f _{crack} > 2, pain=0, no reinforcement)	1.0	0.630
vertical push-off	Freny	N/A	1985	387	241000.000	NW	MO	P	0.315	90	22.40	79.77	1787.0	9818.0	0.0	3197.0	0.005	0.025	0.011	0.011	unavailable	unavailable	unavailable	unavailable	if (f _{crack} > 2, pain=0, no reinforcement)	1.0	0.630
vertical push-off	Sagasta	Vollum	2011	388	PL2	NW	MO	P	0.315	90	4.20	79.77	335.0	7763.0	0.0	703.4	0.005	0.044	0.001	0.001	no	2545.500	no	2545.500	if (f _{crack} > 2, pain=0, no reinforcement)	1.0	0.394
vertical push-off	Sagasta	Vollum	2011	389	PL2b	NW	MO	P	0.315	90	4.20	79.77	335.0	7763.0	0.0	844.1	0.004	0.009	0.008	0.008	unavailable	unavailable	unavailable	unavailable	if (f _{crack} > 2, pain=0, no reinforcement)	1.0	0.394
vertical push-off	Sagasta	Vollum	2011	390	PL3	NW	MO	P	0.315	90	6.40	79.77	510.5	7763.0	0.0	1029.8	0.005	0.015	0.010	0.010	no	2454.500	no	2454.500	if (f _{crack} > 2, pain=0, no reinforcement)	1.0	0.394
vertical push-off	Sagasta	Vollum	2011	391	PL4	NW	MO	P	0.315	90	8.50	79.77	678.0	7763.0	0.0	1029.8	0.005	0.015	0.020	0.020	no	2048.280	no	2048.280	if (f _{crack} > 2, pain=0, no reinforcement)	1.0	0.394
vertical push-off	Sagasta	Vollum	2011	392	PG2	NW	MO	P	0.315	90	6.40	79.77	335.0	4597.0	0.0	521.3	0.011	0.026	0.037	0.037	no	1658.540	no	1658.540	if (f _{crack} > 2, pain=0, no reinforcement)	1.0	0.394
vertical push-off	Sagasta	Vollum	2011	393	PG3	NW	MO	P	0.315	90	6.40	79.77	335.0	4597.0	0.0	312.1	0.003	0.020	0.024	0.024	no	N/A	no	N/A	if (f _{crack} > 2, pain=0, no reinforcement)	1.0	0.394
Horizontal push-off	Rose	N/A	1998	394	VMP2-NSRW	NW	CJ	S	N/A	90	0.00	0.00	0.00	7555.5	0.0	304.0	N/A	unavailable	unavailable	N/A	N/A	N/A	N/A	if (f _{crack} > 2, pain=0, no reinforcement)	N/A	0.750	
Horizontal push-off	Rose	N/A	1998	395	VMP2-NSRW	NW	CJ	S	N/A	90	0.00	0.00	0.00	6932.0	0.0	250.0	N/A	unavailable	unavailable	N/A	N/A	N/A	N/A	if (f _{crack} > 2, pain=0, no reinforcement)	N/A	0.750	
Horizontal push-off	Rose	N/A	1998	396	VMP2-NSPD	NW	CJ	S	N/A	90	0.00	0.00	0.00	5346.5	0.0	445.0	N/A	unavailable	unavailable	N/A	N/A	N/A	N/A	if (f			

additional info (crack opening and slip)															additional info (aggregate and rebars)												
Type of test	Author1	Author2	year	ID	orig. spec. ID	concrete type	interface type	surface preparation	strip diameter	bars at angle, α	ρ	f_y or f_u	f_{yk}	Ext. Normal compressive stress, σ	surface strength or σ	initial residual crack width	crack width at ultimate load	slip at ultimate load	strain in steel at ultimate load	load kept constant while strain increased? Or any unusual	ultimate load reached or not	if stopped before reaching ult. load, the max slip	if stopped before reaching ult. load, the max width	bumps on rebars (see or slow size where 5% or less retained)	max coarse aggregate size (see or slow size where 5% or less retained)		
									[in]		[10 ⁻³]	[ksi]	[psi]	[psi]	[psi]	[in]	[in]	[in]	[microstrain]		(yes=1 no=0)	[in]	[in]	(5 for cracks, 1 for no reinforcement)	[in]		
Horizontal push-off	Jose	N/A	1998	401	VMP2-B45	NW	C	R	N/A	90	0.00	0.00	0.0	5199.0	0.0	245.0	N/A	unavailable	unavailable	N/A	N/A	1.0	N/A	N/A	N/A	0.750	
Horizontal push-off	Jose	N/A	1998	402	VMP1-B90	NW	C	R	N/A	90	0.00	0.00	0.0	5788.0	0.0	216.0	N/A	unavailable	unavailable	N/A	N/A	1.0	N/A	N/A	N/A	0.750	
Horizontal push-off	Jose	N/A	1998	403	VMP2-B90	NW	C	R	N/A	90	0.00	0.00	0.0	5331.5	0.0	260.0	N/A	unavailable	unavailable	N/A	N/A	1.0	N/A	N/A	N/A	0.750	
Horizontal push-off	Jose	N/A	1998	404	VMP3-B90	NW	C	R	N/A	90	0.00	0.00	0.0	5633.0	0.0	292.0	N/A	unavailable	unavailable	N/A	N/A	1.0	N/A	N/A	N/A	0.750	
Horizontal push-off	Jose	N/A	1998	405	VMP1-B90V	NW	C	R	N/A	90	0.00	0.00	0.0	6387.0	0.0	62.00	N/A	unavailable	unavailable	N/A	N/A	1.0	N/A	N/A	N/A	0.750	
Horizontal push-off	Jose	N/A	1998	406	VMP2-B90V	NW	C	R	N/A	90	0.00	0.00	0.0	6641.0	0.0	56.00	N/A	unavailable	unavailable	N/A	N/A	1.0	N/A	N/A	N/A	0.750	
Horizontal push-off	Jose	N/A	1998	407	VN1	NW	MO	U	N/A	90	0.00	0.00	0.0	5981.0	0.0	86.00	N/A	unavailable	unavailable	N/A	N/A	1.0	N/A	N/A	N/A	0.750	
Horizontal push-off	Jose	N/A	1998	408	VN2	NW	MO	U	N/A	90	0.00	0.00	0.0	7184.0	0.0	86.00	N/A	unavailable	unavailable	N/A	N/A	1.0	N/A	N/A	N/A	0.750	
Horizontal push-off	Jose	N/A	1998	409	VN3	NW	MO	U	N/A	90	0.00	0.00	0.0	6655.0	0.0	92.00	N/A	unavailable	unavailable	N/A	N/A	1.0	N/A	N/A	N/A	0.750	
Horizontal push-off	CTA	N/A	1974	410	S-7-5	NW	C	S	N/A	90	0.00	0.00	0.0	5500.0	0.0	42.00	N/A	unavailable	unavailable	N/A	N/A	1.0	N/A	N/A	N/A	unavailable	
Horizontal push-off	CTA	N/A	1974	411	S-8-5	NW	C	S	N/A	90	0.00	0.00	0.0	4060.0	0.0	39.00	N/A	unavailable	unavailable	N/A	N/A	1.0	N/A	N/A	N/A	unavailable	
Horizontal push-off	CTA	N/A	1976	412	P-1	NW	C	S	N/A	90	0.00	0.00	0.0	4340.0	0.0	29.00	N/A	unavailable	unavailable	N/A	N/A	1.0	N/A	N/A	N/A	unavailable	
Horizontal push-off	CTA	N/A	1976	413	SFC-2	NW	C	S	N/A	90	0.00	0.00	0.0	4300.0	0.0	10.00	N/A	unavailable	unavailable	N/A	N/A	1.0	N/A	N/A	N/A	unavailable	
Horizontal push-off	CTA	N/A	1976	414	SFC-4	NW	C	S	N/A	90	0.00	0.00	0.0	4900.0	0.0	23.00	N/A	unavailable	unavailable	N/A	N/A	1.0	N/A	N/A	N/A	unavailable	
Horizontal push-off	CTA	N/A	1976	415	SRC-4	NW	C	S	N/A	90	0.00	0.00	0.0	4900.0	0.0	28.00	N/A	unavailable	unavailable	N/A	N/A	1.0	N/A	N/A	N/A	unavailable	
Horizontal push-off	CTA	N/A	1976	416	LEC-3	NW	C	S	N/A	90	0.00	0.00	0.0	3820.0	0.0	84.0	N/A	unavailable	unavailable	N/A	N/A	1.0	N/A	N/A	N/A	unavailable	
Horizontal push-off	CTA	N/A	1976	417	LEC-3	NW	C	R	N/A	90	0.00	0.00	0.0	3820.0	0.0	14.00	N/A	unavailable	unavailable	N/A	N/A	1.0	N/A	N/A	N/A	unavailable	
Horizontal push-off	CTA	N/A	1976	418	LEC-5	NW	C	S	N/A	90	0.00	0.00	0.0	4090.0	0.0	19.00	N/A	unavailable	unavailable	N/A	N/A	1.0	N/A	N/A	N/A	unavailable	
Horizontal push-off	CTA	N/A	1976	419	REC-5	NW	C	R	N/A	90	0.00	0.00	0.0	4090.0	0.0	15.00	N/A	unavailable	unavailable	N/A	N/A	1.0	N/A	N/A	N/A	unavailable	
Horizontal push-off	CTA	N/A	1976	420	IEE-5	NW	C	S	N/A	90	0.00	0.00	0.0	3970.0	0.0	10.00	N/A	unavailable	unavailable	N/A	N/A	1.0	N/A	N/A	N/A	unavailable	
Horizontal push-off	CTA	N/A	1976	421	IEE-5	NW	C	S	N/A	90	0.00	0.00	0.0	3420.0	0.0	8.0	N/A	unavailable	unavailable	N/A	N/A	1.0	N/A	N/A	N/A	unavailable	
Horizontal push-off	CTA	N/A	1976	422	LR-5	NW	C	R	N/A	90	0.00	0.00	0.0	3970.0	0.0	23.00	N/A	unavailable	unavailable	N/A	N/A	1.0	N/A	N/A	N/A	unavailable	
Horizontal push-off	Scott	N/A	2010	423	LL-9A	SLW	C	R	N/A	90	0.00	0.00	0.0	6250.0	6.6	343.8	N/A	unavailable	unavailable	N/A	N/A	1.0	N/A	N/A	N/A	0.500	
Horizontal push-off	Scott	N/A	2010	424	LL-9B	SLW	C	R	N/A	90	0.00	0.00	0.0	6250.0	6.6	364.6	N/A	unavailable	unavailable	N/A	N/A	1.0	N/A	N/A	N/A	0.500	
Horizontal push-off	Scott	N/A	2010	425	LL-9C	SLW	C	R	N/A	90	0.00	0.00	0.0	6250.0	6.6	465.5	N/A	unavailable	unavailable	N/A	N/A	1.0	N/A	N/A	N/A	0.500	
Horizontal push-off	Scott	N/A	2010	426	NW-6A	NW	C	R	N/A	90	0.00	0.00	0.0	6150.0	6.6	398.4	N/A	unavailable	unavailable	N/A	N/A	1.0	N/A	N/A	N/A	1.000	
Horizontal push-off	Scott	N/A	2010	427	NW-9B	NW	C	R	N/A	90	0.00	0.00	0.0	6150.0	6.6	416.7	N/A	unavailable	unavailable	N/A	N/A	1.0	N/A	N/A	N/A	1.000	
Horizontal push-off	Scott	N/A	2010	428	NW-9C	NW	C	R	N/A	90	0.00	0.00	0.0	6150.0	6.6	406.3	N/A	unavailable	unavailable	N/A	N/A	1.0	N/A	N/A	N/A	1.000	
Horizontal push-off	Scott	N/A	2010	429	NL-9-A	SLW	C	R	N/A	90	0.00	0.00	0.0	6250.0	6.6	464.4	N/A	unavailable	unavailable	N/A	N/A	1.0	N/A	N/A	N/A	0.500	
Horizontal push-off	Scott	N/A	2010	430	NL-9-B	SLW	C	R	N/A	90	0.00	0.00	0.0	6250.0	6.6	341.1	N/A	unavailable	unavailable	N/A	N/A	1.0	N/A	N/A	N/A	0.500	
Horizontal push-off	Scott	N/A	2010	431	NL-9-C	SLW	C	R	N/A	90	0.00	0.00	0.0	6250.0	6.6	513.0	N/A	unavailable	unavailable	N/A	N/A	1.0	N/A	N/A	N/A	0.500	
Horizontal push-off	Scott	N/A	2010	432	LL-3-A	SLW	C	R	0.500	90	1.04	60.00	62.5	6250.0	6.6	630.2	N/A	unavailable	unavailable	N/A	N/A	1.0	N/A	N/A	N/A	0.500	
Horizontal push-off	Scott	N/A	2010	433	LL-3-B	SLW	C	R	0.500	90	1.04	60.00	62.5	6250.0	6.6	382.8	N/A	unavailable	unavailable	N/A	N/A	1.0	N/A	N/A	N/A	0.500	
Horizontal push-off	Scott	N/A	2010	434	LL-3-C	SLW	C	R	0.500	90	1.04	60.00	62.5	6250.0	6.6	489.6	N/A	unavailable	unavailable	N/A	N/A	1.0	N/A	N/A	N/A	0.500	
Horizontal push-off	Scott	N/A	2010	435	NW-1-A	NW	C	R	0.500	90	1.04	60.00	62.5	6150.0	6.6	320.3	N/A	unavailable	unavailable	N/A	N/A	1.0	N/A	N/A	N/A	1.000	
Horizontal push-off	Scott	N/A	2010	436	NW-1-B	NW	C	R	0.500	90	1.04	60.00	62.5	6150.0	6.6	367.2	N/A	unavailable	unavailable	N/A	N/A	1.0	N/A	N/A	N/A	1.000	
Horizontal push-off	Scott	N/A	2010	437	NW-1-C	NW	C	R	0.500	90	1.04	60.00	62.5	6150.0	6.6	495.0	N/A	unavailable	unavailable	N/A	N/A	1.0	N/A	N/A	N/A	1.000	
Horizontal push-off	Scott	N/A	2010	438	NL-1-A	SLW	C	R	0.500	90	1.04	60.00	62.5	6250.0	6.6	440.1	N/A	unavailable	unavailable	N/A	N/A	1.0	N/A	N/A	N/A	0.500	
Horizontal push-off	Scott	N/A	2010	439	NL-1-B	SLW	C	R	0.500	90	1.04	60.00	62.5	6250.0	6.6	455.7	N/A	unavailable	unavailable	N/A	N/A	1.0	N/A	N/A	N/A	0.500	
Horizontal push-off	Scott	N/A	2010	440	NL-1-C	SLW	C	R	0.500	90	1.04	60.00	62.5	6250.0	6.6	476.6	N/A	unavailable	unavailable	N/A	N/A	1.0	N/A	N/A	N/A	0.500	
Horizontal push-off	Scott	N/A	2010	441	LL-3-A	SLW	C	R	0.625	90	0.79	60.00	287.5	5730.0	6.6	523.4	N/A	unavailable	unavailable	N/A	N/A	1.0	N/A	N/A	N/A	0.500	
Horizontal push-off	Scott	N/A	2010	442	LL-3-B	SLW	C	R	0.625	90	0.79	60.00	287.5	5730.0	6.6	580.7	N/A	unavailable	unavailable	N/A	N/A	1.0	N/A	N/A	N/A	0.500	
Horizontal push-off	Scott	N/A	2010	443	LL-3-C	SLW	C	R	0.625	90	0.79	60.00	287.5	5730.0	6.6	590.0	N/A	unavailable	unavailable	N/A	N/A	1.0	N/A	N/A	N/A	0.500	
Horizontal push-off	Scott	N/A	2010	444	NW-3-A	NW	C	R	0.625	90	0.79	60.00	287.5	6150.0	6.6	570.8	N/A	unavailable	unavailable	N/A	N/A	1.0	N/A	N/A	N/A	1.000	
Horizontal push-off	Scott	N/A	2010	445	NW-3-B	NW	C	R	0.625	90	0.79	60.00	287.5	6150.0	6.6	567.7	N/A	unavailable	unavailable	N/A	N/A	1.0	N/A	N/A	N/A	1.000	
Horizontal push-off	Scott	N/A	2010	446	NW-3-C	NW	C	R	0.625	90	0.79	60.00	287.5	6150.0	6.6	596.4	N/A	unavailable	unavailable	N/A	N/A	1.0	N/A	N/A	N/A	1.000	
Horizontal push-off	Scott	N/A	2010	447	NL-3-A	SLW	C	R	0.625	90	0.79	60.00	287.5	5730.0	6.6	630.2	N/A	unavailable	unavailable	N/A	N/A	1.0	N/A	N/A	N/A	0.500	
Horizontal push-off	Scott	N/A	2010	448	NL-3-B	SLW	C	R	0.625	90	0.79	60.00	287.5	5730.0	6.6	619.8	N/A	unavailable	unavailable	N/A	N/A	1.0	N/A	N/A	N/A	0.500	
NW to LW concrete	Scott	N/A	2010	449	NL-3-C	SLW	C	R	0.625	90	0.79	60.00	287.5	5730.0	6.6	476.6	N/A	unavailable	unavailable	N/A	N/A	1.0	N/A	N/A	N/A	0.500	
Vertical push-off	Barbosa	Trep	2017	450	4660-1	NW	C	R	0.500	90	4.17	72.60	302.5	4481.0	0.0	725.6	N/A	0.040	0.047	1950.000	no	1.0	N/A	N/A	N/A	1.0	0.375

Type of test		Author1	Author2	year	ID	orig. spec. ID	concrete type	interface type	surface preparation	strip diameter	bars at angle, α	ρ	fy or fu	fy	fc'	External Normal compressive stress, σ	surface strength, σ or τ	initial residual crack width	crack width at ultimate load	slip at ultimate load	strain in steel at ultimate load	load kept constant while strain increased? Or any unusual	ultimate load reached or not	if stopped before reaching ult. load, the max slip	if stopped before reaching ult. load, the max width	bumps on rebars	additional info (aggregate and rebars)	
Vertical push-off	Barbosa	Tejro	2017	451	4660-2	NW	C	R	C	R	0.500	90.0	4.17	72.60	302.5	4481.0	0.0	688.1	N/A	0.055	0.042	1475.000	no	1.0	N/A	N/A	1.0	0.375
Vertical push-off	Barbosa	Tejro	2017	452	4660-3	NW	C	R	C	R	0.500	90.0	4.17	72.60	302.5	4198.0	0.0	636.7	N/A	0.059	0.050	2000.000	no	1.0	N/A	N/A	1.0	0.375
Vertical push-off	Barbosa	Tejro	2017	453	4660-4	NW	C	R	C	R	0.500	90.0	4.17	72.60	302.5	4198.0	0.0	688.1	N/A	0.028	0.032	1425.000	no	1.0	N/A	N/A	1.0	0.375
Vertical push-off	Barbosa	Tejro	2017	454	4660-5	NW	C	R	C	R	0.500	90.0	4.17	72.60	302.5	4198.0	0.0	702.5	N/A	note	0.042	1600.000	no	1.0	N/A	N/A	1.0	0.375
Vertical push-off	Barbosa	Tejro	2017	455	4660-1	NW	C	R	C	R	0.500	90.0	4.17	93.00	387.5	4372.0	0.0	666.3	N/A	unavailable	0.032	unavailable	no	1.0	N/A	N/A	1.0	0.375
Vertical push-off	Barbosa	Tejro	2017	456	4660-2	NW	C	R	C	R	0.500	90.0	4.17	93.00	387.5	4198.0	0.0	684.2	N/A	0.018	note	1400.000	no	1.0	N/A	N/A	1.0	0.375
Vertical push-off	Barbosa	Tejro	2017	457	4660-3	NW	C	R	C	R	0.500	90.0	4.17	93.00	387.5	4198.0	0.0	672.5	N/A	0.044	0.047	1550.000	no	1.0	N/A	N/A	1.0	0.375
Vertical push-off	Barbosa	Tejro	2017	458	4660-4	NW	C	R	C	R	0.500	90.0	4.17	83.00	375.2	4198.0	0.0	682.9	N/A	0.029	0.044	2075.000	no	1.0	N/A	N/A	1.0	0.375
Vertical push-off	Barbosa	Tejro	2017	459	4660-5	NW	C	R	C	R	0.500	90.0	4.17	93.00	387.5	4198.0	0.0	756.8	N/A	0.055	0.044	1675.000	no	1.0	N/A	N/A	1.0	0.375
Vertical push-off	Barbosa	Tejro	2017	460	5660-1	NW	C	R	C	R	0.625	90.0	6.46	67.60	436.6	4578.0	0.0	948.8	N/A	0.056	0.063	5556.667	unavailable	1.0	N/A	N/A	1.0	0.375
Vertical push-off	Barbosa	Tejro	2017	461	5660-2	NW	C	R	C	R	0.625	90.0	6.46	67.60	436.6	4578.0	0.0	957.8	N/A	0.047	0.067	5833.333	unavailable	1.0	N/A	N/A	1.0	0.375
Vertical push-off	Barbosa	Tejro	2017	462	5660-3	NW	C	R	C	R	0.625	90.0	6.46	67.60	436.6	4149.0	0.0	933.1	N/A	0.042	0.074	5186.667	unavailable	1.0	N/A	N/A	1.0	0.375
Vertical push-off	Barbosa	Tejro	2017	463	5660-4	NW	C	R	C	R	0.625	90.0	6.46	67.60	436.6	4149.0	0.0	945.0	N/A	0.033	0.058	5073.333	unavailable	1.0	N/A	N/A	1.0	0.375
Vertical push-off	Barbosa	Tejro	2017	464	5660-5	NW	C	R	C	R	0.625	90.0	6.46	67.60	436.6	4149.0	0.0	955.4	N/A	0.042	0.063	5906.667	unavailable	1.0	N/A	N/A	1.0	0.375
Vertical push-off	Barbosa	Tejro	2017	465	5660-1	NW	C	R	C	R	0.625	90.0	6.46	86.80	501.6	4578.0	0.0	1067.6	N/A	0.043	0.072	4233.333	unavailable	1.0	N/A	N/A	1.0	0.375
Vertical push-off	Barbosa	Tejro	2017	466	5660-2	NW	C	R	C	R	0.625	90.0	6.46	86.80	501.6	4160.0	0.0	1064.4	N/A	0.046	0.068	4103.333	unavailable	1.0	N/A	N/A	1.0	0.375
Vertical push-off	Barbosa	Tejro	2017	467	5660-3	NW	C	R	C	R	0.625	90.0	6.46	86.80	501.6	4160.0	0.0	1084.8	N/A	0.040	0.065	4480.000	unavailable	1.0	N/A	N/A	1.0	0.375
Vertical push-off	Barbosa	Tejro	2017	468	5660-4	NW	C	R	C	R	0.625	90.0	6.46	86.80	501.6	4160.0	0.0	961.5	N/A	0.033	0.058	4726.667	unavailable	1.0	N/A	N/A	1.0	0.375
Vertical push-off	Barbosa	Tejro	2017	469	5660-5	NW	C	R	C	R	0.625	90.0	6.46	86.80	501.6	4160.0	0.0	1022.1	N/A	0.040	0.073	4730.000	unavailable	1.0	N/A	N/A	1.0	0.375
Vertical push-off	Rahal	Khaleefi	2015	470	35-216-5CC	NW	MO	U			0.236	90.0	3.62	37.42	135.4	884.7	0.0	864.7	N/A	unavailable	unavailable	1657.800	no	1.0	N/A	N/A	unavailable	0.787
Vertical push-off	Rahal	Khaleefi	2015	471	35-216-5CC	NW	MO	U			0.3149608	90.0	6.43	59.176	380.7	6338.161	0.0	1063.129	N/A	unavailable	unavailable	1692.500	yes	1.0	N/A	N/A	unavailable	0.787
Vertical push-off	Rahal	Khaleefi	2015	472	35-216-5CC	NW	MO	U			0.3149608	90.0	9.65	59.176	571.1	6338.161	0.0	1116.793	N/A	unavailable	0.049	2173.230	yes	1.0	N/A	N/A	unavailable	0.787
Vertical push-off	Rahal	Khaleefi	2015	473	35-216-5CC	NW	MO	U			0.3149608	90.0	3.62	59.176	761.5	6338.161	0.0	1274.884	N/A	unavailable	unavailable	unavailable	1.0	N/A	N/A	unavailable	0.787	
Vertical push-off	Rahal	Khaleefi	2015	474	35-216-5CC	NW	MO	U			0.3149608	90.0	12.87	59.176	1142.2	6338.1606	0.0	1406.686	N/A	unavailable	unavailable	1236.200	no	1.0	N/A	N/A	unavailable	0.787
Vertical push-off	Rahal	Khaleefi	2015	475	35-216-5CC	NW	MO	U			0.2322206	90.0	3.62	37.420	135.4	11487.010	0.0	1380.380	N/A	unavailable	unavailable	unavailable	1.0	N/A	N/A	unavailable	0.787	
Vertical push-off	Rahal	Khaleefi	2015	476	70-216-5CC	NW	MO	U			0.3149608	90.0	6.43	59.176	380.7	11487.010	0.0	1657.937	N/A	unavailable	unavailable	unavailable	1.0	N/A	N/A	unavailable	0.787	
Vertical push-off	Rahal	Khaleefi	2015	477	70-216-5CC	NW	MO	U			0.3149608	90.0	9.65	59.176	571.1	11487.010	0.0	1657.937	N/A	unavailable	unavailable	unavailable	1.0	N/A	N/A	unavailable	0.787	
Vertical push-off	Rahal	Khaleefi	2015	478	70-216-5CC	NW	MO	U			0.3149608	90.0	9.65	59.176	571.1	11487.010	0.0	1823.128	N/A	unavailable	unavailable	unavailable	1.0	N/A	N/A	unavailable	0.787	
Vertical push-off	Rahal	Khaleefi	2015	479	70-216-5CC	NW	MO	U			0.3149608	90.0	9.65	59.176	571.1	11487.0096	0.0	1794.0	N/A	unavailable	unavailable	unavailable	1.0	N/A	N/A	unavailable	0.787	
Vertical push-off	Rahal	Khaleefi	2015	480	70-418-5CC	NW	MO	U			0.3149608	90.0	12.87	59.176	761.5	11487.0096	0.0	1852.1	N/A	unavailable	unavailable	unavailable	1.0	N/A	N/A	unavailable	0.787	
Vertical push-off	Rahal	Khaleefi	2015	481	70-418-5CC	NW	MO	U			0.3149608	90.0	19.30	59.176	1142.2	11487.0096	0.0	2298.9	N/A	unavailable	unavailable	unavailable	1.0	N/A	N/A	unavailable	0.787	
Vertical push-off	Rahal	Khaleefi	2015	482	35-216-0	NW	MO	U			0.2322206	90.0	3.62	37.42	135.4	6294.6492	0.0	805.0	N/A	unavailable	unavailable	unavailable	1.0	N/A	N/A	unavailable	0.787	
Vertical push-off	Rahal	Khaleefi	2015	483	35-216-0	NW	MO	U			0.3149608	90.0	6.43	59.176	380.7	6294.6492	0.0	1154.6	N/A	unavailable	unavailable	unavailable	1.0	N/A	N/A	unavailable	0.787	
Vertical push-off	Rahal	Khaleefi	2015	484	35-216-0	NW	MO	U			0.3149608	90.0	9.65	59.176	571.1	6294.6492	0.0	1258.9	N/A	unavailable	unavailable	unavailable	1.0	N/A	N/A	unavailable	0.787	
Horizontal push-off	Hansen	N/A	1960	485	BR56-1	NW	C	R			0.500	90.0	8.18	45.000	409.1	3500.0	0.0	888.3	unavailable	unavailable	0.009	unavailable	unavailable	1.0	N/A	N/A	unavailable	0.750
Horizontal push-off	Hansen	N/A	1960	486	BR56-2	NW	C	R			0.500	90.0	8.18	45.000	409.1	3240.0	0.0	505.4	unavailable	unavailable	0.02	unavailable	unavailable	1.0	N/A	N/A	unavailable	0.750
Horizontal push-off	Hansen	N/A	1960	487	BR56-3	NW	C	R			0.500	90.0	8.18	45.000	409.1	3760.0	0.0	773.3	unavailable	unavailable	0.003	unavailable	unavailable	1.0	N/A	N/A	unavailable	0.750
Horizontal push-off	Hansen	N/A	1960	488	BR52-1	NW	C	R			0.500	90.0	4.09	48.500	198.4	4130.0	0.0	545.2	unavailable	unavailable	0.002	unavailable	unavailable	1.0	N/A	N/A	unavailable	0.750
Horizontal push-off	Hansen	N/A	1960	489	BR52-2	NW	C	R			0.500	90.0	4.09	47.000	192.3	3580.0	0.0	496.7	unavailable	unavailable	0.001	unavailable	unavailable	1.0	N/A	N/A	unavailable	0.750
Horizontal push-off	Hansen	N/A	1960	490	BR52-3	NW	C	R			0.500	90.0	4.09	51.000	208.6	3310.0	0.0	391.7	unavailable	unavailable	0.001	unavailable	unavailable	1.0	N/A	N/A	unavailable	0.750
Horizontal push-off	Hansen	N/A	1960	491	BR52-4	NW	C	R			0.500	90.0	4.09	51.000	208.6	3310.0	0.0	396.7	unavailable	unavailable	0.001	unavailable	unavailable	1.0	N/A	N/A	unavailable	0.750
Horizontal push-off	Hansen	N/A	1960	492	BR52-5	NW	C	R			0.500	90.0	4.09	51.000	208.6	3310.0	0.0	346.5	unavailable	unavailable	0.001	unavailable	unavailable	1.0	N/A	N/A	unavailable	0.750
Horizontal push-off	Hansen	N/A	1960	493	BR52-6	NW	C	R			0.500	90.0	4.09	50.000	204.5	3960.0	0.0	406.7	unavailable	unavailable	0.001	unavailable	unavailable	1.0	N/A	N/A	unavailable	0.750
Horizontal push-off	Hansen	N/A	1960	494	BR52-7	NW	C	R			0.500	90.0	4.09	45.000	204.5	3960.0	0.0	475.8	unavailable	unavailable	0.001	unavailable	unavailable	1.0	N/A	N/A	unavailable	0.750
Horizontal push-off	Hansen	N/A	1960	495	BR52-8	NW	C	R			0.500	90.0	4.09	50.000	204.5	3960.0	0.0	485.8	unavailable	unavailable								

Type of test	Author1	Author2	year	ID	orig. spec. ID	concrete type	interface type	surface preparation	stripping diameter	bars at angle, α	ρ	fy or fu	pH	fc'	External Normal compressive stress, σ	surface strength, σ _{or}	initial residual crack width	crack width at ultimate load	slip at ultimate load	strain in steel at ultimate load	load kept constant while stress increased or any unusual	ultimate load reached or not	if stopped before reaching ult. load, the max slip	if stopped before reaching ult. load, the max width	additional info (aggregate and rebar)	
																									deformed-1, plain=0, no reinforcement	max coarse aggregate size (except on sieve size where 5% or less retained)
horizontal pushoff	Hanson	N/A	1960	501	BR12-6	NW	CJ	R	N/A	90.0	0.00	0.00	0.0	3700.0	0.0	410.0	unavailable	unavailable	0.001	unavailable	1.0	N/A	N/A	1.0	0.750	
horizontal pushoff	Hanson	N/A	1960	502	BR12-7	NW	CJ	R	N/A	90.0	0.00	0.00	0.0	3700.0	0.0	408.0	unavailable	unavailable	0.001	unavailable	1.0	N/A	N/A	1.0	0.750	
horizontal pushoff	Hanson	N/A	1960	503	BR12-8	NW	CJ	R	N/A	90.0	0.00	0.00	0.0	3700.0	0.0	405.0	unavailable	unavailable	0.001	unavailable	1.0	N/A	N/A	1.0	0.750	
horizontal pushoff	Hanson	N/A	1960	504	BR524-1	NW	CJ	R	0.500	90.0	2.05	49.00	100.2	3540.0	0.0	494.1	unavailable	unavailable	0.001	unavailable	1.0	N/A	N/A	1.0	0.750	
horizontal pushoff	Hanson	N/A	1960	505	BR524-2	NW	CJ	R	0.500	90.0	2.05	52.00	106.4	3430.0	0.0	369.0	unavailable	unavailable	0.001	unavailable	1.0	N/A	N/A	1.0	0.750	
horizontal pushoff	Hanson	N/A	1960	506	BR524-3	NW	CJ	R	0.500	90.0	2.05	50.00	102.3	3420.0	0.0	454.7	unavailable	unavailable	0.001	unavailable	1.0	N/A	N/A	1.0	0.750	
horizontal pushoff	Hanson	N/A	1960	507	BR524-4	NW	CJ	R	0.500	90.0	2.05	50.00	102.3	3510.0	0.0	489.3	unavailable	unavailable	0.001	unavailable	1.0	N/A	N/A	1.0	0.750	
horizontal pushoff	Hanson	N/A	1960	508	B55-1	NW	CJ	S	0.500	90.0	8.18	50.00	409.1	3240.0	0.0	179.9	unavailable	unavailable	0.000	unavailable	1.0	N/A	N/A	1.0	0.750	
horizontal pushoff	Hanson	N/A	1960	509	B55-2	NW	CJ	S	0.500	90.0	8.18	50.00	409.1	3240.0	0.0	291.7	unavailable	unavailable	0.001	unavailable	1.0	N/A	N/A	1.0	0.750	
horizontal pushoff	Hanson	N/A	1960	510	B55-3	NW	CJ	S	0.500	90.0	8.18	50.00	409.1	3760.0	0.0	523.8	unavailable	unavailable	0.002	unavailable	1.0	N/A	N/A	1.0	0.750	
horizontal pushoff	Hanson	N/A	1960	511	B55-4	NW	CJ	S	0.500	90.0	8.18	50.00	409.1	3700.0	0.0	287.9	unavailable	unavailable	0.001	unavailable	1.0	N/A	N/A	1.0	0.750	
horizontal pushoff	Hanson	N/A	1960	512	B55-5	NW	CJ	S	0.500	90.0	8.18	50.00	409.1	3700.0	0.0	327.5	unavailable	unavailable	0.001	unavailable	1.0	N/A	N/A	1.0	0.750	
horizontal pushoff	Hanson	N/A	1960	513	B52-1	NW	CJ	S	0.500	90.0	4.09	50.15	205.1	4650.0	0.0	184.8	unavailable	unavailable	0.001	unavailable	1.0	N/A	N/A	1.0	0.750	
horizontal pushoff	Hanson	N/A	1960	514	B52-2	NW	CJ	S	0.500	90.0	4.09	50.15	205.1	4650.0	0.0	134.0	unavailable	unavailable	0.001	unavailable	1.0	N/A	N/A	1.0	0.750	
horizontal pushoff	Hanson	N/A	1960	515	B12-1	NW	CJ	S	N/A	90.0	0.00	0.00	0.0	4650.0	0.0	125.0	unavailable	unavailable	0.001	unavailable	1.0	N/A	N/A	1.0	0.750	
horizontal pushoff	Hanson	N/A	1960	516	B12-2	NW	CJ	S	N/A	90.0	0.00	0.00	0.0	3660.0	0.0	280.0	unavailable	unavailable	0.001	unavailable	1.0	N/A	N/A	1.0	0.750	
horizontal pushoff	Hanson	N/A	1960	517	B12-3	NW	CJ	S	N/A	90.0	0.00	0.00	0.0	3980.0	0.0	130.0	unavailable	unavailable	0.001	unavailable	1.0	N/A	N/A	1.0	0.750	
horizontal pushoff	Hanson	N/A	1960	518	B12-4	NW	CJ	S	N/A	90.0	0.00	0.00	0.0	4150.0	0.0	90.0	unavailable	unavailable	0.000	unavailable	1.0	N/A	N/A	1.0	0.750	
horizontal pushoff	Hanson	N/A	1960	519	B12-5	NW	CJ	S	N/A	90.0	0.00	0.00	0.0	4060.0	0.0	120.0	unavailable	unavailable	0.000	unavailable	1.0	N/A	N/A	1.0	0.750	
horizontal pushoff	Hanson	N/A	1960	520	B24-1	NW	CJ	S	N/A	90.0	0.00	0.00	0.0	4220.0	0.0	109.0	unavailable	unavailable	0.000	unavailable	1.0	N/A	N/A	1.0	0.750	
horizontal pushoff	Hanson	N/A	1960	521	B24-2	NW	CJ	S	N/A	90.0	0.00	0.00	0.0	4220.0	0.0	94.0	unavailable	unavailable	0.000	unavailable	1.0	N/A	N/A	1.0	0.750	
horizontal pushoff	Hanson	N/A	1960	522	B24-3	NW	CJ	S	N/A	90.0	0.00	0.00	0.0	4220.0	0.0	100.0	unavailable	unavailable	0.000	unavailable	1.0	N/A	N/A	1.0	0.750	

Author1	Author 2	year	specimen name	specimen ID	concrete type	grossed- no. increases thickness e-pers	d6, diameter of stud	Hs, height of stud	num of studs/shear plane	length of stud	transverse spacing	length of flange	bf	A flange in contact	p	f y real (stud)	f y real (ply)	ply limited	fc'	fu (stud)	phi	Failure Shear/plane (load per plane)	Failure load per stud	v u (ultimate shear strength)	normal load % of shear load applied (if mentioned)	thickness of flange	Du/Actual	length of nail spacing in terms of ds	transverse spacing in terms of ds	max longitudinal spacing in terms of % slab	Hols		
																																l [in]	l [mm]
		1971	28 (J cone)	51	NW	yes	6.0	3.0	2	0.0	4.00	26.0	8.07	203.92	4.21	unknown	unknown	252.67	4780.0	70.30	285.57	51.00	33.59	263.02	0.0	0.56	57.72	1.34	0.00	5.33	0.0	4.00	
		1971	28 (J cone)	52	NW	yes	6.0	3.0	2	0.0	4.00	26.0	8.07	203.92	4.21	unknown	unknown	252.67	4780.0	70.30	285.57	51.00	25.00	298.30	0.0	0.56	56.39	1.34	0.00	5.33	0.0	4.00	
		1971	Cl-wt fine agg	53	AW	yes	6.0	3.0	4	12.00	4.00	26.0	8.07	203.92	8.42	unknown	unknown	505.33	4490.0	70.30	297.13	79.60	21.30	379.37	0.0	0.56	46.04	1.34	16.00	5.33	2.00	4.00	
		1971	Cl-wt fine agg	54	AW	yes	6.0	3.0	4	12.00	4.00	26.0	8.07	203.92	8.42	unknown	unknown	505.33	4490.0	70.30	297.13	79.60	21.30	406.16	0.0	0.56	46.21	1.34	16.00	5.33	2.00	4.00	
		1971	Cl-wt fine agg	55	AW	yes	6.0	3.0	4	12.00	4.00	26.0	8.07	203.92	8.42	unknown	unknown	505.33	4490.0	70.30	297.13	80.00	21.00	400.34	0.0	0.56	47.53	1.34	16.00	5.33	2.00	4.00	
		1971	Cl-wt fine agg	56	AW	yes	6.0	3.0	4	12.00	4.00	26.0	8.07	203.92	8.42	unknown	unknown	505.33	4490.0	70.30	297.13	86.40	21.60	411.78	0.0	0.56	46.89	1.34	16.00	5.33	2.00	4.00	
		1971	D-wt fine agg	57	AW	yes	6.0	3.0	4	12.00	4.00	26.0	8.07	203.92	8.42	unknown	unknown	505.33	4720.0	70.30	297.13	86.00	21.50	409.98	0.0	0.56	46.67	1.34	16.00	5.33	2.00	4.00	
		1971	D-wt fine agg	58	AW	yes	6.0	3.0	4	12.00	4.00	26.0	8.07	203.92	8.42	unknown	unknown	505.33	4720.0	70.30	297.13	88.80	22.20	452.22	0.0	0.56	50.25	1.34	16.00	5.33	2.00	4.00	
		1971	E-wt fine agg	59	AW	yes	6.0	3.0	4	12.00	4.00	26.0	8.07	203.92	8.42	unknown	unknown	505.33	3600.0	70.30	297.13	96.40	24.10	459.44	0.0	0.56	54.55	1.34	16.00	5.33	2.00	4.00	
		1971	E-wt fine agg	60	AW	yes	6.0	3.0	4	12.00	4.00	26.0	8.07	203.92	8.42	unknown	unknown	505.33	3600.0	70.30	297.13	90.00	23.00	438.47	0.0	0.56	52.06	1.34	16.00	5.33	2.00	4.00	
		1971	E-wt fine agg	61	AW	yes	6.0	3.0	4	12.00	4.00	26.0	8.07	203.92	8.42	unknown	unknown	505.33	3600.0	70.30	297.13	90.00	22.70	432.75	0.0	0.56	51.38	1.34	16.00	5.33	2.00	4.00	
		1971	E-wt fine agg	62	AW	yes	6.0	3.0	4	12.00	4.00	26.0	8.07	203.92	8.42	unknown	unknown	505.33	4300.0	70.30	297.13	86.40	21.60	411.78	0.0	0.56	46.89	1.34	16.00	5.33	2.00	4.00	
		1971	E-wt fine agg	63	AW	yes	6.0	3.0	4	12.00	4.00	26.0	8.07	203.92	8.42	unknown	unknown	505.33	4300.0	70.30	297.13	92.80	23.30	444.19	0.0	0.56	52.74	1.34	16.00	5.33	2.00	4.00	
		1971	E-wt fine agg	64	AW	yes	6.0	3.0	4	12.00	4.00	26.0	8.07	203.92	8.42	unknown	unknown	505.33	4300.0	70.30	297.13	97.60	24.40	465.16	0.0	0.56	52.73	1.34	16.00	5.33	2.00	4.00	
		1971	C	65	SW	yes	6.0	3.0	4	12.00	4.00	26.0	8.07	203.92	8.42	unknown	unknown	505.33	4280.0	70.30	297.13	78.40	19.60	373.65	0.0	0.56	44.37	1.34	16.00	5.33	2.00	4.00	
		1971	C	66	SW	yes	6.0	3.0	4	12.00	4.00	26.0	8.07	203.92	8.42	unknown	unknown	505.33	4280.0	70.30	297.13	78.40	19.20	366.02	0.0	0.56	43.46	1.34	16.00	5.33	2.00	4.00	
		1971	C	67	SW	yes	6.0	3.0	4	12.00	4.00	26.0	8.07	203.92	8.42	unknown	unknown	505.33	4280.0	70.30	297.13	71.20	17.80	339.34	0.0	0.56	40.29	1.34	16.00	5.33	2.00	4.00	
		1971	D	68	SW	yes	6.0	3.0	4	12.00	4.00	26.0	8.07	203.92	8.42	unknown	unknown	505.33	4280.0	70.30	297.13	84.40	21.10	400.98	0.0	0.56	43.29	1.34	16.00	5.33	2.00	4.00	
		1971	D	69	SW	yes	6.0	3.0	4	12.00	4.00	26.0	8.07	203.92	8.42	unknown	unknown	505.33	4280.0	70.30	297.13	90.00	22.90	429.94	0.0	0.56	50.93	1.34	16.00	5.33	2.00	4.00	
		1971	LF low [C]	70	SW	yes	6.0	3.0	4	12.00	4.00	26.0	8.07	203.92	8.42	unknown	unknown	505.33	4300.0	70.30	297.13	86.40	21.60	411.78	0.0	0.56	46.89	1.34	16.00	5.33	2.00	4.00	
		1971	LF low [C]	71	SW	yes	6.0	3.0	4	12.00	4.00	26.0	8.07	203.92	8.42	unknown	unknown	505.33	4300.0	70.30	297.13	74.80	18.70	356.50	0.0	0.56	42.33	1.34	16.00	5.33	2.00	4.00	
		1971	LF low [C]	72	SW	yes	6.0	3.0	4	12.00	4.00	26.0	8.07	203.92	8.42	unknown	unknown	505.33	3200.0	70.30	297.13	78.00	19.20	371.75	0.0	0.56	44.14	1.34	16.00	5.33	2.00	4.00	
		1971	LF low [C]	73	SW	yes	6.0	3.0	4	12.00	4.00	26.0	8.07	203.92	8.42	unknown	unknown	505.33	3200.0	70.30	297.13	78.00	19.20	375.56	0.0	0.56	44.59	1.34	16.00	5.33	2.00	4.00	
		1971	55** [58 Stud]	74	SW	yes	6.0	0.63	3.0	4	12.00	4.00	26.0	8.07	203.92	5.85	unknown	unknown	360.92	4000.0	70.20	403.58	62.80	13.70	299.30	0.0	0.56	51.17	1.12	19.20	6.40	2.00	4.80
		1971	55** [58 Stud]	75	SW	yes	6.0	0.63	3.0	4	12.00	4.00	26.0	8.07	203.92	5.85	unknown	unknown	360.92	4000.0	70.20	403.58	62.80	15.70	299.30	0.0	0.56	51.17	1.12	19.20	6.40	2.00	4.80
		1971	55** [58 Stud]	76	SW	yes	6.0	0.63	3.0	4	12.00	4.00	26.0	8.07	203.92	5.85	unknown	unknown	360.92	4000.0	70.20	403.58	62.80	17.00	324.03	0.0	0.56	55.41	1.12	19.20	6.40	2.00	4.80
		1971	2E [20mm]	77	SW	yes	6.0	0.75	3.0	2	0.0	4.00	26.0	8.07	203.92	4.21	unknown	unknown	252.67	4400.0	70.30	285.57	42.40	21.20	202.08	0.0	0.56	47.99	1.34	0.00	5.33	0.00	4.00
		1971	2E [20mm]	78	SW	yes	6.0	0.75	3.0	2	0.0	4.00	26.0	8.07	203.92	4.21	unknown	unknown	252.67	4400.0	70.30	285.57	46.20	23.10	201.90	0.0	0.56	52.29	1.34	0.00	5.33	0.00	4.00
		1971	2E [20mm]	79	SW	yes	6.0	0.75	3.0	2	0.0	4.00	26.0	8.07	203.92	4.21	unknown	unknown	252.67	4400.0	70.30	285.57	46.40	21.20	216.88	0.0	0.56	51.38	1.34	0.00	5.33	0.00	4.00
		1973	M&E-6	80	NW	no	unknown	0.75	4.00	2	0.0	2.50	22.00	5.00	110.00	8.03	unknown	unknown	481.95	4390.0	64.80	503.90	48.24	24.12	435.97	0.0	0.46	54.60	1.67	0.00	3.33	unknown	5.33
		1973	546.47	81	NW	no	unknown	0.75	4.00	2	0.0	2.50	22.00	5.00	110.00	8.03	unknown	unknown	481.95	4700.0	65.20	523.72	48.80	24.30	441.79	0.0	0.46	55.00	1.67	0.00	3.33	unknown	5.33
		1973	166.4	82	NW	no	unknown	0.75	4.00	2	0.0	2.50	22.00	5.00	110.00	8.03	unknown	unknown	481.95	4440.0	76.20	612.08	53.81	26.90	498.18	0.0	0.46	60.90	1.67	0.00	3.33	unknown	5.33
		1973	166.47	83	NW	no	unknown	0.75	4.00	2	0.0	2.50	22.00	5.00	110.00	8.03	unknown	unknown	481.95	4790.0	85.80	689.19	56.28	28.14	511.67	0.0	0.46	63.70	1.67	0.00	3.33	unknown	5.33
		1973	M&E-8	84	NW	no	unknown	0.75	4.00	2	0.0	2.50	22.00	5.00	110.00	8.03	unknown	unknown	481.95	8990.0	65.00	521.11	66.89	33.44	608.06	0.0	0.46	75.70	1.67	0.00	3.33	unknown	5.33
		1973	M&E-8	85	NW	no	unknown	0.75	4.00	2	0.0	2.50	22.00	5.00	110.00	8.03	unknown	unknown	481.95	3890.0	72.80	589.76	37.98	19.00	345.46	0.0	0.46	48.00	1.67	0.00	3.33	unknown	5.33
		1973	148.19	86	NW	no	unknown	0.75	4.00	2	0.0	2.50	22.00	5.00	110.00	8.03	unknown	unknown	481.95	3980.0	74.30	596.91	37.98	18.80	359.77	0.0	0.46	42.30	1.67	0.00	3.33	unknown	5.33
		1973	M&																														

Author1	Author2	year	specimenname	Specimen ID	concrete type	gressed- no. increases	slab thickness	di. diameter of stud	es, height of stud	Hs, height of stud	num of studs/ shear plane	longitudinal spacing	transvers length of spacing	bf	A flange in contact	p	f (stud)	fy (stud)	fy (real)	ply limited	fc'	f1 (stud)	f2 (stud)	Failure Shear/Plane (load per plane)	Failure load per stud	nu (ultimate strength)	normal load % applied (if load mentioned)	thickness of flange	Qy/Actual	longitudinal spacing in terms of ds	transvers spacing in terms of ds	max longt % spacing in terms of ds	Hols
	Stm			512-82	NV	no	7.87	6.10	4	3.84	20.28	10.04	20.28	10.04	20.28	10.04	66.14	888.89	158.88	39.72	76.66	0.00	0.5	52.11	1.79	20.00	4.00	1.25	6.20				
	Stm	2004	Stm	512-83	NV	no	7.87	6.10	4	3.84	20.28	10.04	20.28	10.04	20.28	10.04	66.14	888.89	158.88	39.72	76.66	0.00	0.5	52.11	1.79	20.00	4.00	1.25	6.20				
	Stm	2004	Stm	512-84	NV	no	7.87	6.10	4	3.84	20.28	10.04	20.28	10.04	20.28	10.04	66.14	888.89	158.88	39.72	76.66	0.00	0.5	52.11	1.79	20.00	4.00	1.25	6.20				
	Mix	2004	Mix	517-A1	NV	no	7.87	1.06	4	3.84	39.4	20.28	10.04	20.28	10.04	20.28	10.04	66.14	888.89	158.88	39.72	76.66	0.00	0.5	49.35	1.93	3.70	1.25	5.74				
	Mix	2004	Mix	517-A2	NV	no	7.87	1.06	4	3.84	39.4	20.28	10.04	20.28	10.04	20.28	10.04	66.14	888.89	158.88	39.72	76.66	0.00	0.5	49.35	1.93	3.70	1.25	5.74				
	Mix	2004	Mix	517-A3	NV	no	7.87	1.06	4	3.84	39.4	20.28	10.04	20.28	10.04	20.28	10.04	66.14	888.89	158.88	39.72	76.66	0.00	0.5	49.35	1.93	3.70	1.25	5.74				
	Stm	2004	Stm	517-A4	NV	no	8.66	1.06	4	3.84	39.4	20.28	10.04	20.28	10.04	20.28	10.04	66.14	888.89	158.88	39.72	76.66	0.00	0.5	52.74	1.93	3.70	1.14	5.74				
	Stm	2004	Stm	517-A5	NV	no	8.66	1.06	4	3.84	39.4	20.28	10.04	20.28	10.04	20.28	10.04	66.14	888.89	158.88	39.72	76.66	0.00	0.5	52.74	1.93	3.70	1.14	5.74				
	Stm	2004	Stm	517-A6	NV	no	8.66	1.06	4	3.84	39.4	20.28	10.04	20.28	10.04	20.28	10.04	66.14	888.89	158.88	39.72	76.66	0.00	0.5	52.74	1.93	3.70	1.14	5.74				
	Concrete	2004	Concrete	513-A1	NV	no	7.87	1.18	4	3.84	39.4	20.28	10.04	20.28	10.04	20.28	10.04	66.14	888.89	158.88	39.72	76.66	0.00	0.5	29.18	2.14	8.33	3.33	1.25	5.17			
	Concrete	2004	Concrete	513-A2	NV	no	7.87	1.18	4	3.84	39.4	20.28	10.04	20.28	10.04	20.28	10.04	66.14	888.89	158.88	39.72	76.66	0.00	0.5	29.18	2.14	8.33	3.33	1.25	5.17			
	Mix	2004	Mix	513-A3	NV	no	7.87	1.18	4	3.84	39.4	20.28	10.04	20.28	10.04	20.28	10.04	66.14	888.89	158.88	39.72	76.66	0.00	0.5	30.33	2.14	8.33	3.33	1.25	5.17			
	Mix	2004	Mix	513-A4	NV	no	7.87	1.18	4	3.84	39.4	20.28	10.04	20.28	10.04	20.28	10.04	66.14	888.89	158.88	39.72	76.66	0.00	0.5	30.33	2.14	8.33	3.33	1.25	5.17			
	Stm	2004	Stm	513-A5	NV	no	8.66	1.18	4	3.84	39.4	20.28	10.04	20.28	10.04	20.28	10.04	66.14	888.89	158.88	39.72	76.66	0.00	0.5	46.71	2.14	8.33	3.33	1.14	5.17			
	Stm	2004	Stm	513-A6	NV	no	8.66	1.18	4	3.84	39.4	20.28	10.04	20.28	10.04	20.28	10.04	66.14	888.89	158.88	39.72	76.66	0.00	0.5	46.71	2.14	8.33	3.33	1.14	5.17			
	Concrete	2004	Concrete	513-A7	NV	yes	9.06	0.87	3.94	2	unrein	0.00	17.00	4.02	69.27	17.38	54.08	926.64	950.64	650.2	70.15	1.233.11	75.42	31.71	1.0445	0.00	0.39	62.85	2.22	unrein	0.00	unrein	4.50
	Concrete	2004	Concrete	513-A8	NV	yes	9.06	0.87	3.94	2	unrein	0.00	17.00	4.02	69.27	17.38	54.08	926.64	950.64	650.2	70.15	1.233.11	75.42	31.71	1.0445	0.00	0.39	62.85	2.22	unrein	0.00	unrein	4.50
	Concrete	2004	Concrete	513-A9	NV	yes	9.06	0.87	3.94	2	unrein	0.00	17.00	4.02	69.27	17.38	54.08	926.64	950.64	650.2	70.15	1.233.11	75.42	31.71	1.0445	0.00	0.39	62.85	2.22	unrein	0.00	unrein	4.50
	Concrete	2004	Concrete	513-A10	NV	yes	9.06	0.87	3.94	2	unrein	0.00	17.00	4.02	69.27	17.38	54.08	926.64	950.64	650.2	70.15	1.233.11	75.42	31.71	1.0445	0.00	0.39	62.85	2.22	unrein	0.00	unrein	4.50
	Concrete	2004	Concrete	513-A11	NV	yes	9.06	0.87	3.94	2	unrein	0.00	17.00	4.02	69.27	17.38	54.08	926.64	950.64	650.2	70.15	1.233.11	75.42	31.71	1.0445	0.00	0.39	62.85	2.22	unrein	0.00	unrein	4.50
	Concrete	2004	Concrete	513-A12	NV	yes	9.06	0.87	3.94	2	unrein	0.00	17.00	4.02	69.27	17.38	54.08	926.64	950.64	650.2	70.15	1.233.11	75.42	31.71	1.0445	0.00	0.39	62.85	2.22	unrein	0.00	unrein	4.50
	Concrete	2004	Concrete	513-A13	NV	yes	9.06	0.87	3.94	2	unrein	0.00	17.00	4.02	69.27	17.38	54.08	926.64	950.64	650.2	70.15	1.233.11	75.42	31.71	1.0445	0.00	0.39	62.85	2.22	unrein	0.00	unrein	4.50
	Concrete	2004	Concrete	513-A14	NV	yes	9.06	0.87	3.94	2	unrein	0.00	17.00	4.02	69.27	17.38	54.08	926.64	950.64	650.2	70.15	1.233.11	75.42	31.71	1.0445	0.00	0.39	62.85	2.22	unrein	0.00	unrein	4.50
	Concrete	2004	Concrete	513-A15	NV	yes	9.06	0.87	3.94	2	unrein	0.00	17.00	4.02	69.27	17.38	54.08	926.64	950.64	650.2	70.15	1.233.11	75.42	31.71	1.0445	0.00	0.39	62.85	2.22	unrein	0.00	unrein	4.50
	Concrete	2004	Concrete	513-A16	NV	yes	9.06	0.87	3.94	2	unrein	0.00	17.00	4.02	69.27	17.38	54.08	926.64	950.64	650.2	70.15	1.233.11	75.42	31.71	1.0445	0.00	0.39	62.85	2.22	unrein	0.00	unrein	4.50
	Mix	1994	An	NSC11	NV	yes	5.91	0.75	2.95	4	3.84	5.91	22.64	11.81	267.38	6.57	60.63	388.59	384.47	448.8	75.27	489.90	103.41	35.86	386.7	0.00	0.75	46.83	1.00	13.16	7.88	1.67	3.95
	Mix	1994	An	NSC12	NV	yes	5.91	0.75	2.95	4	3.84	5.91	22.64	11.81	267.38	6.57	60.63	388.59	384.47	448.8	75.27	489.90	103.41	35.86	386.7	0.00	0.75	46.83	1.00	13.16	7.88	1.67	3.95
	Mix	1994	An	NSC21	NV	yes	5.91	0.75	2.95	4	3.84	5.91	22.64	11.81	267.38	6.57	60.63	388.59	384.47	448.8	75.27	489.90	103.41	35.86	386.7	0.00	0.75	46.83	1.00	13.16	7.88	1.67	3.95
	Mix	1994	An	NSC22	NV	yes	5.91	0.75	2.95	4	3.84	5.91	22.64	11.81	267.38	6.57	60.63	388.59	384.47	448.8	75.27	489.90	103.41	35.86	386.7	0.00	0.75	46.83	1.00	13.16	7.88	1.67	3.95
	Mix	1994	An	NSC11	NV	yes	5.91	0.75	2.95	4	3.84	5.91	22.64	11.81	267.38	6.57	60.63	388.59	384.47	448.8	75.27	489.90	103.41	35.86	386.7	0.00	0.75	46.83	1.00	13.16	7.88	1.67	3.95
	Mix	1994	An	NSC12	NV	yes	5.91	0.75	2.95	4	3.84	5.91	22.64	11.81	267.38	6.57	60.63	388.59	384.47	448.8	75.27	489.90	103.41	35.86	386.7	0.00	0.75	46.83	1.00	13.16	7.88	1.67	3.95
	Mix	1994	An	NSC21	NV	yes	5.91	0.75	2.95	4	3.84	5.91	22.64	11.81	267.38	6.57	60.63	388.59	384.47	448.8	75.27	489.90	103.41	35.86	386.7	0.00	0.75	46.83	1.00	13.16	7.88	1.67	3.95
	Mix	1994	An	NSC22	NV	yes	5.91	0.75	2.95	4	3.84	5.91	22.64	11.81	267.38	6.57	60.63	388.59	384.47	448.8	75.27	489.90	103.41	35.86	386.7	0.00	0.75	46.83	1.00	13.16	7.88	1.67	3.95
	Stm	2004	Stm	SP-1	NV	yes	5.91	0.87	3.94	4	3.84	39.4	23.09	10.24	235.76	10.00	64.54	666.22	593.81	719.4	76.87	788.46	205.92	51.48	873.47	0.00	0.69	87.37	1.16	11.36	4.55	1.67	4.55
	Stm	2004	Stm	SP-2	NV	yes	5.91	0.87	3.94	4	3.84	39.4	23.09	10.24	235.76	10.00	64.54	666.22	593.81	719.4	76.87	788.46	205.92	51.48	873.47	0.00	0.69	87.37	1.16	11.36	4.55	1.67	4.55
	Stm	2004	Stm	SP-3	NV	yes	5.91	0.87	3.94	4	3.84	39.4	23.09	10.24	235.76	10.00	64.54	666.22	593.81	719.4	76.87	788.46	205.92	51.48	873.47	0.00	0.69	87.37	1.16	11.36	4.55	1.67	4.55
	Stm	2004	Stm	SP-2	NV	yes	9.84	0.87	5.91	4	13.78	39.4	36.81	10.55	388.40	6.07	64.54	391.64															

Author1	Author 2	year	specimen name	Specimen ID	concrete type	grossed-up no. of piers	slab thickness	height of stud	ds, diameter of stud	Hs, height of stud	num of studs/shear plane	longitudinal spacing	transverse spacing	length of flange	A flange in contact	p	fy real (stud)	fy real limited	fc' (stud)	fu (stud)	Failure Shear/plane (load per plane)	Failure load per stud	vu (ultimate shear strength)	normal load % of shear load applied (if mentioned)	thickness of flange	Du/Actual	longitudinal spacing in terms of ds	transverse spacing in terms of ds	Max long term spacing	
Others	N/A	1980	855	331	NW	no	5.00	0.75	3.94	1	0.00	0.00	unknown	unknown	unknown	unknown	unknown	429.5	101.95	unknown	23.90	unknown	0.00	unknown	60.04	unknown	0.00	0.00	5.36	
Others	N/A	1980	856	332	NW	no	5.00	0.75	3.94	1	0.00	0.00	unknown	unknown	unknown	unknown	unknown	429.5	101.95	unknown	31.92	unknown	0.00	unknown	72.94	unknown	0.00	0.00	5.36	
Shop	Singhlon	1968	4A	303	NW	yes	unknown	0.90	4.00	4	unknown	unknown	unknown	unknown	unknown	unknown	unknown	338.00	70.79	unknown	57.60	unknown	0.00	unknown	73.34	unknown	unknown	unknown	8.00	
Shop	Singhlon	1968	4B	304	NW	yes	unknown	0.90	4.00	4	unknown	unknown	unknown	unknown	unknown	unknown	unknown	338.00	70.79	unknown	57.60	unknown	0.00	unknown	70.79	unknown	unknown	unknown	8.00	
Shop	Singhlon	1968	5A	305	NW	yes	unknown	0.68	3.94	4	unknown	unknown	unknown	unknown	unknown	unknown	unknown	338.00	68.12	unknown	50.20	unknown	0.00	unknown	71.58	unknown	unknown	unknown	6.30	
Shop	Singhlon	1968	5B	306	NW	yes	unknown	0.68	3.94	4	unknown	unknown	unknown	unknown	unknown	unknown	unknown	338.00	68.12	unknown	50.20	unknown	0.00	unknown	73.34	unknown	unknown	unknown	6.30	
Shop	Singhlon	1968	6A	307	NW	yes	unknown	0.75	3.90	4	unknown	unknown	unknown	unknown	unknown	unknown	unknown	338.00	69.34	unknown	138.00	unknown	0.00	unknown	72.43	unknown	unknown	unknown	5.30	
Shop	Singhlon	1968	6B	308	NW	yes	unknown	0.75	3.90	4	unknown	unknown	unknown	unknown	unknown	unknown	unknown	338.00	69.34	unknown	138.00	unknown	0.00	unknown	73.55	unknown	unknown	unknown	5.30	
Shop	Singhlon	1968	6F	309	NW	yes	unknown	0.75	3.90	4	unknown	unknown	unknown	unknown	unknown	unknown	unknown	338.00	69.34	unknown	138.00	unknown	0.00	unknown	73.55	unknown	unknown	unknown	5.30	
Shop	Singhlon	1968	6G	310	NW	yes	unknown	0.75	3.90	4	unknown	unknown	unknown	unknown	unknown	unknown	unknown	338.00	69.34	unknown	138.00	unknown	0.00	unknown	73.55	unknown	unknown	unknown	5.30	
Shop	Singhlon	1968	7H	311	NW	yes	unknown	0.88	8.44	4	unknown	unknown	unknown	unknown	unknown	unknown	unknown	450.00	73.34	unknown	126.00	unknown	0.00	unknown	71.30	unknown	unknown	unknown	9.33	
concrete	Marieston	1967	53	312	NW	no	6.00	0.75	4.00	2	0.00	3.75	16.00	5.00	80.00	11.04	unknown	450.00	76.97	unknown	130.00	unknown	0.00	unknown	74.84	unknown	unknown	unknown	9.68	
concrete	Marieston	1967	54	313	NW	no	9.00	0.75	4.00	2	0.00	3.75	16.00	5.00	80.00	11.04	unknown	450.00	76.97	unknown	39.40	unknown	0.00	0.95	40.87	1.36	0.00	5.00	0.00	5.33
concrete	Marieston	1967	55	314	NW	no	9.00	0.75	4.00	2	0.00	3.75	16.00	5.00	80.00	11.04	unknown	450.00	76.97	unknown	42.00	unknown	0.00	0.95	47.53	1.36	0.00	5.00	0.00	5.33
concrete	Marieston	1967	56	315	NW	no	9.00	0.75	4.00	2	0.00	3.75	16.00	5.00	80.00	11.04	unknown	450.00	76.97	unknown	48.68	unknown	0.00	0.95	56.23	1.36	0.00	5.00	0.00	5.33
concrete	Marieston	1967	58	316	NW	no	9.00	0.75	4.00	2	0.00	3.75	16.00	5.00	80.00	11.04	unknown	450.00	76.97	unknown	47.80	unknown	0.00	0.95	54.10	1.36	0.00	5.00	0.00	5.33
concrete	Marieston	1967	511	317	NW	no	9.00	0.75	4.00	2	0.00	3.75	16.00	5.00	80.00	11.04	unknown	450.00	76.97	unknown	44.00	unknown	0.00	0.95	49.80	1.36	0.00	5.00	0.00	5.33
concrete	Marieston	1967	516	318	NW	no	9.00	0.75	4.00	2	0.00	3.75	16.00	5.00	80.00	11.04	unknown	450.00	76.97	unknown	42.38	unknown	0.00	0.95	51.25	1.36	0.00	5.00	0.00	5.33
concrete	Marieston	1967	519	319	NW	no	9.00	0.75	4.00	2	0.00	3.75	16.00	5.00	80.00	11.04	unknown	450.00	76.97	unknown	42.38	unknown	0.00	0.95	51.25	1.36	0.00	5.00	0.00	5.33
concrete	Marieston	1967	S22	320	NW	no	9.00	0.75	4.00	2	0.00	3.75	16.00	5.00	80.00	11.04	unknown	450.00	76.97	unknown	42.08	unknown	0.00	0.95	47.62	1.36	0.00	5.00	0.00	5.33
concrete	Marieston	1967	S26	321	NW	no	9.00	0.75	4.00	2	0.00	3.75	16.00	5.00	80.00	11.04	unknown	450.00	76.97	unknown	39.00	unknown	0.00	0.95	44.14	1.36	0.00	5.00	0.00	5.33
concrete	Marieston	1967	S29	322	NW	no	9.00	0.75	4.00	2	0.00	3.75	16.00	5.00	80.00	11.04	unknown	450.00	76.97	unknown	41.00	unknown	0.00	0.95	46.40	1.36	0.00	5.00	0.00	5.33
concrete	Marieston	1964	P41	323	NW	no	6.00	0.75	4.00	2	0.00	2.50	16.00	6.00	96.00	9.20	unknown	552.23	412.00	67.60	622.18	unknown	25.00	0.72	56.59	1.06	0.00	3.33	0.00	5.33
concrete	Marieston	1964	P42	324	NW	no	6.00	0.75	4.00	2	0.00	2.50	16.00	6.00	96.00	9.20	unknown	552.23	412.00	67.60	622.18	unknown	24.60	0.72	55.68	1.06	0.00	3.33	0.00	5.33
concrete	Marieston	1964	P43	325	NW	no	6.00	0.75	4.00	2	0.00	2.50	16.00	6.00	96.00	9.20	unknown	552.23	412.00	67.60	622.18	unknown	24.60	0.72	55.68	1.06	0.00	3.33	0.00	5.33
concrete	Marieston	1964	P44	326	NW	no	6.00	0.75	4.00	2	0.00	2.50	16.00	6.00	96.00	9.20	unknown	552.23	412.00	67.60	622.18	unknown	24.60	0.72	55.68	1.06	0.00	3.33	0.00	5.33
concrete	Marieston	1964	P45	327	NW	no	6.00	0.75	4.00	2	0.00	2.50	16.00	6.00	96.00	9.20	unknown	552.23	412.00	67.60	622.18	unknown	24.60	0.72	55.68	1.06	0.00	3.33	0.00	5.33
concrete	Marieston	1964	P81	328	NW	no	6.00	0.75	4.00	2	0.00	2.50	16.00	6.00	96.00	9.20	unknown	552.23	412.00	67.60	622.18	unknown	24.60	0.72	55.68	1.06	0.00	3.33	0.00	5.33
concrete	Marieston	1964	P81	329	NW	no	6.00	0.75	4.00	2	0.00	2.50	16.00	6.00	96.00	9.20	unknown	552.23	412.00	67.60	622.18	unknown	24.60	0.72	55.68	1.06	0.00	3.33	0.00	5.33
concrete	Marieston	1964	P81	330	NW	no	6.00	0.75	4.00	2	0.00	2.50	16.00	6.00	96.00	9.20	unknown	552.23	412.00	67.60	622.18	unknown	24.60	0.72	55.68	1.06	0.00	3.33	0.00	5.33
concrete	Marieston	1964	P81	331	NW	no	6.00	0.75	4.00	2	0.00	2.50	16.00	6.00	96.00	9.20	unknown	552.23	412.00	67.60	622.18	unknown	24.60	0.72	55.68	1.06	0.00	3.33	0.00	5.33
concrete	Marieston	1964	P81	332	NW	no	6.00	0.75	4.00	2	0.00	2.50	16.00	6.00	96.00	9.20	unknown	552.23	412.00	67.60	622.18	unknown	24.60	0.72	55.68	1.06	0.00	3.33	0.00	5.33
concrete	Marieston	1964	P81	333	NW	no	6.00	0.75	4.00	2	0.00	2.50	16.00	6.00	96.00	9.20	unknown	552.23	412.00	67.60	622.18	unknown	24.60	0.72	55.68	1.06	0.00	3.33	0.00	5.33
concrete	Marieston	1964	P81	334	NW	no	6.00	0.75	4.00	2	0.00	2.50	16.00	6.00	96.00	9.20	unknown	552.23	412.00	67.60	622.18	unknown	24.60	0.72	55.68	1.06	0.00	3.33	0.00	5.33
concrete	Marieston	1964	P81	335	NW	no	6.00	0.75	4.00	2	0.00	2.50	16.00	6.00	96.00	9.20	unknown	552.23	412.00	67.60	622.18	unknown	24.60	0.72	55.68	1.06	0.00	3.33	0.00	5.33
concrete	Marieston	1964	P81	336	NW	no	6.00	0.75	4.00	2	0.00	2.50	16.00	6.00	96.00	9.20	unknown	552.23	412.00	67.60	622.18	unknown	24.60	0.72	55.68	1.06	0.00	3.33	0.00	5.33
concrete	Marieston	1964	P81	337	NW	no	6.00	0.75	4.00	2	0.00	2.50	16.00	6.00	96.00	9.20	unknown	552.23	412.00	67.60	622.18	unknown	24.60	0.72	55.68	1.06	0.00	3.33	0.00	5.33
concrete	Marieston	1964	P81	338	NW	no	6.00	0.75	4.00	2	0.00	2.50	16.00	6.00	96.00	9.20	unknown	552.23	412.00	67.60	622.18	unknown	24.60	0.72	55.68	1.06	0.00	3.33	0.00	5.33
concrete	Marieston	1964	P81	339	NW	no	6.00	0.75	4.00	2	0.00	2.50	16.00	6.00	96.00	9.20	unknown	552.23	412.00	67.60	622.18	unknown	24.60	0.72	55.68	1.06	0.00	3.33	0.00	5.33
concrete	Marieston	1964	P81	340	NW	no	6.00	0.75	4.00	2	0.00	2.50	16.00	6.00	96.00	9.20	unknown	552.23	412.00	67.60	622.18	unknown	24.60	0.72	55.68	1.06	0.00	3.33	0.00	5.33
concrete	Marieston	1964	P81	341	NW	no	6.00	0.75	4.00	2	0.00	2.50	16.00	6.00	96.00	9.20	unknown	552.23	412.00	67.60	622.18	unknown	24.60	0.72	55.68	1.06	0.00	3.33	0.00	5.33
concrete	Marieston	1964	P81	342	NW	no	6.00	0.75	4.00	2	0.00	2.50	16.00	6.00	96.00	9.20	unknown	552.23	412.00	67.60	622.18	unknown	24.60	0.72	55.68	1.06	0.00	3.33	0.00	5.33
concrete	Marieston	1964	P81	343	NW	no	6.00	0.75	4.00	2	0.00	2.50	16.00	6.00	96.00	9.20	unknown	552.23	412.00	67.60	622.18	unknown	24.60	0.72	55.68	1.06	0.00	3.33	0.00	5.33
concrete	Marieston	1964	P81	344	NW	no	6.00	0.75	4.00	2	0.00	2.50	16.00	6.00	96.00	9.20	unknown	552.23	412.00	67.60	622.18	unknown	24.60	0.72	55.68	1.06	0.00	3.33	0.00	5.33
concrete	Marieston	1964	P81	345	NW	no	6.00	0.75	4.00	2	0.00	2.50	16.00	6.00	96.00	9.20	unknown	552.23	412.00	67.60	622.18	unknown	24.60	0.72	55.68	1.06	0.00	3.33	0.00	5.33
concrete	Marieston	1964	P81	346	NW	no	6.00	0.75	4.00	2	0.00	2.50	16.00	6.00	96.00	9.20	unknown	552.23	412.00	67.60	622.18	unknown	24.60	0.72	55.68	1.06	0.00	3.33	0.00	5.33
concrete	Marieston	1964	P81	347																										

Author1	Author 2	year	specimen name	Specimen ID	concrete type	grossed- slab no. (upgrades)	di- diameter of stud	Hs, height of stud	num of studs/ shear plane	longitudi- nal spacing	transvers length of spacing	A flange in contact	p	fy real (stud)	fy real limited	fc' (stud)	Failure Shear/Plane (load per plane)	Failure load per stud	u (ultimate shear strength)	normal load % applied (if load mentioned)	thickness of flange	Qy/Actual	longitudi- nal spacing in terms of ds	transvers spacing in terms of ds	max longt- e spacing in terms of ds	HoVs							
Daham	N/A	1988	I1(184)	401	AIW	no	6.0	0.75	3.50	2	0.0	400	17.0	8.13	138.13	6.40	unknown	unknown	383.83	530.0	72.0	481.22	47.20	23.60	341.72	0.0	0.69	59.42	1.09	0.00	5.33	0.00	4.67
Balfry	N/A	1985	I4(443)	427	SIW	unknown	6.0	0.50	2.69	2	0.0	400	unknown	unknown	unknown	unknown	27.60	13.80	unknown	unknown	71.90	67.80	unknown	70.28	unknown	0.00	8.00	0.00	5.38	0.00	0.00	0.00	5.38
Daham	N/A	1988	I3(184)	403	AIW	no	6.0	0.63	3.69	2	0.0	400	17.0	8.13	138.13	4.44	unknown	unknown	266.63	0.00	0.69	58.67	0.91	0.00	6.40	0.00	5.90	0.00	0.00	0.00	0.00	0.00	5.90
Daham	N/A	1988	I4(184)	404	AIW	no	6.0	0.63	3.69	2	0.0	400	17.0	8.13	138.13	4.44	unknown	unknown	265.54	0.00	0.69	60.63	0.91	0.00	6.40	0.00	5.90	0.00	0.00	0.00	0.00	0.00	5.90
Daham	N/A	1988	I5(184)	405	AIW	no	6.0	0.63	3.69	2	0.0	400	17.0	8.13	138.13	4.44	unknown	unknown	265.54	0.00	0.69	58.70	0.91	0.00	6.40	0.00	5.90	0.00	0.00	0.00	0.00	0.00	5.90
Daham	N/A	1988	I6(184)	406	AIW	no	6.0	0.63	3.69	2	0.0	400	17.0	8.13	138.13	4.44	unknown	unknown	265.54	0.00	0.69	58.70	0.91	0.00	6.40	0.00	5.90	0.00	0.00	0.00	0.00	0.00	5.90
Bahwin	N/A	1970	I3(42)	407	AIW	yes	6.0	0.63	3.69	2	0.0	400	17.0	8.13	138.13	4.44	5120	231.1	290.11	490.0	64.20	285.20	34.40	16.20	24.57	0.00	0.69	52.80	0.91	0.00	6.40	0.00	5.90
Balfry	N/A	1985	I3(42)	408	AIW	yes	6.0	0.63	3.69	2	0.0	400	17.0	8.13	138.13	4.44	5120	231.1	290.11	490.0	64.20	285.20	33.00	16.50	24.93	0.00	0.69	57.78	0.91	0.00	6.40	0.00	5.90
Balfry	N/A	1985	I3(42)	409	SIW	unknown	6.0	0.63	3.69	2	0.0	400	unknown	unknown	unknown	unknown	333.0	64.20	unknown	unknown	26.40	13.20	unknown	43.03	unknown	0.00	6.40	0.00	5.90	0.00	0.00	0.00	5.90
Bahwin	N/A	1970	I3(42)	410	AIW	yes	6.0	0.63	3.69	2	0.0	400	17.0	8.13	138.13	4.44	5120	231.1	290.11	490.0	64.20	285.20	30.00	15.00	27.17	0.00	0.69	48.95	0.91	0.00	6.40	0.00	5.90
Bahwin	N/A	1970	I3(42)	411	AIW	yes	6.0	0.63	3.69	2	0.0	400	17.0	8.13	138.13	4.44	5120	231.1	290.11	490.0	64.20	285.20	37.40	18.70	27.97	0.00	0.69	60.95	0.91	0.00	6.40	0.00	5.90
Daham	N/A	1988	I1(184)	412	AIW	no	6.0	0.50	3.69	2	0.0	400	17.0	8.13	138.13	2.84	unknown	unknown	170.58	unknown	78.30	72.61	17.20	8.60	124.52	0.00	0.69	48.80	0.73	0.00	8.00	0.00	7.28
Daham	N/A	1988	I2(184)	413	AIW	no	6.0	0.50	3.69	2	0.0	400	17.0	8.13	138.13	2.84	unknown	unknown	170.58	unknown	78.30	72.61	17.20	8.60	124.52	0.00	0.69	48.80	0.73	0.00	8.00	0.00	7.28
Daham	N/A	1988	I3(184)	414	AIW	no	6.0	0.50	3.69	2	0.0	400	17.0	8.13	138.13	2.84	unknown	unknown	170.58	unknown	78.30	72.61	17.20	8.60	124.52	0.00	0.69	48.80	0.73	0.00	8.00	0.00	7.28
Daham	N/A	1988	I4(184)	415	AIW	yes	6.0	0.50	3.69	2	0.0	400	17.0	8.13	138.13	2.84	unknown	unknown	170.58	unknown	78.30	72.61	17.20	8.60	124.52	0.00	0.69	48.80	0.73	0.00	8.00	0.00	7.28
Daham	N/A	1988	I5(184)	416	AIW	yes	6.0	0.50	3.69	2	0.0	400	17.0	8.13	138.13	2.84	unknown	unknown	170.58	unknown	78.30	72.61	17.20	8.60	124.52	0.00	0.69	48.80	0.73	0.00	8.00	0.00	7.28
Daham	N/A	1988	I6(184)	417	AIW	yes	6.0	0.50	3.69	2	0.0	400	17.0	8.13	138.13	2.84	unknown	unknown	170.58	unknown	78.30	72.61	17.20	8.60	124.52	0.00	0.69	48.80	0.73	0.00	8.00	0.00	7.28
Bahwin	N/A	1970	I4(42)	418	AIW	yes	6.0	0.50	3.69	2	0.0	400	17.0	8.13	138.13	2.84	6680	189.2	170.58	780.0	78.30	72.61	23.20	11.60	167.98	0.00	0.69	50.08	0.73	0.00	8.00	0.00	7.28
Bahwin	N/A	1970	I4(42)	419	AIW	yes	6.0	0.50	3.69	2	0.0	400	17.0	8.13	138.13	2.84	6680	189.2	170.58	780.0	78.30	72.61	24.80	12.40	179.55	0.00	0.69	61.15	0.73	0.00	8.00	0.00	7.28
Bahwin	N/A	1970	I4(42)	420	AIW	yes	6.0	0.50	3.69	2	0.0	400	17.0	8.13	138.13	2.84	6680	189.2	170.58	780.0	78.30	72.61	24.80	12.40	179.55	0.00	0.69	61.15	0.73	0.00	8.00	0.00	7.28
Balfry	N/A	1985	I4(44)	421	SIW	unknown	6.0	0.50	3.69	2	0.0	400	unknown	unknown	unknown	unknown	330.0	78.30	unknown	unknown	21.40	10.70	unknown	35.99	unknown	0.00	8.00	0.00	7.28	0.00	0.00	0.00	7.28
Balfry	N/A	1985	I4(44)	422	SIW	unknown	6.0	0.50	3.69	2	0.0	400	unknown	unknown	unknown	unknown	330.0	78.30	unknown	unknown	21.40	10.70	unknown	35.99	unknown	0.00	8.00	0.00	7.28	0.00	0.00	0.00	7.28
Zhao	N/A	1994	I1.0	423	NW	unknown	unknown	0.87	1.97	1	0.0	0.00	unknown	unknown	unknown	unknown	13.30	13.30	unknown	0.00	unknown	23.58	unknown	0.00	0.00	unknown	0.00	0.00	unknown	2.27	0.00	0.00	2.27
Zhao	N/A	1994	I3.0	424	NW	unknown	unknown	0.87	1.97	1	0.0	0.00	unknown	unknown	unknown	unknown	313.0	61.90	unknown	0.00	unknown	30.05	unknown	0.00	0.00	unknown	0.00	0.00	unknown	2.72	0.00	0.00	2.72
Zhao	N/A	1994	I4.0	425	NW	unknown	unknown	0.87	2.56	1	0.0	0.00	unknown	unknown	unknown	unknown	313.0	61.90	unknown	0.00	unknown	30.22	unknown	0.00	0.00	unknown	0.00	0.00	unknown	2.72	0.00	0.00	2.72
Zhao	N/A	1994	I5.0	426	NW	unknown	unknown	0.87	2.56	1	0.0	0.00	unknown	unknown	unknown	unknown	313.0	61.90	unknown	0.00	unknown	30.09	unknown	0.00	0.00	unknown	0.00	0.00	unknown	2.96	0.00	0.00	2.96
Zhao	N/A	1994	I6.0	427	NW	unknown	unknown	0.87	2.56	1	0.0	0.00	unknown	unknown	unknown	unknown	313.0	61.90	unknown	0.00	unknown	30.99	unknown	0.00	0.00	unknown	0.00	0.00	unknown	2.96	0.00	0.00	2.96
Balfry	N/A	1985	I6(44)	428	NW	unknown	6.0	0.75	2.50	2	0.0	400	unknown	unknown	unknown	unknown	330.0	62.00	unknown	0.00	unknown	48.80	unknown	0.00	5.38	0.00	3.33	0.00	0.00	0.00	3.33		
Balfry	N/A	1985	I6(44)	429	NW	unknown	6.0	0.75	2.50	2	0.0	400	unknown	unknown	unknown	unknown	330.0	62.00	unknown	0.00	unknown	48.80	unknown	0.00	5.38	0.00	3.33	0.00	0.00	0.00	3.33		
Balfry	N/A	1985	I6(42)	431	NW	unknown	6.0	0.50	1.69	2	0.0	400	unknown	unknown	unknown	unknown	630.0	62.00	unknown	0.00	unknown	48.40	unknown	0.00	24.20	unknown	0.00	4.57	0.00	0.00	4.57	0.00	4.57
Balfry	N/A	1985	I6(42)	432	NW	unknown	6.0	0.50	1.69	2	0.0	400	unknown	unknown	unknown	unknown	630.0	62.00	unknown	0.00	unknown	48.40	unknown	0.00	24.20	unknown	0.00	4.57	0.00	0.00	4.57	0.00	4.57
Balfry	N/A	1985	I6(42)	433	NW	unknown	6.0	0.50	1.69	2	0.0	400	unknown	unknown	unknown	unknown	630.0	62.00	unknown	0.00	unknown	48.40	unknown	0.00	24.20	unknown	0.00	4.57	0.00	0.00	4.57	0.00	4.57
Balfry	N/A	1985	I6(42)	434	NW	unknown	6.0	0.50	1.69	2	0.0	400	unknown	unknown	unknown	unknown	630.0	62.00	unknown	0.00	unknown	48.40	unknown	0.00	24.20	unknown	0.00	4.57	0.00	0.00	4.57	0.00	4.57
Balfry	N/A	1985	I6(42)	435	NW	unknown	6.0	0.50	1.69	2	0.0	400	unknown	unknown	unknown	unknown	630.0	62.00	unknown	0.00	unknown	48.40	unknown	0.00	24.20	unknown	0.00	4.57	0.00	0.00	4.57	0.00	4.57
Steele	N/A	1967	30-C	436	NW	unknown	6.0	0.75	2.63	2	0.0	400	unknown	unknown	unknown	unknown	330.0	76.20	unknown	0.00	unknown	34.50	unknown	0.00	17.25	unknown	0.00	5.34	0.00	3.50	0.00	3.50	
Steele	N/A	1967	30-C	437	NW	unknown	6.0	0.75	2.63	2	0.0	400	unknown	unknown	unknown	unknown	330.0	76.20	unknown	0.00	unknown	34.50	unknown	0.00	17.25	unknown	0.00	5.34	0.00	3.50	0.00	3.50	
Steele	N/A	1967	C63C	438	NW	yes	6.0	0.88	3.50	2	0.0	400	unknown	unknown	unknown	unknown	285.0	76.20	unknown	0.00	unknown	51.60	unknown	0.00	25.80	unknown	0.00	5.94	0.00	3.50	0.00	3.50	
Bahwin	N/A	1970	I7(44)	439	NW	yes	6.0	0.88	3.50	2	0.0	400	17.0	8.13	138.13	8.71	5050	439.70	490.0	30.00	60.00	37.42	60.00	484.38	0.00	0.69	49.83	1.27	0.00	4.57	0.00	4.00	
Bahwin	N/A	1970	I7(44)	440	NW	yes	6.0	0.88	3.50	2	0.0	400	17.0	8.13	138.13	8.71	5050	439.70	490.0	30.00	60.00	37.42	60.00	484.38	0.00	0.69	49.83	1.27	0.00	4.57	0.00	4.00	
Daham	N/A	1988	I7(44)	441	NW	no	6.0	0.88	3.50	2	0.0	400	17.0	8.13	138.13	8.71	5050	439.70	490.0	30.00	60.00	37.42	60.00	484.38	0.00	0.69	53.55	1.27	0.00	4.57	0.00	4.00	
Zhao	N/A	1994	I7.0	442	NW	unknown	unknown	0.87	3.54	1	0.0	0.00	unknown	unknown	unknown	unknown	313.0	61.90	unknown	0.00	unknown	50.59	unknown	0.00	0.00	unknown	0.00	0.00	unknown	4.00	0.00	4.00	
Zhao	N/A	1994	I8.0	443	NW	unknown	unknown	0.87	3.54	1	0.0	0.00	unknown	unknown	unknown	unknown	313.0	61.90	unknown	0.00	unknown	49.81	unknown	0.00	0.00	unknown	0.00	0.00	unknown	4.00	0.00	4.00	
Zhao	N/A	1994	I9.0	444	NW	unknown	unknown	0.87	3.54	1	0.0	0.00	unknown	unknown	unknown	unknown	313.0	6															

Author1	Author2	year	specimen name	Specimen ID	concrete type	grease- no. ungase thickness of eyes	slab diameter of stud	ds, diameter of stud	Hs, height of stud	num of studs/ shear plane	longitudi- nal spacing	transvers e-spacing	Length of flange	A flange bf in contact	fy real (stud)	fy real p	fy limited	fc	fu (stud)	phi	Failure Shear/plane (load/per plane)	Failure load per stud	vu (ultimate shear strength)	normal load % applied (if mentioned)	thickness of flange	Qy/Actual	longitudi- nal spacing in terms of ds	transvers e spacing in terms of ds	max longit spacing in terms of ds	Hs/ds	
concrete		1994	Zb	451	NW	unknown	0.87	0.87	2.55	4	3.94	3.94	unknown	unknown	unknown	unknown	unknown	3865.0	61.90	unknown	51.10	42.78	unknown	0.00	unknown	21.69	unknown	4.55	4.55	unknown	2.96
concrete	N/A	1994	Zb	451	NW	unknown	0.87	0.87	2.55	4	3.94	3.94	unknown	unknown	unknown	unknown	unknown	3865.0	61.90	unknown	51.70	42.93	unknown	0.00	unknown	21.94	unknown	4.55	4.55	unknown	2.96
concrete	N/A	1994	Zc	452	NW	unknown	0.87	0.87	3.54	4	3.94	3.94	unknown	unknown	unknown	unknown	unknown	3865.0	61.90	unknown	61.00	45.35	unknown	0.00	unknown	25.88	unknown	4.55	4.55	unknown	4.09
concrete	N/A	1994	Zc	453	NW	unknown	0.87	0.87	3.54	4	3.94	3.94	unknown	unknown	unknown	unknown	unknown	3865.0	61.90	unknown	66.30	46.63	unknown	0.00	unknown	28.23	unknown	4.55	4.55	unknown	4.09
concrete	N/A	1994	Zc	454	NW	unknown	0.87	0.87	3.54	4	3.94	3.94	unknown	unknown	unknown	unknown	unknown	3865.0	61.90	unknown	57.80	44.45	unknown	0.00	unknown	24.53	unknown	4.55	4.55	unknown	4.09
concrete	N/A	1994	Zc	455	NW	unknown	0.87	0.87	3.54	4	3.94	3.94	unknown	unknown	unknown	unknown	unknown	3865.0	61.90	unknown	57.80	44.45	unknown	0.00	unknown	24.53	unknown	4.55	4.55	unknown	4.09